2nd Annual Workshop Proceedings of the Collaborative Project "Fast / Instant Release of Safety Relevant Radionuclides from Spent Nuclear Fuel"

(7th EC FP CP FIRST-Nuclides)

Antwerp 05 – 07 November 2013

Bernhard Kienzler, Volker Metz, Lara Duro, Alba Valls (eds.)

Bernhard Kienzler, Volker Metz, Lara Duro, Alba Valls (eds.)

**2nd Annual Workshop Proceedings of the Collaborative Project
"Fast / Instant Release of Safety Relevant Radionuclides from Spent Nuclear Fuel"**

(7th EC FP CP FIRST-Nuclides)

Antwerp 05 – 07 November 2013

Karlsruhe Institute of Technology

KIT SCIENTIFIC REPORTS 7676

2nd Annual Workshop Proceedings of the Collaborative Project "Fast / Instant Release of Safety Relevant Radionuclides from Spent Nuclear Fuel"

(7th EC FP CP FIRST-Nuclides)

Antwerp 05 – 07 November 2013

Bernhard Kienzler
Volker Metz
Lara Duro
Alba Valls
(eds.)

KIT Scientific Publishing

Report-Nr. KIT-SR 7676

This report is printed in black and white. The report showing the original colours in several photos, tables, figures and logos can be downloaded from the homepage of KIT Scientific Publishing.

Karlsruher Institut für Technologie (KIT)
Institut für Nukleare Entsorgung

FOREWORD

The present document is the proceedings of the 2nd Annual Workshop (AW) of the EURATOM FP7 Collaborative Project FIRST-Nuclides (Fast / Instant Release of Safety Relevant Radionuclides from Spent Nuclear Fuel). The electronic version of these proceedings is also available in the webpage of the project (http://www.firstnuclides.eu/). The workshop was hosted by SCK·CEN and held in Antwerp (Belgium) 5th – 7th November 2013. The project started in January 2012 and has three years duration. It has 10 beneficiaries and 11 associated groups. Most of them have participated in the 2nd AW as well as external interested groups.

The proceedings serve several purposes. The key purpose is to document and make available to a broad scientific community the outcome of the FIRST-Nuclides project. For this purpose, a considerable part of the project activity reporting is done through the proceedings, together with the outcome of scientific-technical contributions and Topical Sessions on different topics of interest for the development of the project. In the 2nd AW of FIRST-Nuclides, the topical session focused on understanding aging processes of the spent nuclear fuel. InSOTEC and CAST, two European projects, were also presented during the workshop. Additional purposes of the proceedings are to ensure on-going documentation of the project outcome, promote systematic scientific-technical development throughout the project and to allow thorough review of the project progress.

All Scientific and Technical papers submitted for the proceedings have been reviewed by the EUG (End-User-Group). The EUG is a group specifically set up within the project in order to represent the interest of the end users to the project and their needs. To this aim, the composition of the EUG includes organisations representing national waste management or national regulatory interests and competence.

The proceedings give only very brief information about the project structure and the different activities around the project, such as training measures and dissemination of knowledge. Such information about the project can be found in detail under http://www.firstnuclides.eu/.

Thanks are due to all those who submitted Scientific and Technical contributions for review and, especially, the workpackage leaders who provided the summary of the different workpackages for publication in these proceedings. We also want to give a special thanks to the reviewers, members of the EUG, whose effort and hard work reflect their commitment and dedication to the project and ensure a proper direction of the research within the project programme.

Table of Contents

THE PROJECT

The EURATOM FP7 Collaborative Project "Fast / Instant Release of Safety Relevant Radionuclides from Spent Nuclear Fuel (CP FIRST-Nuclides)" started in January 1, 2012 and extends over 3 years. The European nuclear waste management organisations contributing to the Technology Platform "Implementing Geological Disposal (IGD-TP)" considered the fast / instant release of safety relevant radionuclides from high burn-up spent nuclear fuel as one of the key topics in the deployment plan. For this reason, the CP FIRST-Nuclides deals with understanding the behaviour of high burn-up uranium oxide (UO_2) spent nuclear fuels in deep geological repositories.

The project is implemented by a Consortium with ten beneficiaries (Karlsruher Institut fuer Technologie (KIT) Germany, Amphos 21 Consulting S.L. (AMPHOS21) Spain, Joint Research Centre – Institute for Transuranium Elements (JRC-ITU) European Commission, Forschungszentrum Juelich GmbH (JÜLICH) Germany, Paul Scherer Institut (PSI) Switzerland, Studiecentrum voor Kernenergie (SCK•CEN) Belgium, Centre National de la recherche scientifique (CNRS) France, Fundacio Centre Technologic (CTM) Spain, Magyar Tudományos Akadémia Energiatudományi Kutatóközpont (MTA-EK) Hungary, and Studsvik Nuclear AB (STUDSVIK) Sweden). Organisations from France (Commissariat à l'énergie atomique et aux énergies alternatives, CEA), USA (Los Alamos Natonal Laboratory, SANDIA National Laboratories), UK (Nuclear Decommissioning Authority (NDA), National Nuclear Laboratory (NNL), the Department of Earth Sciences of the University Cambridge, and the Center for Nuclear Engineering of the Imperial College London), Finland (Posiva Oy, Teollisuuden Voima (TVO)), Spain (CIEMAT) and Germany (Gesellschaft für Anlagen- und Reaktorsicherheit (GRS) mbH) contribute to the project without receiving any funding as *Associated Groups (AG)*. These groups have particular interest in the exchange of information. Finally, a group of six implementation and regulatory oriented organizations (SKB (Sweden), NAGRA (Switzerland), ONDRAF/NIRAS (Belgium), ANDRA (France), BfS (Germany), ENRESA (Spain) participate as an *"End-User Group (EUG)"*. This group ensures that end-user interests (waste management organisations and one regulator) are reflected in the project work reviewing the project work and the scientific-technical outcome. Further details of the CP, especially on the workpackages and their detailed objectives have been reported somewhere else (Kienzler et al., 2013; Kienzler et al., 2013).

The 2nd Annual Workshop was held shortly after the first reporting period of the CP. As in the previous report (Kienzler et al., 2013), the scientific technical contributions of the beneficiaries have been reviewed by the End-User Group. The objectives of WP1 included the selection of spent nuclear fuel (SNF) samples, the complete characterization of these SNF materials with respect to the individual fuel characteristics and irradiation history, and the installation of experimental and analytical tools. WP1 is almost completed. Remaining results will be included in the final deliverable. Quantification of fission gases and fission gas release (FGR) from the various high burn-up spent nuclear fuels is part of WP2. Fission gas release measurement on PWR fuel were completed as well as measurements of the radial fission gas distribution by Ablation Mass Spectroscopy. The experiments on fast dissolution based release of gaseous and non-gaseous activation and fission products have been started. In contrast to previous instant release studies, it was possible within FIRST-Nuclides, combining FGR and dissolution based release measurements with material of single fuel rod. Further results are obtained on Se speciation in irradiated UO_2 fuel samples by micro-XAS. Rim and grain boundary diffusion experiments cannot be performed within the duration of CP FIRST-Nuclides due to an incident with the autoclave and long lasting repair measures. The objectives of the modelling cover the determination of the speciation of rare fission products in LWR fuel, the multi-scale modelling of themigration / retention processes of fission products in the

spent fuel and the estimation of fission product total release through the spent fuel rod. Detailed results are described in the following chapters.

Indispensable for CP FIRST-Nuclides is the documentation of the scientific and analytical state of knowledge related to the fast/instant release fraction of fission products from SNF as well as conducting activities related with dissemination of the generated knowledge to interested parties and to provide training and education for the next generation of spent nuclear fuel specialists. In this context, a laboratory meeting was held at PSI where different experimental and analytical techniques were discussed. 12 young scientists participated in a 2-days training course held in Karlsruhe (Germany). Three students applied for training mobility measures. Invited talks on the CP FIRST-Nuclides were given at the 14th Int. High Level Rad. Waste Management Conf. "Integrating Storage, Transportation, and Disposal" (Kienzler et al., 2013) and at the EURADWASTE'13 conference (Kienzler et al., 2013) and the state-of-the-art concerning the fast release was also presented (Kienzler and González-Robles, 2013). Reference to CP FIRST-Nuclides was given by the beneficiaries at various conferences. To the present, minimum 25 conference contributions and other publications refer to CP FIRST-Nuclides. Socio-political challenges with regard to CP FIRST-Nuclides were discussed during meetings with representatives of InSOTEC during a meeting held in July at Karlsruhe and during the 2nd Annual Workshop in Antwerp.

References

Kienzler, B., González-Robles. E. (2013). State-of-the-Art on Instant Release of Fission Products from Spent Nuclear Fuel. 15th International Conference on Environmental Remediation and Radioactive Waste Management ICEM2013, 8th-12th September 2013, Brussels.

Kienzler, B., González-Robles, E., Metz, V., Valls, A., Duro, L. (2013). FIRST-Nuclides: European Project on Radionuclide Release from Spent Fuel. 14th Int. High Level Waste Management Conference, Albuquerque, NM, USA. 28th April - 2nd May 2013, American Nuclear Society.

Kienzler, B., Metz, V., Duro, L., Valls, A. (2012). Collaborative Project "Fast / Instant Release of Safety Relevant Radionuclides from Spent Nuclear Fuel". 1st Annual Workshop Proceedings – 7th EC FP – FIRST-Nuclides. 9th – 11th October 2012, Budapest, Hungary.

Kienzler, B., Metz, V., González-Robles, E., Duro, L., Valls, A., Wegen, D., Carbol, P., Curtius, H., Günther-Leopold, I., Froideval Zumbiehl, A., Lemmens, K., Vandenborre, J., de Pablo, J., Casas, I., Clarens, F., Hózer, Z., Roth, O. (2013). CP FIRST-Nuclides: "Fast / Instant Release of Safety Relevant Radionuclides from Spent Nuclear Fuel". EURADWASTE'13, 8th EC Conference on the Management of Radioactive Waste, Community Policy and Research on Disposal, Vilnus, Lithuania, 14th-17th October 2013.

2ND ANNUAL WORKSHOP

The 2nd Annual Project Workshop of the FIRST-Nuclides project was held in Antwerp (Belgium) 5th – 7th November 2013. The workshop was hosted by SCK·CEN. There were 43 attendees at the workshop, representing beneficiaries, associated groups, the End-User Group and project external organizations. The workshop was organized in three days of oral presentations of results obtained within the project and a topical session on gas behaviour and alpha-damage in spent fuel.

Objectives

The Workshop combines different activities and meetings with the following objectives:

- Informing about the scientific progress. For this purpose, plenary sessions and posters are used for communicating results from the different technical workpackages.
- Informing about the administrative status.
- Informing/agreeing upon forthcoming reporting.
- Discussing various topics of interest for the consortium.
- Agreeing upon the forthcoming work program.

Emphasis was on scientific-technical topics with administrative issues kept to the minimum necessary.

RTD sessions

The workshop included plenary sessions where the results from the different workpackages were presented. Next to an overview of the achievements within the respective WP, scientific highlights were presented. The following presentations were given within the project.

WP1 session

- V. Metz. Overview of Activities within WP1 "Samples and Tools".
- V. Metz. Characterization of UOX fuel segments irradiated in the PWR Gösgen.
- D. Serrano-Purroy, D.H. Wegen, R. Sureda. Non-destructive analysis of a PWR fuel segment with a burn-up of 50.4 GWd/t$_{HM}$.
- A. Froideval Zumbiehl, I. Günther-Leopold, H.P. Linder, E. Curti. WP1: Preparation of the spent fuel samples for leach experiments and spectroscopic studies at PSI.
- K. Govers, M. Verwerft, W. Van Renterghem, B. Vos, S. Van den Berghe, T. Mennecart, C. Cachoir, K. Lemmens, L. Adriaensen, A. Dobney, M. Gysemans. Status of the characterization. SCK·CEN samples from Tihange 1 NPP.
- J.Vandenborre, A.Traboulsi, G.Blain, M.Fattahi. Radiolytic corrosion of grain boundaries onto the UO$_2$ TRISO particle surface: WP1 - solid characterization and irradiation cell development.
- O. Roth. Characterization and preparation of spent fuel samples at Studsvik.
- V. Metz, E. González-Robles, B. Kienzler. Characterization of UOX fuel segments irradiated in the PWR Gösgen Contribution of KIT-INE to WP1 "Samples and Tools".

WP2 session

- D.H. Wegen. WP2: Fission Gas Release and Rim and Grain Boundary Diffusion.
- E. González-Robles, E. Bohnert, N. Müller, M. Herm, B. Kienzler, V. Metz. Determination of the fission gas release in the segment N0204 and gas phase results of anoxic leaching experiment.
- A. Puranen, M. Granfors, O. Roth. Laser ablation experiments at Studsvik
- P. Carbol, I. Marchetti, D.H. Wegen. Oxygen and Water Diffusion into 42 GWd/t$_{HM}$ UO$_2$ fuel under reducing conditions.
- H. Curtius, H.W. Müskes, N. Lieck, M. Güngör, D. Bosbach. Instant radionuclide release fraction of high burn-up spent nuclear fuel.
- A. Traboulsi, J. Vandenborre, G. Blain, M. Fattahi. Impact of water radiolysis on uranium dioxide corrosion: effect of molecular species.

WP3 session

- K. Lemmens. Introduction : overview of activities within WP3.
- E. Slonszki, Z. Hózer. Determination of dissolution rates for damaged and leaking VVER fuel stored in water.
- R. Sureda, .J. de Pablo, F. Clarens, I. Casas, D. Serrano-Purroy, L. Aldave, D. Wegen, J.P. Glatz, V. Rondinella. Leaching test of commercial BWR UO$_2$ SNF for fast/instant radionuclide release studies. First results for cladded segment samples.
- O. Roth, A. Puranen, J. Low, M. Granfors, D. Cui, C. Askeljung. Effects of matrix composition on instant release fractions from high burnup nuclear fuel and WP3 status.
- D. Cui, J. Low. WP3: dissolution based fast/instant ^{14}C release.
- E. González-Robles, E. Bohnert, N. Müller, M. Herm, B. Kienzler, V. Metz. State of the leaching experiments under anoxic conditions.
- Th. Mennecart, K. Lemmens, C. Cachoir, L. Adriaensen, A. Dobney. Leaching tests for the experimental determination of IRF radionuclides from Belgian high-burnup spent nuclear fuel: Overview of pre-test fuel characterization, experimental set-up and first results.
- E. Curti, A. Froideval Zumbiehl, I. Günther-Leopold, M. Martin, A. Bullemer, H.P. Linder, C.N. Borca, D. Grolimund, J. Rothe, K. Dardenne. X-ray Absortion Spectroscopy of Se in non-irradiated doped UO$_2$ and HBU spent UO$_2$ fuel.

WP4 session

- J. de Pablo. WP4 – Overview of activities.
- B. Kienzler, E. Bohnert, E. González-Robles, M. Herm, X. Gaona, C. Borkel. Speciation of ^{14}C in Spent Nuclear Fuel.
- J. de Pablo, D. Serrano-Purroy, I. Casas, A. Espriu, A. Martínez-Esparza. IRF modelling from high burn-up spent fuel cladded segments from leaching experiments.
- M. Pękala, A. Idiart, L. Duro, O. Riba. Linking water saturation of SF with instant/fast release.

WP5 session

- A. Valls. Status and overview of WP5.
- V. Metz. WP5 – training activities summary.
- E. Curti. Report on the FIRST-Nuclides Lab meeting (PSI, March 18-19, 2013).

Poster presentations

The following posters were presented during the 2nd Annual Workshop:

- B. Kienzler, V. Metz, L. Duro, A. Valls, V. Montoya. Generic Poster of FIRST-Nuclides project.
- Pekala, M., Idiart, A., Riba, O., Duro, L. Numerical Modelling of spent Nuclear fuel Saturation with Water under Laboratory and Ropository Conditions.

Topical session and external presentation

The main objective of organizing the Topical Sessions is covering the key areas along with the project. One talk was given during the 2nd Annual Workshop Topical session focused on understanding aging processes of the spent nuclear fuel.

- T. Wiss, V.V. Rondinella, D. Staicu, Z. Talip, E. Maugeri, A. Janssen, J.-Y. Colle, O. Benes, R.J.M. Konings, P. Raison, D. Bottomley, P. Pöml, S. Bremier, D. Papaioannou, V. Di Marcello, P. Van Uffelen . Evidence on spent fuel aging: gas behaviour and alpha-damage.

Two presentations presenting the CAST and InSOTEC European projects where given by C. Padovani and J. Schröder, respectively.

- S. Williams, E. Scourse. Project CAST – Carbon-14 Source Term.
- A. Bergmans, J. Schröder. International Socio-Technical challenges implementing geological disposal.

Associated group presentations

Additional presentations were given on a topic of general interest, especially the context of the present project within the EURATOM FP7 program on geologic disposal. These presentations were given by the associated group.

- D.C. Sassani, Carlos F. Jové-Colón, Philippe F. Weck. Brief. Integrated used fuel degradation models into generic performance assessment.
- B. Pastina. Use of IRF data in the safety case for the Finnish disposal project.
- C. Padovani. The characteristics and leaching behaviour of AGR spent fuel – an overview of UK research.
- D. Hambley. Long term behaviour of spent AGR fuel in repository conditions.
- N. Rauff-Nisthar, C. Boxall, R. Wilbraham. Corrosion Behaviour of AGR Simulated Fuels – Evolution of the Fuel Surface Preliminary Studies.
- M. Cooper, R. W. Grimes, S. Middleburgh. WP3. Issues aroung UK specific AGR fuel & atomistic modelling & results so far.

Structure of the proceedings

The proceedings are divided into the following sections:

- Contribution of external experts presenting issues of interest for the project within the Topical Sessions and European Projets Presentations.
- WP activity overviews
- Individual Scientific and Technical Contributions, containing reviewed scientific and technical manuscripts
- Posters presented in the 2nd Annual Workshop
- Additional presentations given by members of the Associated Group

All the scientific-technical contributions submitted were reviewed by the EUG members (End-User-Group).

CONTRIBUTION EXTERNAL EXPERTS (TOP SESS)

EVIDENCE ON SPENT FUEL AGING: GAS BEHAVIOUR AND ALPHA-DAMAGE

T. Wiss[1], V.V. Rondinella[1], D. Staicu[1], Z. Talip[1], E. Maugeri[2], A. Janssen[1], J.-Y. Colle[1], O. Benes[1], R.J.M. Konings[1], P. Raison[1], D. Bottomley[1], P. Pöml[1], S. Bremier[1], D. Papaioannou[1], V. Di Marcello[3], P. Van Uffelen[1]

[1] European Commission, Joint Research Centre, Institute for Transuranium Elements (DE)
[2] Paul Scherrer Institute, PSI (CH)
[3] Karlsruhe Institute of Technology, KIT (DE)

The safety assessment of spent nuclear fuel (SNF) during storage/disposal requires defining/extrapolating the behaviour of the fuel over the timescale of interest, to ensure that the mechanical integrity is retained, hence minimising the possible exposed surface to corrosion processes.

Since no direct measurement of stored fuel can cover the full time extension of interest, additional studies aimed at understanding aging processes of the SNF expected to affect properties and behaviour of spent fuel during many decades of storage are necessary. Tests conducted under accelerated conditions can thus contribute to the safe implementation of extended storage concepts.

Alpha-decay damage and helium accumulation are the key process affecting the microstructure evolution of properties and behaviour of spent fuel. The effects of alpha-decay damage and helium build-up during SNF storage are the object of a dedicated programme of studies carried out at JRC-ITU, which covers in particular the evolution of physical-chemical and mechanical properties as a function of accumulated radioactive decay damage and He. The investigations address processes and mechanisms from the microstructural level (lattice defects and swelling, He behaviour) up to macroscopic properties (fuel swelling, hardness, stored heat, thermal conductivity). Accelerated ageing conditions are obtained by using suitable UO_2 matrices containing short-lived alpha-emitters (the so-called alpha-doped UO_2).

The evolution of the fuel is also directly connected to its microstructure and composition after irradiation. Knowing the location of the various elements present and their chemical nature but also their evolution or migration during storage through diffusion or alpha-radiation enhanced mobility will allow assessing the source term in case of contact with water.

This paper addresses both fundamental studies of aging processes of spent fuel surrogate (the alpha-doped) and the investigation of irradiated nuclear fuel aiming at determining the location and behaviour of the volatile fission products in particular. Several techniques have been used to characterize these two types of material (XRD, TEM, helium thermal desorption, Knudsen-cell mass spectrometry, etc).

PROJECT CAST - UNDERSTANDING THE CARBON-14 SOURCE TERM IN GEOLOGICAL DISPOSAL

Steve Williams[1] and Ellie Scourse[2]

[1] Nuclear Decommissioning Authority, Radioactive Waste Management Directorate (UK)
[2] MCM-international (UK)

The CAST project (CArbon-14 Source Term) aims to develop understanding of the potential release mechanisms of carbon-14 from radioactive waste materials under conditions relevant to waste packaging and disposal to underground geological disposal facilities. The expected increase in understanding should decrease uncertainties in the long-term safety assessment and increase confidence in the safety case. The project focuses on the release of ^{14}C as dissolved and gaseous species from irradiated metals (steels, Zircaloys), irradiated graphite and from ion-exchange materials. CAST is co-funded under the Euratom Seventh Framework programme and began on 1st October 2013.

The CAST consortium brings together 33 partners consisting of national waste management organisations, research institutes, universities and commercial organisations. The objectives of the CAST project are to:

a) gain a scientific understanding of the rate of release of ^{14}C from the corrosion of irradiated steels and Zircaloys and from the leaching of ion-exchange resins and irradiated graphites under geological disposal conditions, its speciation and how these relate to ^{14}C inventory and aqueous conditions;

b) evaluate this understanding in the context of national safety assessments; and

c) disseminate this understanding and its relevance to safety assessments to interested stakeholders and provide an opportunity for training of early career researchers

These objectives will be met through seven Work Packages:

- Work Package 1: 'Management' led by NDA, UK
- Work Package 2: 'Steels' led by Nagra, Switzerland
- Work Package 3: 'Zircaloy' led by Andra, France
- Work Package 4: 'Ion-Exchange Resins' led by CEA, France
- Work Package 5: 'Graphite' led by NDA, UK
- Work Package 6: 'Relevance to Safety Cases' led by Niras/Ondraf, Belgium
- Work Package 7: 'Dissemination' led by Covra, Netherlands

Work Packages 2 to 5 undertake fundamental scientific experiments and develop conceptual models for carbon-14 release from a range of radioactive waste materials. Work Package 6 will relate the results to national safety cases, while Work Package 7 will ensure that the CAST results and the implications are disseminated to all partners and interested stakeholders. Each Work Package will produce a final report to record the findings; these will be published along with a Final Report assimilating all of the results into one overview report. The total duration of CAST is 54 months.

INTERNATIONAL SOCIO-TECHNICAL CHALLENGES TO IMPLEMENTING GEOLOGICAL DISPOSAL (INSOTEC)

Jantine Schröder and Anne Bergmans

University of Antwerp (BE)

InSOTEC is a three-year European FP7 social sciences research project, aiming to generate a better understanding of the complex interplay between the technical and the social in radioactive waste management (RWM) and, in particular, in the design and implementation of geological disposal (GD). This field is classically dominated by techno-scientific research, social science input being limited to e.g. communication and public participation. InSOTEC questions the division between 'technical content' and 'social context' in RWM, by investigating the social shaping of technologies (e.g. the social boundary condition of not wishing to burden future generations leading to the expectation of a passive, final RWM technology) and the technical shaping of societies (e.g. the technical boundary conditions of passive safety leading to the expectation of a future society that will remember where the repository is but refrain from digging into it). In other words, InSOTEC aims to investigate the mutual shaping of the social and the technical throughout RWM, as we see that in RWM activities and debates techno-scientific and socio-political issues are in fact, consciously or unconsciously, concurrently negotiated, weighted and assessed.

Work package (WP) 1 provided a review of national (14 countries) and international RWM programs and activities, focusing on the correlation of socio-political and techno-scientific challenges and whether or not they are acknowledged and dealt with as such. WP2 consists of a further assessment of the main challenges identified throughout WP1, by means of a number of case studies on socio-technical mechanisms related to the topics of siting, technology transfer, reversibility and retrievability, and the demonstration of safety. WP3 looks at arenas where socio-technical decisions on RWM are formed through the co-production of knowledge between different actors. A particular case study is the Implementing Geological Disposal Technology Platform (IGD-TP). The presentation and discussion at the FIRST-Nuclides workshop also belong to this activity, as we want to explore with scientists and technical experts the socio-political dimensions and implications of their work and how they perceive this socio-technical entanglement. To this aim, the workshop participants were asked to share their opinion about questions such as: "How are societal expectations integrated into the RD&D of projects such as FIRST-Nuclides? How do technical projects define their end users and reach out beyond peers? Can long-term safety be demonstrated? How are scenario, model and parameter value uncertainties dealt with?" etc.

Overall, with this project InSOTEC partners hope to create greater understanding and awareness among the technical community of the social implications of their work, as well as of the underlying social assumptions that directly and indirectly colour the solutions they are developing. At the same time the partners hope the project will also provide other parties concerned (such as political decision makers or involved communities) with a better insight into the origins of certain technical concepts, which may help them to be better equipped when dealing with these issues in their own context. To this aim, WP4 will explicitly link the research activities to the practice of RWM and GD by offering concluding reflections and recommendations.

WP OVERVIEW

OVERVIEW WP1: SAMPLES AND TOOLS

Volker Metz

Karlsruhe Institute of Technology (KIT), Institute for Nuclear Waste Disposal (INE), (DE)

Introduction

The basic activities of the project FIRST-Nuclides – coordinated in workpackage #1 "Samples and Tools" - were to select, provide and prepare spent nuclear fuel (SNF) samples for subsequent experimental investigations. The objectives of this workpackage included the complete characterization of the selected SNF materials with respect to the individual fuel characteristics and irradiation history, achieving permission by the fuel owners for publication of key parameters as well as the installation of experimental and analytical tools. All experimentally working partners of the FIRST-Nuclides project (i.e. KIT, JRC-ITU, JÜLICH, PSI, SCK•CEN, CNRS, CTM, MTA EK and STUDSVIK) contributed to this workpackage. Initially the activities within workpackage #1 were planned to be conducted until June 2013. Since there were delays in the documentation and with the sample preparation of SNF materials used by JRC-ITU and CTM, it was decided to extend this workpackage until summer 2014.

Twenty months after the start of the project, the characterisation of the studied spent nuclear fuel samples and the description of methodologies and tools applied in workpackages #1, #2 and #3 were documented in the FIRST-Nuclides Deliverable #1.2 (Metz et al., 2013). In the Proceedings of the 2nd Annual Workshop, an update on the characterisation of the studied samples and activities related to set-up the methodologies and tools for the experimental studies in workpackages #2 and #3 are presented.

Achievements

Most partners dealt with high burn-up SNF, which had been irradiated in commercial nuclear power reactors, while the JÜLICH group studied so-called TRISO fuel irradiated in a research reactor at the Petten EC Joint Research Centre. CNRS worked with unirradiated TRISO particles, which are used in successive corrosion experiments under alpha irradiation. MTA EK studied damaged and leaking VVER fuel rods, which were stored in water for several years after an incident at the Paks-2 reactor. KIT, JRC-ITU, PSI, SCK•CEN, CTM and STUDSVIK investigated six SNF fuels, which were discharged from boiling water reactors (BWR), and six SNF fuels, which were discharged from pressurized water reactors (PWR). The selected BWR fuels were initially enriched with ^{235}U in the range of 3.7 to 4.3% and approached average fuel rod burn-ups between 42.2 to 59.1 GWd/t_{HM} during irradiation. The selected PWR fuels cover a burn-up range of 50.0 to 70.2 GWd/t_{HM} and initial ^{235}U enrichments in the range of 2.8 to 4.3%. Additionally, a PWR mixed oxide fuel with 63 GWd/t_{HM} and an initial Pu_{fiss} enrichment of 5.5% was studied by PSI.

Samples (cladded pellets, pellets, powders, TRISO kernels etc.) of these fuel materials were characterized to a certain extent and prepared for various spectroscopic, metallurgic and chemical analyses as well as subsequent investigations in workpackages #2 and #3. For experimental studies within these workpackages, experimental set-ups (incl. autoclaves, irradiation cells, reaction vessels), specific sampling devices and analytical equipment were provided and installed in the hot cells, shielded box-line and He^{2+} irradiation facility, respectively.

KIT studied the spent nuclear fuel rod segment SBS1108-N0204, which was irradiated in a PWR together with the adjacent segment SBS1108-N0203, achieving an average burn-up, BU, of 50.4 GWd/t_{HM}. Up-dated data on irradiation history of both segments as well as experimental data of SBS1108-N0203 (determined in previous studies) were reported by Metz et al. (2014).

JRC-ITU and CTM characterized BWR spent fuel samples (average burnup of 42 and 54 GWd/t_{HM}, respectively). The properties of the fuels and preparation of segment and powder samples for IRF investigations and oxygen diffusion experiments are described by Wegen et al. (2014).

PSI selected a BWR UO_2 fuel with an average BU of 57.5 GWd/t_{HM} and a PWR UO_2 fuel with 62.2 GWd/t_{HM}. Additionally, a PWR MOX fuel with 63 GWd/t_{HM} was selected for subsequent studies in workpackage #3. Günther-Leopold et al. (2014) described the preparation of samples (cutting and defueling) and the installation of leach equipments in a dissolution box of the PSI hot laboratory.

SCK•CEN collected manufacturing and operational data of a PWR fuel with an average BU of 50 GWd/t_{HM}. Fuel fragments were prepared for consecutive investigations within workpackage #3. Equipment for leaching experiments within workpackage #3 were installed in a SCK•CEN hot cell. Mennecart et al. (2014) described the main experimental parameters, i.e. the type of fuel, the sample preparation, the experimental setup, the leach test conditions, the sampling scheme and the surface and solution analyses.

At the 2nd Annual Workshop, activities of CNRS, JÜLICH, MTA EK and STUDSVIK related to compilation of manufacturing and operational data, preparation of samples and tools were reported in their contributions to workpackages #2 and #3.

Acknowledgement

References

Günther-Leopold, I., Lindner, H.P., Froideval Zumbiehl, A., Curti, E. (2014). Preparation of the spent fuel samples for leach experiments and spectroscopic studies at PSI. 2nd Annual Workshop Proceedings, 7th EC FP – FIRST-Nuclides, November 5th-7th, Antwerp, Belgium.

Mennecart, T., Lemmens, K., Cachoir, C., Adriaensen, L., Dobney, A. (2014). Leaching tests for the experimental determination of IRF radionuclides from Belgian high-burnup spent nuclear fuel. Overview of pre-test fuel characterization, experimental set-up and first results. 2nd Annual Workshop Proceedings, 7th EC FP – FIRST-Nuclides, November 5th-7th, Antwerp, Belgium

Metz, V., González-Robles, E., Müller, N., Bohnert, E., Herm, M., Lagos, M., Kienzler, B., Serrano Purroy, D., Colle, J.Y., Beneš, O., Naisse, F., Wiss, T., Konings, R.J.M., Wegen, D.H., Papaioannou, D., Gretter, R., Nasyrow, R., Rondinella, V. V., Glatz, J. P., Curtius, H., Müskes, H.W., Like, N., Bosbach, D., Günther-Leopold, I., Curti, E., Froideval Zumbiehl, A., Lindner, H.P., Govers, K., Verwerft, W., Van Renterghem, W., Lemmens, K., Mennecart, T., Cachoir, C., Adriaensen, L., Dobney, A., Gysemans, M., Vandenborre, J., Traboulsi, A., Blain, G., Barbet, J., Fattahi, M., Sureda Pastor, R., Slonszki, E., Hózer, Z., Roth, O. (2013). Fast/Instant Release of Safety Relevant Radionuclides from Spent Nuclear Fuel (FIRST-Nuclides):

Characterisation of spent nuclear fuel samples and description of methodologies and tools to be applied in FIRST-Nuclides. Deliverable No 1.2. European Commission, Brussels.

Metz, V., González-Robles, E., Kienzler, B. (2014). Characterization of PWR UOX fuel segments irradiated in the PWR Gösgen. 2nd Annual Workshop Proceedings, 7th EC FP – FIRST-Nuclides, November 5th-7th, Antwerp, Belgium

Wegen, D.H., Papaioannou, D., Nasyrow, R., Gretter, R., Serrano-Purroy, D., Sureda Pastor, R., Carbol, P., Rondinella, V. V., Glatz, J. P., (2014). Characterisation of commercial BWR spent fuel samples for IRF investigations and oxygen diffusion experiments. 2nd Annual Workshop Proceedings, 7th EC FP – FIRST-Nuclides, November 5th-7th, Antwerp, Belgium

OVERVIEW WP2: GAS RELEASE + RIM AND GRAIN BOUNDARY DIFFUSION

Detlef Wegen

Institute for Transuranium Elements, ITU (EC)

Introduction

In the first project year the focus was on setting up experimental facilities, characterisation and preparation of samples. In the second year of the experimental work programme in WP2 first results have been obtained by the partners but also new challenges arose.

Work package two is divided into the two components "Experimental determination of fission gas release" and "Rim and grain boundary diffusion". In the first component, the focus is on the quantification of fission gases and fission gas release in high burn-up (HBU) UO_2 spent nuclear fuels (SNF). Fission gas sampled in the plenum of a fuel rod are analysed as well as the grain boundary inventory and the cross sectional distribution of fission gases and volatile fission products.

The second component "Rim and grain boundary diffusion" deals with investigations on oxygen diffusion in spent UO_2 fuel. The examination of diffusion mechanisms will result in the quantification of water penetration into the fuel (grain and grain boundaries) structures and subsequently couple the diffusion/corrosion phenomena. Furthermore, investigations on irradiated and unirradiated fuel kernels separated from high temperature gas cooled reactor (HTR) fuel are planned which are complementary to those on light water reactor (LWR) fuel.

The experimental part of WP2 started in project month 4 and will end in project month 36 (Wegen et al., 2012; 2012a; 2013a).

The Joint Research Centre – Institute for Transuranium Elements (JRC-ITU) is the leading organization of WP2. In the first project year the fission gas release (FGR) from a spent fuel rod owned by KIT was measured (Wegen et al., 2012; 2013). The determination of the inventory of fission gas and fission products in grain boundaries are foreseen for the third project year.

The Karlsruher Institut Für Technologie (KIT) analysed in the first project year fission and activation products in the fission gas sampled at JRC-ITU from the plenum of a fuel rod segment by puncturing. The development, testing and implementation of analytical methods for fission and activation products have started in the first project year one and were continued in the second. Leaching experiments in which gas and solution analyses are foreseen were started in the first year and last until project month 33 (Wegen et al., 2012).

STUDSVIK Nuclear AB (STUDSVIK) investigates in the frame of WP2, the radial fission gas and volatile fission product distribution (Xe, I, and Cs) by Laser-Ablation Mass Spectroscopy (LA-MS) on HBU boiling water reactor (BWR) SNF (Wegen et al., 2012).

The JRC-ITU is the leading organization of WP2. The investigation of diffusion effects started in the first project year with the characterisation and preparation of spent fuel samples, which will be used for corrosion experiments in $H_2^{18}O$ water at room temperature. In 2013 it was planned to determine the $^{18}O/^{16}O$ depth profiles using a shielded SIMS (secondary ion mass spectrometry) to quantify the oxygen diffusion into spent nuclear fuel (SNF) (Wegen et al., 2012a).

Forschungszentrum Jülich GMBH (JÜLICH) is working on spent high temperature reactor fuel. Within the first half of the project the radionuclide inventory in the fuel kernel and in the coatings were determined and compared to calculated values as well. Further on investigations of the microstructure and of the elemental distribution of the fuel kernel and of the coatings are performed before (first half of the project) and after leaching (second half of the project). After cracking of the tight coatings the fission gas release fraction was measured in the first 18 months. Then static leaching experiments with the separated fuel kernels and coatings were started in 2013 in order to determine the fast instant radionuclide release fraction (Wegen et al., 2012a).

Unirradiated tristructural-isotropic (TRISO) fuel particles are investigated by the Centre National de la Recherche Scientifique (CNRS) at the ARRONAX cyclotron. The particles are irradiated using a He^{2+}-beam in the dose rate range of 0 - 100 Gy/min. The corrosion of UO_2 TRISO particles is investigated in view of grain boundary effects and secondary phase formation and the influence of hydrogen. The experiments started in 2013 with studies on the role of grain boundaries, followed by investigations of fuel particle corrosion under hydrogen and in varying dose rates (Wegen et al., 2012a).

Achievements

Experimental determination of fission gas release

KIT has analysed the experimental FGR data obtained after the plenum puncturing of the PWR fuel segment N0204 and determined the fission gas release from the experimental results and the theoretical inventory for Xe and Kr calculated with the ORIGEN code. The fission gas release was 8.35% of the total inventory (González-Robles et al., 2013; 2013a).

A leaching experiment on a well characterised sample of PWR fuel (N0204) was started under anoxic conditions. A cladded segment pellet was introduced in an autoclave together with 220 ml of bicarbonate water (19 mM $NaHCO_3$ + 1 mM NaCl). Then the autoclave was pressurised with Ar/H_2 (p_T = 40 bar; pH_2 = 3 bar). First gas samples have been analysed. After a cumulative contact time of 57 days, 4.3% of the Xe and 17% of the Kr inventories were released into the gas phase (González-Robles et al., 2013b; 2013c; 2013d).

STUDSVIK evaluated the Laser Ablation data obtained in 2012 on cross sections from a standard UO_2 fuel and an Al/Cr-additive fuel. The findings of the Laser Ablation study on both pellets indicate caesium and iodine profiles that are very similar and appear to follow the radial burn-up profile (as indicated by [140]Ce). Caesium, iodine and to some extent selenium also appear to collect in some fuel cracks. Selenium was tentatively identified by the good agreement of the isotopic ratios of mass 77, 79 and 82 with the calculated inventory. For the additive pellet chromium and especially aluminium are heterogeneously distributed in the pellet. Further analysis of the data is underway (Roth et al., 2013; Puranen et al., 2013; 2013a).

Rim and grain boundary diffusion

After more than one year of experimental work first results were obtained in the HTR related studies, while the oxygen diffusion studies were drawn back by an autoclave failure.

JÜLICH investigates UO_2TRISO coated particles from spent HTR fuel (burn-up ~100 GWd/t_HM). Due to the tight coatings no fission gas is released during the irradiation process, hence the complete activation/fission products are located in the TRISO coated particles. To determine the fission gas fraction a crack device coupled with a gas sampling tool was developed. $^{14}CO_2$ was detected up to (15 ± 5) Bq per fuel kernel. Previous ESEM (environmental scanning electron microscope) investigations revealed the presence of He in the buffer, but

within the gas samples no He was detected. The fission gas ^{85}Kr represented the main gas component. Approximately 35% of the complete inventory was instantaneously released.

During static leaching experiments no actinides Pu, Am, Cm, Np and U were detected in solution (detection limit for U ~ 10^{-8} mol/L). The release of Sr from the fuel matrix was negligible indicating that the UO_2 matrix does not dissolve yet. In contrast a high release of Cs was observed. This finding underlines the location of Cs at the grain boundaries. In addition the formation of a protective $UO_{2.33}$ layer under air condition is assumed as the determined Cs release rates are lower under oxic conditions compared to the values obtained for an anoxic/reducing environment (Curtius et al., 2013; 2013a; 2013b).

CNRS investigates the oxidation of UO_2 in unirradiated HTR fuel kernels by α-radiolysis products of water. Radiolysis products are produced by 66.5 MeV He^{2+} beam irradiation of water in the ARRONAX cyclotron giving a dose rate of 4.37 kGy/min. The UO_2 oxidation is studied by simultaneous characterisation of secondary phases on the UO_2 surface by Raman spectroscopy, quantification of the radiolysis products H_2O_2 in water (UV-VIS spectrophotometry) and H_2 in the gas phase (micro gas chromatography) and determination of U in solution by inductively coupled plasma mass spectrometry (ICP-MS).

The obtained results show that α-radiolysis induced oxidation of the UO_2 surface depend on the composition of the gas phase in the open or closed system and the dose. In open system at a dose of 8.73 kGy Raman spectra show oxidation of UO_2 by radiolytic produced H_2O_2 indicated by formation of studite ($UO_4·4(H_2O)$) on the UO_2 surface. Under irradiation a G-value for hydrogen peroxide production of $G(H_2O_2) = 0.06$ μmol/J is found. The total uranium concentration in solution is $11.5·10^{-7}$ mol/L.

In a closed system the oxidation is slower due to the reducing effect of radiolytically produced H_2. Here, $G(H_2O_2)$ and $G(H_2)$ are respectively 0.10 and 0.02 μmol/J. The concentration of uranium in solution is $5.2·10^{-7}$ mol/L. Despite the fact of a higher H_2O_2 concentration in the closed system, the oxidation of UO_2 is slower. The radiolytically produced H_2 reacts as a reducing agent and limits the oxidation process of UO_2 (Vandenborre et al., 2013; Traboulsi et al., 2013; 2013a; 2014).

JRC-ITU did a literature review of spent fuel oxidation and oxygen diffusivity. It was searched for open publications related to experiments or predictions of oxygen lattice and grain boundary diffusion coefficients with or without coupling to the oxidation of the irradiated fuel (Carbol et al., 2013).

During refurbishment of the autoclave in the hot cell, intended for oxygen diffusion experiments, a Ti-welded tube joint broke. Unfortunately the weld broke at a vital place on the autoclave and as the autoclave was contaminated it could not be taken out of the hot cell and re-welded. For safety reasons a replacement of the complete autoclave setup is necessary. This causes a delay of 6 months. Even by reducing the duration of the experiment to a minimum (9 months) it is not possible to finish the study in the given time frame of FIRST-Nuclides. It was decided to prolong WP2 from 33 to 36 months and to report all results obtained until month 33 in FIRST-Nuclides. Later results will be published in an open journal with reference to FIRST Nuclides (Carbol et al., 2013a).

References

Carbol, P., Marchetti, I., Wegen, D.H. (2013). WP2: Rim and Grain Boundary Diffusion. 2nd Annual Workshop Proceedings, 7th EC FP – FIRST-Nuclides. 5th-7th November, Antwerp, Belgium.

Carbol, P., Marchetti, I., Wegen, D.H. (2013a). Oxygen and water diffusion into 42 GWd/t$_{HM}$ UO_2. 2nd Annual Workshop, 7th EC FP – FIRST-Nuclides. 5th-7th November, Antwerp, Belgium.

Curtius, H., Müller, E., Müskes, H.W., Klinkenberg, M., Bosbach, D. (2013). Selection and Characterisation of HTR Fuel. 1st Annual Workshop Proceedings of the Collaborative Project "FAST/INSTANT release of Safety Relevant Radionuclides from Spent Nuclear Fuel" (7th EC FP CP FIRST-NUCLIDES). 9th-11th October 2012, Budapest, KIT SCIENTIFIC Reports 7639.

Curtius, H., Müskes, H.W., Güngör, M., Liek, N., Bosbach, D. (2013a). Instant radionuclide release fraction of high burn-up spent nuclear fuel. 2nd Annual Workshop Proceedings, 7th EC FP – FIRST-Nuclides. 5th-7th November, Antwerp, Belgium.

Curtius, H. (2013b). Instant radionuclide release fraction of high burn-up spent nuclear fuel. 2nd Annual Workshop, 7th EC FP – FIRST-Nuclides. 5th-7th November, Antwerp, Belgium.

González-Robles, E., Bohnert, E., Loida, A., Müller, N., Metz, V., Kienzler, B. (2013). Fission gas measurements and description of leaching experiments with of KIT's irradiated PWR fuel rod segment (50.4 GWd/t_{HM}). 1st Annual Workshop Proceedings of the Collaborative Project "Fast /Instant Release of Safety Relevant Radionuclides from Spent Nuclear Fuel" (7th EC FP CPFIRST-Nuclides). 9th-11th October 2012, Budapest, KIT SCIENTIFIC REPORTS 7639, 231.

González-Robles, E., Bohnert, E., Müller, N, Herm, M., Metz, V. (2013a). Determination of the fission gas release in the segment N0204 and gas phase result of anoxic leaching experiment. Proceedings of the 2nd Annual Workshop of the FIRST- Nuclides Project. 5th-7th November, Antwerp, Belgium.

González-Robles, E., Wegen, D.H., Papaioannou, D., Kienzler, B., Nasyrow, R., Metz, V. (2013b). Physical characterisation of spent nuclear fuel: First steps to further Instant Release Fractions investigations. 8th EC Conference on the Management of Radioactive Waste, EURADWASTE 2013. 14th-17th October, Vilnius, Lithuania.

González-Robles, E., Bohnert, E., Metz, V., Wegen, D.H., Papaioannou, D., Kienzler, B. (2013c). Physical characterisation and calculation of the initial and boundary conditions of a commercial UO_2 spent nuclear fuel regarding the radionuclide release. 37th Symposium on the Scientific Basis for Nuclear Waste Management. 29th September–3rd October, Barcelona, Spain.

González-Robles, E., Bohnert, E., Müller, N, Herm, M., Metz, V. (2013d). Determination of the fission gas release in the segment N0204 and gas phase result of anoxic leaching experiment. 2nd Annual Workshop of the FIRST- Nuclides Project. 5th-7th November, Antwerp, Belgium.

Puranen, A., Roth, O., Granfors, M. (2013). Investigating the radial distribution of potential rapid release radionuclides in irradiated nuclear fuel. Symposium: E No. 2 15, E-MRS 2013 Spring Meeting. 27th-31st May, Strasbourg, France.

Puranen, A., Granfors, M, Roth, O. (2013a). Laser ablation experiments at Studsvik. 2nd Annual Workshop of the FIRST- Nuclides Project. 5th-7th November, Antwerp, Belgium.

Roth, O., Puranen, A., Low, J., Granfors, M, Cui, D., Askeljung, C. (2013). Spent fuel leaching experiments and laser ablation studies performed in Studsvik - Status and preliminary results. Proceedings of the 2nd Annual Workshop of the FIRST- Nuclides Project. 5th-7th November, Antwerp, Belgium.

Traboulsi, A., Vandenborre, J., Blain, G., Humbert, B., Barbet, J., Fattahi, M. (2013). Impact of Water Radiolysis on Uranium Dioxide Corrosion. 2nd Annual Workshop Proceedings, 7th EC FP – FIRST-Nuclides. 5th-7th November, Antwerp, Belgium.

Traboulsi, A., Vandenborre, J., Blain, G., Barbet, J., Fattahi, M. (2013a). Impact of Water Radiolysis on Uranium dioxide corrosion. Migration 2013. 8th-13th September, Brighton, UK.

Traboulsi, A., Vandenborre, J., Blain, G., Humbert, B., Barbet, J., Fattahi, M. (2014). Radiolytic Corrosion of Uranium Dioxide: Role of Molecular Species. J. Phys.Chem C, Vol. Submitted.

Vandenborre, J., Traboulsi, A., Blain, G., Barbet, J., Fattahi, M. (2013). Radiolytic Corrosion of Grain Boundaries onto the UO_2 TRISO Particle Surface. 1st Annual Workshop Proceedings of the Collaborative Project "FAST/INSTANT release of Safety Relevant Radionuclides from Spent Nuclear Fuel" (7th EC FP CP FIRST-NUCLIDES). 9th-11th October 2012, Budapest, KIT SCIENTIFIC Reports 7639.

Wegen, D.H., González-Robles, E., Puranen, A. (2012). DELIVERABLE (D-N°: 2.1) - Status of fission gas release studies (12 months). FIRST Nuclides (Contract Number: FP7-295722). JRC Scientific and Policy Reports, JRC76116, European Atomic Energy Community, Germany.

Wegen, D.H., Carbol, P., Curtius,H., Vandenborre, J. (2012a). DELIVERABLE (D-N°: 2.2) Status of Rim and Grain Boundary Diffusion Experiments (12 months). JRC Scientific and Policy Reports, JRC77256, European Atomic Energy Community, Germany.

Wegen, D.H., Papaioannou, D., De Weerd, W., Rondinella, V.V., Glatz, J.P. (2013). Fission gas release measurement on one 50.4 GWD/tHM PWR fuel segment. 1st Annual Workshop Proceedings, 7th EC FP – FIRST-Nuclides. 9th–11th October 2012, Budapest, KIT SCIENTIFIC REPORTS 7639.

Wegen, D.H. (2013a). WP2: Gas Release & Rim and Grain Boundary Diffusion. 2nd Annual Workshop, 7th EC FP – FIRST-Nuclides. 5th-7th November, Antwerp, Belgium.

OVERVIEW WP3: DISSOLUTION BASED RELEASE

Karel Lemmens

Belgian Nuclear Research Center, SCK•CEN (BE)

Introduction

The overall objective of WP3 is the quantification of the fast release of radionuclides by means of leach tests with spent nuclear fuel, and – to the extent possible – the determination of their chemical speciation. Such leach tests are performed by INE, PSI, Studsvik, SCK•CEN, ITU and CTM. The experiments are done with PWR fuels having a burnup in the range of 45 to 70 MWd/kg_{HM}, with BWR fuels of 50-60 MWd/kg_{HM}, and a MOX fuel of 63 MWd/kg_{HM} (average burnups).

The radionuclides that are susceptible to fast release are situated in various compartments of the fuels, i.e. in the gap between the fuel and the cladding, in the large fissures, in the grain boundaries, and in the cladding. Hence, the release to be expected in the leach tests depends on the physical preparation of the fuel samples from the fuel rods. The most complete information can be obtained by exposing different fuel compartments to the leachant. The programme therefore foresees tests with cladded fuel segments (segments cut from the fuel rods, a few mm to 2.5 cm long, exposed to the leachant on the top and bottom surface, but radially covered by the cladding), with fuel fragments (not covered by the cladding), and with fuel powder (maximum grain boundary exposure). For some fuels, fragments and powder from the centre and the periphery of the fuel are tested separately. In other leach tests, the cladding is separated from the fuel fragments, and the cladding with the adhering fuel residues is leached together with the fragments. In still other experiments, the cladding with the adhering fuel residues is leached separately (without the fuel fragments). Lastly, the cladding can be leached separately after removal of the fuel residues, to determine the specific release from the cladding.

The radionuclide release measured in the leach tests depends to some extent on the leach test conditions, i.e. the composition of the leachant and the atmosphere. To reduce the related effects and to ease the intercomparison of the results, most tests are done in a harmonized solution of 19 mM NaCl + 1 mM $NaHCO_3$. The atmosphere under which the tests are performed is mostly oxidizing, but the oxidation is limited by closure of the leach vessels. One laboratory uses a reducing atmosphere (argon with hydrogen gas). During the leach test, the composition of the leachant is verified at different time intervals. The last sampling is foreseen 12 months after the start of the experiments, but in some cases (particularly with fuel powder) the sampling will be stopped after 40-60 days.

The exact experimental setup of the leach tests is different for the various laboratories. Some laboratories replace the solution completely at the sampling intervals, other laboratories take only small samples. The equipment and procedures are not standardized.

The radiochemical analyses always include the Cs and I isotopes, which are well known for their fast release and which show a similar behaviour as the fission gasses. Much attention is given also to ^{79}Se and ^{14}C, i.e. isotopes for which the release and speciation is poorly understood. Special efforts are done to lower the detection limit for ^{79}Se. One laboratory plans specific surface analyses to determine the Se distribution on a μm-scale and to determine the oxidation state of the Se in the fuel. Another laboratory foresees specific analytical treatments to distinguish organic from anorganic ^{14}C. Other isotopes are measured as well, e.g. ^{90}Sr and

U isotopes, which allow to estimate the fuel oxidation before and during the leach tests. One laboratory also intends to measure the released gasses (Kr, Xe, H_2, O_2).

As a complement to the leach tests performed on fuel samples under controlled laboratory conditions, the leaching behaviour of damaged and leaking VVER fuels is studied. These fuel rods have been stored since 2003 (damaged fuel) and 2009 (leaking fuel) in pools with a pH 4 and 7, containing 15-21 g/kg boric acid.

Achievements

The first year (2012) has been used to define the detailed experimental matrix and to prepare the leach tests and analytical methods. The sample preparation methods, leachant composition and analytical methods had been discussed between the participating institutes, to come to an optimal program in which the various contributions give complementary information, produced in conditions that are sufficiently harmonized to allow intercomparison. The only laboratory that had already started some of the planned leach tests in 2012 was STUDSVIK.

In the second year (2013), the analytical methods were further developed, the preparations of the leach tests have been continued, most planned experiments have been started, and the first results have become available. Detailed information on the developments in the second year are given in the scientific and technical papers that were prepared for the second annual workshop of FIRST-Nuclides, held in Antwerp (Belgium) on the $5^{th} - 7^{th}$ of November, 2013. A summary of the realisations of each parnter is given hereunder.

SCK•CEN (Mennecart et al., 2013) has started the two planned leach tests (cladded fuel segment and uncladded fuel fragments with cladding) and obtained the first results.

PSI (Curti et al., 2013) has started part of the planned experiments (cladded fuel, segments, fuel fragments, cladding with fuel residues) and plans the remaining tests (cladding without fuel residues) for early 2014. PSI has further used combined X-ray fluorescence (XRF) and X-ray absorption spectroscopy (XAS) on Se doped non-irradiated UO_2 and HBU spent fuel to gain insight into the redox state and the microscopic distribution pattern of selenium in the fuel.

ITU and CTM have started the first leach tests (cladded fuel segments) and obtained the first results. They further have developed a method for the determination and speciation of [79]Se, [126]Sn and [126]Te at trace levels by high resolution ICP-MS coupled to an automated chromatographic system (Serrano-Purroy et al., 2013; Sureda et al., 2013).

KIT (González-Robles et al., 2013) has made further preparations and started the leach leach (cladded and uncladded segments, cladding with residues) in the second semester of 2013.

STUDSVIK (Roth et al., 2013) had started four of the six planned leach tests already in 2012 and has started one more test in 2013. The remaining test will be started in 2014. The first results are available. The radial selenium profile was determined by laser ablation, and the methods for measurement of selenium and carbon-14 in the leaching solutions have been tested.

EK (Slonszki et al., 2013) has determined dissolution rates of different isotopes from damaged and leaking VVER fuel stored in water for several years as planned.

The further planning foresees to continue the leach tests that were started in 2012 and 2013, and to start the few remaining planned tests early 2014. The results will become available gradually, and be integrated in the final report and complementary publications.

References

Mennecart, T., Lemmens, K., Cachoir, C., Adriaensen, L., Dobney, A. (2013). Leaching Tests for the Experimental Determination of Irf Radionuclides from Belgian High-Burnup Spent Nuclear Fuel: Overview of Pre-Test Fuel Characterization, Experimental Set-Up and First Results. Proceedings of the second annual workshop of FIRST-Nuclides. 5th-7th November, Antwerp, Belgium.

Curti, E., Froideval Zumbiehl, A., Günther-Leopold, I., Martin, M., Bullemer, A., Linder, H.P., Borca, C.N., Grolimund, D., Rothe, J., Dardenne, K. (2013). X-Ray Absorption Spectroscopy of Selenium in Non-Irradiated Doped UO_2 and High Burn-Up Spent UO_2 Fuel. Proceedings of the second annual workshop of FIRST-Nuclides. 5th-7th November, Antwerp, Belgium.

Serrano-Purroy, D., Aldave de las Heras, L., Glatz, J.P., Rondinella, V.V., Sureda, R. (2013). WP3. Dissolution Based Release. Proceedings of the second annual workshop of FIRST-Nuclides. 5th-7th October, Antwerp, Belgium.

Sureda, R., De Pablo, J., Clarens, F., Serrano-Purroy, D., Casas, I. (2013). Corrosion Test of Commercial UO_2 BWR Spent Nuclear Fuel for Fast/Instant Release Studies/ First Results for Cladded Segment Samples. Proceedings of the second annual workshop of FIRST-Nuclides. 5th-7th October, Antwerp, Belgium.

González-Robles, E., Bohnert, E., Müller, N., Metz, V., Kienzler, B. (2013). Determination of the Fission Gas Release in the Segment N0204 and Gas Phase Result of Anoxic Leaching Experiment. Proceedings of the second annual workshop of FIRST-Nuclides. 5th-7th November, Antwerp, Belgium.

Roth, O., Puranen, A., Low, J., Granfors, M., Cui, D., Askeljung, C. (2013). Spent Fuel Leaching Experiments and Laser Ablatoin Studies Performed in Studsvik – Status and Preliminary Results. Proceedings of the second annual workshop of FIRST-Nuclides. 5th-7th October, Antwerp, Belgium.

Slonszki, E., Hózer, Z. (2013). Determination of Dissolution Rates for Damaged and Leaking VVER Fuel Stored in Water. Proceedings of the second annual workshop of FIRST-Nuclides. 5th-7th October, Antwerp, Belgium.

OVERVIEW WP4: MODELING

Joan de Pablo

Chemical Engineering Departament, UPC-Barcelona Tech (ES)
Environmental Technology Area, Fundació CTM (ES)

Objectives

The objectives of WP 4 cover initial speciation of fission products in LWR fuel, and multi-scale modelling of the migration / retention processes of fission products in the HBU spent fuel, in the cladding, and the estimation of the fission product total release through the spent fuel rod.

On the other hand, a semi-empirical model will be developed to predict fission product release to water from gap, grain boundaries and grains.

Introduction

In this period, special attention was focused on ^{14}C by KIT, from both thermodynamic calculations and experimental investigation. Speciation of ^{14}C is a key question not yet resolved by theoretical considerations. The formation of oxides or carbides has been discussed in terms of redox state of the High Burn-up Fuel and temperature regime during irradiation.

On the other hand, AMPHOS 21 focused the modelling on how an initially "dry" fracture was invaded by water and the instantaneous radionuclide transfer into the solution upon wetting. This modelling is being combined with the results obtained by UPC-CTM where radionuclide releases are explained taking into account different parts of the fuel: gap, cracks, external or internal grain boundaries, rim structure, and finally grains.

Modeling

1. Radionuclide Characteristics in the Fuel

KIT combined thermodynamic considerations with experimental investigation aiming on the speciation of ^{14}C in the spent nuclear fuel matrix. ^{14}C is a key radionuclide in the safety assessment and in disposal concepts it is assumed, that ^{14}C bearing species are not retained. ^{14}C is an activation product in spent nuclear fuel (SNF) showing low concentrations; its chemical speciation is widely unknown. After formation of ^{14}C by a $^{14}N(n,p)^{14}C$ reaction, the highly exited and charged carbon competes with available reactants within the fuel matrix and will likely form either oxides or in reactions with metals, carbides. In contact with water, these compounds react by forming carbonates or hydrocarbons. The potential for the formation of oxides or carbides is investigated. Free energy of formation for some relevant carbides and oxides are provided. The results of thermodynamic considerations for ^{14}C were compared with experimental gas measurements. According to the initial nitrogen concentration in the fuel between 4 and 11 ppm, the maximal nitrogen content of KIT's fuel rod sample was estimated to be $2.1 \cdot 10^{-4}$ mol. Using the KKG operation characteristics, a formation of $4.3 \cdot 10^{-6}$ mol ^{14}C was expected whereas the measured amount of $^{14}CO_2$ was only $7.2 \cdot 10^{-7}$ mol, corresponding to 17% of the total measured CO_2. However, the speciation of ^{14}C is not yet resolved.

2.   Water saturation of the fuel

Amphos 21 efforts focused on the following issues:

- Improving certain technical aspects of the water saturation model (especially the saturation-retention curve) to improve the numerical performance of the calculation.
- Conceptual linking of the water saturation model with experimental results.
- Developing a simplified preliminary numerical model for linking water saturation with transport.

Fast/instant radionuclide release commonly observed in laboratory experiments could be explained by not only chemical processes (desorption, dissolution), but also by physical processes of saturation with water and solute transport. According to our working hypothesis the characteristic form of the fast/instant (non-gaseous) radionuclide release could be controlled by a combination of the rate at which spent fuel pellet surfaces (and specifically the internal crack surfaces) are contacted by water and by radionuclide transport in the aqueous solution towards the external reservoir (e.g. experimental solution in the laboratory or pore water in the prospective repository). These processes could also be affected by dissolution of the spent fuel surfaces. This hypothesis is supported by similar shapes of radionuclide release versus time curves obtained from laboratory experiments and the curve representing degree of saturation with water of the pellet.

A 1D numerical model was set up and tested. This model couples the previously developed saturation model with diffusive and advective transport of a tracer from a single crack to the outside solution (fully 3D). Several cases were investigated including two bounding variants (instant saturation and "slow" saturation) as well as an in-between case ("fast" saturation). The results indicate that pure diffusive transport of a tracer from the crack is a relatively fast process.

3.   Modeling of radionuclide release to water

UPC-CTM is developing a semi-empirical model is based on the experimental fitting by using three different first-order kinetic equations corresponding to different parts of the fuel as mentioned above.

This model was applied to four cladding segmented fuel sample of different burn-up's, three PWR (48, 52 and 60 MWd/kgU) and one BWR (53 MWd/kgU). The release of Sr, Tc, Cs and U were studied in detail. Results clearly indicated that Sr, Tc and Cs are not congruently dissolved with Uranium. On the other hand, Cs IRF (~8%) determined in 48 BU PWR fuel is high compared to the pessimistic value of 6% compared to literature values. This probably indicates a non-conventional spent fuel. In the case of 60 BU fuel, Cs IRF (in solution) is approximately a third of the total fission gas release (gas). This may be attributed to the lower diffusion of Cs compared to fission gases.

Cs release determined in 53 BU BWR fuel is much lower than estimated for these fuels. Sr and Tc releases are also much lower than those estimated. Two different possibilities could explain this finding, either water has not reached Sr and Tc phases yet, or these phases dissolve slowly.

OVERVIEW WP5: KNOWLEDGE, REPORTING AND TRAINING

Alba Valls

Amphos 21 Consulting S.L. (ES)

Work package 5 (WP5) of the FIRST-Nuclides project is focused on knowledge management and knowledge dissemination, reporting and training. The objectives of this WP are (i) to provide access to all scientific-technical results for all interested parties, (ii) to elaborate a state of the art report on the project and (iii) to organize, within the project, dissemination of the results, training and education for the next generation of spent nuclear fuel specialists.

During the second year of the project several activities have been implemented within WP5, and are described below.

The 2nd Annual **Newsletter** has been produced, which presents a summary of the activities developed during the first half of the project. The document is open to the general public and is available at the project Internet webpage.

July 9th-10th, 2013,

KIT-INE, JRC-ITU and Amphos21 organized a **training course**. The course focused on the radionuclide release from LWR spent nuclear fuel (SNF), experimental methods available to quantify radionuclide release and relevant characteristics of LWR SNF. The course was held in Karlsruhe from 9th to 10th of July 2013. Twelve participants attended the course, from six project partners and three associated groups. After the course closure, the participants were asked for their opinion, and there was a general agreement in the positive value of the initiative, obtaining an average grade of 4.7 over 5.

17 participants from four partner institutions (KIT-INE, JRC-ITU, Studsvik and PSI) have attended at the **Lab-meeting** organized by PSI on March 2013. The aim of the meeting was to serve as a discussion forum for experimentalists of the project to discuss analytical and technical experimental details.

The project has so far allocated resources for three **training mobility measures,** which consider the visit of one student from a participant institution to a different partner organization. This initiative aims at improving the knowledge sharing and taking profit of the synergies that the project can facilitate. Two of the three training mobility have been effective this year: Albert Martínez (PhD student from UPC/CTM) was hosted at KIT-INE for a period of two weeks to improve experimental abilities in working in an inert gas glovebox, gas sampling in a shielded box (gas-MS) or handling of 0.1 wt.% ^{238}Pu doped UO_2(s) pellets, among other technical issues. Péter Szabó (PhD student from EK-MTA) was also at KIT-INE, being trained on sample preparation for ^{14}C analyses (LSC), uranyl solubility analyses, introduction to geochemical modeling, laser fluorescence measurements, and other skills of interest for his scientific development within the project. The last year of the project, David García (PhD student from AMPHOS21) will benefit from a training mobility also at KIT-INE, on development of sorption models.

The planned activities from this work-package for the final project year include:

- publication of the final newsletter
- mobility training of David Garcia (Ph.D student from Amphos21) at KIT-INE on sorption model development
- Preparation of the final update of the State of the Art document

- Preparation of the Final Workshops Proceedings.
- Publication of a half a page notice at the Quarterly, Research Review Policy Focus of the Parliament Magazine, 31st March 2014 Edition

S + T CONTRIBUTIONS

DETERMINATION OF THE FISSION GAS RELEASE IN THE SEGMENT N0204 AND GAS PHASE RESULT OF ANOXIC LEACHING EXPERIMENT

Ernesto González-Robles*, Elke Bohnert, Nikolaus Müller, Michel Herm, Volker Metz, Bernhard Kienzler

Karlsruhe Institute of Technology (KIT), Institute for Nuclear Waste Disposal (INE) (DE)

* Corresponding author: ernesto.gonzalez-robles@kit.edu

Abstract

This paper presents the current status of the experiments performed at INE within the Work-packages 2 and 3 of the EURATOM FP7 Collaborative Project, "Fast / Instant Release of Safety Relevant Radionuclides from Spent Nuclear Fuel (CP FIRST-Nuclides)".

The segment N0204 from the pressure water reactor of Gösgen (KKG) nuclear power plant was selected to carry out this project.

In a first approach and before the performance of leaching experiment, the fission gas release of this segment was determined to be 8.35% (in vol.). Leaching experiment of a cladded fuel pellet in bicarbonate water (19 mM $NaHCO_3$ + 1 mM NaCl) under an Ar and H_2 atmosphere with a total pressure of (40 ± 1) bar (pH_2: 3 ± 1 bar) were started. After a cumulative contact time of 57 days, 4.3% of the Xe and 17% of the Kr inventories of the cladded fuel pellet segment was released into the gas phase.

Introduction

Within the EURATOM FP7 Collaborative Project, "Fast / Instant Release of Safety Relevant Radionuclides from Spent Nuclear Fuel (CP FIRST-Nuclides)" the objective is to have a better comprehension of the IRF, different parameters influence and its evolution as a function of time.

The fast release is due to the segregation of a part of the radionuclide inventory to the gap interface between the cladding and the pellet, the fractures as well as to grain boundaries, especially for the most labile elements. The radionuclides that will be segregated are: fission gases (Kr and Xe), volatiles elements (^{129}I, ^{137}Cs, ^{135}Cs, ^{36}Cl and ^{79}Se) and segregated metals (^{99}Tc, ^{107}Pd and ^{126}Sn) (Johnson et al., 2005; Poinssot et al., 2005). The degree of segregation of the various radionuclide is highly dependent on in-reactor fuel operating parameters such as linear power rating, fuel temperature, burn-up, ramping processes, and interim storage time. In the case of the fission gases, the gas release occurs by diffusion to grain boundaries, grain growth accompanied by grain boundary sweeping, gas bubble interlinkage and intersection of gas bubbles by cracks in the fuel (Johnson and Shoesmith, 1988).

The aim of the experiments is the quantification of instant release from irradiated high burn-up UO_2 during leaching of fuel pellets under anoxic condition. As a first step, emphasis is given to the release of fission gases during the leaching experiments.

Furthermore, a complete description of the leaching experiments under anoxic conditions that are being performed is giving. Finally, the first results obtained related to gas phase analysis are also reported.

Spent nuclear fuel

The fuel rod segment was irradiated in a pressure water reactor placed at Gösgen (KKG) nuclear power plant in Switzerland. The irradiation was carried out in 4 cycles for a period of time of 1226 days with an average linear power of 260 W/cm and achieving an average burn-up of 50.4 GWd/t$_{HM}$. The fuel rod segment was unloaded the 27th May 1989 that implies a cooling time of 24 years before characterisation and cutting of the segment.

Characteristic data of the studied segment N0204 of the KKG-BS fuel rod SBS1108 are given in Metz et al. (2012). The inventory of the SNF was calculated with the ORIGEN code. The results regarding Xe and Kr are summarised in Table 1.

Table 1: *Theoretical inventory (µg/g$_{UO2}$) determined by ORIGEN code.*

Kr	µg/g$_{UO2}$	Xe	µg/g$_{UO2}$
^{80}Kr	$3.4 \cdot 10^{-4}$	^{128}Xe	$3.8 \cdot 0^{0}$
^{82}Kr	$9.7 \cdot 10^{-1}$	^{129}Xe	$4.3 \cdot 10^{-2}$
^{83}Kr	$4.8 \cdot 10^{1}$	^{130}Xe	$1.1 \cdot 10^{1}$
^{84}Kr	$1.4 \cdot 10^{2}$	^{131}Xe	$4.0 \cdot 10^{2}$
^{85}Kr	7.0	^{132}Xe	$1.4 \cdot 10^{3}$
^{86}Kr	$2.4 \cdot 10^{2}$	^{134}Xe	$2.0 \cdot 10^{3}$
		^{136}Xe	$3.1 \cdot 10^{3}$
Total	$4.3 \cdot 10^{2}$	**Total**	$6.9 \cdot 10^{3}$

Determination of the fission gas release

The plenum of segment N0204 was punctured at ITU and gas samples were collected and analysed at INE. A scheme of the puncturing device placed at ITU is shown in Figure 1.

In the previous contribution the results regarding the gas phase were presented but at that moment the FGR was still no determined. Finally, in this work the results of the FGR (Xe + Kr) are given.
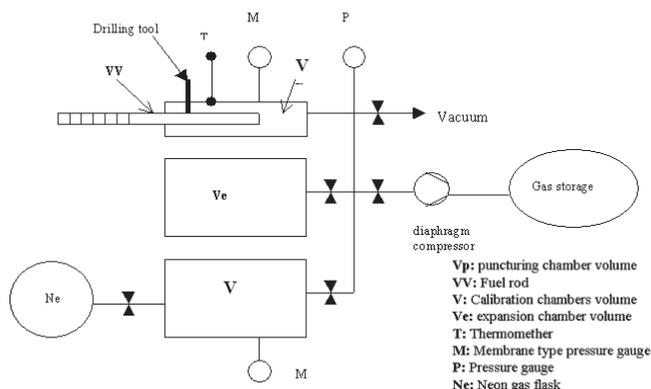
Figure 1: Scheme of the puncturing device (from Wegen et al., 2012a).

Sample preparation for leaching experiments

From the fuel rod a cladded fuel pellet was cut. The procedure was carried out using a cutting machine equipped with a diamond wafering blade (Buehler Isomet ® series 15HC). The dry cutting was performed slowly without any cooling liquid and under N_2 atmosphere. To obtain complete pellet sample, the cut was performed between the axial gap pellets taking into account the γ-scan as reference. The complete description of the process is explained elsewhere (Wegen et al., 2012b).

In Figure 2, the cladded fuel pellet selected to perform the leaching experiments under anoxic conditions is shown.
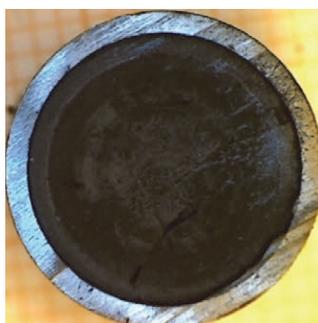
Figure 2: Cross section of the selected cladded fuel sample.

The sample was weighed and measured (length and diameter). Its characteristics are given in Table 2.

Table 2: Characteristic of the cladded fuel pellet.

Parameter	Value
External diameter (mm)	10.75 ± 0.01
Internal diameter (mm)	9.35 ± 0.01
Length (mm)	9.85 ± 0.01
Weight (g)	7.77 ± 0.01
Weight of fuel (g)	6.97 ± 0.01

Experimental set-up of leaching experiments

A static experiment is being performed in 250 ml stainless steel Ti-lined VA autoclaves (Berghof Company, Eningen, Germany) with 2 valves in the lid to allow solution and gas sampling.

The experiment is being carried out under anoxic conditions in Ar and H_2 atmosphere of a total pressure of (40 ± 1) bar ($pH_2=3 \pm 0.5$ bar).

To ensure that both sides of the cladded pellet sample are in contact with the solution, the sample was mounted in special Ti sample holder, see Figure 2.
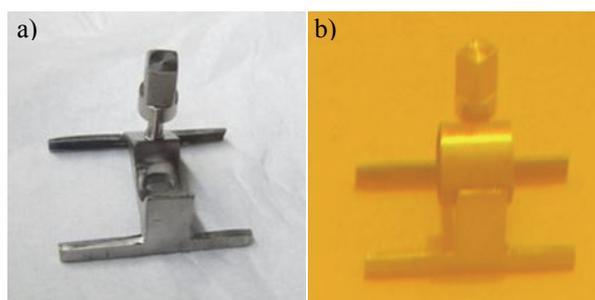

Figure 2: a) sample holder used during the experiment; b) sample holder mounted with pellet before immersion into the solution.

The holder with the sample was placed in the autoclave. The autoclave was closed and fluxed with Ar to avoid the possible presence of air. Afterwards, the autoclave was filled with 220 ml of bicarbonate water (19 mM NaCl + 1 mM NaHCO$_3$), the addition was performed using syringes filled with (50 ± 1) mL of solution and under constant Ar flux into the autoclave to avoid air intrusion.

After one day the solution was completely renewed and a gas sample was collected, it is the so-called wash cycle. Then the autoclave was refilled with 220 ml of bicarbonate solution in the same way as previously explained. Thereafter, gas (50 ± 1) mL and liquids (15 ± 1) mL samples were taken at 1, 7, 21 and 56 days. After the sampling, the remaining gas was purged with Ar, and the initial conditions (40 bar of Ar and H_2 mixture) were again established. On the contrary, the solution was not renewed to replace the amount extracted during sampling.

Leachant composition

The leachant was prepared in a glove-box under Ar atmosphere. The composition according to the agreement within CP FIRST-Nuclides is 19 mM NaCl + 1 mM NaHCO$_3$ with a pH of (8.9 ± 0.2). The Eh (vs SHE) of (-116 ± 50) mV was measured.

Liquid and gas analyses of radionuclides

After each sampling, gas and liquids samples were recovered. Presently, the analysis of the liquids samples is not yet completed.

The gas samples, both for the determination of the FGR as well as those from leaching experiments, were collected in stainless steel single-ended miniature sampling cylinders (SS-4CS-TW-50, Swagelok Company, USA). These gas sampling cylinders are characterised by a volume of (50 ± 2.5) ml, a length of

(159 ± 1.00) mm, an outer diameter for tube fitting of (9.5 ± 0.1) mm and an inner diameter for tube socket weld connection of (6.4 ± 0.1) mm. The volume of the tubes is known; therefore, the moles of gas released could be calculated.

The gas MS (GAM400, In Process Instruments, Bremen, Germany) was equipped with a Faraday and SEV detector and a batch inlet system. The batch-type gas inlet system was optimised for low gas sample consumption. Within the gas dosage and inlet system, the total gas pressure was controlled at four successive positions. It applied three different expansion-volumes to charge relatively low gas contents in the desired pressure range. Ten scans of each gas sample were measured, using the SEV-detector, and the mean value was taken. Calibration of the gas MS analysis was performed in the same pressure range as the respective range for analyses of the sample aliquots.

Results

Fission gas release

The fission gas release (FGR) fraction was calculated from the experimentally determined amount of Xe and Kr extracted from the segment and, the calculated total inventory of fission gases generated in the fuel rod segment over the irradiation time.

The total fission gas inventory was calculated using the ORIGEN code. The result of the fission gas analyses is given in Table 3.

Table 3: *Determination of the fission gases (Xe and Kr) released into the plenum at 24 years (Puncture Test).*

Fission gas release (at 0 °C, 1 bar) (%)	Kr 7.03	Xe 8.48	Kr+Xe 8.35			
Isotopic composition of Kr (% in vol)	^{80}Kr 0.007	^{82}Kr 0.04	^{83}Kr 7.33	^{84}Kr 36.67	^{85}Kr 1.33	^{86}Kr 53.33
Isotopic composition of Xe (% in vol.)	^{128}Xe 0.004	^{129}Xe 0.01	^{130}Xe 0.31	^{131}Xe 3.82	^{132}Xe 25.37	^{134}Xe 28.20	^{136}Xe 42.30
Released volume (at 0 °C, 1 bar) (cm³)	Kr 2.12	Xe 26.09				

Gas phase in leaching experiments

The number of moles released into the gas phase for each contact period was measured and determined. The results, concerning Kr and Xe, are given as cumulative fraction of the inventory released into the gas phase and as fractional release rate.

The fraction of inventory released into the gas phase for an element *i* (*FIG$_i$*) is defined by Equation 1:

$$FIG_i = \frac{m_i}{m_{UO_2} x H_i} \qquad\qquad (1)$$

where m_i, is the mass of element (g)*i* in the gas phase, m_{UO2} is the initial oxide mass (g) in the fuel sample and H_i corresponds to the fraction of inventory for the element *i* (g$_i$/g$_{UO2}$).

The cumulative fraction of the inventory released into the gas phase, FIG_c, is then calculated as the sum of the release for each contact period as described in Equation 2:

$$FIG_C = \sum FIG_i \tag{2}$$

Finally, the fractional release rate for an element I, FRR$_i$) in each contact period as indicate in Equation 3:

$$FRR_i = \frac{FIG_i}{t} \tag{3}$$

where t is the contact time (d).

The cumulative release fraction of Kr and Xe as a function of the cumulative contact time are plotted in Figure 3. It can be observed that the fraction of the inventory released into the gas phase for Kr is much higher than for Xe.

In the initial wash cycle, the fraction released was $(1.6 \pm 0.2) \cdot 10^{-2}$ for Kr and $(9.6 \pm 1.0) \cdot 10^{-4}$ for Xe. After 57 days of cumulative contact, the fraction of the inventory released in the gas phase was $(1.7 \pm 0.2) \cdot 10^{-1}$ for Kr and $(4.3 \pm 0.4) \cdot 10^{-2}$ for Xe. Therefore, a 17% of Kr and a 4.3% of Xe inventories of the cladded fuel pellet was released during the first 57 days of the leaching experiment.
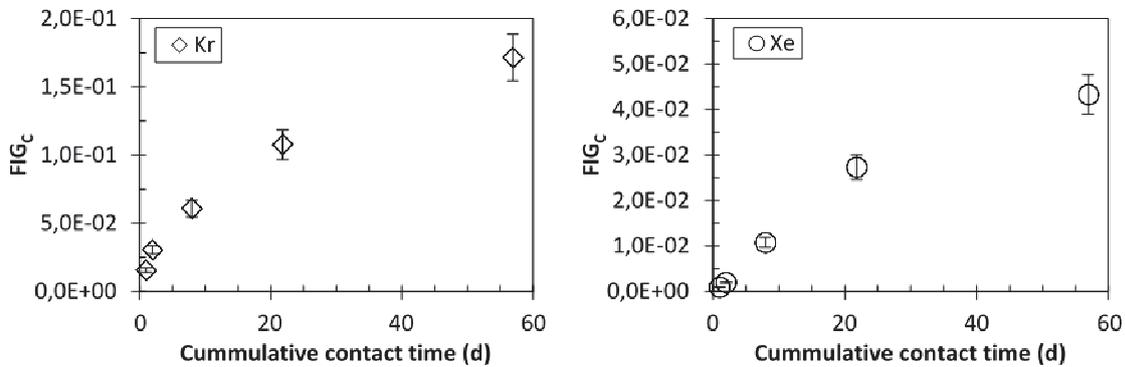

Figure 3: Cumulative release fraction of Kr (left side) and Xe (right side) as function of the cumulative contact time.

The fractional release rate of Kr and Xe as function of the contact time is plotted in Figure 4. It can be noted that after constant initial high fractional release rate of Kr $(1.7 \pm 0.2) \cdot 10^{-2}$ d^{-1}, the fractional release rate decreases one order of magnitude achieving a value of $(1.6 \pm 0.2) \cdot 10^{-3}$ d^{-1}. On the other hand, the fractional release rate of Xe seems to be constant during the first 4 contact period. Afterwards, the fractional release rate drops reaching a value, after cumulative contact time of 57 days, of $(3.9 \pm 0.2) \cdot 10^{-4}$ d^{-1}.
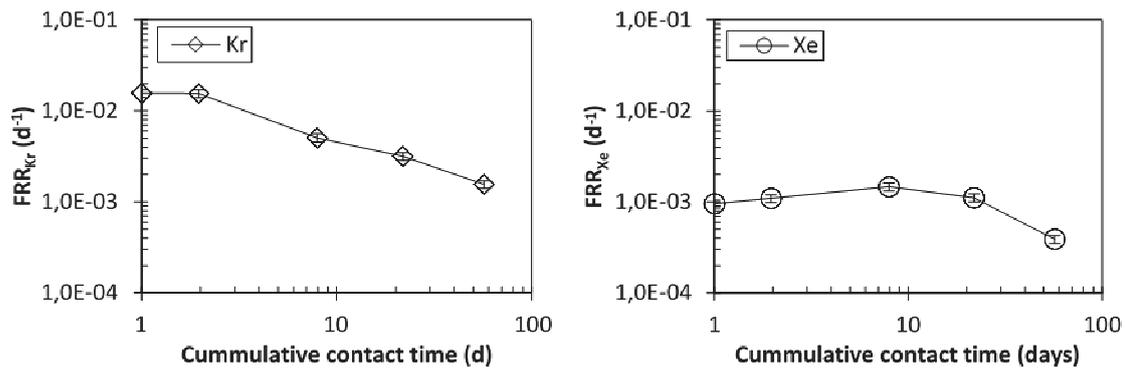
Figure 4: *Fractional release rate of Kr (left side) and Xe (right side) as function of the cumulative contact time.*

Conclusions and Future work

The FGR (Xe + Kr) from the studied Gösgen fuel rod segment N0204 was successfully determined to be 8.35%.

The first leaching experiments under anoxic conditions were started and gaseous and liquid sampling were carried out over a period of 2 months. The results of the gas phase were obtained giving a fraction of the inventory released after a cumulative contact time of 57 days of 4.3% for Xe and 17% for Kr.

The analyses of the liquid samples will be completed, soon. The experiment is still on going, hence, more gaseous and liquid samples will be taken and the results will be presented.

Acknowledgement

References

Johnson, L., Ferry, C., Poinssot, C., Lovera, P. (2005). Spent Fuel Source-Term Model for Assessing Spent Fuel Performance in Geological Disposal. Part I: Assesment of the Instant Release Fraction. Journal of Nuclear Materials, 346, 56-65.

Johnson, L., Shoesmith, D.W. (1988). Spent Fuel in Radioactive Waste Forms for the Future. W. Lutze and R.C. Ewing, Eds., North-Holland, Amsterdam, 635-698.

Metz, V., Loida, A., González-Robles, E., Bohnert, E., Kienzler, B. (2012). Characterization of Irradiated PWR UOX Fuel (50.4GWd/tHM) Used for Leaching Experiments. 1st Annual Workshop Proceedings of the Collaborative Project "Fast/Instant Release of Safety Relevant Radionuclides from Spent Nuclear Fuel" (7th EC FP CP FIRST-Nuclides). KIT Scientific Reports 7639, 117-124.

Poinssot, C., Ferry, C., Lovera, P., Jegou, C., Gras, J.-M. (2005). Spent Fuel Radionuclide Source Term Model for Assessing Spent Fuel Performance in Geological Disposal. Part II: Matrix Alteration Model and Global Performance. Journal of Nuclear Materials, 346, 66-77.

Wegen, D.H., Papaioannou, D., de Weerd, W., Rondinella, V.V., Glatz, J.P. (2012a). Fission Gas Release Measurement on 50.4 GWd/tHM PWR Fuel. 1st Annual Workshop Proceedings of the Collaborative Project "Fast/Instant Release of Safety Relevant Radionuclides from Spent Nuclear Fuel" (7th EC FP CP FIRST-Nuclides). KIT Scientific Reports 7639, 201-205.

Wegen, D.H., Papaioannou, D., Gretter, R., Nasyrow, R., Rondinella, V.V., Glatz, J.P. (2012b). Preparation of Samples for IRF Investigation and Post Irradiation Examinations from 50.4 GWd/tHM PWR Fuel. 1st Annual Workshop Proceedings of the Collaborative Project "Fast/Instant Release of Safety Relevant Radionuclides from Spent Nuclear Fuel" (7th EC FP CP FIRST-Nuclides). KIT Scientific Reports 7639, 193-199.

HERMODYNAMIC CONSIDERATIONS ON THE SPECIATION OF ^{14}C IN SPENT NUCLEAR FUEL

Bernhard Kienzler[*], Elke Bohnert, Ernesto González-Robles, Michel Herm,
Xavier Gaona, Christoph Borkel

Karlsruhe Institute of Technology (KIT), Institute for Nuclear Waste Disposal (INE) (DE)

* Corresponding author: bernhard.kienzler@kit.edu

Abstract

^{14}C is a key radionuclide in the safety assessment of a geological disposal for nuclear waste. For most disposal concepts it is assumed, that ^{14}C bearing species are not retained in the geological or geo-technical barriers. ^{14}C is found as an activation product in spent nuclear fuel (SNF) at low concentrations. For evaluation of ^{14}C retention, information of its chemical speciation is indispensable. Therefore thermodynamic properties of possible phases containing ^{14}C are discussed in the following. After formation of ^{14}C by a ^{14}N(n,p)^{14}C reaction, the highly exited and charged carbon competes with available reactants within the fuel matrix and will likely form either oxides or, in reactions with metals, carbides. In contact with water, these compounds react by forming carbonates or hydrocarbons. The potential for the formation of oxides or carbides is investigated in this contribution.

Introduction

^{14}C in high burn-up UO_2 fuel may be formed by different processes (Table 1) (Magnusson, 2007):

Table 1: Neutron reactions relevant for ^{14}C formation (data taken from www.nuclides.net).

Reaction	Abundance of the mother isotope	Thermal cross section [barn]	Cross section resonance [barn]
^{17}O(n,α)^{14}C	0.038%	0.235	0.106
^{14}N(n,p)^{14}C	99.6%	1.821	0.818
^{13}C(n,γ)^{14}C	1.1%	$1.4 \cdot 10^{-3}$	$5.9 \cdot 10^{-4}$
ternary fission	The yield of ^{14}C was measured to be 0.1 to 1% of the yield of ^{4}He by ternary fission which is $4 \cdot 10^{-3}$% per binary fission reaction (Theobald, Heeg et al. 1989).		
	Neeb (Neeb 1997) reports yields of $1.7 \cdot 10^{-4}$% per thermal ^{235}U fission and $1.8 \cdot 10^{-4}$% per thermal ^{239}Pu fission.		

The concentration of carbon in nuclear fuel was found to be between 4 to 12 ppm (Saiger, 1979). The nitrogen concentration was measured to be in the range of 4 to 11 ppm (Saiger, 1979). A recent Japanese study reports a nitrogen impurity of 10 ppm in the fuel (Sakuragi et al., 2013). The total number of activated atoms depends on the neutron flux and can be calculated by the build-up function (Equation 1) (Loveland et al., 2005).

$$\frac{N}{N_0} = \sigma \cdot \frac{flux}{\lambda} \cdot \left(1 - e^{-\lambda \cdot t}\right) \tag{1}$$

N: ^{14}C atoms at time t;   N$_0$: number of mother atoms in the fuel

σ: cross section [barn] f   lux: neutron flux [s$^{-1} \cdot$cm^{-2}]

λ: decay constant of ^{14}C [s^{-1}]   t: time [s]

Conditions for ^{14}C formation in the KIT fuel sample

For the KIT fuel sample (assembly ID N0206, rod ID SBS1108) which was irradiated for 1,226 days in the Gösgen Pressurized Water Reactor (KKG) with a burn-up of 50.4 GWd/t$_{HM}$, a fast neutron fluence [1] of $9.8 \cdot 10^{21}$ cm^{-2} is reported in the energy range E > 0.82 MeV (Stratton et al., 1991). Using the data of Table 1 in Equation 1 the relation of the ^{14}C formation by thermal and resonance (n,p) reactions can be compared. According to Figure 1, the resonances of the (n,p) reaction cross section occurs in the neutron energy range between $5 \cdot 10^5$ and $1 \cdot 10^7$ eV, corresponding to the range of intermediate to fast neutrons. Assuming constant operating conditions of KKG, the flux of the KIT fuel sample is calculated from the fluence in the range of $9.3 \cdot 10^{13}$ cm$^{-2} \cdot$s^{-1}.
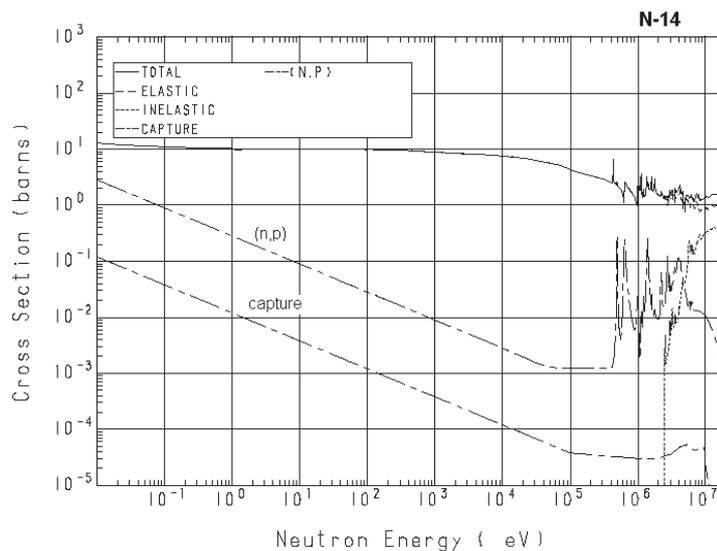

Figure 1: *Point-wise cross-sections from JENDL-3.2 (taken from www.nuclides.net).*

Based on an effective energy release of 205.4 MeV per fission, the f̲issions per i̲nitial m̲etal a̲tom (FIMA in %) is obtained by dividing the burn-up (GWd/t$_{HM}$) by the conversion factor 9.60 (see Kienzler et al., 2013 p. 103). The total number of ternary fissions forming ^{14}C in the KIT fuel sample results an activity of 800 Bq/g.

---

[1] Neutron **flux** (cm$^{-2} \cdot$s^{-1}) is the quantity corresponding to the total length travelled by all neutrons per unit time and volume, nearly equivalent to the number of neutrons travelling through the unit area in unit time. The neutron **fluence** (cm^{-2}) is defined as the neutron flux integrated over a certain time period.

Using the thermal and resonance integral cross section values and an initial concentration of 11 ppm nitrogen impurity in the fuel, an activity of 27,200 Bq ^{14}C/g fuel for the KIT SNF sample is obtained. Measurements for low burn-up spent nuclear fuel revealed 7,000 Bq/g for a 22.4 GWd/t$_{HM}$ BWR fuel and 9,300 Bq/g PWR fuel having a burn-up of 30 GWd/t$_{HM}$ (Bleier et al., 1987).

Formation of ^{14}C compounds

The activities calculated above can be expressed in molar units: ^{14}C concentration in KIT's SNF sample is ~0.016 mol/t$_{HM}$ which is in the range of the molar ^{234}U concentration. This small quantity of ^{14}C is surrounded by a huge concentration of fission products, actinides and oxygen. Table 2 shows some example concentrations.

Table 2: Calculated concentrations of some important elements in the KIT SNF sample.

Element	Concentration [mol/t$_{HM}$]
^{14}C	0.016
Se	0.91
Y	7.4
Sr	14.1
Nb	0.5
Zr	55.2
Mo	48.9
Cs	30.5
Ba	15.7
REE	100.0
Actinides (without U)	52.5
Oxygen	8403

Table 2 shows an excess of about 500,000 oxygen atoms in comparison to ^{14}C atoms. For this reason, after the formation of ^{14}C by the (n,p) reaction, the emission of a proton and the resulting disturbance of the electron shells, the carbon may react with oxygen and a variety of mono-, di-, and trivalent elements. Most probably, the reactions take place directly after the formation of ^{14}C at temperatures in the center of the fuel rod in the range between 1,000 and 1,200°C and about 500°C close to the cladding. If ^{14}C reacts with metallic elements, such as fission products, U, or Pu, carbides may be formed, reactions with oxygen result in ^{14}CO or ^{14}CO$_2$. These types of compounds are discussed in the following sections.

Carbides

Hardfacing alloys such as drill bits achieve their properties by deposit welding. The amount (volume) of the carbides formed and their structure, composition and degree of homogeneity determine the nature of the strengthening of the weld metal and thus its service characteristics. For this reason several data collections and reviews of thermodynamic data have been published (Wicks and Block, 1961; Shatynski, 1979; Iwai et al., 1986; Farkas et al., 1996; Mazurovsky et al., 2004). Carbides of the most abundant additives and fission products in SNF which are of interest for this study are listed in Table 3 with the corresponding functions for calculating their Gibbs free energy of formation ΔG_f^0.

Table 3: *Free energy of formation for some relevant carbides of elements present in the SNF (Shatynski, 1979). Data for Zr, Th, and U (Wicks and Block, 1961).*

Element	Compound	Free Energy of Formation [cal/mol]	T [K]
Fe	$3Fe + C \rightarrow Fe_3C$	$\Delta G_f = +4530 - 5.43T \times \ln T + 1.16 \times 10^{-3}T^2 - 0.40 \times 10^5 T^{-1} + 31.98T$	298 – 463
		$\Delta G_f = +3850 - 11.41T \times \ln T + 9.66 \times 10^{-3}T^2 - 0.40 \times 10^5 T^{-1} + 66.2T$	463 – 1033
		$\Delta G_f = +13130 + 9.68 \times \ln T - 0.99 \times 10^{-3}T^2 - 1.05 \times 10^5 T^{-1} - 78.14T$	1033 – 1179
		$\Delta G_f = -1000 - 7.0T \times \ln T + 3.5 \times 10^{-3}T^2 - 1.05 \times 10^5 T^{-1} + 46.45T$	1179 – 1500
Cr	$\frac{7}{23}Cr_{23}C_6$	$\Delta G_f = -29985 - 7.41 \times T$	1100 – 1720
Nb	$Nb + C \rightarrow NbC$	$\Delta G_f = -31100 + 0.4 \times T$	1180 – 1370
	$2Nb + C \rightarrow Nb_2C$	$\Delta G_f = -46000 + 1.00 \times T$	1180 – 1370
Mo	$2Mo + C \rightarrow Mo_2C$	$\Delta G_f = -12030 - 1.44 \times T$	600 – 900
		$\Delta G_f = -11710 - 1.83 \times T$	1200 – 1340
Ni	$3Ni + C \rightarrow Ni_3C$	$\Delta G_f = +8110 - 1.70 \times T$	298 – 1000
Zr	$Zr + C \rightarrow ZrC$	$\Delta G_f = -44100 + 2.2 \times T$	298 – 2220
Th	ThC_2	$\Delta G_f = -50000$	298
U	UC	$\Delta G_f = -43600$	298
	U_2C_3	$\Delta G_f = -78400$	298
	UC_2	$\Delta G_f = -37500$	298

According to Table 3, zirconium carbide (ZrC) may be formed. In industry, ZrC is used as a refractory metal in sub-stoichiometry. At carbon contents higher than approximately $ZrC_{0.98}$ the material contains free carbon. Stability range of ZrC covers carbon to metal ratios ranging from 0.65 to 0.98 (Baker et al., 1969). It has a cubic crystal structure and is highly corrosion resistant.

Oxides

The burn-up of UO_2 and PuO_2 releases oxygen and the fission products (FP's) may not combine with all of the oxygen liberated. To estimate the partial molal free energy of oxygen (ΔG_{O_2}) in the solid per mole of O_2 (oxygen potential) the following information is required (Olander, 1976):

- Quantification of U and Pu decrease and increase in oxygen binding FP's.
- Chemical and physical state of the FP's.
- Redistribution of O_2 and FP's in the fuel.
- Thermochemistry of solid-gas phase.
- Effect of cladding by forming oxidized layers on the Zircaloy.

Oxygen can exist in the fuel in both forms bonded to actinides or FPs. The charge balance is maintained by reduction of U or Pu as well as by the formation of different Mo phases. Olander's way (Olander, 1976) of calculating the oxygen deficit/excess is applied to the KIT fuel sample using the concentrations of the FP's shown in Table 2. A slight deficit of 26.6 mol O_2 per t_{UO_2} is calculated in the case that Mo exists in the form of MoO_2. Olander's equation is used for estimating the ratio of Mo in the metallic form.

$$y_{Mo} = \frac{(1-f_{Mo}) \cdot N_{Mo}}{N_{Ru} + N_{Rh} + N_{Pd} + N_{Tc} + (1-f_{Mo}) \cdot N_{Mo}} \tag{2}$$

f_{Mo}: partitioning of molybdenum between the fuel matrix and the metallic inclusions; N_{xx}: number of noble metal atoms in the fuel

According to Olander, f_{Mo} is close to zero for UO_2 fuel of ~50 GWd/t burn-up and temperatures during irradiation below 2,000 K. Using the calculated element concentrations of KIT's fuel, about 58% of Mo is in the metallic form. This number results in a deficit of 6.5 mol O_2/t_{UO_2}. An effect of the cladding which may increase the deficit was not considered. However, these relationships are not affected by the time of storage (26 years) since discharge of the KIT fuel sample.

For any particular oxidisable element a value of oxygen potential for the oxidation reaction exists. In a system with higher oxygen potential a metal will be oxidised, but below no oxidation will take place. Thermodynamic calculations over a wide range of temperatures are generally made with algebraic equations representing the characteristic properties of the substances being considered. The following equations for temperature extrapolations of the free energy of formation ΔG_f as well as the fitting parameters are taken from Glassner's report (Glassner, 1957).

For the reaction

$$M + nX_2 \rightarrow MX_{2n} \tag{3}$$

the free energy of formation is calculated by $\qquad\qquad$ (4)

$$\Delta G_f(T) - \Delta H_{f,298}$$

$$= -(2.303\Delta a)T \cdot logT - \frac{1}{2}(\Delta b \cdot 10^{-3})T^2 - \frac{1}{6}(\Delta c \cdot 10^{-6})T^3 - \frac{\frac{1}{2}(\Delta d \cdot 10^5)}{T} - T\Delta(B-a)$$
$$- \Delta A$$

with

$$\Delta h = h(MX_{2n}) - h(M) - n \cdot h(X_2)$$

$\Delta H_{f,298}$: enthalpy of formation at 298 K.
$\Delta G_{f,(T)}$: free energy of formation at given temperature T.
h: incorporates fit data a, b, c, d, (B−a) and A.

The data for oxides are listed in (Glassner 1957). The data are used in metallurgy as the addition of carbon or CO gas is a measure to prevent elements from being oxidized. Nickel, for example, will undergo oxidation to nickel oxide (NiO) in an atmosphere with an oxygen potential greater than −60 kcal/mol at 1,000 °C, or −81 kcal/mol at 500 °C. Chromium has a greater affinity for oxygen than nickel. It would require an oxygen potential of less than −130 kcal/mol at 1,000 °C to prevent oxidation. Thus an atmosphere which is just adequate to prevent nickel from being oxidised, would not protect chromium from oxidation. In many cases, the

chemical stability of compounds decreases with increasing temperature. The calculations enable the level of oxygen potential to be determined for a variety of conditions.

To estimate which oxidation reactions are favoured at different conditions, the oxygen potentials or ΔG values for some oxides of FP's and carbon have been calculated as function of the temperature (Figure 2) using the data of Glassner (Glassner, 1957). Similar figures are shown in many text books (e.g. Olander, 1976), but without considering the minor activation product carbon. Most elements of interest such as Ba, Sr, U, Pu and REE have significantly lower ΔG_f values to form oxides than the oxidation reactions of carbon. The only elements which may compete for oxygen with carbon are Cs and Mo in a small area between 850 K and 1,100 K where ΔG_f of the carbon oxides are below the $\Delta G_f(MoO_2)$. Under these conditions, CO or CO_2 could be formed. Mo data are available up to 1,100 K, only.

As the Glassner data are relatively old, other data bases have been tested, such as the GEMS-specific HERACLES database (Kulik et al., 2013) and Thermo-Calc. Thermo-Calc is a software for thermodynamic calculations on multi-component systems at high temperatures. Databases exist for cemented carbides, solid oxide fuels, etc. Unfortunately Thermo-Calc requires a full license which is not available at KIT, presently.
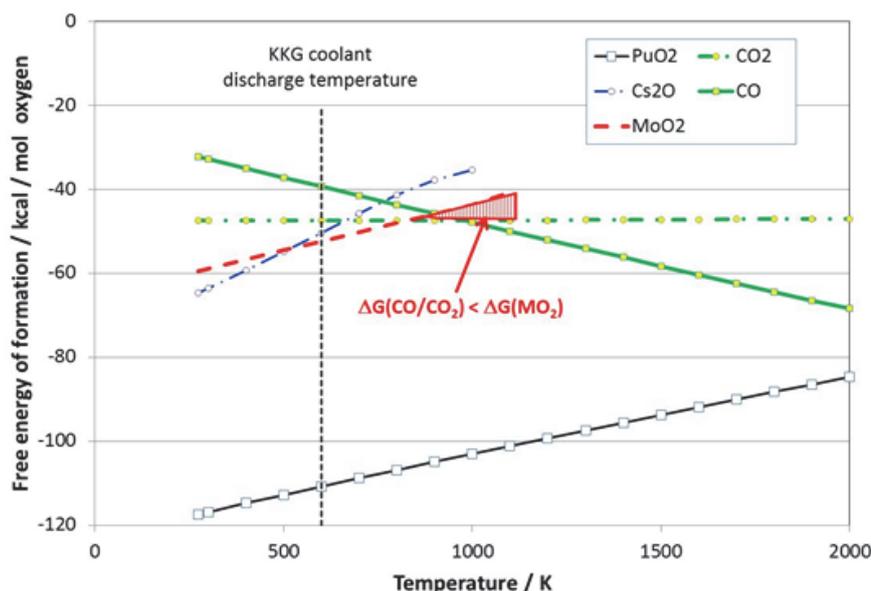

Figure 2: Free energy of formation for carbon oxides, Cs$_2$O, MoO$_2$ and PuO$_2$. The vertical dashed line indicates approximately the surface temperature of the cladding, the red triangle shows the temperature region where ΔG$_f$ of the carbon oxides are below those of MoO$_2$.

Experimental: Gas analyses

In the chapter "Fission Gas Measurements and Description of Leaching Experiments with of KIT's Irradiated PWR Fuel ROD Segment (50.4 GWD/THM)" (p. 61 in Kienzler et al., 2013), a CO_2 concentration of 0.13 vol.% in the gas phase of the fuel rod segment was found, corresponding to 0.016 cm^3. This CO_2 volume corresponds to $7.2 \cdot 10^{-7}$ mol. Figure 3 shows the signals of the quadrupole gas mass spectrometer (GAM400, In Process Instruments) of $^{12}CO_2$, $^{13}CO_2$ and $^{14}CO_2$ in the gas, sampled from the plenum of KIT's SNF rod. Preliminary estimations of the intensities between the measured $^{12}CO_2$ (AMU = 44) to $^{13}CO_2$ (AMU = 45) and to $^{14}CO_2$ (AMU = 46) signals were found to be $1 \cdot 10^{-11}$ and $4.6 \cdot 10^{-13}$ to $1.6 \cdot 10^{-13}$ respectively. This relation allows

the statement, that about 1% of the total CO_2 can be attributed either to $^{14}CO_2$ or to $^{12}C^{18}O^{16}O$. It can be assumed that the concentration of the compound $^{12}C^{18}O^{16}O$ corresponds to the natural abundance of ^{18}O which is about 0.205% of the total oxygen. For this reason, the level of the ^{18}O compound is expected by a factor of 5 below the measured concentration for AMU = 46.
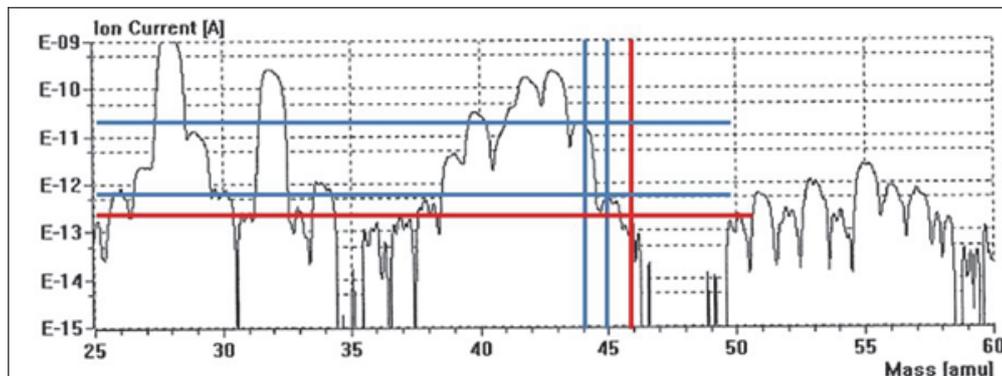

Figure 3: Measured $^{12}CO_2$ (blue), $^{13}CO_2$ (blue), and $^{14}CO_2$ (red) signals in the gas sampled from the plenum of KIT's SNF rod (analysed with a quadrupole gas mass spectrometer (GAM400, In Process Instruments).

The fuel mass of KIT's SNF rod segment is 265.7 g. According to the initial nitrogen concentration in the range between 4 and 11 ppm, a maximal amount of $2.4 \cdot 10^{-4}$ mol nitrogen was present in KIT's rod segment. The total mass of ^{14}C expected from using equation 1 would be in the range of $4.3 \cdot 10^{-6}$ mol (see Table 2), a value which is by a factor of 6 above the measured total CO_2 in the gas phase ($7.2 \cdot 10^{-7}$ mol). The $^{14}CO_2$ concentration is by a factor of 100 below the total CO_2. The comparison of these values indicates, that only a minor part of carbon is released as CO_2 into the plenum. No distinction can be made between CO and N_2 species because of the same masses. Nitrogen detected in the gas phase of the rod segment results from remaining air contamination in the sampling system during the fuel rod puncturing. Formation of N_2O is not expected after the irradiation phase.

Formation of Se compounds

Selenium, especially the isotope ^{79}Se is also considered to be dose relevant and to be rapidly released from SNF. For this reason, potential reaction of Se with oxygen, FPs and actinides under the high temperature conditions are of high interest. According to Table 2, the Se concentration in KIT's fuel rod segment is 0.93 mol/t_{HM}. Using eq. 4 and the data for the formation of SeO_2 given by Glassner (Glassner, 1957), a range $-14.2 \leq \Delta G_f(SeO_2) \leq +2.7$ kcal/mol is calculated for the temperature range from 298 to 2,000 K. This $\Delta G_f(SeO_2)$ value indicates that SeO_2 is not formed. The $\Delta G_f(SeO_2)$ value is significantly above the $\Delta G_f(Cs_2O)$ value (see Figure 2). ΔG_f values for other redox states (Se^{-II}, Se^0 and Se^{+VI}) for the relevant temperature ranges are not available, presently.

Discussion

The results of thermodynamic considerations for ^{14}C were compared with experimental findings. According to the initial nitrogen concentration in the fuel between 4 and 11 ppm, the maximal nitrogen content of KIT's fuel rod sample was estimated to be $2.1 \cdot 10^{-4}$ mol. Using Equation 1 and the KKG operation characteristics, a formation of $4.3 \cdot 10^{-6}$ mol ^{14}C is expected whereas the measured amount of $^{14}CO_2$ was $7.2 \cdot 10^{-7}$ mol. This $^{14}CO_2$

amount corresponds to 16.7% of the total measured CO_2. However, the measurement of the isotopic composition of the gas phase is still pending.

The question as to which compound (oxide or carbide) ^{14}C exists depends strongly on the redox state of the high burn-up fuel and the temperature regime during the irradiation. In the case of an O_2 deficite in the SNF, [14]CO/[14]CO$_2$ can only be formed, if the free energy of formation for these compounds is below the ΔG values of other FP's. For the fuel used in KKG, the average coolant temperature was 305°C/578 K (max. discharge temperature 325°C/598 K). In the small range between 850 and 1,100 K carbon oxides have lower ΔG_f than the fission product MoO_2. Especially Mo may be present in metallic or oxidic compounds. A slight deficite of 26.6 mol O_2 per t_{UO_2} is calculated for the KIT SNF sample in the case, that Mo exists in the form of MoO_2, only, and 6.5 mol O_2/t_{UO_2} in the case that Mo exists in the metallic form to an extend of 58%. These numbers do not vary with the decay time. An effect of oxidation of the Zr of the cladding which may increase the deficite was not considered.

At lower temperatures, the ΔG_f of the oxides of Cs and Mo are lower than ΔG_f of the carbon oxides. However, if the gaseous carbon oxides have disappeared from the fuel and accumulated in the plenum of the fuel rod, a re-formation of solid Cs, Mo, other FP's and actinide oxides may be kinetically hindered.

From available thermodynamic data, formation of $Se^{IV}O_2$ is not expected.

Conclusions

The speciation of ^{14}C is not yet resolved by theoretical considerations. Further measurements, especially of the isotopic composition of the CO_2 in the gas phase and the redox state of the fuel are required. Furthermore a code needs to be applied which solves the equilibrium between the carbides and oxides as function of the temperature.

Acknowledgement

References

Baker, F.B., Storms, E.K., Holley, C.E. (1969). Enthalpy of Formation of Zirconium Carbide. Journal of Chemical & Engineering Data, 14, 244-246.

Bleier, A., R. Kroebel, K.H. Neeb, and H.W. Wiese (1987). Kohlenstoff-14 in LWR-Brennstäben und dessen Verhalten beim Wiederaufarbeitungsprozess. Jahrestagung Kerntechnik '87, Karlsruhe (Germany), Kerntechnische Gesellschaft e.V.417-420.

Farkas, D.M., Groza, J.R., Mukherjee, A.K. (1996). Thermodynamic Analysis of Carbide Precipitates in a Niobium-Zirconium Carbon Alloy. Scripta Materialia, 34, 103-110.

Glassner, A. (1957). The thermochemical properties of the oxides, fluorides, and chlorides to 2500°K. Chicago, USA, Argonne National Laboratory, vol. 5750.

Iwai, T., Takahashi, I., Handa, M. (1986). Gibbs Free Energies of Formation of Molybdenum Carbide and Tungsten Carbide from 1173 to 1573 K. Metallurgical Transactions A, 17, 2031-2034.

Kienzler, B., Metz, V., Duro, L., Valls, A. (2013). 1st Annual Workshop Proceedings of the Collaborative Project 'FIRST-Nuclides'. Karlsruhe, Karlsruhe Institute of Technology (KIT).

Kulik, D.A., Wagner, T., Dmytrieva, S.V., Kosakowski, G., Hingerl, F.F., Chudnenko, K.V., Berner, U.R. (2013). GEM-Selektor Geochemical Modeling Package: Revised Algorithm and GEMS3K Numerical Kernel for Coupled Simulation Codes. Computational Geosciences, 17, 1-24.

Loveland, W.D., Morrissey, D.J., Seaborg, G.T (2005). Modern nuclear chemistry, John Wiley & Sons.

Magnusson, Å. (2007). ^{14}C Produced by Nuclear Power Reactors – Generation and Characterization of Gaseous, Liquid and Solid Waste. Ph.D., Lund University.

Mazurovsky, V., Zinigrad, M., Leontiev, L., Lisin, V. (2004). Carbide formation during crystallization upon welding. In: Third International Conference on Mathematical Modeling and Computer Modeling and Computer Simulation of Materials Technologies MMT.

Neeb, K.H. (1997). The radiochemistry of nuclear power plants with light water reactors. Berlin, Walter de Gruyter.

Olander, D. R. (1976). Fundamental Aspects of Nuclear Reactor Fuel Elements. National Technical Information Service, U. S. Department of Commerce, Springfield, Virginia 22161, Technical Information Center, Office of Public Affairs, Energy Research and Development Administration.

Saiger, S. (1979). Zur Bestimmung von Verunreinigungen in Urandioxidpulvern und -Pellets. Journal of Nuclear Materials, 81, 249-255.

Sakuragi, T., Tanabe, H., Hirose, E., Sakashita, A., Nishimura, T. (2013). Estimation of carbon 14 inventory in hull and end-piece wastes from Japanese commercial reprocessing operation. ASME 15th International Conference on Environmental Remediation and Radioactive Waste Management ICEM2013, September 8th - 12th, Belgium.

Shatynski, S. R. (1979). The Thermochemistry of Transition Metal Carbides. Oxidation of Metals, 13, 105-118.

Stratton, R.W., Botta, F., Hofer, R., Ledergerber, G., Ingold, F., Ott, C., Eindl, J., Zwicky, H.U., Bodmer, R., Schlemmer, F. (1991) A Comparative Irradiation Test of UO2 Shere-pac and Pellet Fuel in the Goesgen PWR. Int. Topical Meeting on LWR Fuel Performance, 21st – 24th April, France, 174 – 183.

Theobald, J.P., Heeg, P., Mutterer, M. (1989). Low-Energy Ternary Fission. Nuclear Physics A, 502, 343-362.

Wicks, C. E., Block, F. E. (1961). Thermodynamic Properties of 65 Elements - Their Oxides, Halides, Carbides, and Nitrides. Bulletin 605 (No. NP-13622). Bureau of Mines. Albany Metallurgy Research Center, Ore.

CHARACTERIZATION OF UOX FUEL SEGMENTS IRRADIATED IN THE GÖSGEN PRESSURIZED WATER REACTOR

Volker Metz*, Ernesto González-Robles and Bernhard Kienzler

Karlsruhe Institute of Technology (KIT), Institute for Nuclear Waste Disposal (INE) (DE)

* Corresponding author: volker.metz@kit.edu

Abstract

Between 1985 and 1989, two adjacent segments N0203 and N0204 of the UOX fuel rod SBS 1108 were irradiated in the PWR Gösgen achieving an average burn-up of 50.4 GWd/t_{HM}. A physical characterization of segment N0203 was performed in the years 1991 to 1992, whereas the characterization of segment N0204 is presently ongoing within the project FIRST-Nuclides. This communication compiles published irradiation data and experimental results of the two fuel rod segments.

Introduction

In the 1980s, a series of fuel rod segments were irradiated in the Swiss Gösgen PWR (KKG) to analyze the performance of UO_2 fuels, which had been fabricated with different sintering and gelation manufacturing methods. For each irradiation test, five segments and additional dummy segments were mounted to make a full-length KKG fuel rod. The fuel of the adjacent segments N0203 and N0204 was fabricated by Kraftwerk Union AG using the NIKUSI sintering process (Stratton et al., 1991). NIKUSI is a short-term fast sintering process under controlled oxidizing condition at a temperature (< 1,300 °C) below the temperature range of conventional UO_2 pellet sintering processes (Kutty et al., 2004). The oxidative sintering in presence of CO_2 gas is followed by a reduction step to stoichiometric UO_2 (Matzke, 1987). Stratton et al. (1991) presents details about comparative tests on rod segments with NIKUSI fuel pellets and rod segments with vibrocompacted spherical UO_2 particle fuel, which were irradiated in the Gösgen PWR between 1986 and 1990.

We compile characteristic data on the fuel segments N0203 and N0204, taken from reports of previous projects funded by the European Commission (Grambow et al., 1996; 2000), data given in Stratton et al. (1991), unpublished results of physical characterizations of segment N0203 at Kernforschungszentrum Karlsruhe, Abteilung Heiße Zellen (KfK-HZ; nowadays KIT) as well as results of physical analyses of the segment N0204 (Wegen, 2012; 2013a; 2013b; 2013c; 2013d).

Characteristics of fuel and rod segment

The characteristics of segments N0203 and N0204 are similar to those of rod segments with NIKUSI fuel pellets described by Stratton et al. (1991). Most fuel pellets had been initially enriched with 3.8 wt.% ^{235}U in N0203 as well as in N0204 and with 4.27 wt.% ^{235}U in the study of Stratton et al. (1991), respectively. Pure UO_2 pellets were fabricated without any additives; a UO_2 stoichiometry of O/U = 2.002 and a fuel density of 95.4% theoretical density is reported by Stratton et al. (1991). In each of the fuel rod segments with NIKUSI pellets, two pellets adjacent to the upper and lower isolation pellets were made of U_{nat} (Figure 1). The initial pellet

dimensions were specified with a diameter of 9.1 to 9.2 mm and a length of 11 mm. According to non-destructive analyses of the irradiated segment N0204 the length of the initially 3.8 wt.% ^{235}U enriched pellets is 11.5 mm in average and the length of the two U_{nat} pellets is 11.3 mm (Wegen et al., 2013b). The cladding material of the fuel rod segments were made of Zircaloy-4 (DX ELS 0.8). Before irradiation the cladding was specified with an external diameter of (10.75 ± 0.05) mm, an internal diameter about 9.3 mm, and a wall thickness of 0.725 mm (Grambow et al., 1996; 2000; Kernkraftwerk Gösgen, 2010; Stratton et al., 1991). After irradiation of segment N0204, an external cladding diameter of $10.67 - 10.73$ mm (10.71 mm mean) was measured by Wegen et al. (2012; 2013c). The internal fill gas pressure of segments N0203 and N0204 was (21.5 ± 1.0) bar He. Accordingly, Stratton et al. (1991) reported a fill gas pressure of 22.5 bar for the NIKUSI fuel segments in their study.
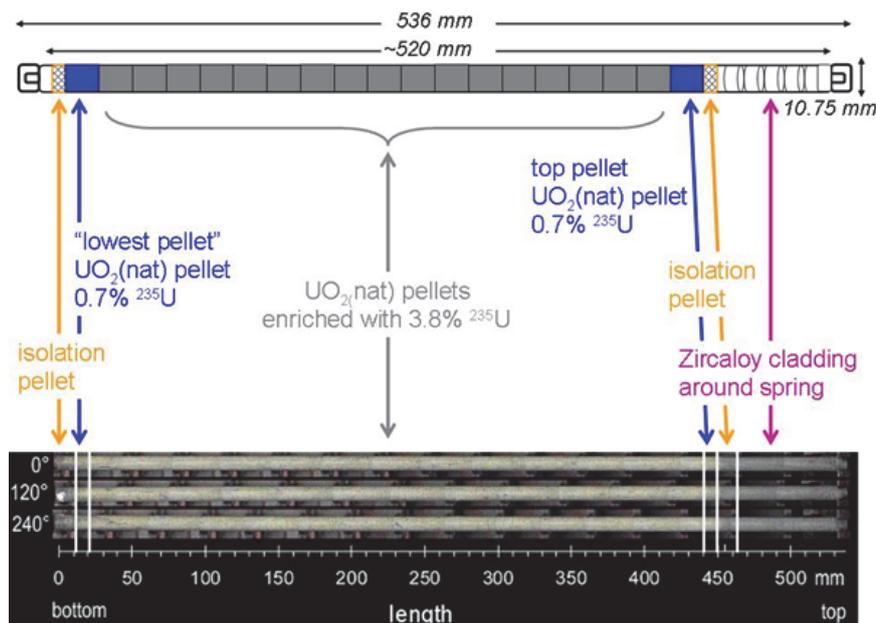
*Figure 1: Schematic cross section and photos of the fuel rod segment SBS1108-N0204. The inserted photo is taken from Papaioannou et al. (2012).*

Irradiation data

The Gösgen PWR operated with a 15×15 fuel assembly design. 205 of the 225 positions of the lattice geometry were occupied with fuel rods, the 20 remaining guide tubes were available for control rods (Gauld et al., 2011; Kernkraftwerk Gösgen, 2010). The fuel rod SBS1108 was inserted in the central region of the 15×15 fuel assembly and irradiated in four cycles for 1,226 days total irradiation, which started in 1985 and ended on May 27, 1989; an average linear heat generation rate (LHGR) and a maximal LHGR of 260 and 340 W/cm, respectively, is reported for SBS1108 (Grambow et al., 1996; 2000). At similar irradiation conditions, another fuel rod with NIKUSI fuel segments (pin 1106) was inserted at the outer edge of the fuel assembly and irradiated for about 1,220 days between June 1986 and 1990 (Stratton et al., 1991). Figure 2 compares the power history of fuel rod 1106 with the published LHGR data for the fuel rod SBS1108. A final rod-average burn-up was estimated as 50.4 GWd/t_{HM} for SBS1108 and 54 GWd/t_{HM} for 1106, respectively (Grambow et al., 1996; 2000; Stratton et al., 1991).
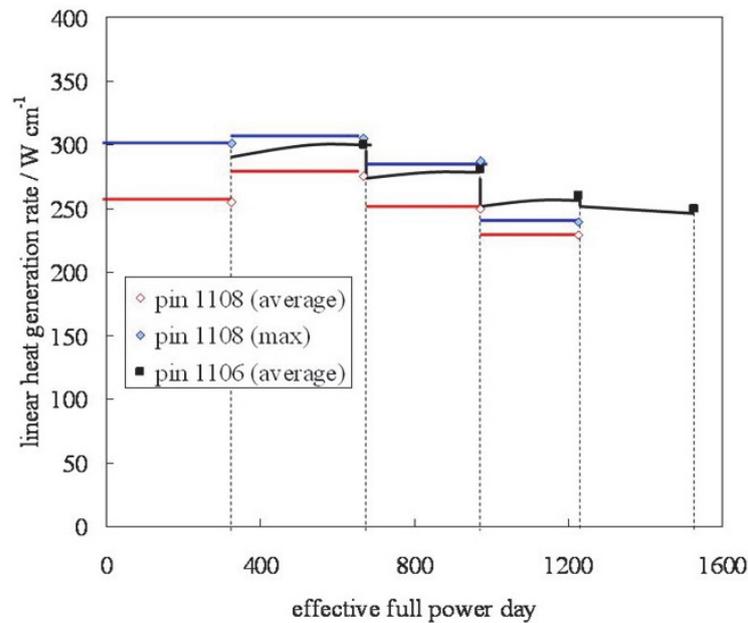
Figure 2: Power history of fuel rod 1106 (average LHGR; after Stratton et al., 1991) compared to average and maximum LHGR data of fuel rod SBS1108.

Fission gas release and morphology of irradiated fuel samples

During irradiation, porosity, grain size distribution and other morphological physical features of UOX fuels change considerably. The morphology of spent nuclear fuels depends on the power history, in particular on the linear heat generation rates and the burn-up. Previous studies showed that the fission gas release (FGR) is correlated to the grain size distribution of the irradiated fuels (e.g. Turnbull, 2005). In a puncturing test of the segment N0204, Gonzalez-Robles et al. (2013) determined a Kr and Xe release corresponding to 8.35% of the calculated fission gas inventory of the fuel rod segment. Comparing the FGR of N0204 with published data of other high burn-up spent nuclear fuel samples, they observed a significant dependency of FGR on the LHGR of the studied fuel rods.

Within the framework of project FIRST-Nuclides, ceramography analyses of fuel rod segment N0204 are in preparation at JRC-ITU. For completeness and comparison with future ceramography results of N0204, we present optical images of N0204 and unpublished ceramography analyses of fuel segment N0203 performed by the group of F. Weiser, Abteilung Heiße Zellen, Kernforschungszentrum Karlsruhe. Macro sections of the studied pellets of N0203 and N0204 show the typical cracking pattern and the porous structure in the outer part of the pellet, the so-called high burn-up structure (Figure 3).
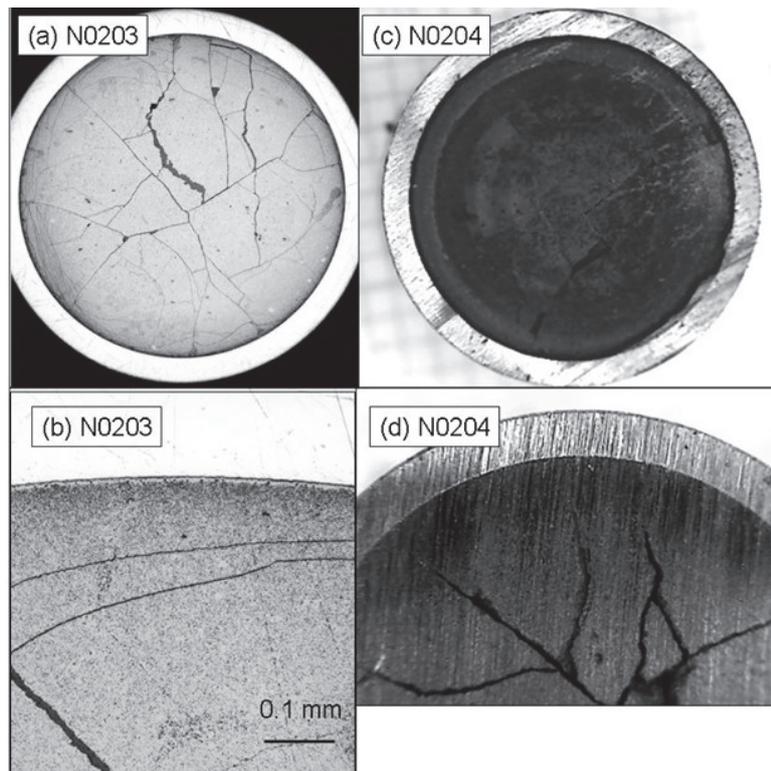
Figure 3: *Exemplary section images of initially 3.8 wt.% [235]U enriched pellets of fuel segments N0203 and N0204. Ceramography images of N0203 are taken from F. Weiser (KfK-HZ). Detail images (b) and (d) display the rim zone close to the cladding.*

Based on ceramography micro sections of N0203, Gonzalez-Robles et al. (2013b) estimated the thickness of the rim zone to be (200 ± 10) µm and a porosity of 20% of the rim (so-called high burn-up structure). According to Koo et al. (2001), the burn-up of the rim zone BU_R is 1.33 times higher than the average pellet burn-up, i.e. 67.0 GWd/t_{HM} for pellets of the rod segment SBS1108. Using the rim zone thickness, R_t, to rim burn-up relation of Koo et al. (2001),

$$R_t = 5.44\ BU_R\ - 281\ (\mu m)$$

a rim zone thickness of 83 µm is calculated (Kienzler et al., 2013). The difference between the measured and calculated rim zone thickness is related to the uncertainty in the estimation of BU_R.

Outlook

Morphological and chemical characterization of pellets from the fuel rod segment SBS1108-N0204 is in preparation by KIT-INE and JRC-ITU. In particular ceramography analyses will be performed to determine accurately the grain size distribution and rim zone thickness. Using the irradiation data, calculations are performed to determine the spatial distribution of radionuclides in irradiated pellets with an initial enrichment of 3.8 wt.% [235]U and with UO_2(nat). The calculated radionuclide distributions will be compared to future laser-ablation mass spectrometry analyses of [235]U enriched and UO_2(nat) pellets of segment N0204.

Acknowledgements

References

Gauld, I.C., Ilas, G., Radulescu, G. (2011). Uncertainties in Predicted Isotopic Compositions for High Burnup PWR Spent Nuclear Fuel. U.S. Nuclear Regulatory Commission, Washington, NUREG/CR-7012.

González-Robles, E., Bohnert, E., Müller, N., Herm, M., Metz, V., Kienzler, B. (2013a). Determination of the Fission Gas Release in the Segment N0204 and Gas Phase Result of Anoxic Leaching Experiment. Proceedings of 7th EC FP – FIRST-Nuclides 2nd Annual Workshop. Antwerp, Belgium.

González-Robles, E., Wegen, D.H., Bohnert, E., Papaioannou, D., Kienzler, B., Nasyrow, R., Metz, V. (2013b). Physico-Chemical Characterization of a Spent UO_2 Fuel with Respect to Its Stability under Final Disposal Conditions. Materials Research Society, Scientific Basis for Nuclear Waste Management, Mat. Res. Symp. Proc. (accepted for publication).

Grambow, B., Loida, A., Dressler, P., Geckeis, H., Gago, J., Casas, I., de Pablo, J., Giménez, J, Torrero, M.E. (1996). Long-Term Safety of Radioactive Waste Disposal: Chemical Reaction of Fabricated and High Burnup Spent UO_2 Fuel with Saline Brines. Final Report. Forschungszentrum Karlsruhe Wissenschaftliche Berichte, FZKA 5702.

Grambow, B., Loida, A., Martínez-Esparza, A., Díaz-Arocas, P., de Pablo, J., Paul, J.L., Marx, G., Glatz, J.P., Lemmens, K., Ollila, K., Christensen, H. (2000). Long-Term Safety of Radioactive Waste Disposal: Source Term for Performance Assessment of Spent Fuel as a Waste Form. Final report. Source term for performance assesment of spent fuel as a waste form. European Commission, Nuclear Science and Technology Series. Forschungszentrum Karlsruhe Wissenschaftliche Berichte, FZKA 6420.

Kernkraftwerk Gösgen (2010). Technik und Betrieb – Technische Hauptdaten. Kernkraftwerk Gösgen-Däniken AG, Däniken, Solothurn, Switzerland.

Kienzler, B., Bube, C., González-Robles, E., Metz, V. (2013). Modelling of Boundary Conditions for Upscaling Migration / Retention Processes of Fission Products in the Spent Nuclear Fuel Structure. Proceedings of 7th EC FP – FIRST-Nuclides 1st Annual Workshop (eds. B. Kienzler et al.). KIT Scientific Reports 7639, Karlsruhe, ISBN 978-3-86644-980-0, Budapest, Hungary, 103-110.

Koo, Y.H., Lee, B.H., Cheon, J.S., Sohn, D.S. (2001). Pore Pressure and Swelling in the Rim Region of LWR High Burnup UO_2 Fuel. J. Nucl. Mat., 295, 213-220.

Kutty, T.R.G., Hegde, P.V., Khan, K.B., Jarvis, T., Sengupta, A.K., Majumdar, S., Kamath, H.S. (2004). Characterization and Densification Studies on ThO$_2$–UO$_2$ Pellets Derived from ThO$_2$ and U$_3$O$_8$ Powders. Journal of Nuclear Materials, 335, 462-470.

Matzke, Hj. (1987). Atomic Transport Properties in UO$_2$ and Mixed Oxides (U,Pu)O$_2$. J. Chem. Soc., Faraday Trans. II, 83, 1121-1142.

Papaioannou, D., Nasyrow, R., de Weerd, W., Bottomley, D., Rondinella, V.V. (2012). Non-Destructive Examinations of Irradiated Fuel Rods at the ITU Hot Cells. 2012 Hotlab conference. 24th-27th September 2012, Marcoule, France.

Stratton, R.W., Botta, F., Hofer, R., Ledergerber, G., Ingold, F., Ott, C., Reindl, J., Zwicky, H.U., Bodmer, R., Schlemmer, F. (1991). A Comparative Irradiation Test of UO$_2$ Sphere-Pac and Pellet Fuel in the Goesgen PWR. Int. Topical Meeting on LWR Fuel Performance "Fuel for the 90's". Avignon, France, 174-83.

Turnbull, J.A. (2005). Fission Gas Release as a Function of Burnup at High Power (52-55 MWd/kg). NEA report IFPE/IFA-534.14REV1. Nuclear Energy Agency, NEA, Paris

Wegen, D.H., Papaioannou, D., Nasyrow, R., Gretter, R., De Weerd, W. (2012). Non-Destructive Testing of Segment N0204 of the Spent Fuel Pin SBS1108. Contribution to WP1 of the collaborative project FIRST Nuclides, JRC75272, European Atomic Energy Community, Karlsruhe, Germany.

Wegen, D.H., Papaioannou, D., Gretter, R., Nasyrow, R., Rondinella, V.V., Glatz, J.P. (2013a). Preparation of Samples for IRF Investigations and Post Irradiation Examinations from 50.4 GWd/tHM PWR Fuel (eds. B. Kienzler et al.). Proceedings of 7th EC FP – FIRST-Nuclides 1st Annual Workshop, Budapest, Hungary. KIT Scientific Reports 7639, Karlsruhe, ISBN 978-3-86644-980-0.

Wegen, D.H., Papaioannou, D., Nasyrow, R., Rondinella, V.V., Glatz, J.P. (2013b). Non-Destructive Analysis of a PWR Fuel Segment with a Burn-Up of 50.4 GWd/tHM (eds. B. Kienzler et al.). Proceedings of 7th EC FP – FIRST-Nuclides 1st Annual Workshop, Budapest, Hungary. KIT Scientific Reports 7639, Karlsruhe, ISBN 978-3-86644-980-0.

Wegen, D.H., Papaioannou, D., Nasyrow, R., Rondinella, V.V., Glatz, J.P. (2013c). Non-Destructive Analysis of a PWR Fuel Segment with a Burn-Up of 50.4 GWd/tHM – Part I: Visual Examination And Gamma-Scanning (eds. B. Kienzler et al.). Proceedings of 7th EC FP – FIRST-Nuclides 1st Annual Workshop, Budapest, Hungary. KIT Scientific Reports 7639, Karlsruhe, ISBN 978-3-86644-980-0.

Wegen, D.H., Papaioannou, D., Nasyrow, R., Rondinella, V.V., Glatz, J.P. (2013d). Non-destructive analysis of a PWR fuel segment with a burn-up of 50.4 GWd/tHM – Part II: Defect determination. Proceedings of 7th EC FP – FIRST-Nuclides 1st Annual Workshop, Budapest, Hungary (eds. B. Kienzler et al.), KIT Scientific Reports 7639, Karlsruhe, ISBN 978-3-86644-980-0.

MODELS FOR FISSION PRODUCTS RELEASE
FROM NUCLEAR FUEL AND THEIR APPLICABILITY TO
THE FIRST-NUCLIDES PROJECT

Marek Pękala[*], Andrés Idiart , Lara Duro, Olga Riba

Amphos 21 Consulting (ES)

* Corresponding author: marek.pekala@amphos21.com

Abstract

This contribution provides an overview of conceptual and mathematical models for the Instant Release Fraction (IRF) under repository conditions. To this end a variety of models, including those for fission products release under in-reactor conditions, are reviewed. Correlative models are used to give direct prediction of IRF based on the measured or estimated release of fission gases (FGR). Semi-empirical models applied to experimental results allow conceptual models of radionuclide release to be constructed and verified against measured data. In addition, physics-based mechanistic models for fission products release under in-reactor conditions are being continually developed. These models are often included into larger coupled codes for the assessment of fuel performance, and can be used to accurately predict the release of fission gases and some other fission products during reactor operation. Such information is valuable for estimating IRF under the conditions expected for repository of spent nuclear fuel.

Introduction

Safety assessment of a repository for spent UO_2 fuel requires that the potential release of radioactivity upon breaching of the engineered barriers system due to degradation processes be quantified. From the point of view of the performance assessment (PA) of a repository for spent fuel, the instant release fraction (IRF) is the fraction of the radioactive inventory that will be released from the waste "immediately" after the fuel rod cladding fails, and the waste containment is compromised. The IRF may have important implications for PA because some of the preferentially released radionuclides are characterised by both relatively long half-lives and high degrees of mobility (e.g. ^{129}I and ^{36}Cl – Johnson et al., 2012). As a result a great deal of effort has been directed into improving the understanding and quantifying the physico-chemical processes involved in the instant release of radionuclides from spent nuclear fuel (SNF). These goals are being achieved through a combination of experimental and modelling work (Johnson et al., 2012; Poinssot et al., 2005; Johnson et al., 2004; Sneyers, 2008; Grambow et al., 2010; Ferry et al., 2007; Lovera et al., 2003; Johnson et al., 2005). In-reactor irradiation with neutrons causes a continuous production of fission products within the fuel. The fission products include isotopes of noble gases (mainly Xe and Kr) and others, such as ^{3}H, ^{14}C, ^{79}Se, ^{99}Tc, ^{107}Pd, ^{125}Sn ^{129}I, ^{135}Cs, and ^{137}Cs. Fission products may occur in the fuel as volatiles (I, Br, Cs, Rb, Te), metallic precipitates (Mo, Tc, Ru, Rh, Pd, Ag, Cd, In, Sn, Sb, Te), oxide precipitates (Rb, Cs, Sr, Ba, Zr, Nb, Mo, Te) or oxides in the UO_2 structure (Cs, Nb, Te, Y, Zr, the earth alkaline elements Sr, Ba, Ra and the lanthanides La, Ce, Pr, Nd, Pm, Sm, Eu) (Metz et al., 2012).

In a rod containing stacked pellets of polycrystalline UO_2 fuel during reactor operation, concentration and thermal gradients drive diffusive redistribution of some of the fission products into the inter-granular space, and outside the pellet towards the inner-rod void space. It is thought that under repository conditions, breaching of the cladding would lead to a rapid release of the inventory accumulated in the void space of the rod. Also, some radionuclides segregated at the fuel grain boundaries would be released relatively quickly. Both of these inventory fractions are typically considered to constitute the IRF. In contrast, a much slower radionuclide release would occur over long periods of time due to dissolution of the UO_2 matrix (Johnson et al., 2005; Johnson and Tait, 1997).

Typically, the rapid release of radioactivity when spent UO_2 fuel is contacted by water is assessed through laboratory experiments. These, however, are technically and economically challenging due to the high levels of radioactivity retained by the spent fuel. The measured IRF depends on the type and in-reactor history of the fuel, which requires that a large number of a variety of spent UO_2 materials be studied. This work progresses steadily and simple models of IRF have been developed based on the available data.

In this contribution a review of available conceptual and mathematical models related to the IRF from spent UO_2 fuel is given. A special focus is placed on modelling of the release of fission gases from UO_2 under reactor operation conditions, which has been investigated for a long time and is relatively well understood. The modelling approaches developed for fission gas release and the results obtained using them can be helpful in estimating the IRF from UO_2 under repository conditions.

Modelling Approaches

Empirical and Semi-empirical Models for IRF

The release of fission products from nuclear fuel has been investigated experimentally (Johnson et al., 2012; Johnson et al., 2004; Johnson and Tait, 1997; Johnson and McGinnes, 2002). The fission gas inventory in the inner-rod void can be collected and analysed, the release of fission product radionuclides from the spent UO_2 fuel can be investigated through leaching experiments, and the results obtained can be compared with reactor operating conditions and various fuel properties. Despite the limited amount of experimental data useful correlations of this type have been obtained, which form the basis of empirical models used to estimate the IRF.

Most empirical models rely on the observation that the quantities of radionuclides in the inner-rod void and those leached from the fuel grain boundaries correlate with fission gas release (FGR) (Johnson et al., 2004; Johnson et al., 2005; Johnson and Tait, 1997; Johnson and McGinnes, 2002). These correlations can be used inversely to estimate the IRF (within the calibration range) if the FGR is known. With respect to the fission radionuclides for which there are no experimental data and no such empirical correlations exist (e.g. Cd), bounding IRF values can be defined based on consideration of their diffusion coefficient during irradiation relative to other radionuclides for which such data are available (Johnson et al., 2005).

Semi-empirical models have been developed based on experimental leaching data with the aim to provide insight into the underlying processes that control the release of fission products from UO_2 spent fuel. For example, Casas and co-workers (Casas et al., 2012) analysed the results of static (batch) and dynamic (flow-through) leaching experiments performed on powdered samples of high burn-up fuel. They developed a kinetic dissolution model whose parameters where fitted to the experimental data.

Empirical and Semi-empirical Models for Fission Gas Release

FGR can be correlated with the release of other fission products, thus providing useful information on IRF. FGR can be measured during post-irradiation inspection (PIE), but this is costly, impractical for large numbers of rods and does not offer predictive capability. Because FGR from fuel during reactor operation is an important safety and economic consideration, predictive models for this process have been in development since the early days of the nuclear power generation. In general, these models fall into two broad categories: (1) empirical and semi-empirical correlations and (2) process-oriented mechanistic models that often are incorporated into fuel performance assessment codes.

It has been observed that in-reactor FGR from UO_2 fuel correlates strongly with linear heating rate, which depends on fuel temperature (Kamimura, 1992). Increasing degree of burn-up causes a reduction of thermal conductivity of the fuel, hence a correlation of FGR with the degree of burn-up is also observed (at burn-up > 40 GWd/t_{iHM}) (Spino, 1998).

In UO_2 fuels characterised by high degree of burn-up (>40 GWd/t_{iHM}) restructuring of the peripheral parts of the fuel is observed (Johnson et al., 2005). The rim region of the fuel pellet undergoes recrystallization resulting in smaller grain sizes and increased porosity filled with over-pressurised fission gas bubbles (Johnson et al., 2005). Experimental data indicate that the thickness of the rim is a function of the degree of burn-up experienced by the rim area (Koo et al., 2001). Koo et al. (2001) have developed a model to calculate the fraction of the total amount of Xe produced in the fuel pellet, which is retained in the rim pores. In radionuclide release models, the inventory contained in these bubbles can either be treated as part of the IRF or can be considered to be released during matrix dissolution only (Johnson et al., 2005). However, Johnson et al. (2005) argue that fission gas retained in rim pores can be considered to be released from the fuel matrix and should therefore be considered to be part of the IRF even though it is not released into the cladding gap. Moreover, other fission products, which do not form a solid solution with UO_2, are expected to be released from the matrix into the inter-grain space during recrystallization of the rim and could be released if contacted by water (Johnson et al., 2005).

Mechanistic Models

The main limitation of empirical models is that their applicability is restricted to a specific fuel type used under specific reactor operation conditions. In other words, extrapolation to other conditions and/or ranges must be considered with caution. In addition, such models offer little in the way of system behaviour understanding. This deficiency is however remedied by more mechanistic, process-oriented models, which are being increasingly developed.

Conceptual models for Fission Products

Fission gas generation and transport during irradiation contributes to fuel swelling and has the potential to cause damage to the cladding due to strong pellet-cladding mechanical interactions. As such, it is a significant safety consideration and considerable amount of effort has been dedicated to better understand these processes.

Underlying mechanistic models are conceptualisations of fission gas generation and transport within the fuel. For UO_2 fuel characterised by high burn-up, the following processes are typically considered (Blair, 2008):

- *Gas generation due to the fission of ^{235}U.*
- *Recoil and knock-out.*
- *Lattice (intra-granular) diffusion.*
- *Grain-boundary diffusion.*

- *Trapping (intra- and inter-granular)*
- *Irradiation-induced resolution.*
- *Intra-granular bubble motion.*
- *Grain growth.*
- *Grain boundary bubble development.*

Mathematical Implementation

Adequate modelling of the fission gas generation and release requires considering a number of mutually interdependent processes (described above). A more detailed description of how these processes can be represented mathematically is given in Blair (2008), Van Uffelen (2002) and Pastore (2012).

The first attempt to model intra-granular diffusion of fission gas out of a fuel element is that of Booth (Booth, 1957). To simplify calculations, the Booth model considers a sinter composed of a collection of uniform spheres with an equivalent radius. This model considers the single process of atomic diffusion in the spherical grain using the Fick's law and assuming constant, single-atom diffusion coefficient. The original Booth model ignores fission gas release due to recoil and knock-out near grain boundary surfaces. This limitation is overcome in some codes by, for example, the implementation of an empirical release term, which is a function of burn-up (Berna et al., 1997).

The model of Booth was later extended by Speight (1969) by further accounting for the presence of (immobile) intra-granular gas bubbles into which diffusing gas atoms can be trapped and re-dissolved due to irradiation. The model is described by a single diffusion equation and in the absence of bubbles is mathematically equivalent to the Booth model. In the Speight model, gas atom trapping and re-solution is expressed by multiplying the diffusion coefficient by a constant expression, which renders the single-atom diffusion coefficient an effective diffusion coefficient.

Van Uffelen and collaborators (2011) have further extended the Speight model by considering the mobility of intra-granular fission gas bubbles. The mobility of fission gas trapped in bubbles is accounted for by adding an extra term to the effective diffusion coefficient of Speight.

The migration of fission gases in the UO$_2$ lattice can be treated using diffusion theory, where the effect of temperature on the diffusion coefficient can be approximated using the Arrhenius theory. However, this situation is complicated by several factors (Blair, 2008):

- *Radiation induced damage to the crystal lattice, which acts both to retard (by trapping in intra-granular bubbles) and to speed up (by re-solution and radiation-enhanced diffusion) diffusion*
- *Chemical effects related to the production of fission products (e.g. changes in oxygen to metal ratio)*

In order to represent the above-mentioned effects the single-atom diffusion coefficient is typically defined as a sum of three components, each expressing a different contribution (e.g. the intrinsic diffusivity and the thermal and athermal impact of irradiation). The components of the diffusion coefficient are represented using analytical expressions based on empirical correlations (Blair, 2008; Van Uffelen et al., 2011; Bernard et al., 2002).

As mentioned earlier, the growth of fuel grains has the effect of fission gas sweeping at the grain boundaries, which provides an accumulation mechanism. In addition, the diffusion distance towards the grain boundary surface increases which slows down diffusive transport. Incorporating the growth of fuel grain size requires that the differential diffusion equation be solved with a moving boundary thus increasing the level of complexity of the model. Some models disregard the impact of grain size growth on diffusive transport and consider the

sweeping effect only, for instance the model of Hargreaves and Collins (1976). Other models attempt to represent both the radionuclide sweeping and a moving boundary diffusion transport, such as the model of Ito and collaborators (1985). However, most models neglect the grain-size distribution, which has been shown to over-estimate the fission gas release fraction (El-Saied and Olander, 1993). White (2004) proposed a model for calculating intra-granular fission gas bubble growth rate based on a calculation of the number of vacancies and gas atoms present. The process of bubble intersection, merging and growth is termed coalescence. This can be modelled, for example, after White (2004), Veshchunov (2008) or Pastore (2012) by considering a change in bubble surface area when bubbles merge.

The release of fission gas from the grain boundaries is usually modelled by assuming that the gas atoms diffuse from inside of the grain to the grain boundaries, where they accumulate until a saturation threshold is reached. Once saturation has been reached, the gas atoms at the rim are released (Bernard et al., 2012). This concentration can be calculated following White and Tucker (1983). However, this model relies on the assumption that the gas is ideal and that the bubble is in mechanical equilibrium. This problem can be circumvented by considering mechanistic kinetic models, where coupling between hydrostatic pressure, temperature, gas swelling and release is represented on a physical basis (White and Tucker, 1983; Pastore, 2012).

Fuel Performance Assessment Codes

As the possibility to study the performance of nuclear fuel through experiments in reactor and post-irradiation examinations (PIE) is limited, it has been recognised that adequate models capable of representing relevant processes affecting nuclear fuel during reactor operation were needed. Fuel performance predictions are required by safety-based calculations, for design purposes and performance assessment. In addition, such codes are also useful in optimising the reactor operation conditions in order for the reactors to be run economically. The ultimate goal of these codes is to reliably predict the in-reactor behaviour of a rod during both normal and abnormal operation conditions. Such codes are now being extensively used across the nuclear industry by fuel manufacturers, power plant operators, regulatory and licensing authorities, and by research centres and universities (Aybar and Ortego, 2005; NEA, 2000).

The in-reactor fuel behaviour is affected by a range of processes including: thermal, mechanical, irradiation, densification, swelling, fission gas generation and release. Modelling of processes related to fission gas generation, transport and release during irradiation in reactor is an important component of the thermo-mechanical behaviour of the fuel. One reason for this is that fuel swelling due to fission gas generation promotes pellet-cladding interactions. Moreover, FGR into the free volume inside the rod causes pressure build-up and degrades thermal properties of the rod-filling gas. Therefore, the thermal, mechanical and fission gas release processes, and their impact on the fuel performance are closely linked. The thermo-mechanical processes are described in terms of dimensional equations, thus defining the dimensionality of the model. When simulating the behaviour of a complete fuel rod, efforts are made to decrease the dimensions of the model in order to reduce computational costs. Most codes are 1-D or quasi-2-D (so called 1.5-D), where radial calculations are coupled axially by the coolant energy equation, common internal rod gas pressure and, sometimes, by a 1-D model for the axial friction forces (Pastore, 2012).

Even though some specific capabilities and the numerical implementation vary broadly between the different codes, the following features are typically calculated by modern fuel performance assessment codes (such as the TRANSURANUS):

- **Thermal Analysis**

    - *Axial heat transfer in the coolant*
    - *Heat transfer in the cladding*
    - *Heat transfer from cladding to fuel*
    - *Heat transfer in the fuel*

- **Mechanical Analysis**

    - *Elastic strains*
    - *Inelastic strains: swelling*
    - *Inelastic strains: plasticity and creep*
    - *Inelastic strains: pellet fragment relocation*

- **Fission gas generation, transport and release**

    - *Swelling due to gaseous fission products*

- **Thermal and irradiation induced densification of the fuel**
- **Volume changes due to phase changes**
- **Neutronics**

Several codes are currently being developed with a special focus on the FGR analysis. MFPR (Model for Fission Products Release) represents a state-of-the-art implementation of such coupled mechanistic models. Recent developments in the code take account of the influence of microscopic defects (vacancies, interstitial and fission atoms, bubbles, pores and dislocations) in the UO_2 structure on the transport of fission gases. The code provides a mechanical description of the behaviour of chemically active elements based on the multi-phase and multi-component thermo-chemical equilibrium at the grain boundary and fuel oxidation state calculation (Veshchunov et al., 2007). MFPR incorporates an advanced model for inter-granular bubble mobility in irradiated UO_2, which considers three mechanisms: volume diffusion, evaporation/condensation and surface diffusion Veshchunov and Shestak. (2008). Moreover, the code includes an advanced model for grain face transport of gas atoms that consistently considers the effects of atom diffusion, trapping and irradiation-induced re-solution (Veshchunov and Tarasov, 2009; Tarasov and Veshchunov, 2009). FASTGRASS (Rest and Zawadzki, 1992) is an example of a fuel performance code with the capability to simulate the release of not only fission gases, but also other fission products: volatiles (I, Te, Cs) and alkaline earth elements (Sr and Ba).

Developments in Fuel Performance Assessment Codes

As of today simplified correlations are still used in many fuel assessment codes to represent complex material behaviour (Pastore, 2012). However, recent efforts in computational algorithms, computer hardware and parallel computing are progressively replacing these simplified approaches by more realistic (and computationally expensive) coupled, pure physics-based models. There are currently several codes under development that take advantage of the recent advances in the field. These include: AMP (ORNL, USA – Clarno et al., 2012), Bison (INL, USA – Novascone et al., 2012), BACO (CNEA, Argentina – Demarco and Marino, 2011) and PLEIADES/ALCYONE (CEA-EDF, France – Michel et al., 2008). These codes rely on state-of-the-art solution methods to simulate in 2-D and 3-D the behaviour of the fuel nominal operation and expected transients (Clarno et al., 2012).

Recently, simulations based on statistical physics concepts, such as the phase-field theory, have been successfully applied to modelling the 3-D structure evolution of irradiated fuels. Processes modelled using the phase-field approach include: solidification, grain growth, martensitic transition, precipitation,

ferroelectric/ferromagnetic transition, dislocation dynamics, deformation twin, sintering, and microstructure evolution in irradiated materials (Li et al., 2010; Steinbach, 2009). Li and co-workers (2012) developed a phase-field model to simulate intra-granular fission gas bubble evolution in a single crystal during post-irradiation thermal annealing. In a follow-up work, Li and co-workers (2012a) presented a phase-field model of intra-granular gas atom and bubble behaviour extended to incorporate thermodynamic and kinetic properties at grain boundaries, to simulate fission gas bubble growth kinetics in polycrystalline UO_2 fuels. The model takes into account gas atom and vacancy diffusion, vacancy trapping and emission at defects, gas atom absorption and resolution at gas bubbles, internal pressure in gas bubbles, elastic interaction between defects and gas bubbles, and the difference of thermodynamic and kinetic properties in matrix and grain boundaries. The enhanced phase-field model was used to simulate gas atom segregation at grain boundaries and the effect of interfacial energy and gas mobility on gas bubble morphology and growth kinetics in a bi-crystal UO_2 during post-irradiation thermal annealing. The application of phase-field models has the potential to reduce many of the simplifying assumptions used to calculate the gas deposition rate at grain boundaries (Li et al., 2012).

Research is being conducted attempting to incorporate multi-scale atomic-level simulations into fuel performance assessment codes (Samaras et al., 2009; Vega, 2008; Harp, 2010). Vega (2008) presented a proof-of-principle for the inclusion of atomic-level (molecular dynamics) simulations of thermal expansion and thermal conductivity of UO_2 into the FRAPCON performance code. Vega found that modifying FRAPCON in such a way as to accept input from the atomistic simulations is possible for a number of thermo-mechanical properties. Harp (2010) used multi-scale atomistic-level simulations to model macroscopic-level diffusion of fission gases in the UO_2 TRISO fuel (for High Temperature Gas Reactor) and explored the link between the experimentally measured fission gas release and the results of the simulations. The modelling involved molecular dynamics simulation of thermal properties of the UO_2 and its validation against available experimental data. Self-diffusion of O and U in UO_2 was explored using molecular dynamics simulations and included an evaluation of the influence of radiation damage and crystal grain boundaries. The results were used in a kinetic Monte Carlo simulation of Xe and Kr migration in UO_2. This approach allows the calculation of lattice diffusion coefficients for noble gases at different temperatures in the fuel from first principles (2010).

Application to the FIRST-Nuclides project

Most FGR models focus on the release under reactor operation conditions. Nevertheless, such models can provide valuable information regarding the future release of radioactivity from spent fuel assemblies under repository conditions.

Firstly, the mechanistic FGR models presented here are capable of accurately predicting the amount of fission gases captured within the inner-rod voids, which would constitute a part of the IRF. Secondly, the release of some fission products upon contact of the fuel with water has been demonstrated experimentally to correlate with the amount of FGR. Therefore, information on FGR obtained from the mechanistic models can be combined with such empirical correlations to make predictions of IRF under repository conditions. In addition, mechanistic FGR models can forecast numerous properties of the fuel and cladding (e.g. cracking, porosity, grain size distribution, etc.), which can be used as boundary conditions for other models, specifically focusing on IRF under repository conditions.

Mechanistic models exist that are capable of quantifying the inventory of fission gases and other fission products segregated at UO_2 grain boundaries. However, to what extent this inventory is susceptible to release remains unresolved (Johnson et al., 2012). As explained earlier, the IRF is typically considered to comprise (1) the release of fission products from the fuel/cladding gap and (2) the release of material segregated at fuel grain

boundaries (Johnson et al., 2012). However, the extent to which preferential release of fission products from grain boundaries occurs is currently unresolved. Leaching experiments do not provide an unambiguous indication of when the transition from rapid release to dissolution-based release takes place, because simultaneous release of fission products present at grain boundaries may also occur during the experiment. Although, Johnson and co-workers indicate that experimental data do not support the hypothesis that fission products occupying grain boundaries are easily leached (Johnson et al., 2012), they emphasize that methods for differentiating between fission products released from the inner-rod gap and grain boundaries should be further explored. This is important for the application of FGR models to estimating IRF from spent fuel assemblies under repository conditions.

The release of non-volatile fission products from the fuel grain surfaces requires wetting the surface with water in order to dissolve them and provide the possibility for aqueous diffusion out of the fuel. Under repository conditions this could happen after the engineered barriers are corroded through and the host-rock pore water contacts the fuel. The rate of release of these fission products would therefore be related to the rate of wetting of the fuel grain surfaces. Numerical modelling of spent fuel pellet saturation with water has been attempted as part of the FIRST-Nuclides project (Pękala et al., 2012). This work is currently under development and is hoped to provide estimates on the time required for saturation with water of spent fuel pellets under different conditions (e.g. experimental leaching of fuel materials in the laboratory and at the repository depth). Ultimately, the water saturation model will be linked with radionuclide transport and relevant retention processes to help better understand the rapid release phase of fission products from UO$_2$ spent fuel.

Acknowledgement

References

Aybar, H. S., Ortego, P. (2005). A Review of Nuclear Fuel Performance Codes. Progress in Nuclear Energy 46, 127-141.

Berna, G. A., Beyer, C. E., Davis, K. L., Lanning, D. D. (1997). FRAPCON-3: A Computer Code for the Calculation of Steady-State, Thermal-Mechanical Behavior of Oxide Fuel Rods for High Burnup. Pacific Northwest National Laboratory Report NUREGKR-6534, vol. 2, PNNL-11513.

Bernard, L.C., Jacoud, J.L., Vesco, P. (2002). An Efficient Model for the Analysis of Fission Gas Release. Journal of Nuclear Materials, 302, 125-134.

Blair, P. (2008). Modelling of Fission Gas Behaviour in High Burnup Nuclear Fuel. PhD Thesis, École Polytechnique Fédérale de Lausanne.

Booth, A. H. (1957). A Method for Calculating Fission Gas Diffusion from UO2 Fuel and Its Applications to the X-2-F Loop Test. AECL Report, 496.

Casas, I., Espriu, A., Serrano-Purroy, D., Martínez-Esparza, A., de Pablo, J. (2012). IRF Modelling from High Burn-Up Spent Fuel Leaching Experiments. 1st Annual Workshop Proceedings of the 7th EC FP – First Nuclides. 9th-11th October 2012, Budapest, Hungary.

Clarno, K.T., Philip, B., Cochran, W.K., Sampath, R.H., Srikanth, A., Barai, P., Simunovic, S., Berrill, M.A., Ott, L.J., Pannala, S., Dilts, G.A., Mihaila, B., Yesilyurt, G., Lee, J.H., Banfield, J.E. (2012). The AMP (Advanced MultiPhysics) Nuclear Fuel Performance Code. Nuclear Engineering and Design, 252, 108-120.

Demarco, G.L., Marino, A.C. (2011). 3D Finite ElementsModelling for Design and Performance Analysis of UO_2 Pellets. Science and Technology of Nuclear Installations, 2011, doi:10.1155/2011/843491.

El-Saied, U.M, Olander, D.R. (1993). Fission Gas Release During Grain Growth in a Microstructure with a Distribution of Grain Sizes. Journal of Nuclear Materials 207, 313-326.

Ferry, C., Piron, J.P., Poulesquen, A., Poinssot, C. (2007). Radionuclides Release from the Spent Fuel under Disposal Conditions: Re-Evaluation of the Instant Release Fraction. In: Scientific Basis for Nuclear Waste Management, Sheffield, UK, 2007.

Grambow, B., Bruno, J., Duro, L., Merino, J., Tamayo, A., Martin, C., Pepin, G., Schumacher, S., Smidt, O., Ferry, C., Jegou, C., Quiñones, J., Iglesias, E., Villagra, N.R., Nieto, J.M., Martínez-Esparza, A., Loida, A., Metz, V., Kienzler, B., Bracke, G., Pellegrini, D., Mathieu, G., Wasselin-Trupin, V., Serres, C., Wegen, D., Jonsson, M., Johnson, L., Lemmens, K., Liu, J., Spahiu, K., Ekeroth, E., Casas, I., de Pablo, J., Watson, C., Robinson, P., Hodgkinson, D. (2010) Final Report of the Project MICADO: Model uncertainty for the mechanism of dissolution of spent fuel in nuclear waste repository.

Hargreaves, R., Collins, D.A. (1976). A Quantitative Model for Fission Gas Release and Swelling in Irradiated Uranium Dioxide. Journal of British Nuclear Energy Society, 15, 311-318.

Harp, J.M. (2010). Examination of Noble Fission Gas Diffusion in Uranium Dioxide Using Atomistic Simulation. PhD Thesis, North Carolina State University.

Ito, K., Iwasaki, R., Iwano, Y. (1985). Finite Element Model for Analysis of Fission Gas Release from UO_2 Fuel. Journal of Nuclear Science and Technology 22, 129-138.

Johnson, L.H., Tait, J.C. (1997). Release of Segregated Nuclides from Spent Fuel. SKB Technical Report TR-97-18.

Johnson, L.H., McGinnes, D.F. (2002). Partitioning of Radionuclides in Swiss Power Reactor Fuels. Nagra Technical Report NTB 02-07.

Johnson, L., Poinssot, C., Ferry, C., Lovera, P. (2004). Estimates of the Instant Release Fraction for UO_2 and MOX Fuel at T=0. In: a report of the spent fuel stability (SFS) project of the 5th Euratom Framework program, NAGRA Technical Report 04-08, Wettingen, Switzerland.

Johnson, L., Ferry, C., Poinssot, C., Lovera, P. (2005). Spent Fuel Radionuclide Source-Term Model for Assessing Spent Fuel Performance in Geological Disposal. Part I: Assessment of the Instant Release Fraction. Journal of Nuclear Materials, 346, 56-65.

Johnson, L., Günther-Leopold, I., Kobler, W.J., Linder, H.P., Low, J., Cui, D., Ekeroth, E., Spahiu, K., Evins, L.Z. (2012). Rapid Aqueous Release of Fission Products from High Burn-Up LWR Fuel: Experimental Results and Correlations with Fission Gas Release. Journal of Nuclear Materials, 420, 54-62.

Kamimura, K. (1993). FP Gas Relesase Behaviour of High Burn-up MOX Fuels for Thermal Reactors. In: Proceedings of the Technical Committee Meeting on Fission Gas Release and Fuel Rod Chemistry Related to Extended Burnup. IAEA-TECDOC-697, 28th April–1st May 1992, Pembroke, Ont., Canada, 82.

Koo, Y.H., Lee, B.H., Cheon, J.S., Sohn, D.S. (2001). Pore Pressure and Swelling in the Rim Region of LWR High Burnup UO_2 Fuel. Journal of Nuclear Materials, 295, 213-220.

Li, Y., Hu, S., Sun, X., Gao, F., Henager, Jr. C.H., Khaleel, M. (2010). Phase-Field Modeling of Void Migration and Growth Kinetics in Materials under Irradiation and Temperature Field. Journal of Nuclear Materials 407, 119-125.

Li, Y., Hu, S., Montgomery, R., Gao, F., Sun, X. (2012). Mesoscale Benchmark Demonstration Problem 1: Mesoscale Simulations of Intragranular Fission Gas Bubbles in UO$_2$ under Postirradiation Thermal Annealing. Report for the U. S. Department of Energy (DoE), PNNL-21295, FCR&D-MDSM-2012-000098.

Li, Y., Hu, S., Montgomery, R., Gao, F., Sun, X. (2012a). Enhanced Generic Phase-field Model of Irradiation Materials: Fission Gas Bubble Growth Kinetics in Polycrystalline UO$_2$. Report for the U. S. Department of Energy (DoE), PNNL-21417, FCRD-NEAMS-2012-000134.

Lovera, P., Férry, C., Poinssot, C., Johnson, L. (2003). Synthesis Report on the Relevant Diffusion Coefficients of Fission Products and Helium in Spent Nuclear Fuel. In: CEA, Direction de L'Énergie Nucléaire, Département de Physico-Chimie, Service d'Études du Comportement des Radionucléides Saclay.

Metz, V., Gonzáles-Robles, E., Loida, A., Bube, C., Kienzler, B. (2012). Radionuclide Behaviour in the Near-Field of a Geological Repository for Spent Nuclear Fuel. Radiochimica Acta, 100, 699-713.

Michel, B., Sercombe, J., Thouvenin, G. (2008). A New Phenomenological Criterion for Pellet-Cladding Interaction Rupture. Nuclear Engineering and Design, 238, 1612-1628.

NEA (2000). Fission Gas Behaviour in Water Reactor Fuels. Seminar Proceedings, Nuclear Energy Agency (NEA). 26th-29th September 2000, Cadarache, France.

Novascone, S.R., Hales, J.D., Spencer, B.W., Williamson, R.L. (2012). Assessment of Simulation Using the Multidimensional Multiphysics BISON Fuel Performance Code. Top Fuel: Reactor Fuel Performance 2012. INL Report INL/CON-12-24744.

Pastore, G. (2012). Modelling of Fission Gas Swelling and Release in Oxide Nuclear Fuel and Application to the TRANSURANUS Code. Doctoral Thesis, Politecnico de Milano.

Pękala, M., Idiart, A., Duro, L., Riba, O. (2012). Modelling of Spent Fuel Saturation with Water – Approach, Preliminary Results and Potential Implications. 1st Annual Workshop Proceedings of the 7th EC FP – First Nuclides. 9th-11th October 2012, Budapest, Hungary.

Poinssot, C., Ferry, C., Kelm, M., Granbow, B., Martínez, A., Johnson, L., Andriambolona, Z., Bruno, J., Cachoir, C., Cavendon, J.M., Christensen, H., Corbel, C., Jégou, C., Lemmens, K., Loida, A., Lovera, P., Miserque, F., de Pablo, J., Poulesquen, A., Quiñones, J., Rondinella, V., Spahiu, K., Wegen, D.H. (2005). Spent Fuel Stability under Repository Conditions – Final Report of the European (SFS) Project. In: Commissariat à l'énergie atomique (CEA), France, 2005.

Rest, J., Zawadzki, S.A. (1992). FASTGRASS: A Mechanistic Model for the Prediction of Xe, I, Cs, Te, Ba, and Sr Release from Nuclear Fuel under Normal and Severe-Accident Conditions. User's Guide for Mainframe, Workstation, and Personal Computer Applications. Argonne National Laboratory (ANL), NUREG/CR-584O, ANL-92/3.

Samaras, M., Victoria, M., Hoffelner, W. (2009). Nuclear Energy Materials Prediction: Application of the Multi-Scale Modelling Paradigm. Nuclear Engineering and Technology, 41, 1-10.

Sneyers, A. (2008). Understanding and Physical and Numerical Modelling of the Key Processes in the Near Field and their Coupling for Different Host Rocks and Repository Strategies (NF-PRO). SCK•CEN, Brussels, 2008.

Speight, M.V. (1969). A Calculation on the Migration of Fission Gas in Material Exhibiting Precipitation and Re-Solution of Gas Atoms under Irradiation. Nuclear Science and Engineering, 37, 180-185.

Spino, J. (1998). State of the Technology Review. In: Advances in Fuel Pellet Technology for Improved Performance at High Burnup. Proc. of a Technical Committee Meeting IAEA-TECDOC-1036, 28th October – 1st November 1996, Tokyo.

Steinbach, I. (2009). Phase-Field Models in Materials Science. Modelling and Simulation in Material Science and Engineering, 17, doi:10.1088/0965-0393/17/7/073001.

Tarasov, V.I., Veshchunov, M.S. (2009). An Advanced Model for Grain Face Diffusion Transport in Irradiated UO2 Fuel. Part 2: Model Implementation and Validation. Journal of Nuclear Materials, 392, 85-89.

Van Uffelen, P. (2002). Contribution to the Modelling of Fission Gas Release in Light Water Reactor Fuel. Doctoral Thesis, University of Liege.

Van Uffelen, P., Pastore, G., Di Marcello, V., Luzzi, L. (2011). Multiscale Modelling for the Fission Gas Behaviour in the Transuranus Code. Nuclear Engineering and Technology, 43, 477-488.

Vega, D.A. (2008). Atomistically Informed Fuel Performance Codes: A Proof of Principle Using Molecular Dynamics and FRAPCON Simulations. PhD Thesis, University of Florida.

Veshchunov, M.S., Dubourg, R., Ozrin, V.D., Shestak, V.E., Tarasov, V.I. (2007). Mechanistic Modelling of Urania Fuel Evolution and Fission Product Migration during Irradiation and Heating. Journal of Nuclear Materials, 362, 327-335.

Veshchunov, M.S. (2008). Modelling of Grain Face Bubbles Coalescence in Irradiated UO_2 Fuel. Journal of Nuclear Materials, 374, 44-53.

Veshchunov, M.S., Shestak, V.E. (2008). An Advanced Model for Intragranular Bubble Diffusivity in Irradiated UO_2 Fuel. Journal of Nuclear Materials, 376, 174-180.

Veshchunov, M.S., Tarasov, V.I. (2009). An Advanced Model for Grain Face Diffusion Transport in Irradiated UO_2 Fuel. Part 1: Model Formulation. Journal of Nuclear Materials, 392, 78-84.

White, R.J., Tucker, M.O. (1983). A New Fission-Gas Release Model. Journal of Nuclear Materials, 118, 1-38.

White, R.J. (2004). The Development of Grain-Face Porosity in Irradiated Oxide Fuel. Journal of Nuclear Materials, 325, 61-77.

CHARACTERISATION OF COMMERCIAL BWR SPENT FUEL SAMPLES FOR IRF INVESTIGATIONS AND OXYGEN DIFFUSION EXPERIMENTS

Detlef H. Wegen[1*], Dimitrios Papaioannou[1], Ramil Nasyrow[1], Ralf Gretter[1],
Daniel Serrano Purroy[1], Rosa Sureda[2], Paul Carbol[1],
Vincenzo V. Rondinella[1] and Jean-Paul Glatz[1]

[1] European Commission, Joint Research Centre, Institute for Transuranium Elements (EC)
[2] Fundació CTM Centre Tecnològic (ES)

* Corresponding author: Detlef.Wegen@ec.europa.eu

Abstract

This article describes the properties of two commercial spent fuels selected by JRC-ITU for instant release fraction studies in the frame of WP3 and for ^{18}O-tracer investigations to study oxygen diffusion and water penetration into the fuel performed in WP2.

Introduction

In the past many of the published results that are used for the evaluation of the fast/instant release (IRF) have been performed with spent fuel test rods which have been irradiated under non-normal conditions. Such fuels are not representative for the present world-wide spent fuel inventory. Therefore two commercial BWR spent fuels denominated as BWR42 and BWR54 with burn-ups of 42 GWd/t_{HM} and 54 GWd/t_{HM} have been selected to perform studies on the instant release fraction (IRF). BWR42 is also foreseen to study oxygen diffusion and water penetration into the fuel using an ^{18}O-tracer technique. To get access to this commercial spent fuel itself and to the irradiation history data of the fuel, JRC-ITU has carried out intensive negotiations with the fuel owners and vendors. The negotiations were finalised in 2013 and agreements with the utilities have been signed.

Commercial BWR spent fuel data

The properties and irradiation data of these fuels are given in Table 1. Both are UO_2 fuels with an initial enrichment of 3.7 and 4.2% [235]U, respectively. The fission gas release differs about a factor two. For this reason a larger IRF is expected for BWR54. At the rod positions where the samples have been taken the burn-up was estimated from rod γ-scans. A higher burn-up of about 3 GWd/t_{HM} (45 GWd/t_{HM} for BWR42 and 57 GWd/t_{HM} for BWR54) is calculated. A better value of the local burn-up will be given after chemical analysis of the samples. The power history is also presented for the actual sample position. The BWR42 fuel sample was exposed to a higher maximal and average linear power during irradiation (292 W/cm and 215 W/cm) than that of the BWR54 fuel (275 W/cm, 163 W/cm). A more detailed power history is given in Figure 1 and Figure 2.

Table 1: *Properties and irradiation data of commercial BWR fuel samples selected for oxygen diffusion studies (WP2) and IRF investigations (WP3).*

|	BWR54	BWR42
Reactor	BWR light water coolant	BWR light water coolant
Fuel assembly design information	Lattice geometry: 10 x 10 Fuel rod outer diameter: 10.05 mm Fuel rod inner diameter: 8.84 mm	Lattice geometry: 9 x 9 Fuel rod outer diameter: 10.987 mm Fuel rod inner diameter: 9.4 mm
Fuel rod data	Standard rod Fission gas release: 3.9% Internal rod pre-pressure: 6.5 bar$_{abs}$	Standard rod Fission gas release: 2.3% Internal rod pre-pressure: 6.5 bar$_{abs}$
Fuel material data	UO$_2$ fuel, initial enrichment 4.2% ^{235}U Pellet diameter: 8.67 mm Pellet height: 10.5 mm Fuel density: 10.45 g/cm^3 Grain size: 10.1 μm Calculated radionuclide inventory with ORIGEN-ARP code (see Serrano-Purroy et. al., 2013)	UO$_2$ fuel, initial enrichment 3.67% ^{235}U Pellet diameter: 9.5 mm Pellet height: 11.53 mm Fuel density: 10.52 g/cm^3 Grain size: 15 μm (intercept) Calculated radionuclide inventory with ORIGEN-ARP code (see Serrano-Purroy et. al., 2013)
Cladding data	Zircaloy-2 Oxide thickness: 21 μm	Zry-2 LTP Fe enhanced Zr liner Oxide thickness: 11 μm
Irradiation data	Rod average burn-up: 54.24 GWd/t$_{HM}$ Number of cycles: 7 *At sample position*: Estimated burn-up: 57 GWd/t$_{HM}$ Average linear power: 163 W/cm Maximal linear power: 275 W/cm Date of loading: 22. March 2002 Discharge date: 23. June 2007 Irradiation duration: 1792 days	Rod average burn-up: 42.22 GWd/t$_{HM}$ Number of cycles: 5 *At sample position*: Estimated burn-up: 45 GWd/t$_{HM}$ Average linear power: 215 W/cm Maximal linear power: 292 W/cm Date of loading: 08. November 1993 Discharge date: 15. June 1998 Irradiation duration: 1442 days Average fuel centreline temperature <u>at sample position</u>: 911°C
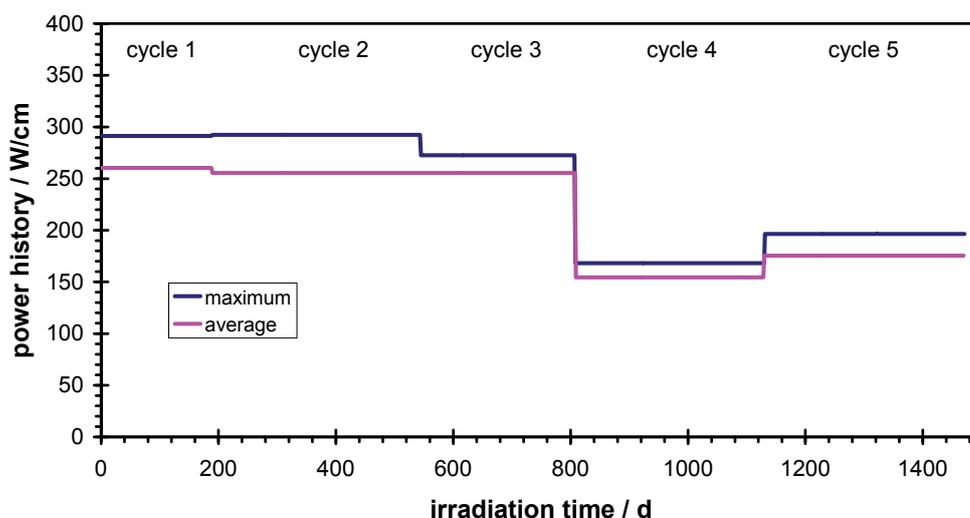
Figure 1: *More detailed power history of BWR42 at sample position.*
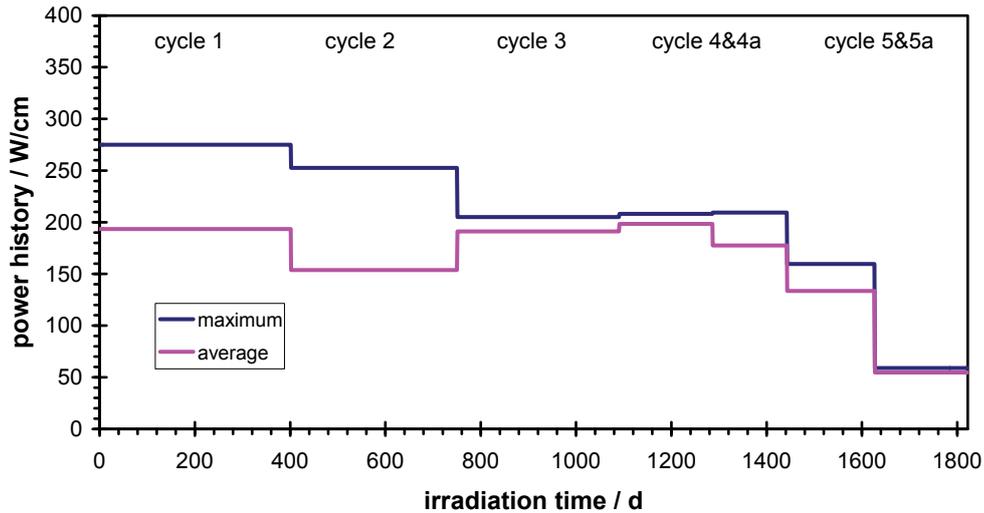
Figure 2: More detailed power history of BWR54 at sample position.

Preparation of spent fuel samples for IRF studies

For both fuels the samples were selected at positions where the total γ-scan shows a flat profile indicating a homogeneous local burn-up. For the preparation of the small IRF-samples the positions of the fuel pellets and the pellet-pellet gaps must be exactly known. The procedure to achieve this is described in the following text taking the BWR42 fuel as example. The fuel pin was cut at position 2283 mm (see Figure 3). In a next step the pin was cut open at the bottom end side, approximately 20 mm in axial direction. Now the pellet-pellet gaps are visible and the position precisely determined. Knowing the pellet length (here 11.6 mm) and the γ-scan all pellet positions in the fuel pin sample can be determined.
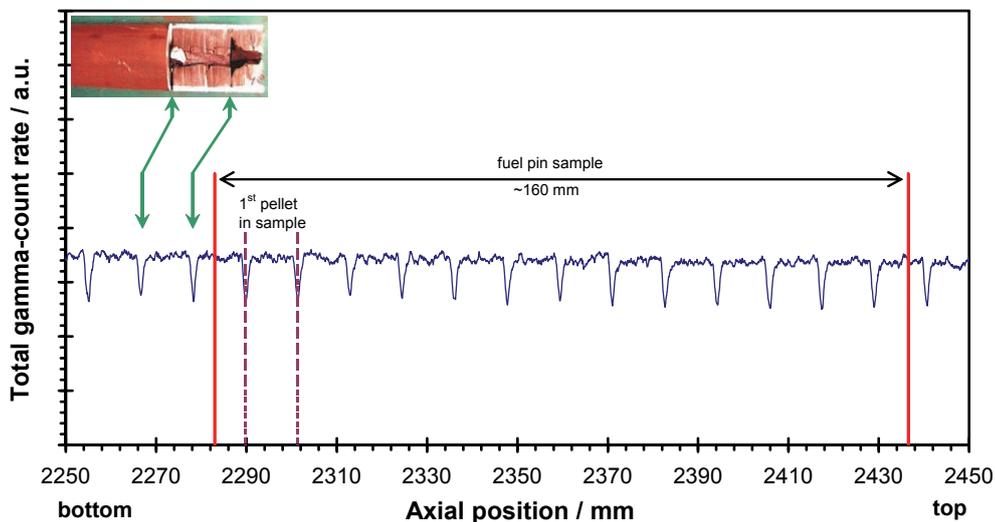
Figure 3: γ-scan of BWR42 illustrating the location of the fuel pin sample and showing the pellet positions in the sample (see also the macrograph of the axially cut open pin in the upper left corner).

The cutting procedure was carried out as described in Wegen et al. (2013). Samples for leaching were cut in mid-pellet position. Additional samples were prepared for chemical analysis and morphology examinations. The positions of the individual samples are shown in the cutting plans in Figure 4 and Figure 5.
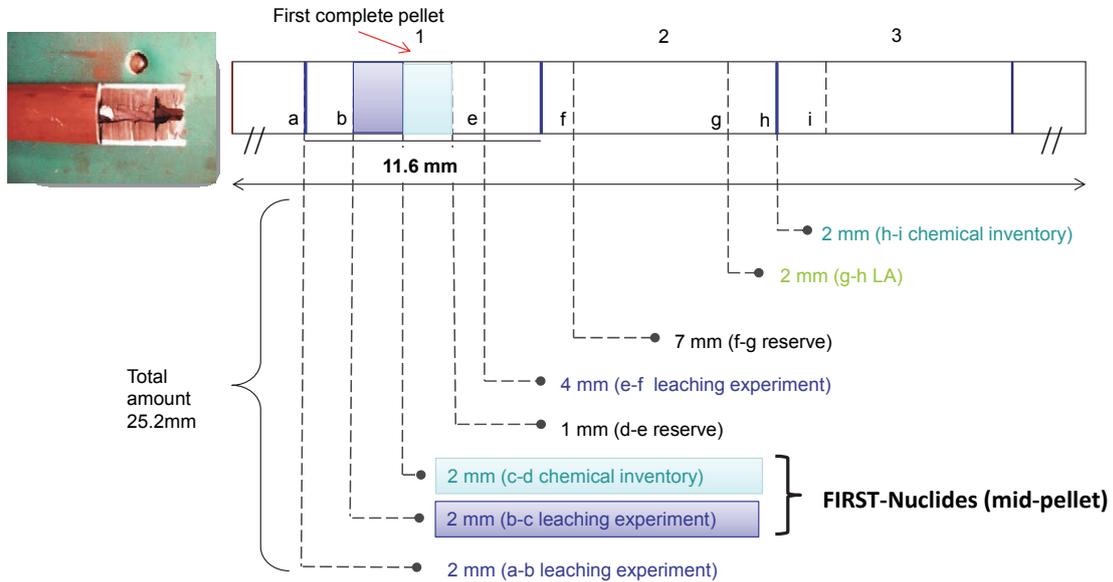

Figure 4: BWR42 cutting plan showing the position and the nominal length of samples cut mid-pellet for IRF leaching studies and for further characterisations (solid vertical lines indicate pellet-pellet gaps; dashed lines indicate cut positions).
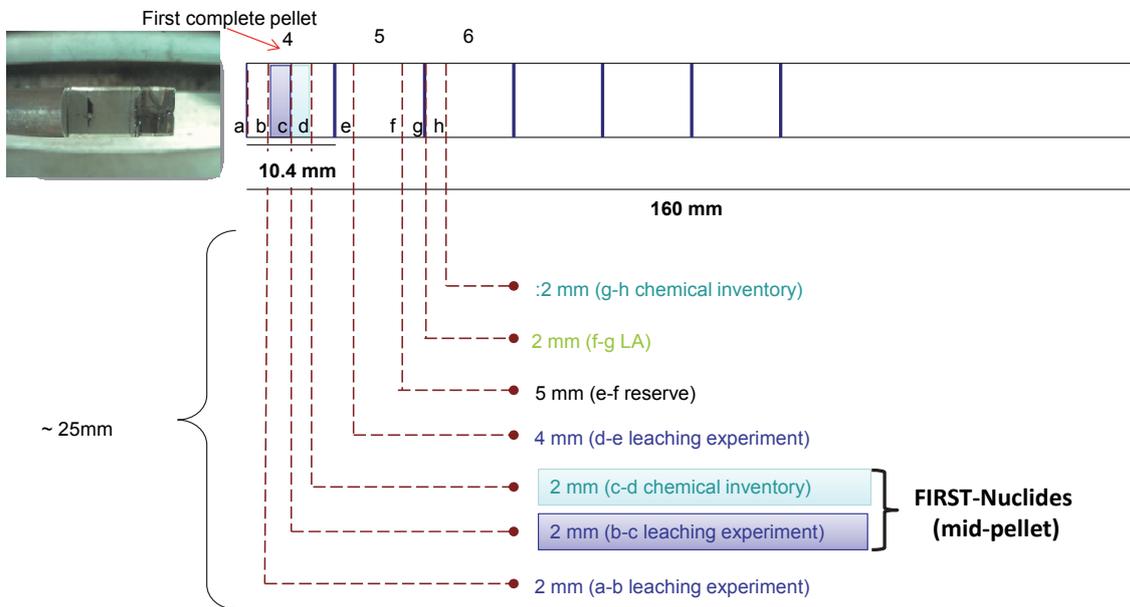
Figure 5: BWR54 cutting plan showing the position and the nominal length of samples cut mid-pellet for IRF leaching studies and for further characterisations (solid vertical lines indicate pellet-pellet gaps; dashed lines indicate cut positions).

Characterisation of fuel samples for IRF studies

Table 2 shows characteristic data of mid-pellet samples for IRF leaching experiments.

Table 2: Properties of mid-pellet samples prepared for IRF studies.

Fuel	Length mm	Pellet diameter mm	Weight total g	Weight fuel* g	Surface area** mm^2
BWR54	2.5±0.1	8.7±0.1	2.0613	1.6823	475
BWR42	2.8±0.1	9.4±0.1	2.3614	1.9269	555

(*) The weight of the fuel without cladding was estimated from previous experiments with BWR pellets and with the given density. It will be corrected after complete pellet dissolution performed before inventory determination.

(**) The surface area exposed was calculated taking into account the surface in contact with solution (both faces of the cut segment) and a roughness factor of 4.

Figure 6 and Figure 7 show macrographs of top and bottom sides of these leaching samples. In all pictures a crack network pattern is visible. This fuel cracking results in a larger surface area in contact with the aqueous phase and where corrosion processes and radionuclide release occur. Therefore, the geometric surface area of the cracks of the segments used in the leaching experiments was determined from cross sectional images taken with a digital colour camera installed in the hot cell.

Images were analysed using the software ImageJ (Rasband, 1997-2013). The colour information was used to enhance the contrast between the crack and the fuel surface by splitting the digital picture into the individual; red, green and blue channels. In our case the blue channel was used for area quantification. After setting the scale and calibration of the image, the wand (tracing) tool was used to delineate the outside boundaries of the cracks. The surface areas of the digitally traced boundaries were automatically calculated in each case and the ratio of the cracked area to the total geometric pellet area was obtained (Figure 6 and Figure 7). The ratio for the BWR54 sample is 4.4% and for the BWR42 sample 6.9%.
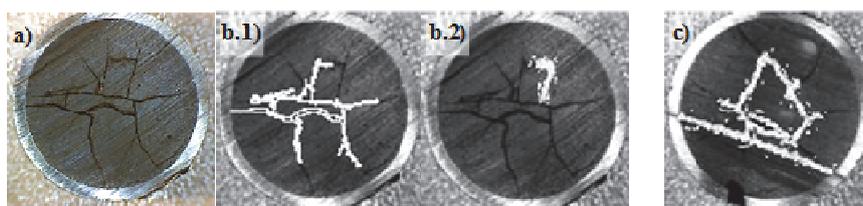

Figure 6: Macrograph of BWR54 fuel sample a)top side. b) Top and c) bottom surface with cracks marked. The top side cracked surface area estimated from image b.1) and b.2) was 2.7 mm^2. From the bottom side cracks were 2.5 mm^2 obtained (image c). For visibility reasons the crack markings are enlarged.
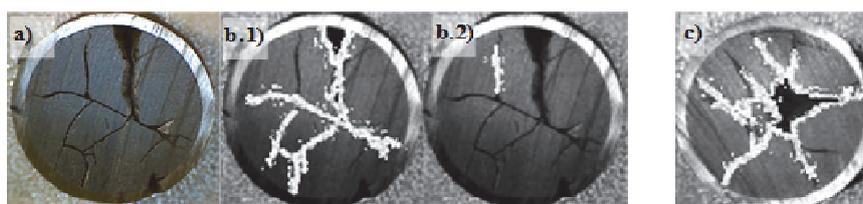
Figure 7: Macrograph of BWR42 fuel sample a)top side. b) Top and c) bottom surface with cracks marked. The top side cracked surface area estimated from image b.1) and b.2) was 3.2 mm^2. From the bottom side cracks were 6.6 mm^2 obtained (image c). For visibility reasons the crack markings are enlarged.

Conclusions and future work

After finalising the negotiations and signing of the agreements with the utilities, the fuel characterisation data and irradiation history were made available for the commercial spent fuels BWR42 and BWR54. These fuels are foreseen to be used for ^{18}O-tracer diffusion and IRF studies. From the latter segment, samples have been prepared and the morphological characterisation started. Powder samples for IRF studies have also been prepared and described elsewhere (Serrano-Purroy, 2013).

BWR42 samples for oxygen diffusion and water penetration studies (WP2) are still to be prepared and the morphological and chemical characterisation will be finalised and summarised in deliverable D1.3, in spring 2014.

Acknowledgement

References

Rasband, W.S. (1997-2013). ImageJ. U. S. National Institutes of Health, Bethesda, Maryland, USA, http://imagej.nih.gov/ij/.

Serrano-Purroy, D., Sureda Pastor, R., Colle, J.Y., Beneš, O., Naisse, F., Wiss, T., Konings, R.J.M., Wegen, D.H., Papaioannou, D., Gretter, R., Nasyrow, R., Rondinella, V.V., Glatz, J.P. (2013). JRC-ITU Contribution to Deliverable (D-N°: 1.2), Characterisation of Spent Nuclear Fuel Samples and Description of Methodologies and Tools to Be Applied in FIRST-Nuclides. JRC Scientific and Policy Report 83524, European Atomic Energy Community, Karlsruhe, Germany.

Wegen, D.H., Papaioannou, D., Gretter, R., Nasyrow, R., Rondinella, V.V., Glatz, J.P. (2013). Preparation of Samples for IRF Investigations and Post Irradiation Examinations from 50.4 GWd/tHM PWR fuel. In: 1st Annual Workshop Proceedings, 7th EC FP – FIRST-Nuclides. KIT SCIENTIFIC REPORTS 7639, 9th–11th October 2012, Budapest, Hungary, pp 193.

WP2: RIM AND GRAIN BOUNDARY DIFFUSION CONTRIBUTION FROM ITU

Paul Carbol, Ilaria Marchetti, Detlef H. Wegen, Antonio Bulgheroni

European Commission, Joint Research Centre, Institute for Transuranium Elements (EC)

* Corresponding author: Paul.CARBOL@ec.europa.eu

Abstract

The aim of this study is to measure the oxygen/water diffusion coefficient in irradiated UO_2 fuel under repository condition. The surface oxidation will be mapped by secondary ion mass spectrometry (SIMS) in order to assess grain boundaries, pores and micro-cracks for potentially preferential reaction with and intrusion of water. Using the combination of spent nuclear fuel, simulated groundwater and addition of H_2-gas (simulating anoxic corrosion of Fe-canisters) the study will take into account the effect of radiolysis and the counteracting UO_2-ε-particles catalysed H_2 reduction reaction. The experimental study is based on:

- static fuel corrosion experiments with ^{18}O-labeled water in presence of H_2,
- high-resolution profilometry and SIMS depth profiling of the fuel matrix
- solution analysis by ICP-MS

A summary of the work carried out at ITU, so far, for the WP2 task "Rim and grain boundary diffusion experiments" of the FIRST-Nuclides Project is reported here. In addition an updated work program is provided.

1. Literature review of spent fuel oxidation and oxygen diffusivity

The scientific literature was searched for open publications related to experiments or predictions of oxygen lattice and grain boundary diffusion coefficients with or without coupling to the oxidation of the irradiated fuel.

No publications were found related to the oxygen lattice and grain boundary diffusion in spent fuel under aqueous conditions. Relatively few publications were found connected to air oxidation of spent fuel. It should be noted that most that the reason to review non-aqueous oxidation of UO_2 is to establish what is known about oxygen diffusion in UO_2 grains and in grain boundaries at low temperatures. These papers are summarised in the next two paragraphs.

1.1. Air oxidation of UO_2 and spent fuel

The overall oxidation mechanism of spent fuel and UO_2 are quite different. The oxidation rate is much larger for irradiated fuel than for non-irradiated UO_2 materials. Irradiated light water reactor (LWR) fuel samples show parabolic kinetics similar to that of oxidation of UO_2 powder with particle size equal to the grain diameter. This means that spent fuel is characterised by rapid grain boundary oxidation, due to the fact that closely packed fission gas bubbles along grain boundaries create easy pathways for penetration of oxygen and thereby internal oxidation (Einziger and Woodley, 1985; Woodley, Einziger et al., 1988; Einziger, Thomas et al., 1992).

The overall rate of oxidation of spent fuel is therefore given by a combination of matrix and grain boundary oxidation (McEachern, 1997). Initially the oxidation rate is slow because only the geometric surface area is

available for oxidation, but the rate continuously increases until all grain boundaries are oxidised and the total grain surface area becomes accessible to further oxidation.

The oxidation of UO_2 affects the mechanical stability of the fuel. Formation of U_3O_8 in a defected fuel element can lead to splitting of the fuel and detachment of grains due to the 36% volume increase as a consequence of UO_2 oxidation. The formation of the intermediate U_3O_7 is considered to have less impact on fuel integrity (Tempest, Tucker et al., 1988) but the kinetics of its formation strongly affects the sub-sequent oxidation step, as for non-irradiated UO_2.

In the oxidation of spent fuel, the U_4O_9 phase is encountered rather than U_3O_7 but with stoichiometry as high as $\sim UO_{2.4}$. A possible explanation is that the presence of fission products stabilizes the U_4O_9-type cubic structure (McEachern and Taylor, 1998). In fact, the same behaviour is encountered in SIMFUEL (Matzke, 1996). SIMFUEL is a chemical analogue of irradiated UO_2. It consists of UO_2 mixed with non-radioactive elements representing fission products and actinides. The elements are dry-mixed with UO_2 powder in amounts equivalent to certain nuclear fuel burn-up.

Spent fuel oxidation at temperatures above 100-300 °C seems to occur slightly faster than UO_2 oxidation but with a higher activation energy than that of UO_2 (134 kJ/mol instead of 104 kJ/mol). With decreasing temperature the rate of the two processes become almost identical. Considering the high concentration of defects in spent fuel, it is not likely that the oxidation rate of spent fuel will be lower than that of UO_2 indicating that the activation energy should not be used for extrapolation to room temperature (Grambow, 1989).

On exposure in low temperature air, a standard pressurised water reactor (PWR) spent fuel initially oxidizes by forming U_4O_9 along UO_2 grain boundaries beginning simultaneously from the UO_2 grain corners without indication of enhancement at the fragment surfaces (Thomas and Einziger, 1992). The U_4O_9/UO_2 interface advances then into the grains with an average rate that was measured at 195 °C to be 4.7 nm per hour.

As the fuel oxidizes from UO_2 to the denser U_4O_9, the grains contract, and thus opens up the grain boundaries. However, some of the stress of this phase transition is accommodated by cracking of the oxidized outer "rind" of individual grains (Thomas and Einziger, 1992), thereby reducing the effective grain size. Even more cracking occurs during the formation and spallation of U_3O_8. The original distribution of grain sizes present from the fabrication process, the variable grain growth that occurs due to axial and radial temperature distributions, and the effective reduction in grain size caused by cracking, result in a log-normal distribution of grain sizes. Stout et al. (1990) have shown that the rate of oxidation depends inversely upon the grain size. Thus, models for the oxidation of U_4O_9 to U_3O_8 must account for both the log-normal distribution of grain sizes and the burn-up dependence of the activation energy to accurately predict the oxidation of spent fuel in a repository.

Significant U_3O_8 formation due to dry air oxidation is not expected to occur in an unsaturated geological repository provided that the maximum temperature does not exceed 150 °C, after spent fuel exposure to oxygen (Kansa, 1999). This finding is predicted to be valid also for high burn-up fuels that have undergone restructuring and tend to have rather small UO_2 fuel grains. The exponential temperature dependence of the activation energy for U_3O_8 formation is the dominating mechanism.

1.2. Grain-boundary diffusivity in UO₂ and spent fuel

It has been reported (Woodley, Einziger et al., 1988; Grambow, 1989) that in spent fuel the penetration of oxygen into grain boundaries is much faster than in UO_2 and that most likely the grain boundary oxidation can be described as a diffusion process.

Weight-gain curves obtained by Einziger and Woodley (Einziger and Woodley, 1985; Einziger and Woodley, 1987) from oxidation of PWR fuel with ~3 % burn-up could be used to obtain an estimation of the diffusion coefficient of oxygen in grain boundaries at 200 °C with a factor two of uncertainty (Grambow, 1989):

$$D_B(200\ °C)= 1.4·10^{-13}\ m^2/s$$

According to Woodley (Woodley et al., 1988) the activation energy for grain boundary oxidation is similar to that for fuel matrix, i.e. 104 kJ/mol. Applying this value, an estimation of the grain boundary diffusion coefficient at 25 °C would give:

$$D_B(25\ °C)= 2.3·10^{-20}\ m^2/s$$

Grambow (Grambow, 1989) speculate that within the uncertainty of the data the dependence of the calculated diffusion coefficient on the transport mechanism can be neglected. A comparison of the oxygen diffusion coefficients, at 200 °C, in grain boundaries (D_B) with UO_2 lattice (D_L), shows that the diffusion in the grain boundaries is 4-5 orders of magnitude faster than lattice diffusion. Nevertheless, it would take 800 years for oxygen to penetrate to a fuel depth equal to the grain diameter (25 μm in this calculation) and therefore grain boundary oxidation at room temperature should be an extremely slow process and almost impossible to be observed.

Nevertheless, it is important to consider that Grambow's estimation is highly speculative, since it depends strictly on the activation energy used for the extrapolation, which is difficult to estimate.

Despite that most other studies of oxygen diffusion in UO_2 minerals show that grain boundary diffusion is much faster than lattice diffusion (Cole et al., 2001), many authors reported that measured diffusivities in polycrystalline UO_2 are approximately equal to those in a single crystal of UO_2 (Marin et al., 1969; Sabioni et al., 2000), and therefore suggested that grain boundary diffusion does not play a major role and oxygen diffusion in uraninite largely depends on temperature and stoichiometry.

Fayek *et al*. (Fayek et al., 2011) speculate that the assumed single crystals used in those studies of oxygen diffusion in uraninite were not real single crystals or that the methods used to separate lattice versus grain boundary diffusion were inadequate. In fact, Fayek et al. (2011) reported that their experimental findings showed evidence of two diffusion mechanisms: an initial, extremely fast mechanism that overprinted the oxygen isotopic composition of the entire crystals regardless of temperature and may reflect diffusion along sub-grain boundaries and micro-fractures (e.g., fast-path diffusion); and a slower volume-diffusive mechanism in which oxygen may have moved through defect clusters that displaced or ejected nearest-neighboring oxygen atoms to form two interstitial sites and two partial vacancies, and by vacancy migration.

Marchetti et al., 2011 exposed a UO_2 pellet to ^{18}O-labelled water at room temperature for 3 months and studied the ^{18}O-tracer diffusion into the UO_2 lattice and grain boundaries using secondary ion mass spectrometry. Depth profiling up to 22 μm beneath the pellet surface indicated a combination of oxygen diffusion into the UO_2 lattice and water species diffusion along grain boundaries and behaving as high-diffusivity-paths. The relevant coefficients were estimated to be ~1.4·10^{-24} m^2/s for lattice diffusion and ~2.3·10^{-16} m^2/s for grain boundary diffusion.

It can be concluded that determination of grain boundary diffusion coefficient of oxygen in spent fuel is difficult to be obtained:

- from SF oxidation in air at elevated temperatures >200 °C as the oxidation mechanism is different than in aqueous spent fuel corrosion (complicated by radiolysis and redox reactions).
- from UO_2 and UO_2 minerals diffusion experiments as the stabilizing oxidation effect of fission products (mainly trivalent lanthanides) in the grain boundaries are missing. On the other hand, data from ^{18}O diffusion into SIMFUEL (UO_2 and presence of lanthanides) under semi-oxidative conditions indicate an oxidation of the SIMFUEL surface layer to U_4O_7 and a $[U]_{tot}$ of ~10^{-10} M and could therefore be partly representative for SF (still missing the radiolysis component) (Marchetti, 2013a).

In general, data for grain boundary diffusion of oxygen into UO_2 or UO_2 minerals measured at room temperature are scarce (Marchetti et al., 2013b).

Finally, it should be pointed out that having searched the literature we could not find any room temperature data for grain boundary diffusion coefficient of oxygen in spent fuel obtained from aqueous studies, neither in oxidising or reducing conditions.

2. Selection, characterization and preparation of materials and set-up tools

2.1. Spent nuclear fuel sample

One standard UO_2 boiling water reactor (BWR) fuel with an average burn-up of 42.2 GWd/t$_{HM}$ will be used in this study. The UO_2 fuel has, before irradiation, a standard enrichment of 3.67 wt.% ^{235}U. The ownership of the 160 mm long fuel rod segments has been transferred from EnBW Kernkraft GmbH to JRC-ITU. Comprehensive in-core fuel characterisation data of the selected fuel segment will be published in the FIRST-Nuclides WP1-report (Wegen et al., 2013).

From the 160 mm long selected rod section a 50 mm long segment has been cut and is stored under oxygen free conditions. One axial part of the fuel segment will be polished. There after a 1-mm thick slice will be cut from this segment and de-cladded right before the start of the diffusion experiment. The diffusion experiment will be carried out using a fuel fragment, with one side polished and the other un-polished.

2.2. Physical and chemical characterization of the fuel sample

The sample will be characterized using Scanning Electron Microscopy (SEM), with a JEOL 6400 (Japan) microscope, modified to analyze active samples. The thickness of the high burn-up structure (HBS), mean grain size and the percentage of the HBS in the samples will be determined from SEM images, using the UTHSCSA *ImageTool* program (developed at the University of Texas Health Science Center at San Antonio, Texas). A comprehensive description of the planned characterization methodology can be found in (Serrano et al., 2012).

The chemical inventory of the used fuel segment will be determined experimentally. The fuel sample will be dissolved in acid, diluted and the aliquots analysed by high-resolution ICP-MS (Element 2, Thermo Fisher, Germany) and γ-spectroscopy (HPGe-detector, EG&G Ortec, USA). In addition, the theoretical inventories will be calculated using the ORIGEN-ARP code.

2.3. Autoclave

During hot cell refurbishment of the MOX-autoclave, intended for this experiment, a Ti-welded tube joint broke. Unfortunately the weld broke at a vital place on the autoclave and as the autoclave was contaminated it could not be taken out of the hot cell and re-welded.

From a safety point of view it was assessed that replacement of only the broken part was not allowed since the complete autoclave setup must, after exchange of pressure parts, be pressure tested to be authorised for use. As it is forbidden to make pressure tests (up to 60 bar) inside our hot cells this was not an option.

It was immediately decided that the old autoclave needed to be replaced with a new one but with a new design to avoid the same problem. To avoid a lengthy safety approval procedure the new autoclave (pressure vessel and lid) is identical with the broken autoclave. A safety approval exists for this type of autoclave. The new autoclave has been purchased but the delivery time is several months long. The CAD-design of the new autoclave head (the part where all the valves, pressure gauges and safety valves are located) and adaption for hot cell manipulation is completed (Figure 1).
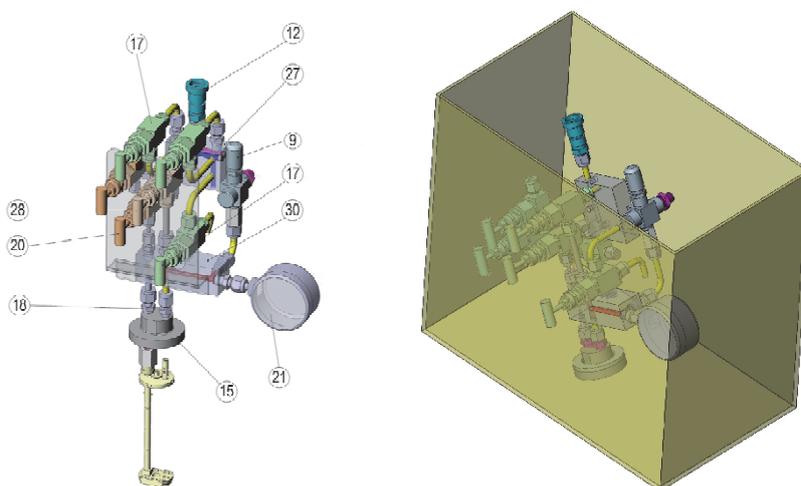
Figure 1: Design of autoclave head (left) and the tested dimension of the head in the hot cell conveyer container (right).

The purchase of the autoclave head parts has been made. Parallel with the autoclave purchase the head part has been assembled (Figure 2).

Figure 2: Manufactured autoclave head.

In order to ensure reliable Ti-welds, as Ti welding must be performed with absence of O_2 (the requirement is <12 ppm O_2) a new welding glovebox has been manufactured (Figure 3).

The inside of the autoclave will be fitted with a PEEK (polyether ether ketone) insert (vessel, lid and dip-tube) to minimise the influence of metallic (foremost Fe) surfaces on the fuel corrosion process.
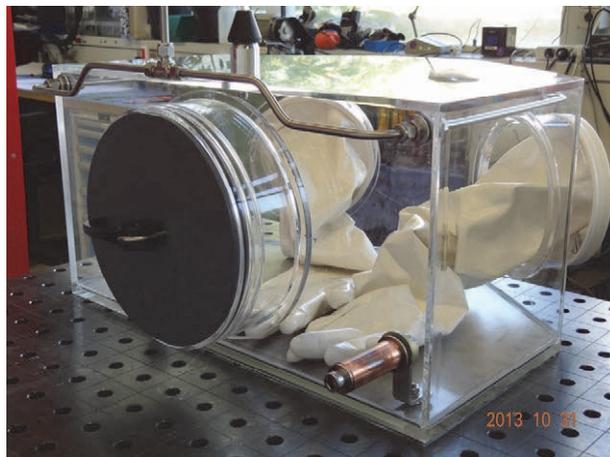

Figure 3: *Glovebox for oxygen-free welding (≈7ppm O_2 and <1ppm H_2) of Ti parts.*

2.4. $H_2^{18}O$ solution

The ^{18}O-labelled water has been purchased and delivered to ITU during 2012.

2.5 SIMS analysis of spent nuclear fuel sample

After 9 months exposure of the fuel fragment to approximately 100 ml $H_2^{18}O$ in the autoclave at 40 bar H_2 the experiment will be terminated and the fuel fragment transferred to a SIMS holder.

The standard procedure is that the fuel fragment is embedded in a resin and thereafter polished. This procedure is unsuitable since we want to study the corroded surface and can therefore not polish the fuel surface. Additionally, it is planned to analyse both sides of the fragment, since the fragment will have one polished side and one non-polished (see sub-section 2.1). To meet these experimental requirements a special SIMS holder was designed and manufactured at ITU (Figure 4). The ^{18}O-depth profiling will be made using the shielded SIMS (Cameca 6F, France).

Figure 4: *SIMS holder for spent fuel fragment.*

3. Studies of ^{18}O diffusion into poly-crystalline UO$_2$

In parallel with the preparation work for this experiment we have continued our studies of ^{18}O diffusion into non-irradiated poly-crystalline UO$_2$. The outcome of these studies will help us to interpret the data from the ^{18}O diffusion experiments into spent fuel. The outcome can be found in (Marchetti, 2013a; Marchetti et al., 2013b). Further publications are in progress.

4. Updated work program

An updated time schedule for the rim and grain boundary task is given in Figure 5 In order to recover the time lost during fabrication of the new autoclave the contact time, between the spent fuel and the leachant, has been reduced from planned 12 months to 9 months. A shorter contact time was predicted to give a too small ^{18}O-diffusion into the spent fuel.
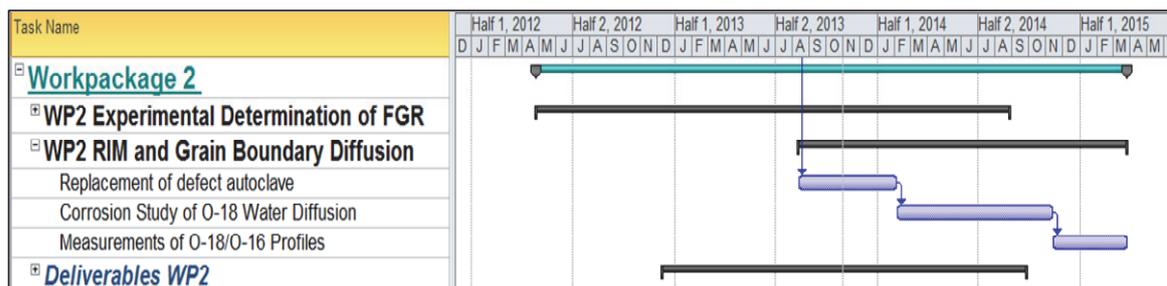
Figure 5: *Updated time schedule for the WP2: Rim and grain boundary project.*

The duration of the experiment goes beyond the end of the FIRST-Nuclides project. This issue was addressed to the coordinator. As was decided at the EXCOM meeting of the FIRST-Nuclides in Antwerp (Duro et al., 2013) an extension of CP FIRST-Nuclides over the planned end date (31st Dec. 2014) is not considered. WP2 will be extended until the end of the project. JRC-ITU will provide all data obtained until month 33. A paper on grain boundary effects is expected to be drafted in the first semester of 2015.

Acknowledgement

References

Cole, D.R., S. Chakraborty (2001). Rates and mechanisms of isotopic exchange. Reviews in Mineralogy and Geochemistry 43, 83-123.

Duro, L., et al. Minutes of the 4th ExCom meeting held during the 2nd Annual Workshop of the FIRST-Nuclides project, 5th November 2013, Antwerp, Belgium.

Einziger, R.E., Woodley, R.E. (1987). Predicting spent fuel oxidation states in a tuff repository. Westinghouse Hanford Company, Richland, WA, USA.

Einziger, R.E., Woodley, R.E. (1985). Low temperature spent fuel oxidation under tuff repository conditions. Westinghouse Hanford Company, Richland, WA, USA.

Einzigera, R.E., Thomasa, L.E., Buchanana, H.C., Stoutb, R.B. (1992). Oxidation of spent fuel in air at 175 to 195°C. J. Nucl. Mater. 190(0): 53-60.

Fayeka, M., Anovitzb, L.M., Colec, D.R., Bostick, D.A. (2011). O and H diffusion in uraninite: implications for fluid-uraninite interactions, nuclear waste disposal, and nuclear forensics. Geochim. et Cosmochim. Acta 75(13), 3677-3686.

Grambow, B. (1989). Spent fuel dissolution and oxidation. An evaluation of literature data. SKB Technical Report. Swedish Nuclear Fuel and Waste Management Co., Stockholm, Sweden.

Kansa, E.J. (1999). Grain size and burn-up dependence of spent fuel oxidation: Geological repository impact. Materials Research Society Symposium - Proceedings

Marchetti, I., Belloni, F., Himbert, J., Carbol, P., Fanghänel, Th. (2011). Novel insights in the study of water penetration into polycrystalline UO_2 by secondary ion mass spectrometry. J. Nucl. Mater. 408, 54-60.

Marchetti, I. (2013a). Characterisation of water penetration into polycrystalline UO_2. PhD- thesis defended at Ruprecht-Karls-Universität, Heidelberg, Germany (19 April, 2013).

Marchetti, I., Carbol, P., Himbert, J., Belloni, F., Fanghänel, T. (2013b). Room-temperature diffusion coefficients for oxygen and water in UO_2 matrices: a SIMS study. Surf. Interface Anal. 45, 360-363.

Marin, J.F., Contamin, P. (1969). Uranium and Oxygen Self-Diffusion in UO_2. J. Nucl. Mater. 30, 16-25.

Matzke, H. (1996). Analysis of the structure of layers on UO_2 leached in H_2O. J. Nucl. Mater. 238(1), 58-63.

McEachern, R.J., Taylor, P. (1998). A review of the oxidation of uranium dioxide at temperatures below 400°C. J. Nucl. Mater. 254(2-3), 87-121.

McEachern, R.J. (1997). A review of kinetic data on the rate of U_3O_7 formation on UO_2. J. Nucl. Mater. 245(2-3), 238-247.

Sabionia, A.C.S., Ferrazb, W.B., Millotc, F. (2000). Effect of grain-boundaries on uranium and oxygen diffusion in polycrystalline UO_2. J. Nucl. Mater. 278(2), 364-369.

Serrano-Purroy, D., Clarens, F., González-Robles, E., Glatz, J.P., Wegen, D.H., de Pablo, J., Casas, I. Giménez, J., Martínez-Esparza, A. (2012). Instant Release Fraction and Matrix Release of High Burn-up UO_2 Spent Nuclear Fuel: effect of High Burn-up Structure and leaching solution composition, J. Nucl. Mater. 427, 249-258.

Stout, R. B., Shaw, H.F., Einziger, R.E. (1990). Statistical Model for Grain Boundary and Grain Volume Oxidation Kinetics in UO_2 Spent Fuel. Mat. Res. Soc. Symp. Proc. Vol. 176, 475-488.

Tempest, P.A., Tucker, P.M., Tyler, J.W. (1988). Oxidation of UO_2 fuel pellets in air at 503 and 543 K studied using X-ray photoelectron spectroscopy and X-ray diffraction. J. Nucl. Mater. 151(3), 269-274.

Thomas, L.E., R.E. Einziger (1992). Grain Boundary Oxidation of Pressurized-Water Reactor Spent Fuel in Air. Materials Characterization 28, 149-156.

Wegen, D.H. et al. (2013). FIRST-Nuclides WP1 report, delivery D1.3.

Woodley, R.E., R.E. Einziger *et al.* (1988). Measurement of the oxidation of spent fuel between 140°C and 225°C by thermogravimetric analysis. WHC Technical Report, Westinghouse Hanford Company**: 84.**

WP3. DISSOLUTION BASED RELEASE

IRF CORROSION TESTS OF COMMERCIAL UO₂ BWR SPENT NUCLEAR FUEL: PRELIMINARY RESULTS

Daniel Serrano-Purroy[1*], Laura Aldave de las Heras[1], Rosa Sureda[2],
Jean Paul Glatz[1], Vincenzo V. Rondinella[1]

[1] European Commission, Joint Research Centre, Institute for Transuranium Elements (EC)
[2] Fundació CTM Centre Tecnològic (ES)

* Corresponding author: Daniel.serrano-purroy@ec.europa.eu

Abstract

This report summarizes the work carried out at ITU in the frame of WP3 during the second year of the FIRST-Nuclides project. It includes both preliminary IRF results with SNF cladded pieces under oxidising conditions and recent developments in ^{79}Se and ^{126}Sn determinations.

Introduction

In the frame of the FIRST Nuclides project, ITU's main objective in WP3 is the quantification of the instant/fast release fraction of fission products into bicarbonated aqueous phase (19 mM NaCl + 1 mM NaHCO₃) during corrosion leaching test using a commercial BWR spent nuclear fuel. The work will be carried out using samples from the same SNF but with different morphologies: cladded pieces of about 2 mm length and powder samples from the centre and the periphery (enriched in high burnup structure) of the fuel.

During the reporting period and according to a prepared cutting plan, two neighbouring cladded pieces from the middle of a pellet were cut: one to carry out the corrosion experiment and one to chemically determine the inventory by acid dissolution. In addition some extra pieces of approximately 2 cm of cladded fuel were also cut and will be used to prepare the required amount of powder samples.

After taking macroscopic views of the samples, the experiment with the cladded piece was started beginning of the summer and preliminary results are presented in this report.

Moreover, some effort was dedicated to develop Se and Sn determination methodologies and preliminary results are also reported.

Experimental

Cladded segment samples

According to a prepared cutting plan, two neighbouring cladded pieces of approximately 2 mm length selected from the middle of a pellet were cut: one to carry out the corrosion experiment and one to chemically determine the inventory by acid dissolution. Whereas the experimental inventory determination will be carried out at the end of this year, the experiments with the second piece already started beginning of last summer.

Table 1 shows the sample characteristics, the experimentally set S/V ratio and some important irradiation history parameters. These parameters are reported because of the importance they will have for later comparisons with experiments carried out by other partners within the frame of the project.

Table 1: SNF cladded sample selected for the corrosion experiment.

Sample	42BWR
Length (mm)	2.8 ± 0.1
Diameter without cladding (mm)	9.4 ± 0.1
Weight with cladding (g)	2.3614 ± 0.0001
Weight without cladding (g)[*]	1.9269 ± 0.0001
Surface area (mm^2)[**]	472 ± 1
S/V (m^{-1})	11 ± 1
FGR (%)	2.3
Burnup (GWd/t$_{HM}$)[***]	45
Av. Linear Power Rate (W/cm)	215

[*]The weight of the pellet without cladding was estimated from previous experiments with BWR pellets. It will be corrected after complete pellet dissolution for inventory determination.

[**]The surface area exposed was calculated taking into account the surface in contact with solution (both faces of the slice) and a roughness factor of 3.4 (Iglesias et al., 2008).

[***]Estimated from gamma scanning and cutting plan positions. It will also be experimentally determined during the course of the project.

Figure 1 shows macroscopic views of both sides the selected segment. A typical irradiation cracking profile can be seen. However, in one of the faces a small part of the pellet fell during the sample preparation. The amount of cracks in relation to the total surface area is calculated to be 1.7 and 4.2% in each face.

Figure 1: Two-face macroscopic view of the selected SNF cladded piece.

Experimental set-up

Starting beginning of last summer, a static corrosion experiment is being carried out under oxidizing conditions at hot-cell temperature (25 ± 5 °C). The selected SNF cladded segment is leached in bicarbonate water (19 mM NaCl + 1 mM NaHCO$_3$). The sample is suspended with a platinum (element that does not interfere with the

measurements) wire from the top of a 50 mL plastic bottle (Figure 2) and continuously stirred (Vibrax, IKA, Germany) during the complete duration of the experiment (see Figure 3).

*Figure 2:* SNF sample suspended in a Pt wire.
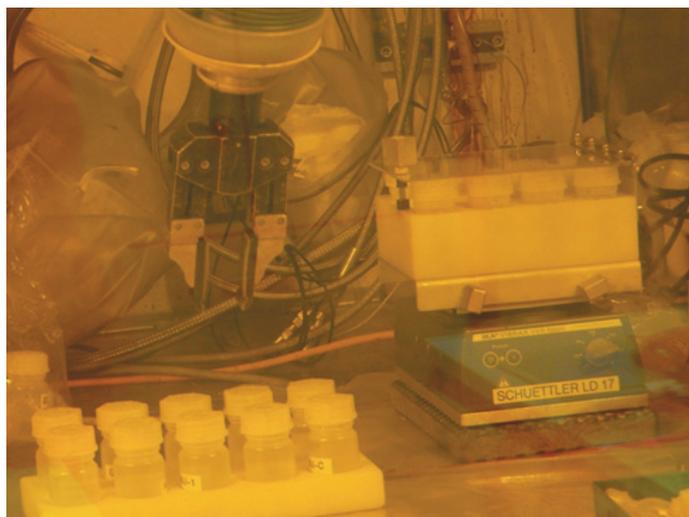
Figure 3: Experimental set-up (orbital stirrer).

The solution is replaced completely at pre-set intervals, shorter at the beginning of the experiment. Non-filtered solutions are further diluted in 1 mol/L nitric acid according to the levels of concentration and dose rate required for subsequent analysis by ICP-MS.

No initial washing of the sample by aqueous solution is performed to avoid pre-leaching of the fuel sample and to prevent losses of IRF information at the very beginning stage of corrosion.

The pH is measured at each sampling interval with an Orion 525A+ pH-meter and a gel pH Triode L/M, (9107BN, Thermo-Electron, USA. The pH electrode is calibrated with commercial pH buffer solutions (METLER TOLEDO Inc., USA; pH 4.01 (Ref. 501307069), pH 7.00 (Ref.51302047), pH 9.21 (Ref. 51302070)).

Based on these results, the behavior of U as matrix main component and of some selected IRF elements (Cs, Rb, Sr, Mo and Tc) is discussed.

Data treatment

The total released or cumulative moles in solution for element *i*, *moles(i)*, is calculated considering the total amount of radionuclide *i* removed in each sampling (Equation 1):

$$moles(i) = \sum_0^n moles_{sample}(n, i) \qquad (1)$$

where *moles$_{sample}$ (n,i)* correspond to the moles in solution before each complete replenishment *n*.

The cumulative concentration *cumC$_i$* of an element *i* in moles/dm^3 is then calculated as:

$$cumC_i = \frac{moles(i)}{V} \qquad (2)$$

where *V* corresponds to the average volume of the dissolution samples in dm^3.

The Cumulative Fraction of Inventory of an element *i* released in the Aqueous Phase (Cum*FIAPi*) is given by Equation 3.

$$CumFIAP_i = \frac{m_{i,aq}}{m_{i,SNF}} = \frac{c_i \, V_{aq}}{m_{SNF} \, H_i} \qquad (3)$$

where *mi,$_{aq}$* is the mass of element *i* in the aqueous phase in g, *mi,$_{SNF}$* the mass of element *i* in the SNF sample in g, *m$_{SNF}$* the mass of SNF used in the experiment in g, *H$_i$* corresponds to the fraction of inventory for the nuclide *i* in g/g, *c$_i$* is the cumulative concentration of element *i* in solution in g/mL and *V$_{aq}$* is the volume of solution in mL.

The Fractional Release for an element *i* Normalised to the total Surface area (*FNS$_i$*) is:

$$FNS_i = \frac{FIAP_i}{S} \qquad (4)$$

where *S* is the total surface area (m^2).

The Fractional Release Normalised to Uranium for an element *i* (FNU$_i$) is given by Equation 5.

$$FNU_i = \frac{FIAP_i}{FIAP_U} \qquad (5)$$

where *FIAP$_i$* and *FIAP$_U$* are the FIAP of element *i* and uranium, respectively.

Finally, the Instant Release Fraction for an element *i* (*IRF$_i$*) is given by Equation 6.

$$IRF_i = FIAP_i - FIAP_U \qquad (6)$$

Results

pH evolution

During the experiment pH measurements are carried out at each sampling time. Figure 4 shows the pH evolution versus the contact time of the sample with the solution (not to mix up with the total experimental time which

corresponds to the cumulative sampling time and that will be used in some of the later discussions). The pH decreases from initially 8.4 at short contact times down to 7.8 for contact times bigger than 5 days. This might be a result of the uranium oxide surface buffer capacity.
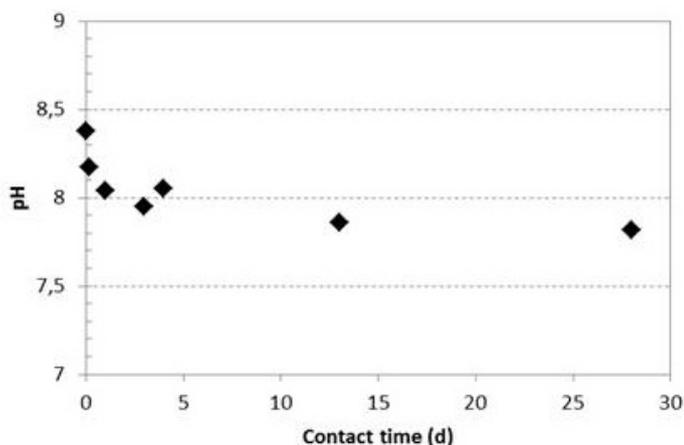

Figure 4: pH evolution vs. sample contact time for each complete replenishment.

Concentration in solution (speciation and secondary phase formation studies)

Table 2 shows measured concentrations in solution at each contact sampling time.

Table 2: Elemental concentration in solution (moles dm^{-3}) at the end of each sampling contact time.

Time (d)	0,01	0,16	1,00	3,00	4,00	13,00	28,00
Rb	7,4E-09	1,0E-08	1,4E-08	5,7E-09	1,2E-08	3,4E-08	3,0E-08
Sr	5,5E-09	1,3E-08	2,6E-08	3,0E-08	3,4E-08	6,5E-08	4,5E-08
Mo	1,1E-07	1,1E-07	1,5E-07	1,2E-07	1,9E-07	2,9E-07	2,4E-07
Tc	2,4E-08	1,7E-08	2,1E-08	1,8E-08	3,1E-08	5,5E-08	4,7E-08
Cs	3,9E-07	2,0E-07	1,7E-07	1,6E-07	3,1E-07	2,5E-07	1,8E-07
U	5,8E-07	1,8E-06	3,0E-06	2,8E-06	4,9E-06	8,2E-06	6,7E-06

*Note that isotopic concentrations can be calculated from the inventory determination reported in WP1. These numbers are reported with the appropriate number of significant digits.

In order to obtain reliable results it is important to avoid the presence of uranium secondary phase formation throughout the experiment. Calculations of uranium speciation in bicarbonate water (19 mM NaCl + 1 mM $NaHCO_3$) were assessed using the geochemical code CHESS (Van der Lee et al., 2002). Most internationally known databases have been made available for use with CHESS, here among the EQ3/6, MINTEQ, PHREEQC and NEA databases. The CHESS default database is based on a moderated version of the LLNL's EQ3/6. For this study, both the default CHESS and the NEA databases were used. A summary of the thermodynamic stability constants used for U can be provided under request. All calculations were based assuming the local equilibrium, oxidising conditions and a temperature of 25 °C. Figure 5 shows the uranium speciation under the experimental conditions. Measured uranium concentrations at each sample are also included.

As can be seen, in all the samples analysed uranium concentration in solution is well below uranium secondary phase formation levels.
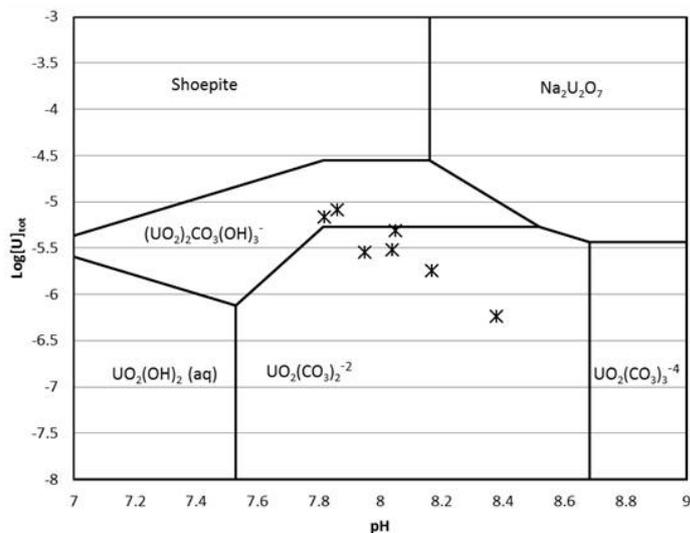

Figure 5: *Speciation diagram of uranium in the studied experimental conditions (NEA and CHESS databases were used for the calculation). Measured uranium concentrations for each sample are also included.*

To properly follow the evolution of the experiment, the cumulative concentration was calculated according to equation 2, see Figure 6.
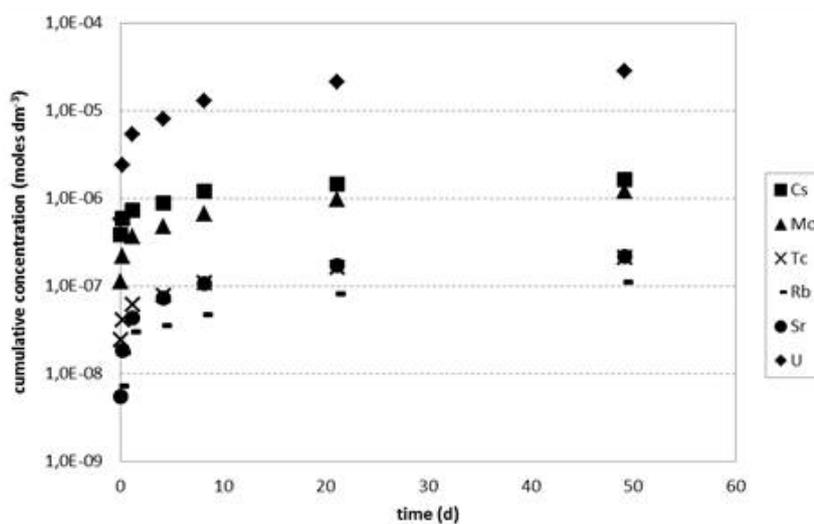
Figure 6: Elemental cumulative concentration (moles/dm) vs time.

The dissolution release of both matrix (uranium) and IRF (Cs, Mo, Tc, Rb and Sr) is faster at the beginning of the experiment and slows down at the end. In the case of uranium the initial higher release is attributed to surface preoxidation while for the IRF elements this is attributed to the fraction immediately available for dissolution after contacting the sample with the aqueous solution, i.e. segregated fraction to the gap and the cracks. The second dissolution mechanism, slower and long-term, is attributed to matrix dissolution in the case of uranium and to internal grain boundary IRF dissolution for the other elements.

However, it is difficult to go further at this point of the experiment and draw anymore conclusions on long term matrix congruent elemental dissolution; more points are needed to accurately calculate normalised dissolution rates. This work will be done at the end of the experiment in the coming months.

Cumulative FIAP(%) and FNU

In addition to cumulative concentration, and taking into account the theoretical inventory, cumulative FIAP values were also calculated (see Figure 7).
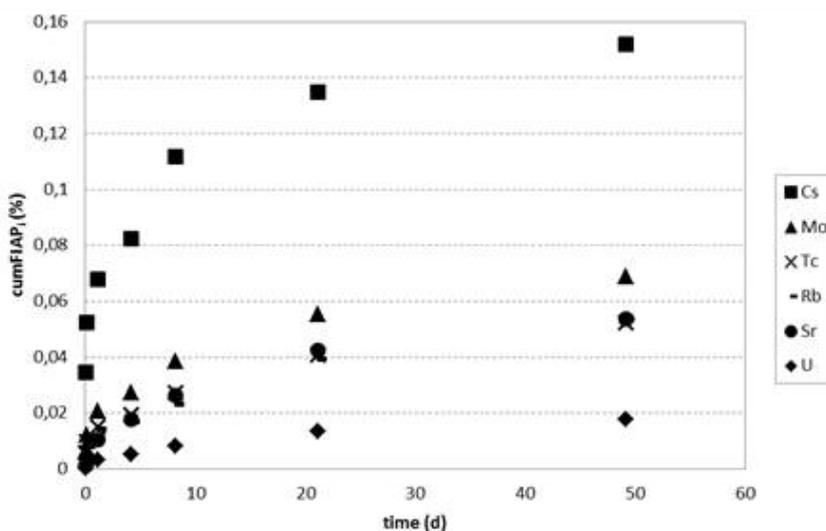

Figure 7: *Cumulative FIAP(%) vs time.*

Cs is the element with the biggest release, followed by Mo, Tc, Rb and Sr with similar release. Finally, uranium presented the lowest release.

In addition, FNU at each sampling time was also calculated, see Table 3. As expected, all the studied IRF elements have FNU higher than 1, being especially significant the case of Cs. The longer the experiment runs the smaller is the calculated FNU indicating that with enough time the IRF will be completely dissolved an all these elements will approach matrix dissolution.

Table 3: *FNU at each sampling solution versus cumulative sampling time.*

Time (d)	0,01	0,17	1,17	4,17	8,17	21,17	49,17
Rb	8	3	3	1	2	2	3
Sr	3	2	2	3	2	2	2
Mo	14	4	3	3	3	3	2
Tc	13	3	2	2	2	2	2
Cs	86	140	7	7	8	4	4

Finally, and based on Equation 6, IRF(%) was calculated taking into account cumulative FIAPs, Figure 7.
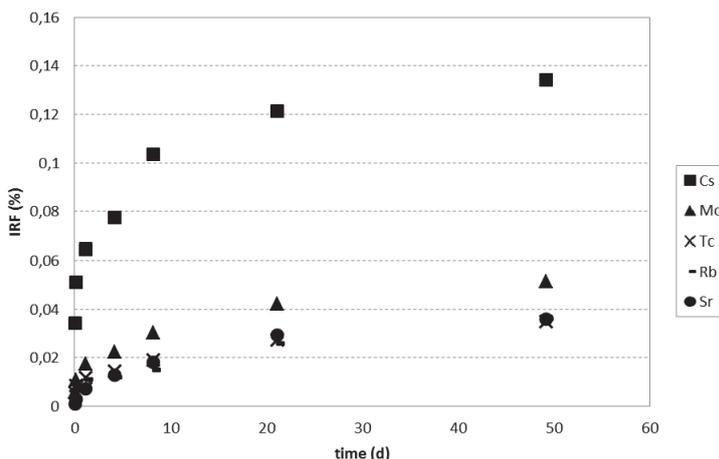
Figure 7: IRF(%) vs. time.

After 50 days of experiment, the highest and most significant IRF(%) corresponds to Cs (0.134%), followed by Mo (0.051%) and Tc, Rb and Sr (0.035%). These numbers are only indicative, they are not normalised by the specific surface area and the amount of fuel used to calculate the FIAP is the total one of the piece selected. Careful comparison with the literature and the other partner's findings will be carried out at the end of the experiment.

Se speciation in leachates

A method for the determination of ^{79}Se species at trace levels by high resolution ICP-MS coupled to an automated chromatographic system has been developed for the determination of Se species. The FAST system uses one high purity valve to take up an aliquot of sample and separate Se species on a PFA column packed with an ion exchange resin. Se species are eluted into a PFA nebulizer attached to the ICP-MS spray chamber. In Figure 8 are shown the Se species elution profiles at different concentration in bicarbonate water (19 mM NaCl + 1 mM NaHCO$_3$) at pH 7.6 in synthetic analogue spent nuclear fuel leachates as well as the analytical figures of merit of the method developed.

| Table 1: Analytical figures of merit:		
	Se (IV)	Se(VI)
Repeatibility (%)	0.2 -1	
Total Se		
Detection limits (pg/g)	23.5	25.3
Absolute amount (pg)	5.9	6.3
^{82}Se		
Detection limits (pg/g)	2.2	2.3
Absolute amount (pg)	0.5	0.6
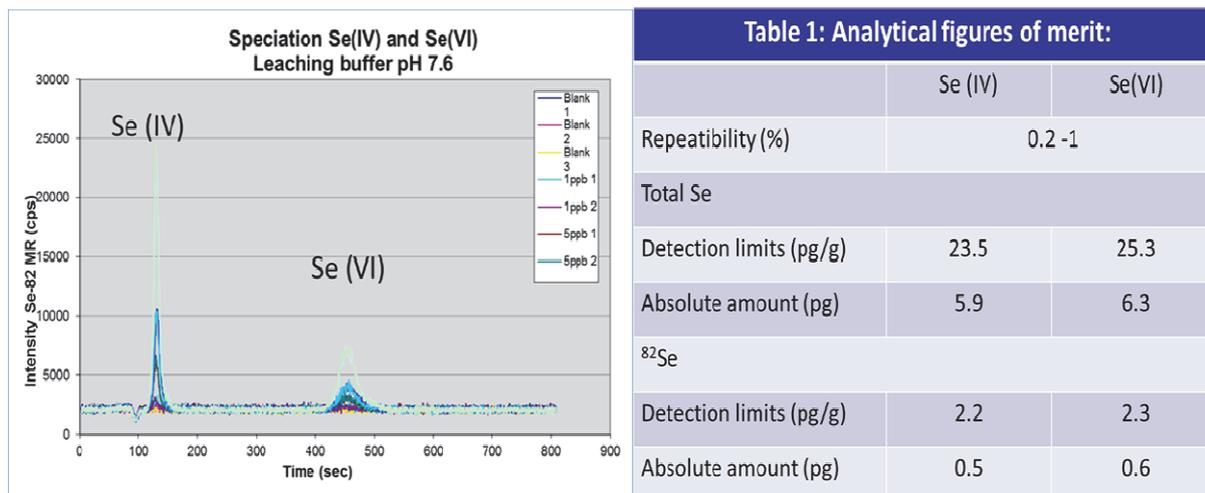
Figure 8:. (A) Se species elution profiles at different concentrations. (B) Analytical figures of merit.

The new method offers an easy and efficient determination of Se species at low pg/g concentrations in analogue spent nuclear fuel leachates. It shows high potential for application in real spent fuel leachates, the detection limits being below the expected concentration levels. Although the method only detects [82]Se, which is not relevant for the safety case, it does allow to calculate the amount of [79]Se present using the K-Origen code. In the near future this developed method will be applied using a new ICP-MS equipped with a collision/reaction cell that overcomes polyatomic interferences and that allows the direct determination of [79]Se and its speciation.

Preliminary results in the determination of [126]Sn

A method has been developed using a chelating resin in an online pre-concentration manifold with high resolution inductively coupled plasma spectrometry (ICP-MS) detection for the analysis of trace metals in spent nuclear fuel leachates. Flow injection analysis was performed using the seaFAST system, a fully-automated online system that improves elemental detection limits in spent nuclear leachates by both preconcentrating analyte and eliminating matrix components. The targeted elements from an aliquot of sample are trapped on a mixed resin preconcentration column while the matrix ions pass through to the waste. Nitric acid then elutes the concentrated metals from the column into the ICP-MS nebuliser.

The determination of [126]Sn by mass spectrometry suffers from isobaric interference of [126]Te which cannot be resolved even with modern high resolution mass spectrometers. Therefore, if Te is not previous chemically separated, it can yield incorrect [126]Sn concentration in nuclear waste analysis. The different behaviour of Sn and Te in the chelating column allows determining [126]Sn because Te is not retained in the column. In Figure 9 are shown the preliminary results on the determination of [126]Sn in spent nuclear fuel leachates. In addition the same method can be used for Te determination, another relevant fast release radionuclide.
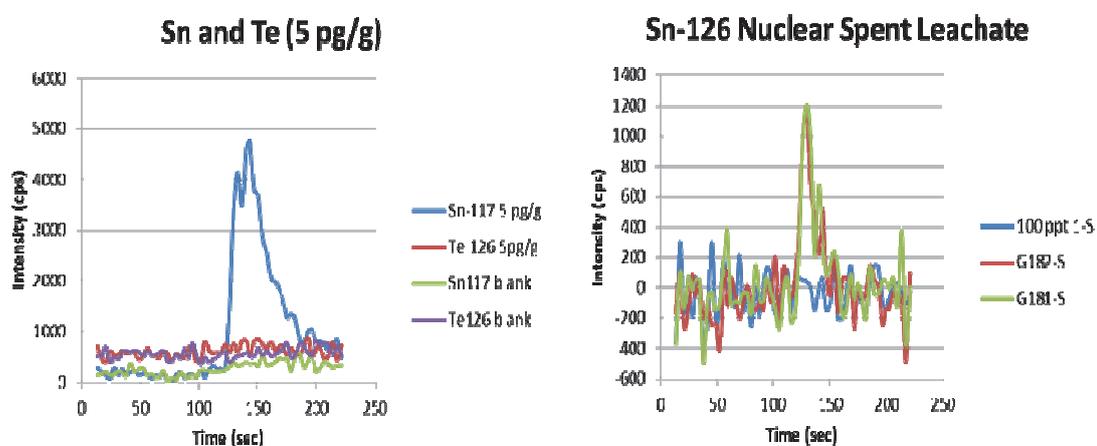

Figure 9:. (A) Behaviour of Sn and Te in the chelating column. (B) Detection of [126]Sn in nuclear spent fuel leachates (dilution 1/10).

Conclusions and Future work

An IRF experiment using a cladded piece of BWR (42GWd/t$_U$) commercial SNF has started and preliminary results from the first 50 days are reported.

Uranium speciation studies show no secondary phase formation during the experiment.

Among the elements measured by ICP-MS, Cs, Mo, Tc, Rb and Sr dissolve faster than the matrix (uranium) and therefore, are identified as IRF. Among them, Cs presents the higher release, followed by Mo. Finally Tc, Rb and Sr follow a very similar release pattern.

Higher release is found at the beginning of the experiment, assumed to be that coming from the gap and the cracks. A second IRF contribution, longer and slower, is also detected. This is assumed to arise from the fraction segregated to the internal grain boundaries, not immediately accessible to water at the beginning of the experiment. However, it is necessary to wait until the end of the experiment to make proper comparisons and draw more conclusions.

Promising preliminary results for ^{79}Se and ^{126}Sn determinations using ICP-MS are also reported with spent fuel analogue materials. Further development is needed before applying these finding to SNF leachates.

Acknowledgement

References

Iglesias, E., Quiñones, J. (2008). Analogous Materials for Studying Spent Nuclear Fuel: The Influence of Particle Size Distribution on the Specific Surface Area of Irradiated Nuclear Fuel. Applied Surface Science, 254, 6890-6896.

Van der Lee, J., De Windt, L. (2002). CHESS Tutorial and Cookbook (version 3.0). Ecole des Mines de Paris, CIG Fontainebleau.

FIRST RESULTS ON INSTANT RADIONUCLIDE RELEASE FRACTION FROM SPENT UO$_2$TRISO COATED PARTICLES

Hilde Curtius[*], Hans Walter Müskes, Murat Güngör, Norman Liek, Dirk Bosbach

Institute of Energy and Climate Research, IEK-6: Nuclear Waste Management and Reactor Safety, Forschungszentrum Jülich (DE)

* Corresponding author: h.curtius@fz-juelich.de

Abstract

Spent UO$_2$ TRISO (Tri-structural-Iso-tropic) coated particles (high burn up of approximately 100 GWd/t) are used by Jülich within the project FIRST. The main working goals in work package 2 (WP2) are the characterisation of the fission gas fraction and of the fast/instant release fraction of volatile radionuclides after contact with groundwater. For the determination of the fission gas fraction a special crack device equipped with a gas sampling tool was constructed. During the crack process of the tight coatings the released gas fraction was collected and analysed by gas chromatography (GC) and radio gas-chromatography (RGC) measurements. Six coated particles were cracked separately. In the analysed samples the fission gas ^{85}Kr represented the main contributor. Compared to the calculated inventory of ^{85}Kr, the results indicate that approximately 35% of ^{85}Kr was released instantaneously. ^{14}CO$_2$ was detected as well. Each sample contained approximately (15 ± 5) Bq. Xe was not detected, although previous ESEM (Environmental Scanning Electron Microscope) investigations revealed an accumulation in the buffer region.

First results of the fast/instant release fraction of volatile radionuclides in contact with groundwater under oxic (air) and anoxic/reducing (Ar/H$_2$) conditions were obtained.

^{90}Sr was released (indicator for UO$_2$ dissolution) in negligible amounts, although the higher values were measured under anoxic/reducing conditions. Under air the formation of a protective UO$_{2.33}$ layer is assumed. Approximately 16% of the inventory of ^{134}Cs respectively 8% of the inventory of ^{137}Cs were released instantaneously from the fuel kernel after contact with the groundwater under anoxic/reducing conditions. Under oxic (air) conditions lower amounts (formation of a protective UO$_{2.33}$ layer on the fuel surface) of ^{134}Cs (9%) respectively of ^{134}Cs (4.8%) were detected in solution. In conclusion the release values of Cs from the spent fuel samples under investigation are high, indicating the open access to grain boundaries (sites of preferential solution attack), where Cs is located.

Introduction

At the High Flux Reactor in Petten five fuel pebbles from the German production AVR GLE-4/2 were irradiated for 249 full effective power days. One pebble was called HFR-EU1bis/2. The burn-up of this pebble was determined to be 10.2% FIMA (Fissions per initial heavy metal atom). From this pebble Jülich obtained irradiated UO$_2$ TRISO coated particles. In Figure 1 the design of a coated particle is shown. In Table 1 the irradiation characteristics of the pebble HRF-EU1bis/2 are summarized. More irradiation details are given in (Fütterer et al., 2006).

Within WP2, Jülich first investigated the microstructure of the TRISO coated particle by ESEM. Within the prepared polished specimen big pores, large grains and metallic precipitates were visible. The elements Cs, O, U, Mo, Xe, Zr and Si were identified whereas higher amounts of the volatile elements Cs and Xe were detected in the surrounding buffer. The periphery of an isolated fuel kernel revealed big grains and small pores. The metallic islands appear here as hexagonal platelets and the elements Mo, Zr and Tc were identified clearly. The activities of the elements Cs, Eu, Ce, Ru, Sb, Rh, Pr and Am present in a coated particle were determined by γ-spectroscopy and agreed with the calculated values. The distribution of these radioisotopes between coatings and fuel kernel was analysed as well by different analytical tools (α-, β-, and γ-spectroscopy). According to these results the elements Am, Pu, Cm, U, Eu, Ce, Sr, Tc, and Pr are located quantitatively within the kernel, while Cs is mainly present in the coatings.

This paper presents first results with respect to the determination of the fission gas fraction and of the fast/instant release fraction of volatile radionuclides after contact with groundwater.
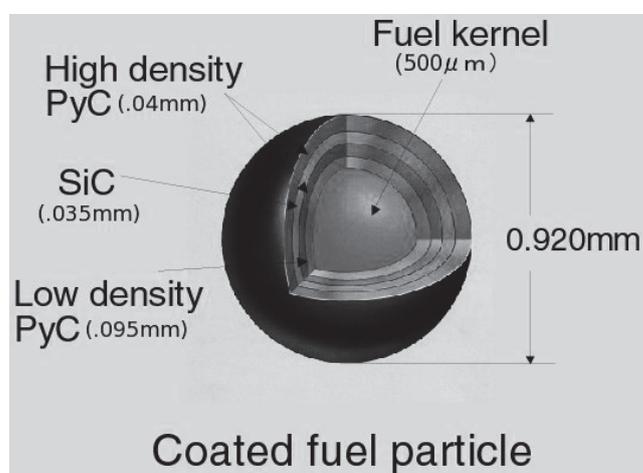

Figure 1: *Design of a TRISO coated fuel particle.*

Table 1: *Main irradiation data for the pebble HFR-EU1bis/2.*

Enrichment	16.76 wt% ^{235}U
Irradiation at:	High Flux Reactor Petten
Reactor cycles:	10
Irradiation:	249.55 (efpds)
Thermal fluences:	2.23 x 10^{25} m^{-2}
Fast fluences:	3.98 x 10^{25} m^{-2}
Central temperature of pebbles:	1250 °C
Power density:	30 W/cm^3
FIMA:	10.2 %, (95.57 GWd/t)

5. Fission gas release

A TRISO coated particle (1,000 µm in diameter) was placed in the sample holder (drill depth: 600 µm) of the crack device (Figure 2).
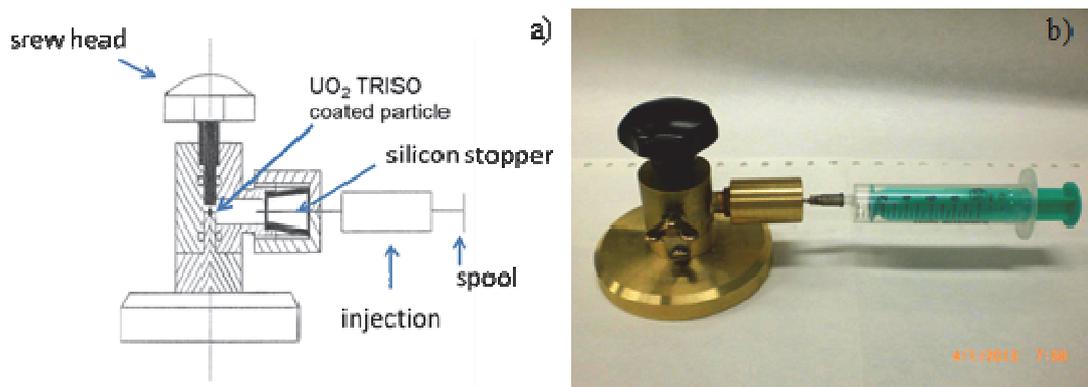
Figure 2: a) Schematic illustration and b) the constructed crack device.

The equipment was closed and the screw head was moved till the drill depth was reached. A further movement is not possible. A drawing out of the connected spool of the injection to a volume of 6mL was performed. Then the spool was held constant while the injection was moved backwards within the silicon stopper. When the middle position in the silicon stopper was reached the spool was released. Immediately the spool moved back till the volume within the injection reached a stable value of 1.5 mL. The screw equipped with the silicon stopper and the injection was disconnected from the crack device and then connected to the gas chromatograph (Siemens Sichromat II, thermal conductivity detector, detection limit: $6 \cdot 10^{-9}$ g/mL N_2 in H_2: first column: molecular sieve 5A 80/100, length 3 m ; second column: Porapack QS 80/100, length 1 m). Ar was used as carrier gas. The complete volume of the gas sample (1.5 mL) was used. An average pressure of 0.2 bar was determined for each gas sample. The radioisotopes were detected within the connected proportional gas flow-through counter. The sensitivity for ^{3}H and for ^{14}C is 50 Bq respectively 3 Bq.

High amounts of the fission gas ^{85}Kr were detected in all samples. Compared to the calculated inventory approximately 35% of ^{85}Kr was released instantaneously. Besides this fission gas, $^{14}CO_2$ was identified and in each gas sample an activity of (15 ± 5) Bq was measured. ^{14}C forms as a fission product in fuel and is produced through fast neutron reactions with ^{14}N (present as impurity). The formation of CO_2 can be explained by graphite oxidation, a reaction which is known to consume oxygen and hence contribute to the low oxygen potential. Further gas components especially Xe were not detected, although previous ESEM/EDX investigations revealed an accumulation in the buffer (low density carbon layer) region.

6.   Leaching

Experimental procedure

Ten TRISO coated particles were cracked and the obtained UO_2 kernels were isolated from the coatings. A low molar salt solution containing 19 mM NaCl and 1 mM $NaHCO_3$ (pH value of this solution was 7.4 ± 0.1) was used for the subsequent leaching procedure at room temperature. Five UO_2 kernels and their corresponding coatings were leached separately in 20 mL under oxic (air) conditions. Leaching also was performed under anoxic/reducing (Ar/H_2: 96% of Ar (type:4.8 (4.8 indicate the pureness to 99.998%) and 4% of H_2 (type 3.0 (3.0 indicates the pureness to 99.9%)) conditions using equal amounts of UO_2 kernels and coatings respectively. At different time intervals 1.5 mL aliquots of the solutions were taken. In order to keep the solid/solution ratios constant 1.5 mL of the prepared salt solution was added to each leaching flask.

The aliquots were filtered (450 nm) and the pH values were determined to be in the pH range of 7.3 ± 0.1 to 7.5 ± 0.1. The stability of these pH values indicate a stable environment in which no dissolution process (consuming or releasing protons) occur so far.

One milliliter of each filtrate was diluted with 9 mL of a 0.1 M HNO_3 solution resulting in a 10 mL sample solution. Then 0.1 mL from each sample solution was vaporized directly on metal disks and an alpha-measurement (alpha-spectrometer: Octete, company Ortec, PIPS-detector (planar implanted passivated silicon)) was performed for 250,000 sec to analyze the activities of the radionuclides U, Pu, Am, Np and Cm.

The activity of ^{90}Sr was determined after the following selective separation steps; 1 mL of each sample solution was diluted with 0.67 mL of 14 M HNO_3 solution. Then 1 mL of this solution was used to quantify the ^{90}Sr activity. A colum (6 mL in volume) was filled with a suspension of 1 g resin (Sr-Resin, Eichrom-Company) in 5 mL of a 2 M HNO_3 solution. The colum was washed two times with 5 mL of a 2 M HNO_3 solution and then 5 ml of a 8 M HNO_3 solution was added. Afterwards the sample solution was added to the column. The sample vial was rinsed with 1 mL of a 8 M HNO_3 solution and this solution was added to the colum as well. Then a washing step with 10 mL of a 8 M HNO_3 solution was performed. The washing solution was collected. After the washing steps ^{90}Sr was eluated by using 10 mL of a 0.05 M HNO_3 solution. Immediatly 1mL of the eluate was used for the β-measurement (Liquid Scintillation Counter:Packard Canberra, TRICARB 2200 A). The measurement time was fixed to 3,600 sec and the detection limit for ^{90}Sr is 0.1 mBq/sample.

Then 5 mL from each sample solution was filled in a polyethylene vial and a γ-measurement was performed (HPGe detector type PGC 2018, Bias:2,500 V positiv, counting time: 86,400 sec, software: Gamma-W Version: 2.44 using ^{152}Eu as standard solution with the same geometry, distance 0.15 m). The uncertanties of the measured activities are in the range between 2% to 5% . The activity of $^{134/137}Cs$ for a TRISO coated particle and the activity distribution between coatings and fuel kernel was determined before (Curtius et al., 2013).

For all elements the measured values were analysed according to the following equations:

The Fraction of Inventory of an element i released in the Aqueous Phase (FIAP) is given by the following equation:

$$FIAP_i = m_{i, aq}/m_{i, SNF} \qquad (1)$$

where $m_{i,aq}$ is the mass of the element i in the aqueous phase (g) and $m_{i,SNF}$ is the mass of the element in the SNF sample (g). The Instant Release Fraction of an element i (IRF_i) is the Fraction of Inventory of the element i in the Aqueous Phase (FIAPi) reduced by FIAP of uranium. For the reported time period no uranium was detected in solution, hence the $FIAP_i$ of the elements represent the IRF_i.

The Fractional Release Rate for an element i (FRR_i) in d^{-1} is given by the equation :

$$FRR_i = \Delta FIAP_i/\Delta t \qquad (2)$$

where Δt is the time range in days and $\Delta FIAP_i$ refers to the difference of the FIAPi values within this time range.

Generally spoken, the FRR_i describes the elemental FIAP evolution with time.

Experimental results

So far, the results indicate that none of these radionuclides was detected in solution, hence no matrix dissolution occurred in this time frame of investigation, independent on oxic or anoxic/reducing conditions.

After 91 days the determined value of the FIAPs of ^{90}Sr differ approximately one order of magnitude with respect to the environmental conditions (Figure 3). The highest FIAP (0.17%) was determined under anoxic/reducing environment, whereas under oxic conditions a value of 0.02% was reached (Figure 3). The FIAPs are quite small, indicating no fuel matrix dissolution effects so far. The lower FIAP values under oxic conditions however can point to the formation of a protective $UO_{2.33}$ layer, which diminish further U(IV) oxidation.

Taking all FIAP data points into consideration two different regions are visible (Figure 3) under oxic and under anoxic/reducing conditions as well.

The first region (region-I in Figure 3) corresponds to the higher release rates at the beginning of the experiment (0 to 5 days). Under oxic conditions, the first FIAP value reached approximately 0.018% within this time period,. This high release represents the dissolution of the grain boundaries which have an open access to the groundwater. Although the contribution of fines leaching (fines located at the periphery of the fuel kernels) are included in this first FIAP value. The second region (region-II in Figure 3) shows a slower release (within this region the second FIAP values were taken for an arbitarry chosen time of 5 days after the intersections of the two FRR regression lines (Figure 3). The time of 5 days was choosen in order to compare these results with those coming from the first region, which took place in the same time frame). Under oxic conditions the second FIAP value reached approximately 0.002%. Here the grain boundaries have no direct open access to the groundwater, hence the water needs to diffuse towards these less accessible places. Under anoxic/reducing conditions the determined first and second FIAP values were 0.13% respectively 0.04%.
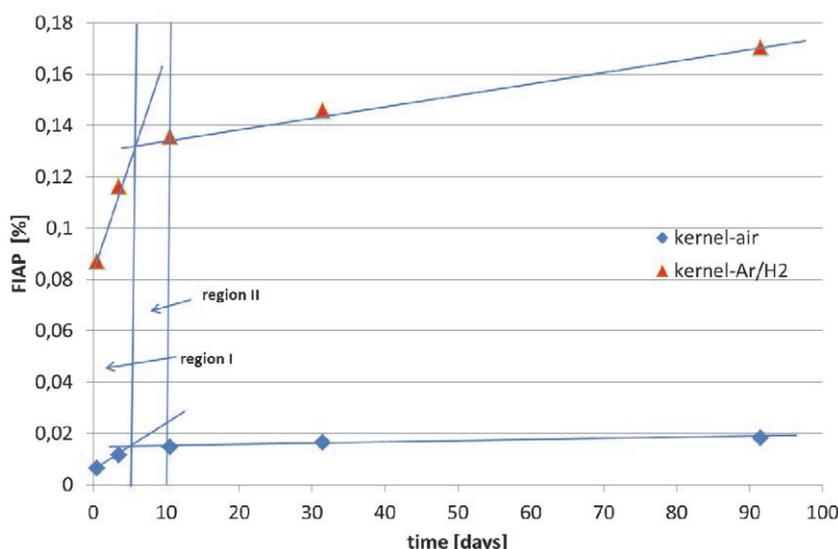

Figure 3: *FIAP ^{90}Sr (%) vs. time under oxic and under anoxic/reducing conditions.*

Figures 4 a) and b) reveal the calculated FIAP values (%) for ^{134}Cs and ^{137}Cs vs. time under oxic and under anoxic/reducing conditions. Chemically, like expected, the radiosisotopes ^{134}Cs and ^{137}Cs reacted identically (comparable curve progression). However the FIAP values obtained for ^{134}Cs were twice as much as the determined values for ^{137}Cs.

In addition, under oxic conditions the FIAP % values are twice as low compared to the values determined for anoxic/reducing conditions. The formation of a protective $UO_{2.33}$ layer on the fuel surface cannot be ruled out.

As we have already observed for ^{90}Sr, two regions are visible. The first region (region-I, first 5 days of the experiment) corresponds to high release rates, indicating leaching of fines and of grain boundaries, which have an open access to the groundwater. FIAP values of 9% for ^{134}Cs and 4.8% for ^{137}Cs respectively were reached within these first five days In contrast to ^{90}Sr the radionuclide Cs is incompatible with the UO_2 lattice. Therefore, during irradiation Cs is mainly excluded to grain boundaries, and grain boundaries represent sites of preferential solution attack.. The second region (region-II) is characterized by very low release rates, indicating the leaching of less accessible grain boundaries.

As mentioned before the FIAP values strongly depend on the environmental conditions. Under anoxic/reducing conditions the FIAP values are twice as high as the values determined under oxic environment. Already after 0.5 days an IRF of 16% for ^{134}Cs and 8.4% for ^{137}Cs was reached. Then, unexpectedly, within the first five days of the experiment, the release rates decreased to 15% for ^{134}Cs and to 7.8% for ^{137}Cs respectively. The second region (region II) is characterized by decreasing release rates as well. These first results may indicate, that the contribution of fines leaching under anoxic/reducing conditions may play an important role. In future work more data points will be obtained and it is of interest to investigate these trends in detail.
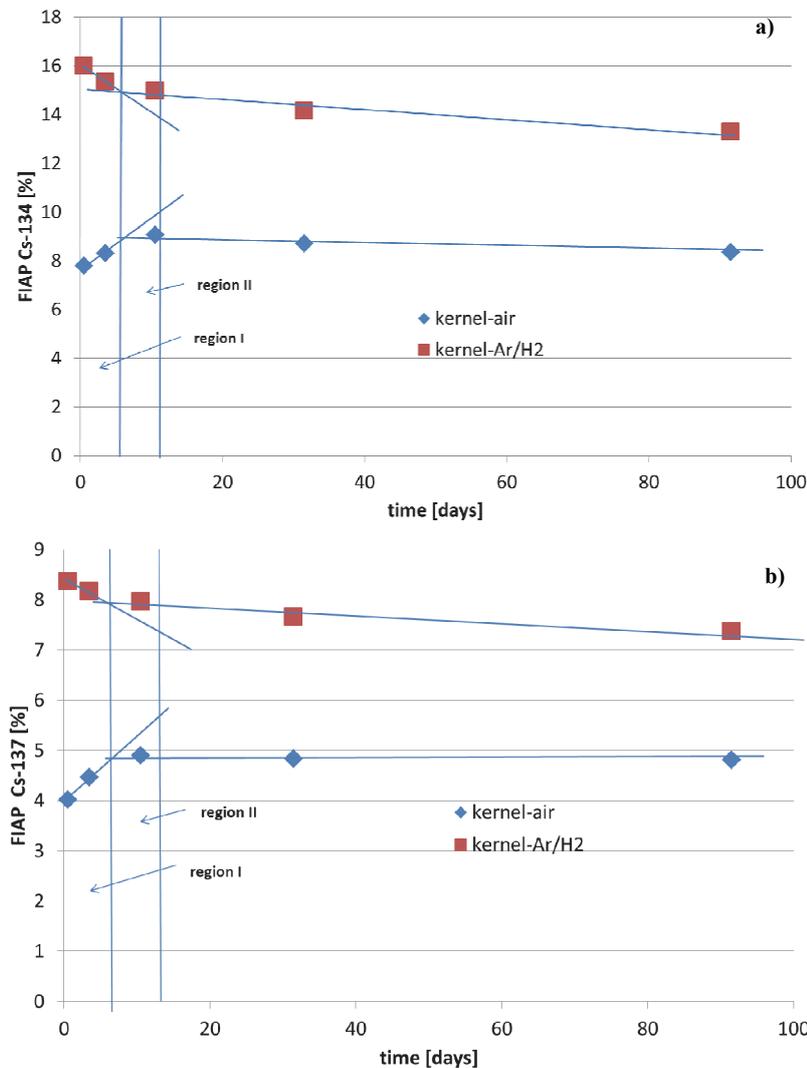

Figure 4: *FIAP values for a) ^{134}Cs (%) and b) ^{137}Cs (%) under oxic and anoxic/reducing conditions.*

Conclusions and Future work

Within the project FIRST, UO_2 TRISO coated particles are used as very high-burn up (approximately 100 GWd/t) spent fuel samples. These coated particles can be described as miniature fuel elements. Due to the tight coatings, no fission gas released during the irradiation process, hence the complete activation/fission products are located in the TRISO coated particles.

A crack device coupled with a gas sampling tool was developed. $^{14}CO_2$ was detected up to (15 ± 5) Bq per fuel kernel. Previous ESEM investigations revealed the presence of He in the buffer, but within the gas samples no He was detected. The fission gas ^{85}Kr represented the main gas component. Approximately 35% of the complete inventory released instantaneously. This enormous release and the results from previous ESEM investigations reflect the high porosity of the fuel lattice. In general, a high porosity alleviates an open access of the groundwater towards the grain boundaries. The grain boundaries represent preferential sites of solution attack hence high release rates of the elements located at grain boundaries are expected. Leaching experiments have been performed in order to measure the release of ^{90}Sr (indicator for UO_2 dissolution) and Cs that accumulates at grain boundaries (not soluble in the UO_2 matrix) during irradiation.

In the time period of investigations, the release of ^{90}Sr from the fuel matrix was negligible indicating that the UO_2 matrix does not dissolve yet. In contrast a high release of Cs was observed. This finding strongly underlines the location of Cs at the grain boundaries. In addition the formation of a protective $UO_{2.33}$ layer under air condition is assumed as the determined Cs release rates are lower compared to the values obtained for an anoxic/reducing environment.

In future work, the leaching will be continued till February 2014. Afterwards the fuel kernels will be investigated by ESEM (detection of secondary phases on the surface, microstructure at the fuel periphery and elemental distribution). These results will be compared to the data obtained before leaching. Dissolution of the fuel kernel is aspired as well to determine the radionuclide inventory.

Acknowledgement

References

Fütterer, M.A., Berg, G., Toscano, E., Bakker, K. (2006). Irradiation Results of AVR Fuel Pebbles at Increased Temperature and Burn-Up in the HFR Petten. 3rd International Topical Meeting on High Temperature Reactor Technology. Johannesburg, South Africa, B00000035.

Curtius, H., Müller, E., Müskes, H.W., Klinkenberg, M., Bosbach, D. (2013). Selection and Characterisation of HTR Fuel. KIT SCIENTIFIC Reports 7639, ISBN 978-3-86644-980-0.

PREPARATION OF THE SPENT FUEL SAMPLES FOR LEACHING EXPERIMENTS AND SPECTROSCOPIC STUDIES AT PSI

Ines Günther-Leopold[*], Hans-Peter Linder, Annick Froideval Zumbiehl, Enzo Curti

Paul Scherrer Institut, Nuclear Energy and Safety Research Department, PSI (CH)

* Corresponding author: ines.guenther@psi.ch

Abstract

The PSI contribution to the FIRST-Nuclides project comprises leaching experiments on selected high burn-up spent nuclear fuel samples from the Swiss nuclear power plants Gösgen and Leibstadt, as well as synchrotron-based spectroscopic investigations of these fuel samples before and after leaching. The present report describes the sample preparation within the hot cells and the installation of the experimental setup in the dissolution box of the PSI hot laboratory.

Introduction

The test matrix for the PSI leaching experiments was defined by selecting three sample types (cladded fuel, cladding without fuel residues, fuel fragments) from an UO_2 fuel rod irradiated in the Leibstadt boiling water reactor (BWR; KKL), as well as six samples (cladded fuel, fuel fragments, cladding with and without fuel residues) irradiated in the Gösgen pressurized water reactor (PWR; KKG), of which four samples originate from an UO_2 fuel rod and two samples from a MOX fuel rod. A detailed characterization of the material (type of fuel rod and cladding, irradiation data, sampling position etc.) was compiled earlier (Günther-Leopold et al., 2012). In addition to the previously published study (Johnson et al., 2012), fuel fragments and cladding of the MOX fuel rod will now be leached separately in order to complete the available data set for this material, especially for the nuclide ^{14}C where a relevant contribution from the cladding can be expected. Furthermore, synchrotron-based spectroscopic investigations of selected fuel samples before and after the leaching process are proposed (Curti et al., 2013; Froideval Zumbiehl et al., 2012).

Cutting and defueling of the leach samples

Based on the knowledge gained from earlier leaching experiments it was decided that the length of the fuel rod specimens used for the leaching experiments should be 20 mm each, whereas a size of 10 mm is sufficient for the fuel rod specimen used to determine the local burn-up and of 3 mm for the samples for the spectroscopic investigation, respectively. Based on these preconditions the cutting plans were created and the cutting was performed in summer 2013 by the operators of the PSI Hot Cell group. The cutting plans for the three selected fuel rod segments are given below together with some pictures of the prepared specimens.

Up to now the preparation of all specimens of "cladded fuel", "cladding with fuel residues" and "fuel fragment" sample types is finished and the samples were transferred to the dissolution box for the leaching experiments. However, the three "cladding" samples (cladding material from the outer part of the fuel rod without fuel

Fuel segment: KKG-14b-4021-01-0129-D

Length		Pos.	sample name	remark
	labelling	2037.0 2038.5		
579.5	rest	2616.5	KKG-14b-4021-01-0129-D	storage
3.0	beamline sample 1	2620.0	KKG-14b-4021-01-0129-DA	beamline sample (without leaching)
3.0	beamline sample 2	2623.5	KKG-14b-4021-01-0129-DB	beamline sample (for leaching)
20.0	leach sample A	2644.0	KKG-14b-4021-01-0129-DC	sample type: cladded fuel
20.0	leach sample B	2664.5	KKG-14b-4021-01-0129-DD	sample type: cladding
20.0	leach sample C/D	2685.0	KKG-14b-4021-01-0129-DE	sample type: cladding + fuel fragments
10.0	burn-up sample	2695.5	KKG-14b-4021-01-0129-DF	burn-up determination
20.0	rest	2716.0	KKG-14b-4021-01-0129-DG	storage

Figure 3: *Segment cutting plan of the selected UO$_2$ PWR fuel.*
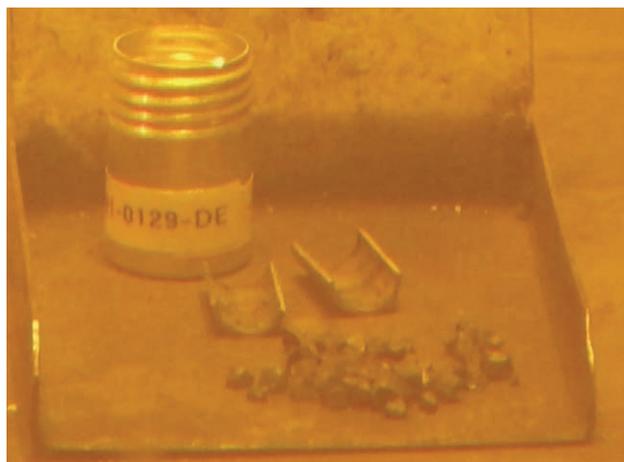
Figure 4: *Sample KKG-14B-4021-01-0129-DE after cutting and defueling (sample type: cladding + fuel fragments).*

MOX PWR fuel (KKG-13-5024-10-K-676-EC)

The cutting plan of the segment KKG-13-5024-10-K-676-EC and the sample sizes (in mm) are illustrated in Figure 5. Figure 6 shows a picture of the specimen KKG-13-5024-10-K-676-ED after cutting and fragmentation.

Fuel segment: KKG-13-5024-10-K-676-EC

			sample name	remark
Length		**Pos.**		
		2007.0		
20.0	rest	2027.0	KKG-13-5024-10-K-676-EF	storage
20.0	leach sample	2047.5	KKG-13-5024-10-K-676-EE	sample type: cladding
20.0	leach sample	2068.0	KKG-13-5024-10-K-676-ED	sample type: fuel fragments
	rest			
252.0	labelling	2320.5	KKG-13-5024-10-K-676-EC	storage

Figure 5: Segment cutting plan of the selected MOX PWR fuel.

Figure 6: Sample KKG-13-5024-10-K-676-ED after cutting and defueling (sample type: fuel fragments).

Installation of the leach equipment in the dissolution box

The experimental setup consists of glass columns (total volume approx. 200 mL) with a sealed outlet cock for sampling, an integrated glass filter in order to prevent the clogging of the cock by solid particles and in-house manufactured pistons made of Plexiglas. The equipment to be used in frame of the FIRST-Nuclides project at PSI is shown in Figure 7. An assembly of ten of such leaching columns was installed in the shielded dissolution box. Finally, the first set of leaching experiments has been started with six fuel samples and one blank (t_0: September 16th, 2013; leaching solution: 19 mM NaCl, 1 mM $NaHCO_3$). The allocation of the samples in the leaching vessels is given in Table 1, whereas the experimental setup in the dissolution box is shown in Figure 8.

Figure 7: PSI leaching equipment before installation in the dissolution box.

Table 1: Sample allocation in the leaching vessels.

Vessel No.	Sample	Sample type	Remark
1	Blank		started
2	KKG-14B-4021-01-0129-DC	cladded fuel	started
3	KKG-14B-4021-01-0129-DE	fuel fragments	started
4	KKG-14B-4021-01-0129-DE	cladding with fuel residues	started
8	KKG-14B-4021-01-0129-DD	cladding	to be prepared
5	KKLAIA003-H6-C3	cladded fuel	started
6	KKLAIA003-H6-C5	fuel fragments	started
9	KKLAIA003-H6-C4	cladding	to be prepared
11	KKG-13-5024-10-K-676-EE	cladding	to be prepared
7	KKG-13-5024-10-K-676-ED	fuel fragments	started
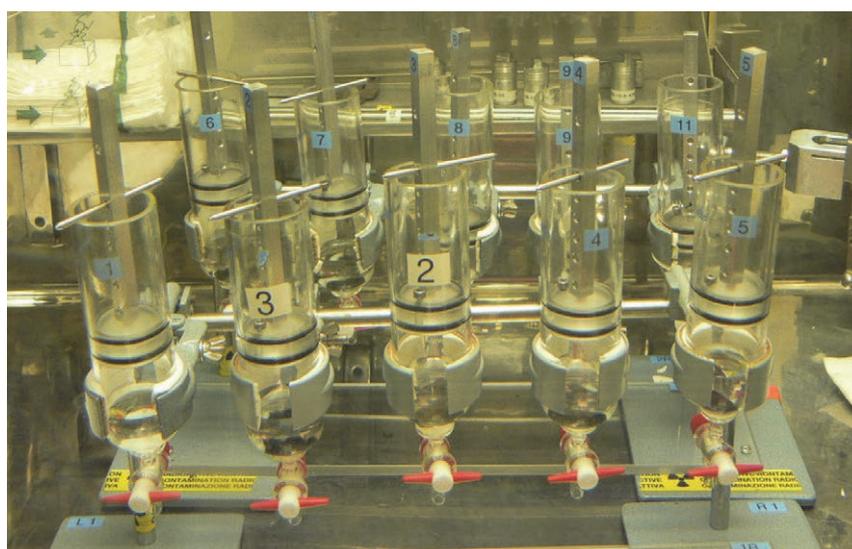
Figure 8: Experimental setup installed in the dissolution box of the PSI Hot Laboratory.

Future work

The leaching experiments of the three "cladding" specimens will start as soon as the samples will have been prepared and transferred to the dissolution box. For all leaching experiments a complete exchange of the solution will be/has been performed after 7 days ("pre-leaching"). Further sampling is scheduled for 28, 56, 182 and 364 days after starting of the leaching experiments followed by the analysis of the leach solutions by gamma spectrometry, ICP-MS and liquid scintillation counting.

Acknowledgement

References

Curti, E., Froideval Zumbiehl, A., Günther-Leopold, I., Martin, M., Bullemer, A., Linder, H.P., Borca, C.N., Grolimund, D., Rothe, J., Dardenne, K. (2013). X-Ray Absorption Spectroscopy of Selenium in Non-Irradiated Doped UO_2 and High Burn-Up Spent UO_2 Fuel. FIRST-Nuclides 2nd Annual Workshop Proceedings. 5th - 7th November 2013, Antwerpen.

Froideval Zumbiehl, A., Curti, E., Günther-Leopold, I. (2012). A Combined XRF/XAS Study of Some Instant Release Fraction Radionuclides in High Burn-Up UO_2 Spent Nuclear Fuel. FIRST-Nuclides 1st Annual Workshop Proceedings, 9th - 11th October 2012, Budapest.

Günther-Leopold, I., Linder, H.P., Froideval Zumbiehl, A., Curti, E. (2012). Selection of High Burn-Up Fuel Samples for Leach Experiments and Spectroscopical Studies at PSI. FIRST-Nuclides 1st Annual Workshop Proceedings, 9th – 11th October 2012, Budapest.

Johnson, L., Günther-Leopold, I., Kobler Waldis, J., Linder, H.P., Low, J., Cui, D., Ekeroth, E., Spahiu, K., Evins, L.Z. (2012). Rapid Aqueous Release of Fission Products from High Burn-Up LWR Fuel: Experimental Results and Correlations with Fission Gas Release. J. Nucl. Mat., 420, 54-62.

X-RAY ABSORPTION SPECTROSCOPY OF SELENIUM IN NON-IRRADIATED DOPED UO$_2$ AND HIGH BURN-UP SPENT UO$_2$ FUEL

E. Curti[1]*, A. Froideval Zumbiehl[1], I. Günther-Leopold[1], M. Martin[1], A. Bullemer[1], H.P. Linder[1], C.N. Borca[2], D. Grolimund[2], J. Rothe[3] and K. Dardenne[3]

[1] Paul Scherrer Institut, Nuclear Energy and Safety Research Department (CH)
[2] Paul Scherrer Institut, Synchrotron Radiation and Nanotechnology Research Department, Swiss Light Source, PSI (CH)
[3] Karlsruhe Institute of Technology, Institut für Nukleare Entsorgung (DE)

* Corresponding author: enzo.curti@psi.ch

Abstract

In this study, we have investigated the oxidation state and the coordination environment of selenium (Se) in a non-leached, high-burnup UO$_2$ (HBU) spent fuel sample (79 GWd/t$_U$) from the Leibstadt reactor (Switzerland) by means of micro X-ray absorption near-edge spectroscopy (μ-XANES) and micro X-ray fluorescence (μ-XRF). In spite of the low Se concentrations (about 100 ppm), the heavy UO$_2$ matrix and the extremely small particle size (max. ~10 μm x 10 μm x 2 μm), we were able to collect Se K-edge XANES spectra on a number of fuel particles from the central and the core regions of a pellet.

The data were evaluated in terms of linear combination fits (LCF) of reference compounds, indicating that Se in spent fuel occurs either as a mixture of Se(0) and Se(IV) or as pure Se(-II), with spectral features closely resembling those of the reference compound ZnSe(-II). The latter option is preferred based on crystal chemical reasons. Theoretical spectra calculations are presently performed in order to test both options.

Additional X-ray absorption measurements were carried out on non-irradiated UO$_2$ powdered samples containing Se traces at concentrations of ~10, 100 and 2,000 ppm. The purpose of these measurements was to assess the technical feasibility of similar spectroscopic measurements in spent nuclear fuel at the INE-beamline (ANKA). This test was successful, indicating that even Extended X-ray Absorption Fine Structure spectra (EXAFS) may be successfully recorded on spent fuel across the Se-K edge.

An internal co-operation with the FIRST-Nuclides partner Studsvik has been initiated, with the goal of carrying out new XANES measurements on leached and non-leached UO$_2$ spent fuel from the Swedish Oskarshamn reactor, using an optimized sample preparation technique based on Focused Ion Beam (FIB) milling. It is expected that such a sample preparation will considerably improve the quality of the spectra.

Introduction

The present contribution focuses on the fate of ^{79}Se, a long-lived safety-relevant nuclide (half-life 3.3·10^5 y), which is traditionally considered as a potentially significant instant release fraction (IRF) contributor owing to the appreciable volatility of this element and to the high solubility of oxidized selenium species (Scheinost et al., 2008; Curti et al., 2013). This view is based on the implicit assumption that selenium is present as oxidized Se(IV) or Se(VI) in the fuels and segregates towards grain boundaries during in-reactor irradiation. So far, no data are available to support this assumption.

Selenium may occur in different oxidation states. The oxidized species Se(IV) and Se(VI) form soluble salts, whereas the reduced forms Se(0) and Se(-II) are sparingly soluble (Scheinost et al., 2008; Curti et al., 2013) and have thus limited Se mobility in aqueous solutions. Recent leaching experiments on HBU fuels from two Swiss nuclear power plants (Johnson et al., 2012) failed to detect dissolved [79]Se after leaching in aqueous solutions during up to 56 days, in spite of the low detection limit (0.5 ppb) of the experimental setup, suggesting that selenium in spent fuel is not as mobile as commonly assumed.

In order to test this hypothesis, we carried out X-ray absorption spectroscopy (XAS) experiments on small (15 μm maximum size) non-leached HBU spent fuel particles from the Leibstadt nuclear power plant using the microfocused X-ray beam delivered at the microXAS beamline (Swiss Light Source (SLS), PSI, Villigen). The main objective of this study was to assess the oxidation state of selenium in the irradiated fuel prior to any leaching in aqueous solution. Such information is expected to give clues for understanding the behavior of [79]Se during aqueous leaching of spent fuel.

The feasibility of XAS measurements recorded at the Se-K edge on spent fuel was also successfully tested at the INE-beamline (ANKA) by means of measurements carried out on non-irradiated UO_2 powdered samples doped with trace Se concentrations.

1. Materials and Methods

1.1. Sample preparation

A high-burnup spent fuel pellet (78.7 GWd/t_U) from the Leibstadt boiling water reactor was used for the spectroscopic investigations (fuel: Westinghouse SVEA96+ Optima 2, assembly AGB108, rod position G6). The fuel was unloaded in August 2004 after 9 fuel cycles. Due to radiation protection limitations at the SLS, only samples containing very small dispersed UO_2 fuel particles could be used. The sample was thus generated by applying the peeling method, which allows recovering tiny amounts of highly active material (Degueldre et al., 2012). A section of a fuel pellet was impregnated with resin and polished using a silicon carbide disc and sand paper, which loosened micrometer-sized fuel particles. The surface of the so-prepared fuel section was then pressed on adhesive Kapton tape, allowing the freed micrometer-sized spent fuel particles (max. 10-15 μm) to stick to the Kapton tape. These micrometer-sized spent fuel particles were then fixed by covering them with a second Kapton tape strip. Afterwards, the sample was removed and isolated in Petri dishes to avoid any contamination (Figure 1). A sub-sampling was necessary in order to reduce the activity to the Swiss licensing limit of 100 LA allowed for a single sample to be measured at the microXAS beamline (rectangles in Figure 1). Sub-sampling was carried-out in such a way to conserve a fuel pellet area covering the center to the rim region and a fortiori to enable the spectroscopic investigations of this extended center to rim area. Two beamtime periods (in November 2012 and in May 2013) were allocated at the microXAS beamline. While a unique and large sub-sample covering the entire center to rim region was produced and analyzed during the November 2012 campaign, two sub-samples from the same pellet – one from the rim region and one from the center part of the pellet – were produced and analyzed during the May 2013 campaign. Figure 1 shows the sub-samples prepared for the May 2013 campaign.

Prior to measurement, each spent fuel sample was mounted on a special sample holder dedicated to the measurements of radioactive samples at the microXAS beamline. This sample holder minimizes the radiation exposure and prevents any risk of direct contact with radioactive materials, at the same time allowing (by means of Kapton windows) the primary X-ray beam and the fluorescence/transmitted signals to reach sample and detector, respectively.
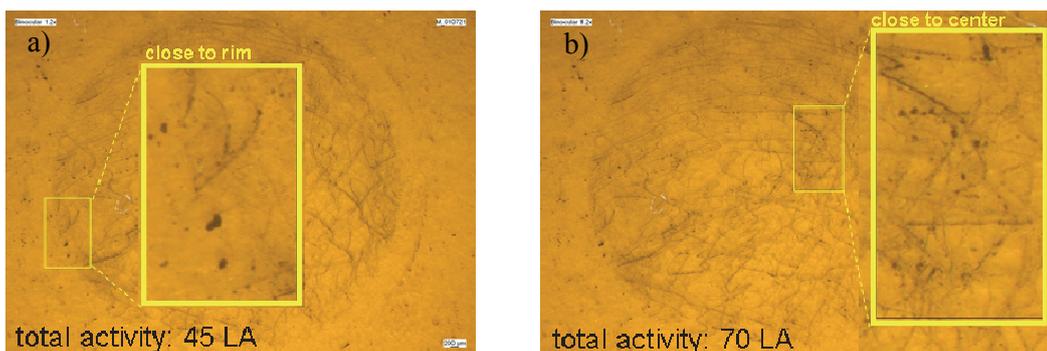
Figure 1: Optical microscopy images of the dispersed high burn-up spent UO₂ fuel particles removed by abrasion from the cross sectional area of the Leibstadt fuel pellet, the two selected regions of the sample ((a) region „rim" and (b) region „center") analyzed by µ-XRF and µ-XANES at the microXAS beamline are highlighted. These two sample regions have been prepared in the HotLab and mounted on two sample holders dedicated to the measurements of radioactive samples at the microXAS beamline. The total activity of each sample was maintained below the allowed limit of 100 LA for a single sample, i.e. 45 LA for the „rim" sample and 70 LA for the „center" sample.

In addition to the previously described samples, low-activity samples aiming at testing the feasibility of synchrotron-based spent fuel measurements were prepared by mixing and homogenizing fine-grained powders of non-irradiated UO_2 (depleted uranium) and trace concentrations of IRF nuclides. Table 1 lists the concentrations and compounds used in detail. Barium was also mixed in order to test spectral interferences (both in absorption and fluorescence mode) with iodine and cesium that would be unavoidable in irradiated fuel.

Table 1: Nominal elemental concentrations in the three prepared powdered samples of non-irradiated UO_2, doped with SeO_2, CaI_2O_6, $BaSO_4$ and CsCl. The sample with concentrations closest to the expected level in the spent nuclear fuel is marked in yellow.

Sample ID	Se (ppm)	I (ppm)	Cs (ppm)	Ba (ppm)
U0030-2000ppm-75mg	2,016	4,098	1,739	2,068
U0030-100ppm-56mg	101	205	87	103
U0030-10ppm- 67mg	10	20.3	8.6	10.3

1.2.X-ray spectroscopy: experimental conditions and data reduction

All measurements conducted on UO_2 spent fuel samples were carried out at the microXAS beamline (SLS) in fluorescence mode, using a micro-focused monochromatic X-ray beam of about 2-3 µm (vertical) x 5 µm (horizontal) size in the photon energy ranges 12.6 - 13.2 keV (Se-K edge and Se-K_α fluorescence regions) and 17.2 - 17.3 keV (U-L_α fluorescence). The energy calibration was carried out using a Se(0) reference.

Micro X-ray fluorescence (µ-XRF) maps of the Se-K_α, U-L_α and the transmission signals were obtained by scanning the surface of the dispersed spent fuel sample with the appropriately tuned micro-focused X-ray beam, while collecting "on the fly" the emitted fluorescence intensity with a Ketek® single element Si detector, within element-specific energy windows. Micro X-ray absorption near edge structure spectra (µ-XANES) were collected for several spent fuel particles and for the reference compounds grey Se(0), Se(IV)O_2 and

$Na_2Se(VI)O_4$ with focused X-ray beam. ZnSe(-II) reference spectra measured during an earlier campaign at the same beamline were also used, after a careful alignment procedure, for the interpretation of the results.

The high percentage of transmitted X-ray beam intensity (> 80%) implies that the thickness of the spent fuel particles did not exceed 2 μm and thus a poor fluorescence yield. This explains, together with the low Se concentrations (about 100 ppm) and the heavy UO_2 matrix, the poor quality of the spectra obtained from the spent fuel sample. Therefore, micro-extended X-ray absorption fine structure (μ-EXAFS) spectra could not be collected. On the other hand, the small thickness of the particles makes self-absorption corrections unnecessary.

XANES data normalization was carried out using the ATHENA package (Ravel and Newville, 2005). Due to the unfavorable signal/noise ratio, the in-built ATHENA interpolative smoothing procedure was applied to allow a careful determination of the edge position (usually, 10 iterations were sufficient). Figure 2 shows a typical example of raw and smoothed spectra obtained from the spent fuel sample.

Linear combination fits (LCF) of the measured reference compounds Se(0), $Se(IV)O_2$ and ZnSe(-II) were calculated in the attempt to reproduce the experimental XANES spectra obtained on the spent fuel sample, using the ATHENA in-built utility and a range from -20 eV to +30 eV with respect to the edge energy. The spectrum of $Na_2Se(VI)O_4$ was not used, since it was evident from the edge position of the spent fuel spectra that no contribution could come from this compound. Deviations of the fits from the measured spectra were quantified as R-factors according to the formula

$$R = \frac{\sum_{j=1}^{N}\left(\chi_{j,meas} - \chi_{j,fit}\right)^2}{\sum_{j=1}^{N}\left(\chi_{j,meas}\right)^2}$$

where N is the total number of data points and χ is the normalized XANES function.
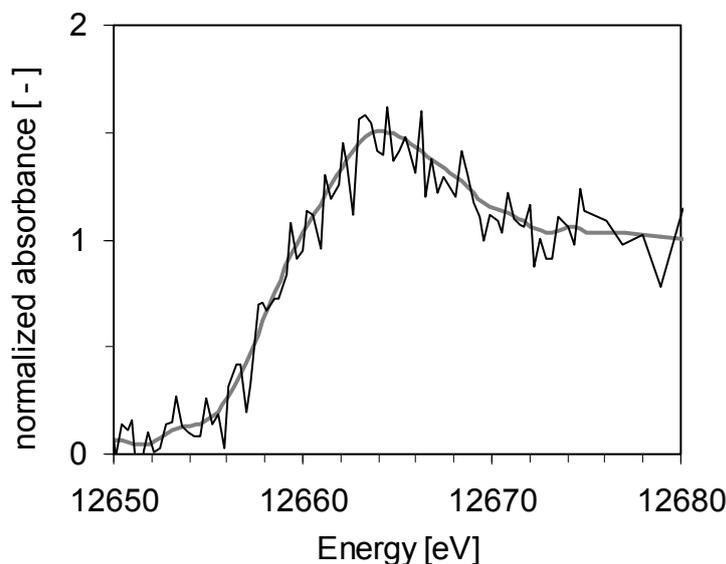

Figure 2: Typical example of raw (black) and smoothed (grey) Se-K XANES spectra from the spent fuel sample (Se "hot-spot" C3 (see Table 2) from location C (see Figure 3a)).

2. Results

2.1. *μ-XRF maps recorded on spent fuel samples*

Figure 3 a-d shows a 1.3 mm × 1.0 mm section of the 4.6 mm × 1.5 mm sample from the intermediate (M) region of the pellet (second beam time, May 2013). Figure 3a is an image obtained from the optical microscope, showing the locations (letters) at which Se-K XANES spectra were successfully recorded. Figures 3 b, c, d show the corresponding μ-XRF maps of the $U\text{-}L_\alpha$, $Se\text{-}K_\alpha$ and transmitted signals, respectively. The maps were recorded at an X-ray energy of 17.3 keV (above the $U\text{-}L_{III}$ edge) allowing us to identify the location of the scattered, tiny spent fuel particles dispersed across the "imprint" of the pellet on the kapton tape and to choose locations exhibiting the highest Se concentrations. The Se fluorescence signal was as expected very weak and rarely exceeded a few hundreds counts per second.

2.2. *Linear combination fits of spent fuel spectra*

The spectra of reference compounds measured during the two beam times are shown in Figure 4 in comparison with the average and envelope of the (smoothed) spectra obtained from the spent fuel particles. The narrow range of the envelope shows that the individual spectra from the spent fuel sample are very similar. A good portion of the envelope thickness can be ascribed to the background noise, so that the individual spectra may be regarded as almost identical. In total, 14 different locations were probed successfully, covering the major part of the pellet region. However, on many other particles our attempt to record usable absorption spectra failed, particularly in the rim (R) region, in spite of the presence of particles with similar fluorescence signals for Se and U as in the areas corresponding to the middle (M) and center (C) of the pellet.

Visual inspection readily shows that combinations of the Se(0) and $Se(IV)O_2$ spectra are likely to reproduce the spent fuel spectra, whereas contributions from the $Na_2Se(VI)O_4$ spectrum can be excluded. Therefore, in a first step we attempted to reproduce the experimental data by linear combination fits of the Se(0) and $Se(IV)O_2$ spectra alone. The numerical results of these fits are shown in Table 2. Figure 5 displays a typical example of fit results for an individual spent fuel spectrum. The results are acceptable and indicate that the experimental spectra obtained on the spent fuel sample may be acceptably represented by a linear combination of the Se(0) and $Se(IV)O_2$ spectral components with about equal weights (i.e. about 50% - 50% mixture on atomic basis).

Figure 6 shows the comparison of the Se-K spectrum for "spot 10" from the spent fuel sample with the carefully aligned ZnSe(-II) spectrum. The two normalized XANES spectra are practically identical. Table 2 also shows the results of the fits obtained from the contributions of Se(0) and ZnSe(-II) alone. LCFs obtained including also $Se(IV)O_2$ always showed negligible contribution by the $Se(IV)O_2$ spectrum, which was therefore discarded. The LCF calculations for "spot 10" and "spot 19" yielded a 100% contribution of the ZnSe(-II) component. All other spent fuel spectra are dominated by this component as well, requiring at most 20% contribution of the Se(0) spectral component. The statistical score is comparable to that of the aforementioned Se(0) - $Se(IV)O_2$ LCFs.

Se-Zn binding is very unlikely in spent fuel, since both are trace elements in this material. However, the close similarity with ZnSe spectral features suggests that Se in the spent fuel may be present as selenide, rather than Se(0) or Se(IV). The existence of stable U(IV) selenide compounds, notably various polymorphs of USe_2 (Beck and Dausch, 1989; Kohlmann and Beck, 1997) suggests direct Se(-II) - U(IV) bonding, e.g. via Se(-II) for O(-II) substitution in the UO_2 lattice, in which case Se would form a dilute solid solution of USe_2 in UO_2.
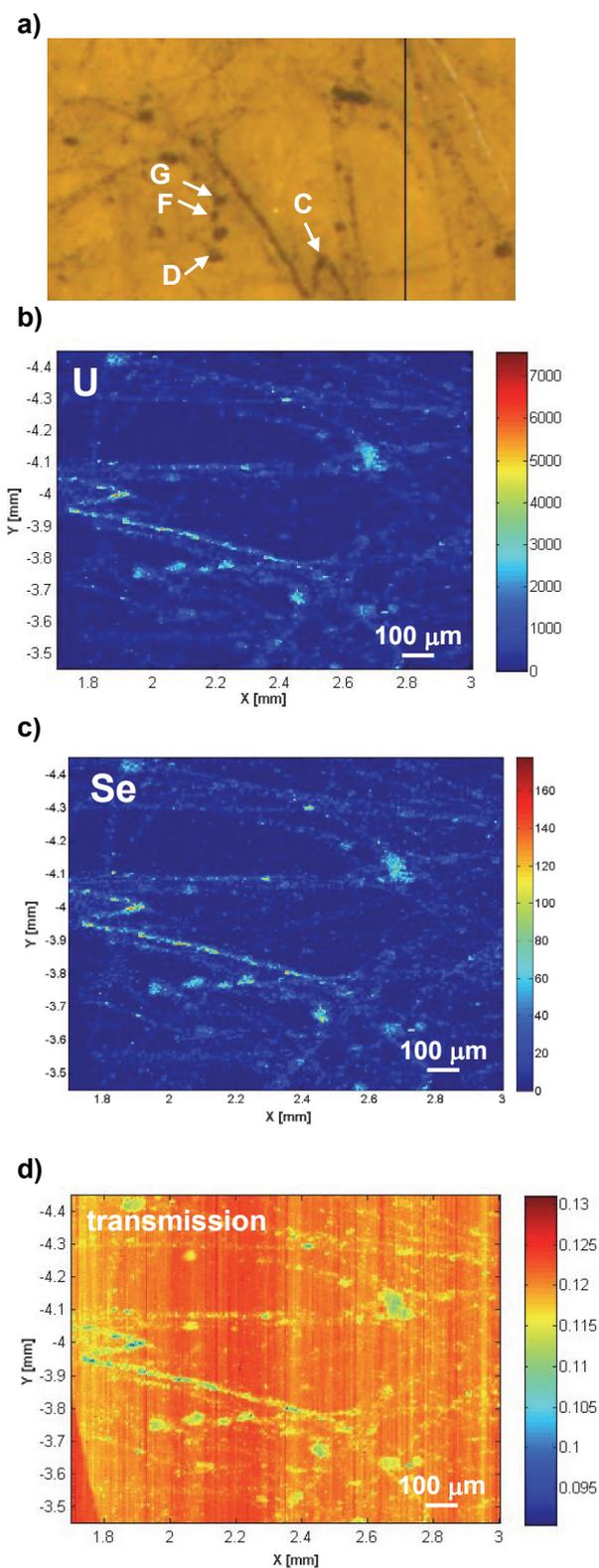
Figure 3: *Optical microscope (a), μ-XRF maps corresponding to the U (b) and Se (c) fluorescence signals and transmitted intensity (d) of a section in the middle region of the dispersed UO$_2$ spent fuel sample investigated in May 2013. Letters and arrows in the microscopic image denote locations where Se K-edge XANES spectra were recorded. Map coordinates are in mm. Color coding represents detector counts (b, c) and voltages of the diode (d) used to measure the transmitted signal.*

In contrast, an occurrence of Se as mixture of Se(0) and Se(IV) at almost constant ratio over the entire location of the sample appears quite unlikely. The similarity among all Se-K XANES spectra recorded rather points to a unique chemical state of Se in the investigated spent fuel sample. Se as a fission product is generated with a very low yield and even in high burnup fuel represents no more than a trace component. It is therefore unlikely that Se may form concentrated phases in spent fuel. Dissemination of Se as trace element, e.g. as dispersed substituent in the UO_2 lattice or adsorbed on the fuel grain surfaces, is the more probable option.

Table 2: LCF results of raw (non-smoothed) spectra with statistics for Se(0) - Se(IV)O_2 combinations.

| | *Position | Se(0) + Se(IV)O_2 | | | Se(0) + ZnSe(-II) | | |
		at% Se(0)	±	R	at% ZnSe(-II)	±	R
1st beamtime							
spot 4	M	54.1	3.6	0.044	91.9	5.7	0.028
spot 5	M	52.2	2.6	0.023	84.2	3.9	0.018
spot 7	M	48.7	2.0	0.012	89.5	2.7	0.008
spot 8	M	56.2	3.7	0.050	79.7	5.8	0.044
spot 10	M	41.0	2.6	0.018	100.0	n.d.	0.013
spot 14	C	47.6	2.1	0.012	88.8	3.6	0.012
spot 15	C	52.3	2.0	0.011	82.0	3.4	0.011
spot 19	C	42.0	2.8	0.023	100.0	n.d.	0.021
mean		**49.3 ± 5.5**	**2.7**	**0.024**	**89.5 ± 7.6**	**4.2**	**0.019**
2nd beamtime							
C1	M	49.8	4.3	0.041	81.1	7.5	0.045
C2	M	57.7	3.3	0.032	71.8	5.5	0.032
C3	M	41.9	2.8	0.020	98.3	5.4	0.025
D1	M	41.0	4.0	0.041	98.2	7.4	0.048
F2	M	44.7	4.2	0.040	82.1	7.5	0.045
G1	M	48.3	3.1	0.024	85.2	5.8	0.028
G3	M	46.7	2.8	0.020	91.9	5.7	0.028
mean		**47.2 ± 5.6**	**3.5**	**0.031**	**86.9 ± 9.7**	**6.4**	**0.036**

*Position of the probed location in the fuel pellet: R=rim, M=middle, C=center; the Se amount found in the region corresponding to the rim (R) of the pellet was not sufficient to provide usable spectroscopic data.

n.d.: ATHENA LCF routine was unable to determine error bars, implying that one of the used components, in this case Se(0), is unsuitable.
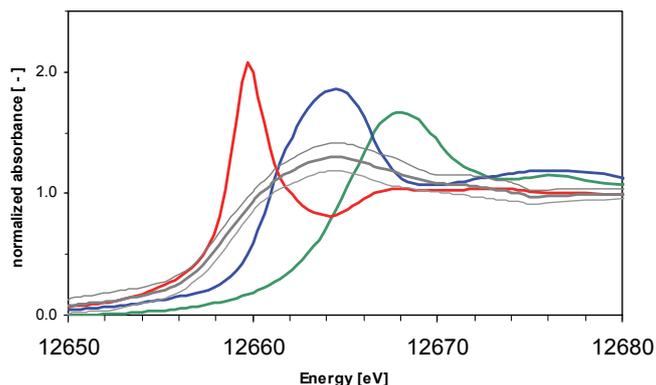
Figure 4: *Average smoothed Se K-edge XANES spectra from all measurements recorded on the spent fuel samples from the same fuel pellet (thick grey line) and envelope of all individual spectra (thin grey lines) compared with the Se K-edge XANES spectra recorded on several Se reference compounds (red = Se(0), blue= Se(IV)O$_2$, green = Na$_2$Se(VI)O$_4$).*
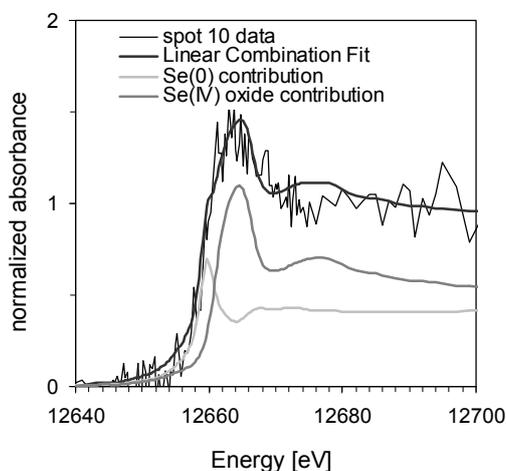

Figure 5: *Example of a LCF of the Se K-edge XANES data from Se(0) and Se(IV) reference compounds for an individual Se K-edge XANES spectrum collected on the spent fuel sample (spot 10).*
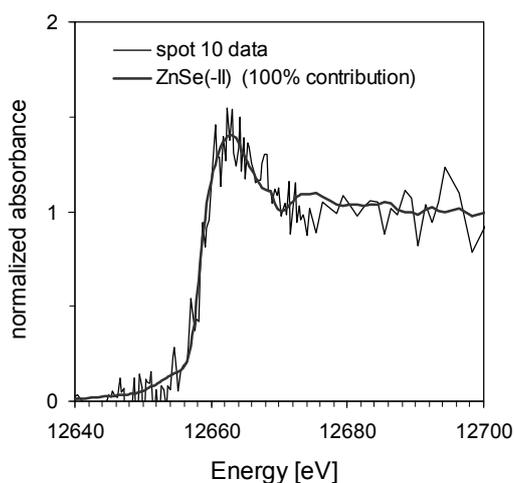
Figure 6: *Using the Se(0) and ZnSe(-II) K-edge XANES spectra as standards for the LCF also leads to acceptable fits of the Se K-edge XANES spectra recorded on spent fuel samples, always with a major contribution by the latter compound. In some cases (e.g. "spot 10") the ZnSe(-II) spectral contribution is 100%.*

2.3.   *XAS measurements on non-irradiated doped UO₂ powdered samples*

X-ray absorption spectra (XAS) of the non-irradiated UO_2 samples described in Section 1.1 were measured at the INE beamline (ANKA synchrotron, Eggenstein-Leopoldshafen, Rothe et al., 2012) using in-house beamtime kindly granted to us by KIT-INE (November 14th-16th, 2012). The purpose of such measurements was to evaluate whether similar measurements with highly active spent fuels would be technically feasible, considering the low concentrations of the nuclides of interest and the heavy UO_2 matrix.

XAS measurements were carried out using an X-ray beam size of 500 μm (horizontal) x 200 μm (vertical) (at 13 keV) at the Se-K edge. Due to beamtime limitations, absorption spectra across the I-L and Cs-L edges could not be measured.

The essential results from these feasibility measurements are illustrated in Figure 7, which shows good quality XANES spectra for the samples doped with 2,000 and 100 ppm Se and still acceptable spectra at the lowest Se concentration (10 ppm). Moreover, it was even possible to obtain a usable EXAFS spectrum for the 100 ppm Se sample, which is the most representative (i.e. the closest) concentration expected in high burn-up spent fuel.

In summary, the feasibility test was positive, indicating that Se-K edge absorption spectroscopy measurements on real spent fuel samples are likely to be successful at the INE beamline and might even have a quality sufficient for EXAFS analyses.
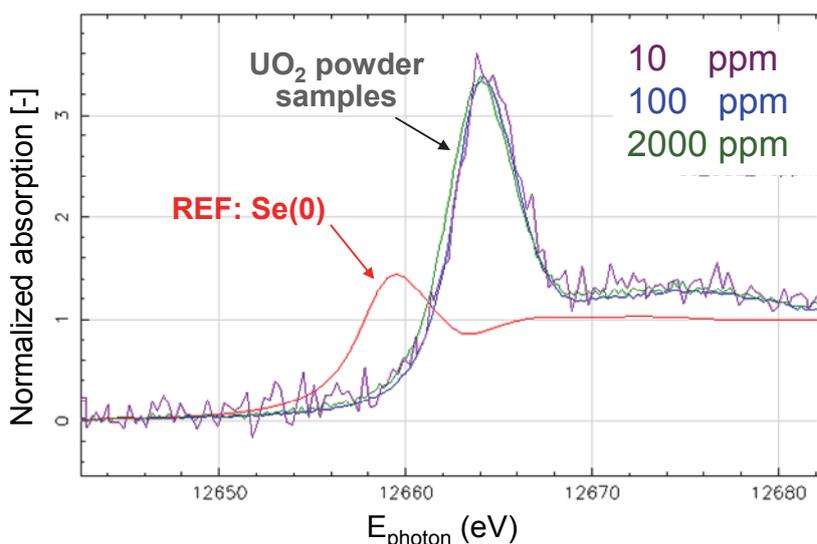

Figure 7: *Se K-edge XANES of the three doped non-irradiated UO₂ powdered samples listed in Table 1, compared to the Se K-edge spectrum of a metallic Se reference.*

c)	Fit Se-O	SeO$_2$ model compound
R [Å]	1.66 ± 0.02	1.62
CN	4.0 ± 1.1	4
σ^2	0.002 (fixed)	
S$_0$	0.91 (fixed)	
E$_0$	0.00 (fixed)	
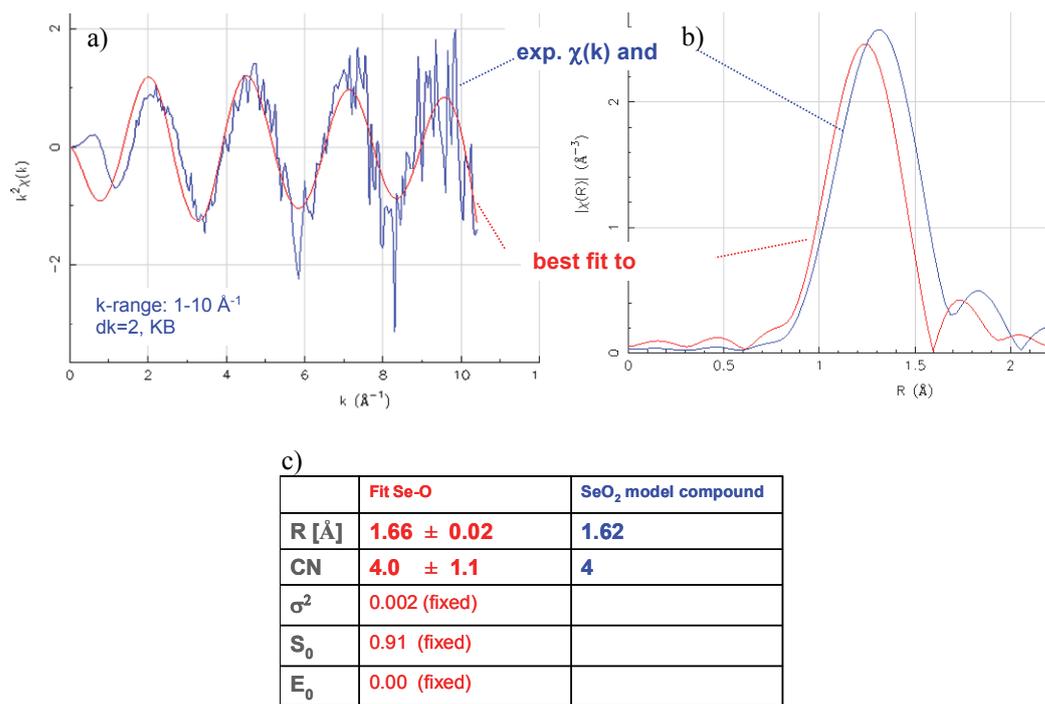
Figure 8: *(a) EXAFS signal (in blue) extracted from the Se K-edge XAFS spectrum recorded on a non-irradiated UO$_2$ powdered sample and (b) Fourier transform (FT) of the EXAFS signal (in blue) with corresponding fits of both the EXAFS and FT signals (in red). (c) The structural parameters - Se-O distance (R) and coordination number (CN) - obtained from the fits for the first coordination shell around the Se absorbing atom are listed in red and match the values determined by X-ray diffraction of the compound used as dopant (SeO$_2$) (in blue). The Debye-Waller factor (σ^2), the amplitude reduction factor (S$_0$), and the energy shift (E$_0$) were fixed at the indicated values.*

Conclusions and Future Work

The spectroscopic data so far available indicate that Se in the investigated (non-leached) HBU fuel sample is at least partly present in reduced form, either as Se(0) or Se(-II). Both oxidation states are characterized by low solubilities and should therefore limit the release of Se to aqueous solutions. Nevertheless, the linear combination fits do not allow us to exclude the presence of substantial amounts of oxidized, soluble Se(IV) species.

Because only XANES spectroscopy is accessible at such low Se concentrations, we propose to resolve the dilemma via theoretical XANES spectra calculations using the Feff (Ankudinov et al., 1998) and FitIt (Smolentsev and Soldatov, 2007) codes. Such calculations have been recently started and should be completed shortly. The idea is to calculate spectra for different assumed coordination environments of Se in the UO$_2$ matrix and compare the theoretical spectra with the experimental spectra. Calculations will be carried out assuming either Se(-II) substitution for O(-II) or Se(IV) substitution for U(IV), under account of lattice deformations induced by the different sizes of substituent and substituted ions. The results of these theoretical calculations will be documented in the final report.

Another important issue is the generalization of the results, i.e. whether the findings obtained for the Leibstadt spent fuel samples can be extended to spent fuel from other reactors. To this aim a prospective collaboration with the FIRST-Nuclides partner Studsvik has been initiated. The plan is to carry out similar XANES measurements on a high burn-up UO$_2$ spent fuel from the Swedish Oskarshamn reactor, both before and after

aqueous leaching. At the same time, an optimization of the sample preparation procedure will be attempted using the focused ion beam (FIB) facility at Studsvik. The aim is to obtain a sufficiently thick sample with plane surfaces, by cutting 20 μm x 20 μm rectangular chips of 5 μm thickness from different pellet locations (center and rim) with the ion beam milling technique. This should improve the signal-to-noise-ratio of the experimental spectra and reduce the time consuming procedure for particle localization during the beamtime. A SLS beamtime proposal has been recently submitted. However, the realization of this plan in the framework of FIRST-Nuclides will only be possible if some logistic and financial issues are resolved (limitation of preparation and transport costs).

Acknowledgement

References

Ankudinov, A.L., Ravel, B., Rehr, J.J., Conradson, S.D. (1998). Real-Space Multiple-Scattering Calculation and Interpretation of X-Ray-Absorption Near-Edge Structure. Phys. Rev. B, 58, 7565.

Beck, H.P., Dausch, W. (1989). The Refinement of α-USe$_2$, Twinning in a SrBr$_2$-Type Structure. J. Solid State Chem., 80, 32-39.

Curti, E., Aimoz, L., Kitamura, A. (2013). Selenium Uptake onto Natural Pyrite. J. Radioanal. Nucl. Chem., 295 1655-1665.

Degueldre, C., Martin, M., Kuri, G., Grolimund, D., Borca, C. (2011). Plutonium–Uranium Mixed Oxide Characterization by Coupling Micro-X-Ray Diffraction and Absorption Investigations. J. Nucl. Mat., 416, 142-150.

Johnson, L., Günther-Leopold, I., Kobler Waldis, J., Linder, H.P., Low, J., Cui, D., Ekeroth, E., Spahiu, K., Evins, L.Z. (2012). Rapid Aqueous Release of Fission Products from High Burn-Up LWR Fuel: Experimental Results and Correlations with Fission Gas Release. J. Nucl. Mat., 420, 54-62.

Kohlmann, H., Beck, H.P. (1997). Synthesis and Crystal Structure of the γ-Modifications of US$_2$ and USe$_2$. Z. anorg. Allg. Chem., 623, 785-790.

Ravel, B., Newville, M. (2005). ATHENA, ARTEMIS, HEPHAESTUS: Data Analysis for X-Ray Absorption Spectroscopy Using IFEFFIT. J. Synchrotron Rad., 12, 537-541.

Rothe, J., Butorin, S., Dardenne, K., Denecke, M. A., Kienzler, B., Löble, M., Metz, V., Seibert, A., Steppert, M., Vitova, T., Walther, C., Geckeis, H. (2012). The INE-Beamline for Actinide Science at ANKA. Rev. Sci. Instrum., 83, 043105.

Scheinost, A.C., Kirsch, R., Banerjee, D., Fernandez-Martinez, A., Zaenker, H., Funke, H., Charlet, L. (2008). X-Ray Absorption and Photoelectron Spectroscopy Investigation of Selenite Reduction by Feii-Bearing Minerals. J. Cont. Hydrol., 102, 228-245.

Smolentsev, G., Soldatov, A.V. (2007). FitIt: New Software to Extract Structural Information on the Basis of XANES Fitting. Comp. Matter. Sci., 39, 569-574.

LEACHING TESTS FOR THE EXPERIMENTAL DETERMINATION OF IRF RADIONUCLIDES FROM BELGIAN HIGH-BURNUP SPENT NUCLEAR FUEL: OVERVIEW OF PRE-TEST FUEL CHARACTERIZATION, EXPERIMENTAL SET-UP AND FIRST RESULTS

Thierry Mennecart*, Karel Lemmens, Christelle Cachoir, Adriaensen Lesley, Dobney Andrew

Belgian Nuclear Research Centre, SCK•CEN (BE)

* Corresponding author: thierry.mennecart@sckcen.be

Abstract

In the framework of the FIRST-Nuclides program, SCK•CEN is conducting leaching experiments on a PWR UOX fuel, taken from the Belgian Tihange 1 reactor, with a rod average burnup of 50 MWd/kg$_{HM}$ in order to determine the rapid release of some of the most critical radionuclides. The main experimental parameters were defined, i.e. the type of fuel, the number of tests and the sample preparation, the experimental setup, the leaching test conditions (medium, atmosphere), the sampling scheme and the surface and solution analyses. The leaching tests started in April 2013. This paper describes how the leaching experiments were started in April 2013, and presents some preliminary results.

Introduction

As one of the partners of FIRST-Nuclides with a hot-cell infrastructure and the required analytical laboratories, SCK•CEN is performing leaching tests on spent fuel samples with a relatively high burn-up. For this purpose, a fuel rod was selected from the spent fuel stock available at SCK•CEN for which the characteristics are known and can be made public.

The selected fuel samples originate from a PWR UOX fuel from the Belgian Tihange 1 reactor with an average burnup of 50 MWd/kg$_{HM}$. More information about this fuel was given in the paper from SCK•CEN's contribution to WP1 of FIRST-Nuclides (Govers et al., 2012).

The results obtained from leaching tests depend on how the fuel samples are prepared before leaching commences. Cladded fuel segments and decladded fuel fragments, or fragments from the centre or the periphery of the pellet will exhibit different leaching behaviours. A combination of differently prepared samples provides the most complete information, but for budgetary reasons, the number of tests with different samples has been limited to two at SCK•CEN.

In the following sections, we describe the sample preparation, the sample pre-test characterization, the experimental setup, the leachate composition, the solution analyses and the first results, before ending with our conclusions and future work.

Sample preparation

Two fuel segments, about 2.4 cm long, including one whole and two half pellets, were taken from the central part of the fuel rod (Govers et al., 2012), and prepared as samples for leaching test. The samples were prepared in hot cells under ambient atmosphere, implying that we can expect the formation of a thin oxidized $UO_{2.33}$ layer at the fuel surface by taking up oxygen at the interstitial sites in the UO_2 lattice (Johnson et al., 1988).

As agreed with the other partners in WP3, every participating laboratory should perform at least one test with an intact cladded fuel segment. So the first segment is used as it is after cutting, without any further treatment. For a second test with the decladded sample, the rod is cut in three parts of 0.8 cm (Figure 1). For each piece of 0.8 cm, the cladding is removed by pressure using a hydraulic pump with a piston which has a diameter close to the inner diameter of the cladding. Due to the strong exerted pressure during this operation, the fuel pellets were broken in fragments and powder of different sizes. In order to compare the two leaching tests, the three parts of the cladding and all the different fuel fragments and the fuel powder were leached together. Like this, we got the exact equivalent sample for the two leaching tests. Only the accessibility of the spent fuel for the leaching solution differs between these two leaching tests.
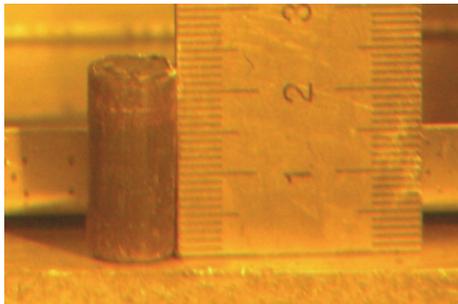

Sample of SNF for leaching test 1 'Intact sample'
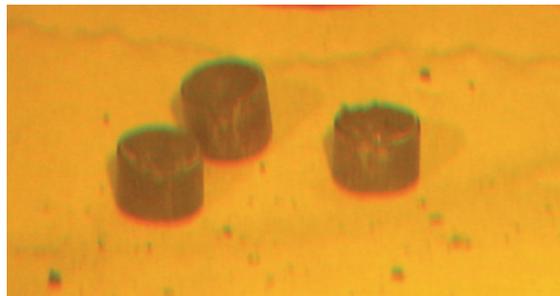
The three pieces (0.8 cm each) of the sample prepared for leaching test 2 'Decladded sample'

Figure 1: *Samples prepared for the two leaching tests with spent nuclear fuel.*

A third, adjacent segment was cut in order to determine the burnup by means of radiochemical analysis. A fourth, shorter segment, was cut for the microstructural characterization of the fuel before leaching. That same sample was also analysed by electron-probe microanalysis (EPMA) to determine the local concentration of various elements.

A rotary disk using a cooling solution (diamond saw) was used to cut the sample set aside for the determination of the burnup and the optical measurements. The aim of the FIRST Nuclides program is to study the release of the most soluble radionuclides when the spent nuclear fuel is in contact with a solution for the first time. Consequently, the classic method using a cooling solution was not conceivable to cut the rod segments for the leaching test. Hence, a commercial tube cutter was used (tool of plumbing) to cut these segments under dry conditions. Only the cladding was cut with this tool. The fuel pellet is manually broken at the cutting plane.

Sample pre-test characterization

Although fabrication data and detailed irradiation history will be available for the project, a cross-check between these estimations and experimental observations of the state of the irradiated fuel is needed in order to reduce

uncertainties on e.g. available free surfaces for leaching and on fission product inventory and location at the end of the irradiation. Good agreement between experiments and theoretical models for the behavior of "observable" fission products should allow us to make firm hypotheses about the location of the few isotopes for which the experimental sensitivity is too low.

Burnup analyses

The average pellet burnup will be determined by radiochemical analysis (RCA) of a small fuel segment (equivalent of 2 pellets) cut in the vicinity of the test samples. The proposed cutting scheme specifies a cutting from mid-pellet to mid-pellet in order to keep a relevant inventory of Cs, bearing in mind the relocation of Cs to the pellet-pellet interface observed upon γ-scanning. The burnup determination is based on the measurement of various burnup indicators, mainly Nd isotopes, by Thermal Ionization Mass Spectrometry (TIMS), and confirmed by ^{137}Cs and ^{144}Ce, using γ-spectrometry. Other relevant isotopes in terms of the fast/instant release fraction will also be measured, within the range permitted by the technique. The analysis is foreseen for the second semester of 2013.

Microstructure analysis – Electron-probe microanalysis

A segment of the rod fuel was examined using different surface analysis techniques. After polishing, optical microscopy and Scanning Electron Microscopy (SEM) were used to observe the surface state and the different zones before the leaching test. The same sample was also subjected to Electron-Probe MicroAnalysis (EPMA). The instrument can analyse all elements from C to Cm. The radial distribution of Xe, Cs and Nd (together with U and Pu) was measured using this technique. The analyses were already done but need to be validated before publication.

Experimental setup

The experiments are performed inside a hot cell under an air atmosphere. The experimental setup is based on previous work performed at the Paul Scherrer Institute (PSI). The materials have a good resistance under high radiation fields. Pictures of the glass column used for the experimental work are shown in Figure 2. The setup consists of glass tubes, used as leaching vessels, each equipped with a piston that fits tightly in the glass tube. After filling the tube with the leaching solution, the air in the headspace is pushed out by the piston via an overflow. Because there will be little or no further exchange between the solution in the vessel and the air in the hot cell, fuel oxidation by atmospheric oxygen should be limited during the leaching test (Johnson et al., 2012). At the bottom of each glass tube, a glass frit prevents the loss of spent fuel fragments during sampling. A moderate pressure on the piston is sufficient to force the solution through the frit. The sample volume at each sampling point depends on the number and height of the perforations in the metal rod that fixes the piston at the desired height.

Screw

Pin

Magnetic stirrer

Frit

Teflon valve

Holder for the leaching tests
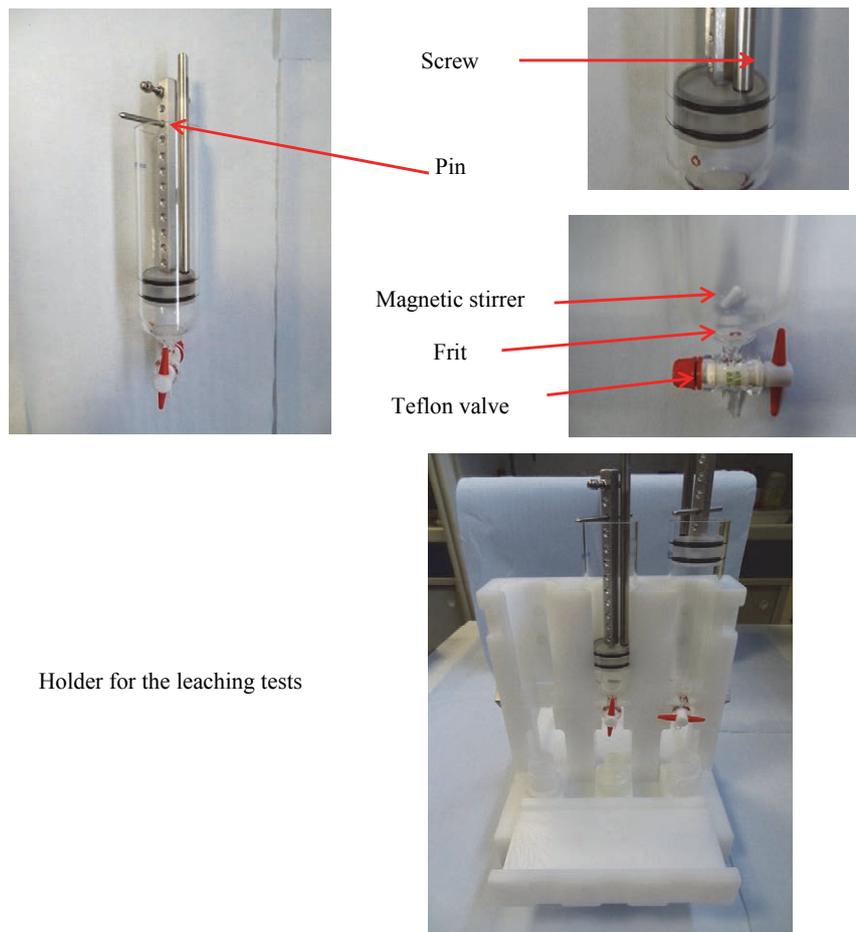
Figure 2: *Experimental setup used for the leaching of the spent fuel*

Three parallel leaching tests are conducted: one leaching unit contains the intact fuel segment, a second unit contains the 'decladded' (fragment of different size + powder) sample, and a third unit is only filled with the leachate, as a blank test to estimate the cross contamination.

Leachant composition

To eliminate the uncertainty linked to the use of different leachates when the tests with different fuels are compared, there is agreement within WP3 of FIRST-Nuclides to use a standard leachant, consisting of 19 mM NaCl + 1 mM NaHCO$_3$. The pH of this solution is around 7.4. No pH buffer will be added to the solution, because important pH changes are not expected to occur.

Preleaching, leaching tests

During the preparation of the sample, the spent fuel samples were never in contact with a liquid. At contact with the leachant we thus expect a further oxidation by dissolved atmospheric oxygen or oxidizing radicals following the half-reaction:

$$UO_{2.33} + 0.33\ H^+ \rightarrow (UO_2^{2+})_{ads} + 0.33\ OH^- + 1.33\ e^-$$
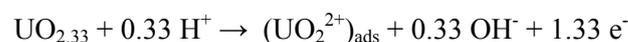
The thus formed U(VI) will dissolve quickly by formation of $UO_2(CO_3)_3^{4-}$ with dissolved CO_2 (Johnson et al., 1988). Consequently, we expect a high initial release of the most mobile elements and a rapid dissolution of the oxidized uranium. This information is crucial for the interpretation of the experiments. If the initial dissolution of the spent fuel leads, however, to high concentrations in solution of the considered radionuclides, the smaller further variation of these concentrations in function of time could be less obvious to observe. Consequently, a preleaching was performed. Thus, the spent fuel samples were two times preleached with 50 mL of the solution during 3 – 4 days. At the end of the second preleaching, the column was filled with 150 mL of fresh solution to cover the whole test duration of 1 year. After 7, 35, 180 and 360 days (end of the experiment) samplings of 20 mL are foreseen. At the present time, the two preleaching samples and the two first leaching samples after 7 and 35 days have been taken. The two leaching samples correspond to 14 and 49 days of cumulative time.

All (pre-)leached solutions are analyzed to determine the concentrations of the radionuclides by various techniques (see section solution analyses). The same procedure is also applied for test 3 (blank), but only solutions after 7 and 360 days will be analyzed. The other samples will be kept in the hotcell for analysis in case of questionable results.

In the case of test 1 (with the intact spent fuel sample), the solution looks translucent and any detached fuel particles were retained in the column thanks to the frit on the bottom of the column. In the case of test 2 with the decladded spent fuel, the solution is cloudy due to the fine particles of spent fuel in suspension. During the replacement of the solution for the two preleaching and the sampling solutions, some of the finest powder particles have passed through the frit into the solution for analysis. To estimate the loss of material during these steps, the solutions were filtered with a previously tarred paper filter. After drying, the filter was weighed and the mass of spent fuel was estimated. The amount of powder on the filter represents less than 1% of the total mass of the spent fuel used per test, and it is considered as negligible for the further calculations.

Solution analyses

Only the most relevant radionuclides are measured, using either mass-spectrometry or radioanalytical techniques.

The concentration of ^{238}U is used to estimate the dissolution rate of the fuel and is measured by means of ICP-MS. ICP-MS also gives the concentrations of ^{93}Zr, ^{129}I, ^{135}Cs, ^{137}Cs, ^{99}Tc, ^{107}Pd and ^{126}Sn in the leachates. Some of these radionuclides (especially ^{107}Pd, ^{129}Sn and ^{99}Tc) may have concentrations close to the detection limit.

The concentrations of ^{59}Ni, ^{94}Nb and ^{137}Cs are measured by γ- or X-ray-spectrometry. The concentrations of ^{14}C, ^{63}Ni and ^{90}Sr are determined using liquid scintillation counting (LSC).

In some cases, prior to the analyses, a separation is required to avoid interference with others radionuclides. This is the case for ^{14}C, ^{59}Ni, ^{63}Ni, ^{94}Nb and ^{90}Sr.

Although the measurement of the ^{14}C-, ^{59}Ni-, ^{63}Ni- and ^{94}Nb-content of waste matrices is performed routinely at SCK•CEN, their analysis in spent fuel and/or leachates has not been performed at SCK•CEN previously. An evaluation and optimization of existing methodologies has to be performed. Analyses of ^{79}Se is not planned.

Results

The complete analysis of the samples takes time. Only the gamma measurements for the ^{134}Cs and ^{137}Cs from the two preleaching samples (P1 and P2) and the two first leaching samples (14 and 49 days of cumulative time) are currently available (Figure 3).

The ^{134}Cs and ^{137}Cs follow the same trend. We observe a high initial release in solution during the preleaching period. Afterwards, the Cs release is slower and seems to have reached a plateau after 50 days. This tendency has to be confirmed with the next samplings. The maximal value is, however, reached faster in the experiments with the decladded fuel than with the intact fuel even if the value of activity tends toward the same value in both systems i.e. ~ 75 kBq and ~ 1.5 MBq for the ^{134}Cs and ^{137}Cs, respectively. The Cs activity thus increases faster in the decladded fuel system, where the fuel is more accessible for water, than in the cladded system.
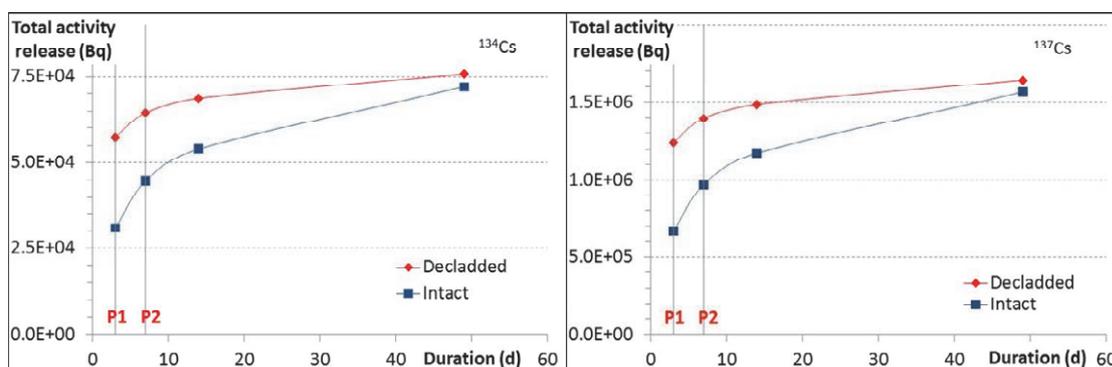

Figure 3: *Evolution of the activity of ^{134}Cs (left side) and ^{137}Cs (right side) for the test with the "intact" and "decladded" fuel. P1 and P2 correspond to the two renewals of the solution during the preleaching steps.*

Conclusions and future work

The experiments performed by SCK•CEN on cladded and decladded UOX PWR fuel segments allow the determination of the fast release in solution of the easily soluble radionuclides. After the preparation of the spent fuel samples in dry conditions, the samples were leached with a standard solution and samplings were performed for the analysis of the main radionuclides. The experiments started in April 2013. The results are not yet fully available. Nevertheless, the first Cs results already indicate a faster release for the decladded fuel than for the intact fuel. The next samplings are planned by the end of 2013 (6 months) and in April 2014 (1 year).

Acknowledgement

References

Johnson, L.H., Shoesmith D.W. (1988). Radioactive Waste Forms for the Future. Eds.: Lutze, W. and Ewing, R.C., North Holland.

Govers, K., Verwerft, M., Lemmens, K. (2012). Characterization of SCK•CEN Fuel Samples Used for Leaching Test Experiments in the Framework of FIRST-Nuclides. 1st Annual Workshop Proceedings – 7th EC FP – FIRST-Nuclides, 9th – 11th October 2012, Budapest, Hungary.

Johnson, L., Günther-Leopold, I., Kobler Waldis, J., Linder, H.P., Low, J., Cui, D., Ekeroth, E., Spahiu, K., Evins, L.Z. (2012). Rapid Aqueous Release of Fission Products from High Burn-Up LWR Fuel: Experimental Results and Correlations with Fission Gas Release. Journal of Nuclear Materials, 420, 54-63.

IMPACT OF WATER RADIOLYSIS ON URANIUM DIOXIDE CORROSION

Johan Vandenborre[1*], Ali Traboulsi[1], Guillaume Blain[1], Jacques Barbet[2], Massoud Fattahi[1]

[1] SUBATECH, UMR 6457, Ecole des Mines de Nantes, CNRS/IN2P3, Université de Nantes (FR)
[2] Cyclotron ARRONAX (FR)

* Corresponding author: johan.vandenborre@subatech.in2p3.fr

Abstract

In this work, the oxidation of UO_2 by the radiolysis products of water at the solid/solution interface is investigated in function of the dose under open and close atmospheres. Irradiation is realized by He^{2+} beam provided by the ARRONAX cyclotron with an energy of 66.5 MeV and a dose rate of 4.37 kGy/min. The aim of this investigation is to determine the effect of the atmosphere (presence of H_2) and the dose on the UO_2 oxidation in order to couple for the first time (1) characterization of the secondary oxidized phases, (2) quantification of H_2O_2 and H_2 produced by water radiolysis and (3) determination of the quantity of uranium released into the solution. The kinetic of the solid surface oxidation is followed by Raman spectroscopy. H_2O_2 and H_2 are measured respectively by UV-VIS spectrophotometry and micro Gas Chromatography (μ-GC). Inductively Coupled Plasma Mass Spectrometry (ICP-MS) is used to quantify the soluble uranium species released into the solution. Our results show that He^{2+} irradiation of water induced oxidation of the UO_2 surface which depended on the atmosphere and the dose rate. We present below the results obtained for two samples irradiated at a dose of 8.73 kGy under the two atmospheres mentioned above. Results shows the Raman spectra of unirradiated UO_2 (a) and a sample irradiated under open atmosphere (b, c, d). The spectra of the irradiated sample are obtained 0.3, 42 and 169 hours after contact with the irradiated water. When comparing the two spectra, 2 identical Raman signals can be observed at 445 and 560 cm^{-1}. The first one characterizes the U-O bonding distance in the fluorite structure of UO_2 and the second one indicates the presence of defects in the matrix. After irradiation, two Raman signals appear at 820 and 865 cm^{-1}. These vibration bands indicate the presence of studtite ($UO_4 \cdot 4(H_2O)$) formed by oxidation of the UO_2 surface by H_2O_2 produced by water radiolysis. We have verified that studtite is not formed by oxidation of the UO_2 surface by O_2 present in the atmosphere. For the irradiated sample, $G(H_2O_2)$ formed by water radiolysis is 0.06 μmol/J and the quantity of uranium species released in the irradiated solution is $11.5 \cdot 10^{-7}$ mol/L. For the sample irradiated under close atmosphere, oxidation is much slower due to the inhibition effect of H_2 produced by water radiolysis. In these conditions, $G(H_2O_2)$ and $G(H_2)$ are respectively 0.1 and 0.02 μmol/J. The concentration of Uranium species in the solution is $5.3 \cdot 10^{-7}$ mol/L which is comparable to that published in the literature.

$G(H_2O_2)$ obtained in open atmosphere is two times lower than that obtained in close one. In this last condition, H_2O_2 yield is equal to that of ultra-pure water which means that this molecule was not consumed. Moreover, $G(H_2)$ obtained in this work is lower than that obtained by radiolysis of ultra-pure water in similar conditions. From this, we can conclude that H_2 has an inhibition effect on the UO_2 oxidation and this inhibition does not take place by direct effect on H_2O_2 as oxidant consumer but by interaction between H_2 and the UO_2 surface.

Introduction

This article deals with the radiolytic corrosion at the UO_2 surface. We study the impact of water radiolysis onto the corrosion of the grain boundaries (GB) present at the TRISO particle surface from irradiated fuel. The influence of H_2 produced by water radiolysis on the UO_2 corrosion is also studied. More details on the context of this study is published elsewhere (Kienzler et al., 2012). The aim of this work was to investigate experimentally the effect of molecular radiolytic species (H_2 and H_2O_2) produced by localized $^4He^{2+}$ radiolysis of water on UO_2 corrosion in function of different parameters. Water in contact with UO_2 particles was then irradiated by $^4He^{2+}$ beam at different absorbed doses and under different atmospheres in order to evaluate the effect of H_2 and the absorbed dose on the corrosion process. To fulfill this work, we choose to investigate the corrosion of the surface of solid particles by Raman Spectroscopy which is known to be very efficient in surface characterization of solid state materials. Soluble uranium species leached into the solution were analyzed by Inducted Coupled Plasma Mass Spectrometry (ICP-MS) technique. H_2O_2 and H_2 produced by water radiolysis were respectively quantified by UV-VIS Spectrophotometry and Gas Chromatography (μ-GC) in order to calculate their radiolytic yields, compare them to those of pure water and clarify the role of these two species in the UO_2 corrosion.

Material and Methods

The experimental section (analytical tools and irradiation conditions) is described elsewhere (Kienzler et al., 2012). 3 irradiations were performed for 3 sets of samples: (1) irradiation under open air atmosphere (oxidative conditions without H_2), (2) closed with air atmosphere (oxidative conditions with H_2 produced by water radiolysis), and (3) closed with Ar/H_2 (4%) atmosphere (reductive atmosphere where H_2 is initially added into the system before irradiation by the Ar/H_2 (4%) gas).

Results

1. UO_2 Surface Characterization

UO_2 TRISO particle is constituted of UO_2 based kernel (500 μm of diameter) composed by grains and grain boundaries (Figure 1). The grain size has been measured between 10 and 20 μm. After irradiation, SEM pictures were realized on the surface particles in order to determine the zones most affected by the corrosion process (Figure 2). Figure 2 clearly shows that regardless the irradiation atmosphere, the grain boundaries are much more degraded than the UO_2 grains. It appears too that the corrosion did not occur homogeneously on the entire surface. Some regions of the grains surface are indeed more corroded. The corrosion can be considered as localized on GB.
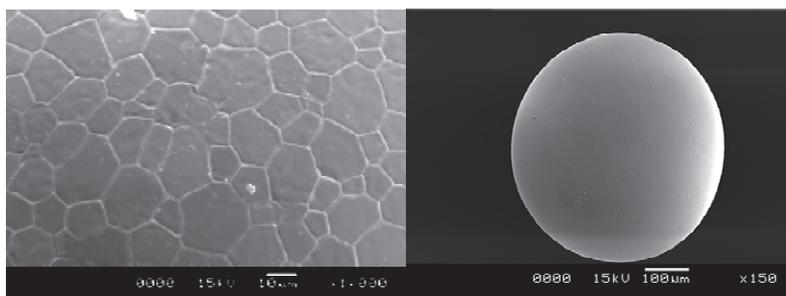

*Figure 1: SEM picture of the surface of an unirradiated UO_2 particle.*
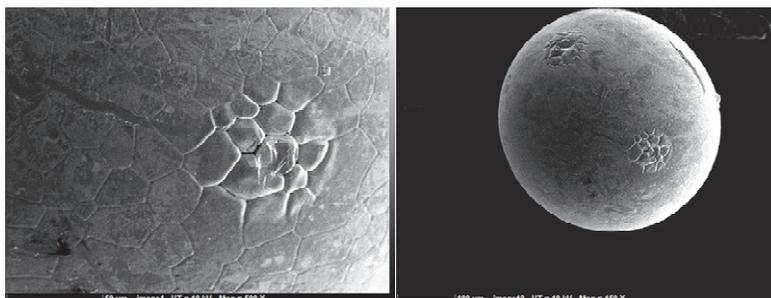
Figure 2: *SEM pictures of the surface of a UO₂ particle corroded in open air atmosphere.*

The Raman spectra of the unirradiated UO_2 is presented in Figure 3. It presents two characteristic bands around 445 cm^{-1} and 560 cm^{-1}. The former is affected to the triply degenerated Raman active mode (T_{2g}) of U-O bond (Amme et al., 2002; Amme et al., 2005; Desgranges et al., 2012; He and Shoesmith, 2010; Manara and Renker, 2003) whereas the latter characterizes defects present initially in the UO_2 fluorite structure (He and Shoesmith, 2010).

To estimate the Raman spectral modifications brought by the radiolytic products of water in the different studied atmospheres, a comparison was made between the UO_2 spectra before and after irradiation. The results showed that after irradiation in close atmospheres, the spectra of the UO_2 particles remained stable in function of the dose (not presented in this paper). When water in contact with the UO_2 particles was irradiated in open to air atmosphere, no spectral modifications were observed until 21.8 kGy deposited in the solution. From 43.7 kGy, modifications can be seen between 800 and 900 cm^{-1} and appear clearly at the dose of 87.3 kGy. Two peeks appear indeed at 825 and 860 cm^{-1}. They characterize the metastudtite ($UO_2(O_2)\cdot 2H_2O$) (Amme et al., 2002; Canizarès et al., 2012; Guimbretière et al., 2011) formed on the UO_2 surface by oxidation with H_2O_2 produced by water radiolysis according to the Reaction (i) (Corbel et al., 2006):

$$UO_2 \;+\; 2H_2O_2 \;\rightarrow\; UO_2(O_2)\,(H_2O)_2 \tag{i}$$

After irradiation, temporal evolution of the solid particles was followed by Raman spectroscopy. The results showed that Raman spectra of the samples irradiated with an irradiation time t = 1 min remained unchanged after two months of the experiment. It seems that in these conditions, the concentration of H_2O_2 produced by water radiolysis was not sufficient to oxidize the UO_2 surface. For t ≥ 3 min, Raman spectra of the irradiated particles evolved slightly in function of time until one week after irradiation and then remained stable.

(a) : unirradiated UO$_2$
(b) : 0.3 hours
(c) : 42 hours
(d) : 169 hours

Formation of Studtite
by oxidation of UO$_2$

Raman signals
of UO$_2$
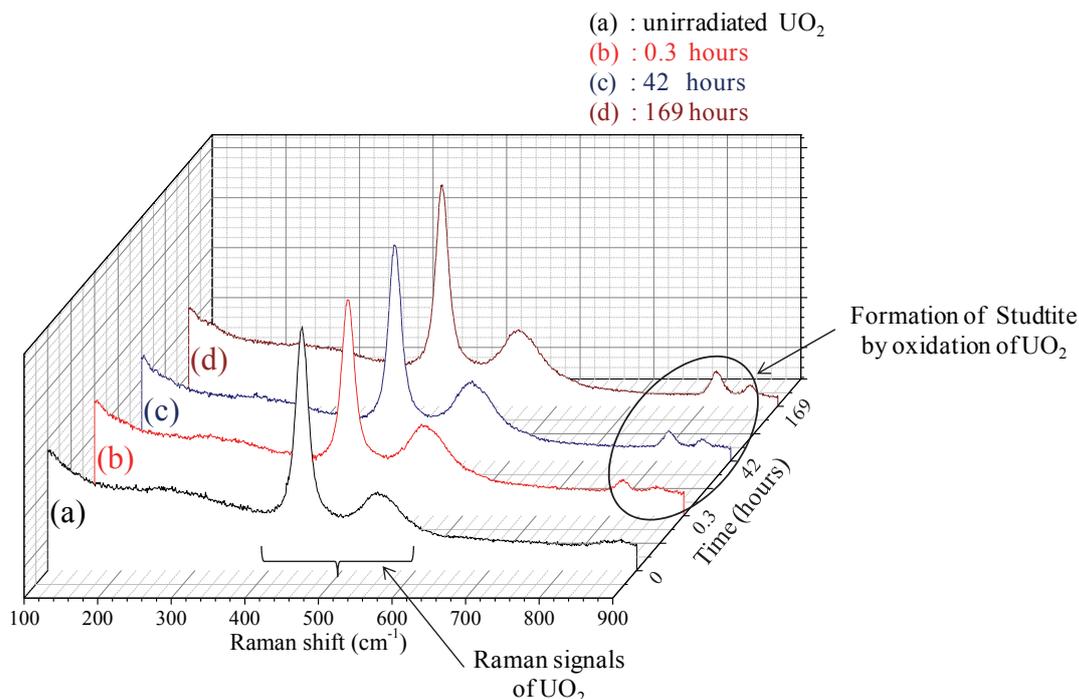
Figure 3: Raman spectra of unirradiated UO$_2$ ((a)) and a sample irradiated at 8.73 kGy under open atmosphere ((b), (c) and (d)). The spectra (b), (c) and (d) are obtained 0.3, 42 and 169 hours after contact with the irradiated solution.

2. Uranium Solubility and Dissolution Rate

After irradiation, water in contact with the UO$_2$ particles was collected to quantify the soluble uranium species leached into the solution. Indeed, the metastudtite phase formed on the UO$_2$ surface after oxidation by H$_2$O$_2$ produced by water radiolysis underwent later a dissolution step where uranyl ions (UO$_2$$^{2+}$) were leached into the solution. The mechanism of this dissolution reaction in ultra-pure water was rarely discussed in the literature. According to some authors (Sattonnay et al., 2001), the dissolution step occurs according to Reaction (ii):

$$UO_2^{2+}{}_{(s)} \quad + \quad H_2O \quad \rightarrow \quad UO_2(OH)^+ \quad + \quad H^+ \tag{ii}$$

However, Sattonnay et al. (2001) proposed this dissolution mechanism based on a pH decreasing observed in their case after the solution irradiation. But, in our work measurement of the irradiated solutions acidity after each irradiation showed that pH did not evolve significantly and remained between 6.5 and 7.5. This means that the above proposed mechanism (Reaction ii) does not occur in our case.

We have followed the variation of the soluble uranium species concentration leached into the solution after irradiation in function of the dose and the irradiation time in both open and close atmospheres. Regardless the irradiation atmosphere, the quantity of soluble uranium species increased with the dose and then remained constant from 43.6 kGy. At this latter dose, concentration of soluble uranium species found in close with air atmosphere (5.25·10^{-7} mol/L) is two-fold lower than that observed in open to air atmosphere (11.49·10^{-7} mol/L) due to inhibition of UO$_2$ oxidation by H$_2$ produced by water radiolysis. Values of [U] measured in our system at the steady state are presented in Table 1 for an irradiation time of 10 min together with the normalized leaching rate (r). Moreover, Table 1 presents also UO$_2$ dissolution rate values obtained from literature in order to compare it to our data. When UO$_2$ particles were irradiated between 10 and 20 min in close with air atmosphere,

concentration of Uranium species remained practically constant. The obtained values were respectively (4.44 ± 0.5) and $(5.25 \pm 0.5) \cdot 10^{-7}$ mol/L for the latter mentioned irradiation time. These values are comparable to most solubility data reported in the literature (Casas et al., 2009; Grambow et al., 2004; Jégou et al., 2003; Shoesmith and Sunder, 1992). However, we believe that in our work the thermodynamic equilibrium of the UO_2 particles dissolution was not achieved due to their composition of grains and grain boundaries. In these conditions, the dissolution rate was equal to 13.5 $g/m^2/d$. A comparison of our dissolution rates with literature data is given in Table 1. Despite the similarity with [U] reported in the literature, r values obtained in this investigation are at least 10^3 fold higher. It seems then that with the irradiation conditions used in our work, the UO_2 oxidation/dissolution mechanism occurred with a faster kinetic. This is very probably due to the impact of the high doses deposited into the irradiated solution for this work. In order to apprehend the dose impact on the UO_2 corrosion, we propose here a new methodology to express the dissolution rate. This methodology consists in calculating the dissolution rate in function of the dose deposited into the solution and not in function of the irradiation time. Thus, the new dissolution rate r' can be defined as follow:

$$r' = \frac{V}{S} \frac{d[U]}{dd} M_{UO_2}$$

Where $d[U]/dd$ (mol/m^3) is the variation of soluble uranium species in function of the dose deposited into the solution. In our case the r' values are 2.01 $\mu g/m^2/Gy$ for the open with air atmosphere experiment and 1.11 $\mu g/m^2/Gy$ for the close with air atmosphere one. These results confirm that the reducing atmosphere (in presence of H_2) has a strong diminishing impact onto the UO_2 dissolution rate. Moreover, we have recalculated the same new dissolution rate r' from literature data (Grambow et al., 2004; Jégou et al., 2003) (Table 1) in order to compare it to our results. Even after taking into account the effect of the dose, r' values obtained in this investigation still higher (Table 1). However, the dose rate used in our work is very high. It appears then that the dose rate is the main parameter which controls the UO_2 dissolution rate under irradiation.

Table 1: Steady state U concentrations, Dissolution rates (r and r') of UO2 and experimental conditions used in this study and others found in the literature.

Ref.	Physical aspect UO_2	$^4He^{2+}$ Beam	Dose Rate Gy/min	Atm.	[U] 10^{-7} mol/L	Diss. rate r $mg/m^2/d$	Diss. rate r' $\mu g/m^2/Gy$
This work	Particle	External source*	4,366	Ox	11.49	13,500	2.01
				Red	5.25	7,000	1.11
Shoesmith and Sunder (1992)	Pellet	Internal	No	Ox		0.5	X
Casas et al. (2009)	Particle	No	0	Red		23.3	X
Grambow et al. (2004)	Colloid	External source*	52.7	Red		15.7	0.246
Jégou et al. (2003)	Pellet	Internal**	18	Ox		2.5	0.095
			1.8	Ox		0.2	0.076

* $^4He^{2+}$ Beam produced by cyclotron facility

** Doped UO_2 with Pu

3.   H$_2$ and H$_2$O$_2$ Chemical Yields

When the UO$_2$ particles were irradiated in close with air atmosphere, H$_2$ produced by water radiolysis was quantified by calculating its radiolytic yield (G) in order to compare it to that of pure water and explain any gas consumption due to the inhibition of the UO$_2$ corrosion process. In our work, the solution used during irradiation is ultra-pure water (ρ = 1 kg/L) and the mean G(H$_2$) was 0.02 ± 0.002 μmol/J. It corresponds to the slope of the curve representing the variation of H$_2$ concentration in function of the dose. (Crumière et al., 2013) irradiated ultra-pure water by a cyclotron ^{4}He^{2+} beam with a 64.7 MeV energy and doses up to 800 Gy in Argon saturated atmosphere. G(H$_2$) obtained in their work was 0.061 ± 0.006 μmol/J which is three-fold higher than that found in this investigation (G(H$_2$) = 0.02 ± 0.002 μmol/J). The irradiation conditions used by (Crumière et al., 2013) are very similar to those used in our work which means that for the system UO$_2$/ultra-pure water, a non negligible part (around 2/3) of the H$_2$ produced by water radiolysis was consumed certainly by inhibition of the UO$_2$ oxidation process.

In both open to air and close with air atmospheres, concentrations of H$_2$O$_2$ produced by water radiolysis was determined by the Ghormley method (Ghormley and Hochanadel, 1954) to analyze the effect of the irradiation atmosphere on its consumption by the UO$_2$ oxidation process. During this study, we have followed the variation of H$_2$O$_2$ concentration produced by water radiolysis under open to air and close with air atmospheres in function of the dose. It shows that concentration of H$_2$O$_2$ produced by water radiolysis increased with the dose and then reached a steady state from 21.8 kGy and 65.5 kGy in open to air and close with air atmospheres respectively. At these latter doses, [H$_2$O$_2$] values were respectively $1.4 \cdot 10^{-4}$ and $5.5 \cdot 10^{-4}$ mol/L which means that H$_2$O$_2$ concentration was four-fold higher when the UO$_2$ particles were irradiated in presence of H$_2$. It seems then that in the latter conditions consumption of H$_2$O$_2$ and thus oxidation of the UO$_2$ surface was mainly inhibited by H$_2$ produced by water radiolysis. Radiolytic yields of H$_2$O$_2$ were also calculated and the values obtained were 0.06 ± 0.006 and 0.1 ± 0.01 μmol/J in open to air and close with air atmospheres respectively. G(H$_2$O$_2$) obtained in open to air atmosphere is two fold lower than that obtained in close with air one. In this last condition, H$_2$O$_2$ yield is equal to that of ultra-pure water (LaVerne, 2004; Pastina and LaVerne, 1999; Yamashita et al., 2008a; Yamashita et al., 2008b) which means that this molecule was not consumed whereas a non-negligible part of H$_2$ was consumed. From this, we can conclude that in open to air atmosphere, half of the H$_2$O$_2$ produced by water radiolysis was consumed by oxidation of the UO$_2$ surface leading to the formation of metastudtite secondary phase. We can conclude too that H$_2$ has an inhibition effect on the UO$_2$ oxidation and this inhibition does not take place by direct effect on H$_2$O$_2$ but by interaction between H$_2$ and the UO$_2$ surface.

Conclusions and Future work

In conclusion, this work brings some light on the radiolytic corrosion of UO$_2$ by identification of (1) the oxidized secondary phase formed (metastudtite) and following its temporal evolution, (2) the H$_2$ role as an inhibitor agent, (3) the oxidative role of H$_2$O$_2$ and (4) the quantity of U species released. Detailed mechanisms of UO$_2$ corrosion/oxidation will be proposed taking into account the phenomena of water radiolysis.

Furthers studies will be performed in order to determine the role of the radical speces produced by water radiolysis on UO$_2$ corrosion. Moreover, spacial resolution technique will be used in future surface characterization experiments in order to localize the corrosion on the grain boundaries as shown with SEM pictures.

Acknowledgement

References

Amme, M., Renker, B., Schmid, B., Feth, M.P., Bertagnolli, H., Döbelin, W., (2002). Raman Microspectrometric Identification of Corrosion Products Formed on UO_2 Nuclear Fuel During Leaching Experiments. Journal of Nuclear Materials, 306, 202-212.

Amme, M., Wiss, T., Thiele, H., Boulet, P., Lang, H., (2005). Uranium Secondary Phase Formation during Anoxic Hydrothermal Leaching Processes of UO_2 Nuclear Fuel. Journal of Nuclear Materials, 341, 209-223.

Canizarès, A., Guimbretière, G., Tobon, Y.A., Raimboux, N., Omnée, R., Perdicakis, M., Muzeau, B., Leoni, E., Alam, M.S., Mendes, E., Simon, D., Matzen, G., Corbel, C., Barthe, M.F., Simon, P. (2012). In Situ Raman Monitoring of Materials under Irradiation: Study of Uranium Dioxide Alteration by Water Radiolysis. Journal of Raman Spectroscopy, 43, 1492-1497.

Casas, I., de Pablo, J., Clarens, F., Giménez, J., Merino, J., Bruno, J., Martinez-Esparza, A. (2009). Combined Effect of H_2O_2 and HCO_3^- on UO_2(s) Dissolution Rates under Anoxic Conditions. Radiochimica Acta, 97, 485-490.

Corbel, C., Sattonnay, G., Guilbert, S., Garrido, F., Barthe, M.F., Jegou, C. (2006). Addition versus Radiolytic Production Effects of Hydrogen Peroxide on Aqueous Corrosion of UO_2. Journal of Nuclear Materials, 348, 1-17.

Crumière, F., Vandenborre, J., Essehli, R., Blain, G., Barbet, J., Fattahi, M. (2013). LET effects on the Hydrogen Production Induced by the Radiolysis of Pure Water. Radiation Physics and Chemistry, 82, 74-79.

Desgranges, L., Baldinozzi, G., Simon, P., Guimbretière, G., Canizares, A. (2012). Raman Spectrum of U_4O_9: a New Interpretation of Damage Lines in UO_2. Journal of Raman Spectroscopy, 43, 455-458.

Ghormley, J.A., Hochanadel, C.J. (1954). The Yields of Hydrogen and Hydrogen Peroxide in the Irradiation of Oxygen Saturated Water with Cobalt γ-Rays. Journal of the American Chemical Society, 76, 3351-3352.

Grambow, B., Mennecart, T., Fattahi, M., Blondiaux, G. (2004). Electrochemical Aspects of Radiolytically Enhanced UO_2 Dissolution. Radiochimica Acta, 92, 603-609.

Guimbretière, G., Canizares, A., Simon, P., Tobon-Correa, Y.A., Ammar, M.R., Corbel, C., Barthe, M.F. (2011). In-Situ Raman Observation of the First Step of Uranium Dioxide Weathering Exposed to Water Radiolysis. Spectroscopy Letters, 44, 570-573.

He, H., Shoesmith, D. (2010). Raman Spectroscopic Studies of Defect Structures and Phase Transition in Hyper-Stoichiometric UO_{2+x}. Physical Chemistry Chemical Physics, 12, 8108-8117.

Jégou, C., Broudic, V., Poulesquen, A., Bart, J.M. (2003). Effects of α and γ Radiolysis of Water on Alteration of the Spent UO$_2$ Nuclear Fuel Matrix. MRS Online Proceedings Library, 807.

Kienzler, B., Metz, V., Duro, L., Valls, A. (2012). Collaborative Project "Fast / Instant Release of Safety Relevant Radionuclides from Spent Nuclear Fuel". 1st Annual Workshop Proceedings – 7th EC FP – FIRST-Nuclides. 9th – 11th October 2012, Budapest, Hungary.

Manara, D., Renker, B. (2003). Raman Spectra of Stoichiometric and Hyperstoichiometric Uranium Dioxide. Journal of Nuclear Materials, 321, 233-237.

Sattonnay, G., Ardois, C., Corbel, C., Lucchini, J.F., Barthe, M.F., Garrido, F., Gosset, D. (2001). α-Radiolysis Effects on UO$_2$ Alteration in Water. Journal of Nuclear Materials, 288, 11-19.

Shoesmith, D.W., Sunder, S. (1992). The Prediction of Nuclear Fuel (UO$_2$) Dissolution Rates under Waste Disposal Conditions. Journal of Nuclear Materials, 190, 20-35.

IRF MODELLING OF HIGH BURN-UP SPENT FUEL CLADDED SEGMENTS FROM LEACHING EXPERIMENTS – APPROACH AND FIRST RESULTS

Ignasi Casas[1*], Alexandra Espriu [1], Daniel Serrano-Purroy[3], Aurora Martínez-Esparza[4], Joan de Pablo[1,2]

[1] Chemical Engineering Departament, UPC-Barcelona Tech (ES)
[2] Environmental Technology Area, Fundació CTM (ES)
[3] European Commission, JRC, ITU (DE)
[4] ENRESA (ES)

* Corresponding author: ignasi.casas@upc.edu

Abstract

This work focuses on the Instant Release Fraction (IRF) modeling of several leaching experiments performed with spent nuclear fuel (SNF) cladding segments of different burn-up´s: 48, 52, 53 and 60 MWd/kgU. Uranium, strontium, technetium and cesium release have been evaluated by using a kinetic model which is the sum of three first order kinetics corresponding to different parts of the fuel. Good fitting has been obtained in all the cases.

Introduction

Instant is a word where the concept of time is useless. However, when we experimentally study the Instant Release Fraction (IRF) we are assigning this to the cumulative fraction of the radionuclide inventory released to the aqueous phase up to a certain point in time. Depending on the authors this point in time varies from 10 to 60 days (Roudil et al., 2007; Serrano-Purroy et al., 2012). In Figure 1, the released fraction per day against time is schematically shown and assigned which part of the fuel is considered: gap, grain boundaries and matrix.


Figure 1. *Schematic release of fission product from three parts in SNF (Johnson et al., 1985).*

According to Figure 1, the fission product release from the gap lasts around 30 days, while the release from grain boundaries continues more than 10,000 days (27 years). Its contribution to the total release is higher than that provided by the grains (matrix).

In this work, experimental dissolution data from four high burn-up spent fuel cladded segments are studied by applying the semi-empirical model described in Casas et al. (2012).

1. Samples

The characteristics and preparation of the spent fuel samples that we have used in the model exercise are described in detail elsewhere (González-Robles, 2011). A summary of these characteristics is given in Tables 1 and 2.

Table 1. *Characteristics of the Spent Fuel cladded segmented samples.*

SNF	48BU	52BU	53BU	60BU
Reactor type	PWR	PWR	BWR	PWR
Burn-Up (MWd/kgU)	48	52	53	60
Length cycle (days)	322	325	274	352
^{235}U enrichment (weight %)	4.3	4.9	4.7	3.95
Irradiation cycles	3	3	5	5
FGR(%)	Aprox 15	-	3.9	15
End of irradiation	July 2000	June 2004	April 2003	March 2001

Table 2. *Physical characteristics of the cladded segments.*

SNF	Length (mm)	Diameter (mm)	Weight (g)
48BU	10.7 ± 0.1	10.7 ± 0.1	7.7735 ± 0.0001
60BU	12.7 ± 0.1	10.7 ± 0.1	8.9647 ± 0.0001
52BU	10.4 ± 0.1	10.0 ± 0.1	8.4296 ± 0.0001
53BU	10.2 ± 0.1	10.0 ± 0.1	7.5911 ± 0.0001

Theoretical determination of the SNF inventories was carried out using the ORIGEN-ARP code (ORIGEN, 2000). The inventory is shown in Table 3. Calculations were performed taking into account the irradiation history of the SNF and the impurity content indicated in the American Society for Testing Material (ASTM) standards for the UO$_2$ composition (as sintered) and for the Zircaloy material used in cladding fabrication.

Table 3. Theoretical inventory for the four cladding segments (μg $_{element}$/g $_{SNF}$).

Element	48BU	52BU	53BU	60BU
Rb	450	500	510	520
Sr	1070	1190	1170	1150
Y	590	660	660	670
Zr	4700	5100	5200	6500
Mo	4300	4700	4800	5300
Tc	1010	1100	1100	1180
Ru	2700	2900	2900	3540
Rh	550	600	600	610
Cs	3300	3500	3500	3900
Ba	2100	2300	2500	2900
La	1600	1700	1700	1900
Nd	5000	5500	5600	6100
U	830000	823000	824000	815000
Np	620	700	600	740
Pu	9700	9700	8600	10300
Am	450	400	500	810
Cm	60	60	70	150

Rim thickness for each segmented sample has been calculated by using the following equation proposed by Johnson et al. (2004):

$$R_t = 5.44 \, BU_R - 281$$

Where R_t is the rim thickness in microns and BU_R is the rim burn-up estimated by the average burn-up (Johnson et al. 2004). Results are collected in Table 4.

Table 4. Rim thickness calculation from Burn-up.

Average Burn-up (MWd/kgU)	Rim Burn-up (MWd/kgU)	Rim Thickness (μm)
48	64	67,2
52	65	72,6
53	66,25	79,4
60	80	154,2

The increase of rim thickness with increasing burn-up leads to a gap closing and probably hinders the penetration of the water, and consequently the fission product release.

1. Approach, results and discussion

In the modeling exercise performed in this work, we assume that total radionuclide mass measured in solution is coming from different parts of the fuel sample: gap, external grain boundary, internal grain boundary, rim porosity, rim grain and matrix grain. In principle, each part can have different kinetics. Taking into account experimental results, it is not possible to distinguish each part. Therefore, modeling is based on fitting the following general kinetic equation:

$$m_{RN}(t) = \sum_{i=1}^{N} m_{RN,i\infty} \cdot (1 - e^{-k_i \cdot t})$$

In all the cladding segments for U, Sr, Tc and Cs, it was possible to fit these data to an expression with three different kinetic constants (k_1, k_2 and k_3):

$$m_{RN}(t) = m_{RN,1\infty} \cdot \left(1 - e^{-k_1 \cdot t}\right) + m_{RN,2\infty} \cdot \left(1 - e^{-k_2 \cdot t}\right) + m_{RN,3\infty} \cdot (1 - e^{-k_3 \cdot t})$$

This expression is the proposed model to predict the release of any radionuclide. It is necessary to determine the following six parameters: $m_{RN,1\infty}$, $m_{RN,2\infty}$, $m_{RN,3\infty}$, k_1, k_2 and k_3. Though, since the total mass of a certain radionuclide is known from the inventory, then $m_{RN,3\infty}$ is deduced from $m_{RN,1\infty}$ and $m_{RN,2\infty}$.

In the case of uranium, in all the cladding segments the cumulative total moles dissolved showed a relatively fast release followed by a slower and steady dissolution. Modeling this behavior, the initial mass dissolved (m_{u1}) during the fast step is lower than 0.01% which could correspond to an initial oxidized phase or fines. On the other hand, the kinetic constant (k_3) value for the slow step is $6.8 \pm 5 \cdot 10^{-8}$ d^{-1} which is at least two orders of magnitude lower than the values of matrix dissolution rates obtained in oxidizing conditions with powder samples, indicating that in cladding segments the matrix dissolution rate cannot be probably measured since water has difficulties for saturating the sample.

Fission product releases of Sr, Tc and Cs for the four cladding segments were determined. The semi-empirical model has been applied to the radionuclides by fitting cumulative moles as a function of time, only the two initial steps were considered which correspond to the IRF. As an example, in Figure 2 both the release of Cs and the corresponding model are shown.

The Cs release from Power Water Reactor (PWR) fuels is higher than that from Boiling Water Reactor (BWR). It is important to point out that this behavior is also observed for Fission Gas Release (FGR) showing that diffusion processes depend on fuels coming fron different reactors.

We assume, as in the case of uranium that the third step, see Figure 2 for Cs as an example, is basically related to the water penetration. So, the fission product release has been focused on the two first steps. In Tables 5, 6 and 7 the values of m_1, m_2 (given as the percentage of the total inventory), k_1 and k_2 for Sr, Tc and Cs, respectively, are shown.

Figure 2. *Cesium cumulative mole release as a function of time,* ▲ *48BU;* ■ *60BU;* ● *52BU;* ♦ *53BU. Continuous line corresponds to the model.*

Table 4. *Model parameters determined for Strontium.*

	m$_1$ (%)	m$_2$ (%)	k$_1$ (d^{-1})	k$_2$ /d
48 BU	0.04±0.015	0.07±0.017	1.436	0.03356
52 BU	0.10±0.06	0.13±0.06	0.1236	0.007019
53 BU	0.02±0.007	0.68±0.3	0.3551	0.0002432
60 BU	0.22±0.05	0.42±0.15	0.3964	0.0003077

Table 5. *Model parameters determined for Technetium.*

	m$_1$ (%)	m$_2$ (%)	k$_1$ (d^{-1})	k$_2$ /d
48 BU	0.017±0.002	0.18±0.1	1.869	1.0E-3
52 BU	0.011±0.001	0.15±0.05	0.3226	1.41E-06
53 BU[2]	0.0005±0.0001	0.2±0.2	8.547	0.003683
60 BU	0.014±0.001	0.0005±0.0005	5.648	0.547

---

[1] Cumulative moles for this sample showed a great variability.

Table 6. *Model parameters determined for Cesium.*

	m_1	m_2	k_1 (d^{-1})	k_2/d
48 BU	5.06±2	2.88±2	3.12	0.06541
52 BU	2.03±0.8	2.23±1	34.82	0.2739
53 BU	0.39±0.06	0.45±0.05	0.39	3.34E-03
60 BU	3.23±0.52	1.40±0.40	8.80	1.659

$m_2 > m_1$ indicates for Sr and Tc that the main release is probably from grain boundaries. On the contrary, $m_1 > m_2$ for Caesium corroborates the predominant presence of this radionuclide in the gap.

The values of m_1 and m_2 are independent on time. m_1 is attributed to the percentage of the radionuclide which is easily released, i.e. gap, fines, oxidized layer. m_2 is attributed to the percentage of the radionuclide not so easy accessible by water though, dissolving faster than the matrix (i.e. water accessible grain boundary or external grain boundary).

In Table 7, $m_1 + m_2$ are given as instant release fraction for Sr, Tc Cs and U. Results clearly indicate that the fission products evaluated in this work do not congruently dissolve with uranium. Therefore, they are segregated from the matrix.

Table 7. *modeled instant release fraction.*

	Sr	Tc	Cs	U
	m_1+m_2	m_1+m_2	m_1+m_2	m_1+m_2
	(%)	(%)	(%)	(%)
48 BU	0.11	0.20	7.94	0.0018
52 BU	0.23	0.16	4.26	0.010
53 BU	0.70	0.20	0.84	0.0008
60 BU	0.64	0.0014	4.63	0.0025

The Cs IRF (~8%) determined in 48BU PWR fuel is high compared to the pessimistic value of 6% given in (Johnson et al., 2004). This probably indicates a non-conventional spent fuel. In the case of 60 BU fuel, Cs IRF (in solution) is approximately a third of the total fission gas release (gas). This may be attributed to the lower diffusion of Cs compared to fission gases.

Cs release determined in 53 BU BWR fuel is much lower than estimated for these fuels in (Johnson et al., 2004). Sr and Tc releases are also much lower than those estimated (Johnson et al., 2004). Two different possibilities could explain this finding, either water has not reached Sr and Tc phases yet, or these phases dissolve slowly.

Values of kinetic constants (*k*) are difficult to interpret; the rate of water penetration may cover the rate of radionuclide dissolution.

Conclusions and Future work

Modelling allows determining the percentage of the total mass of a radionuclide segregated from the matrix, i.e. attributing it to different parts of the SNF and as IRF. Besides this, its rate of release is depending on several factors such as the rate of phase dissolution, rate of matrix dissolution and furthermore on the rate of water penetration into the SNF etc.

This modeling is currently being applied to the experimental data generated in the FIRST-Nuclides project for different fuels.

The combination of this modeling with modeling of water saturation in spent fuel (Pekala et al., 2013) is expected to give some interesting insights into some of the still open questions such as time needed to saturate a cladding segment and radionuclide release and water penetration through grain boundaries

Acknowledgement

References

Casas, I., Espriu, A., Serrano-Purroy, D., Martínez-Esparza, A., de Pablo, J. (2012). IRF Modelling from High Burn-Up Spent Fuel Leaching Experiments. 1st Annual Workshop Proceedings – 7th EC FP – FIRST-Nuclides. 9th – 11th October 2012, Budapest, Hungary.

González-Robles, E. (2011). Study of Radionuclide Release in Commercials UO_2 Spent Nuclear Fuels. Effect of Burn-Up and High Burn-Up Structure. PhD Thesis, UPC-Barcelona Tech.

Johnson, L.H., Garisto, N.C., Stroes-Gascoygne, S. (1985). Used Fuel Dissolution Studies in Canada. In: Waste Management'85, 1, 479-481.

Johnson, L., Ferry, C., Poinssot, C., Lovera, P. (2004). Estimates of the Instant Release Fraction for UO_2 and MOX Fuels at t=0. Nagra Technical Report 04-08.

ORIGEN-ARP (2000) Automatic Rapid Process for Spent Fuel depletion, Decay, And Source Term Analysis NUREG/CR-0200. Revision 6, Volume1, SectionD1, ORNL/NUREG/CSD-2/V1/R6.

Marek Pękala, Andrés Idiart, Lara Duro, Olga Riba (2013). Modelling of Spent Nuclear Fuel saturation with water: implications for the Instant/Fast Release Fraction. Scientific Basis for Nuclear Waste Management, MRS, Barcelona, October 2013.

Roudil, D., Jégou, C., Broudic, V., Muzeau, B., Peuget, S., Deschanels, X (2007). Gap and grain boundaries inventories from pressurized water reactors spent fuels. Journal of Nuclear Materials, 362, 411-415.

Serrano-Purroy, D., Clarens, F., González-Robles, E., Glatz, J., Wegen, D., de Pablo, J., Casas, I., Giménez, J., Martínez-Esparza, A.(2012). Instant Release Fraction and Matrix Release of High Burn-Up UO_2 Spent Nuclear Fuel: Effect of High Burn-Up Structure and Leaching Solution Comosition. Journal of Nuclear Materials, 427, 249-258

.

CORROSION TEST OF COMMERCIAL UO$_2$ BWR SPENT NUCLEAR FUEL FOR FAST/INSTANT RELEASE STUDIES: FIRST RESULTS FOR CLADDED SEGMENT SAMPLES

Rosa Sureda[1*], Joan de Pablo[1,2], Frederic Clarens[1], Daniel Serrano-Purroy [3], Ignasi Casas[2]

[1] Fundació Centre Tecnològic de Manresa (ES)
[3] Department of Chemical Engineering, Universitat Politècnica de Catalunya (ES)
[2] European Commission, Joint Research Centre, Institute for Transuranium Elements (EC)

* Corresponding author: Rosa-Maria.Sureda-Pastor@ec.europa.eu

Abstract

The release behaviour of commercial UO$_2$ spent nuclear fuel was studied using batch leaching experiments performed in the hot cell facilities of JRC-ITU (Karlsruhe, Germany) in the framework of the FIRST-Nuclides program. This paper describes the experimental methodology used and preliminary results after approximately two months of the on-going experiment.

Introduction

A standard BWR fuel rod was selected for leaching test investigations. The fuel has an standard ^{235}U enrichment and an average burn-up of 54 GWd/t$_{HM}$. All the main parameters can be found in previous report D.1.2 for WP1. Two types of fuel samples with different morphologies: fuel cladded segments and powder are provided. The preparation of the powder fraction and characterization is in progress at JRC-ITU.

In the present work, cladded segment sample has been leachate in specific conditions in order to study the Instant Release Fraction (IRF). This concept takes into account the amount of radionuclides that can potentially be released during the initial contact period between fuel and solution, although there is not a clear consensus in the definition. These results, together with the ones performed with powder samples prepared from the same fuel, will be useful in order to identify the different radionuclide contributions: gap, grain boundary and fuel matrix.

Experimental

Fuel Sample

The cladded segment sample was a disk of (2.5 ± 0.1) mm cut at the middle of the pellet avoiding inter-pellets zones as referred in previous report including the characteristics of the fuel (*D.1.2. report spent nuclear fuel samples characterization/description of methodologies*). The total weight of the sample including the cladding was (2.0617 ± 0.0001) g with a fuel pellet diameter of (8.7 ± 0.1) mm. Based on previous observations (Gonzalez-Robles, 2011), the initial mass of the fuel sample can be calculated as approximately 81.6% of the total weight (fuel +cladding), which corresponds to a fuel sample weight of (1.6823 ± 0.0001) g. An image of

the cross sections of the sample is shown in Figure 1 where the typical fractures are observed due to the high thermal gradients during reactor operation.


Figure 1: *Cross sections of spent fuel samples used in leaching experiments.*

The surface are of the fuel samples used in our test is not exactly known but minimum values are calculated from direct geometric measurement. Considering two-cross sections of the segment exposed to the solution, the surface area is 118.9 mm^2. However, a higher specific surface area for a fractured pellet is assumed with a surface roughness factor of 4 (Forsyth, 1995; Iglesias et al., 2008), corresponding to a specific surface area of $4.75 \cdot 10^{-4}$ m^2.

Finally, the theoretical inventory was calculated using the ORIGEN code (ORIGEN-ARP, 2000).

Methodology and analytical methods

The experiments were performed in carbonated solution (1mM NaHCO$_3$ + 19mM NaCl, with initial pH of (8.4 ± 0.1) that were initially equilibrated with air under oxic conditions and a normal hot cell temperature (25 ± 5) °C. For all experiments a volume solution of (50 ± 1) ml was used.

The cladded segment samples were suspended into a plastic vessel through a platinum thread. The vessel was placed in to a stirrer to keep it under continuous orbital rotation. The system, see Figure 2, ensures full contact within sample-leaching solution as well as the homogenization of the solution at all contact times. No previous washing steps were performed in cladded segment samples to avoid the loss of valuable information concerning the IRF.

Figure 2: *Experimental set-up.*

Blank tests were also carried out using the same procedure but without the fuel sample to check for possible cross-contamination in the hot cell.

The contact periods were: 0.01, 0.2, 1, 3, 4, 13 and 28 days. After each one, the whole solution was renewed. Unfiltered and filtered (through a 0.2 micron pore size membrane) aliquots of fuel solutions were diluted and acidified with 1 M HNO_3. Samples were analysed by ICP-MS using a Thermo ELEMENT 2 instrument (Thermo Electron Corporation, Germany).

Calibration curves were produced using a series of dilutions of certified multi-element standard solutions in the concentration range of the major elements in solution. All the samples were measured with the addition of In, Ho, Co and Th as internal standards. The concentrations of the elements were calculated from the isotopic data. Whenever was possible, isobaric interferences were corrected based on isotopic ratios previously calculated with the ORIGEN code (ORIGEN-ARP, 2000) as reference.

Measurements of pH have been performed during the entire experiment using an Orion 525A+ pH-meter, a gel pH Triode L/M (reference 9107BN) supplied from Thermo-Electron, USA. The pH electrode was calibrated with commercial pH buffer solutions (METLER TOLEDO Inc., USA; pH 4.01 (Ref. 501307069), pH 7.00 (Ref.51302047), pH 9.21 (Ref. 51302070).

Static leaching results

In order to analyse the results from leachate of the experiment with fuel 54BWR, data will be presented focussing on: uranium concentration evolution as function of time, Fraction of Inventory in the Aqueous Phase ($FIAP_x$), and $FIAP_x$ normalized to the uranium fraction (FNU_x).

Uranium concentration

Measured uranium concentration as a function of the leaching time is shown in Figure 3. The horizontal dashed line represents the solubility limit for schoepite, $[(UO_2)_8O_2(OH)_{12} \cdot 12H_2O]$, calculated using NEA database. In all cases, U concentrations in solution varies from $3.5 \cdot 10^{-7}$ to $4.9 \cdot 10^{-6}$ mol/dm^3 which corresponds to a range below the expected for the solubility of U(VI) hydroxide phase, schoepite.

Figure 3: *Uranium concentration as a function of the leaching time. The horizontal dashed line represents the solubility limit for schoepite.*

On the other hand, predominance diagrams were used to identify which are the main aqueous or solid phases for uranium that may be formed under the experimental conditions of our system. Speciation calculations were performed with the CHESS v.2.5 (Chemical Equilibrium with Species and Surfaces) computer code based on a combination of the default CHESS and NEA database. Under oxidising conditions, and in the pH and carbonate concentrations of this study which are similar to the ones found in most natural waters, the predominant aqueous species of hexavalent uranium are carbonates, as seen in Figure 4.

Figure 4: *Predominance diagram of main uranium species present in our system. Symbols represent our experimental data.*

Measured Fraction of the inventory in aqueous phase (FIAP)

In order to better compare the results obtained for different nuclides the FIAP was calculated. In this sense, the fraction of inventory of an element x released in aqueous phase (FIAPx) was calculated for an element x according to Equation 1 (Hanson and Stout, 2004):

$$FIAPx = \frac{m_{x,aq}}{m_{x,SNF}} = \frac{c_x \, V_{aq}}{m_{SNF} \, H_x}$$

(1)

Where: $m_{x,aq}$ is the mass of element x in the aqueous phase and m_{xSNF} is the mass of element x in the SNF; c_x corresponds to the concentration of element x in solution (g/mL); V_{aq} is the volume of solution (ml), m_{SNF} is the initial mass of SNF sample (g) and H_x represents the fraction of the inventory in the SNF for the element x (g/g).

The cumulative FIAP, FIAPc, of an element x in sample n can be calculated following Equation 2:

$$FIAP_C(n) = \sum_{i=1}^{n} FIAP_x(i)$$

(2)

Improved FIAP values will be recalculated after completion of the experimental inventory determination as a part of an action in WP1. To use a conservative approach, FIAP had been calculated from the concentration of non-filtered samples although a good reproducibility has been found between both, except for technetium. As example of the behaviour for filtered and non-filtered samples the cumulative moles released as a function of time is shown in Figure 5 for Tc and Mo. An interaction of Tc with the filters is clearly observed and for this reason these data are discarded.

Figure 5: Cumulative mass release in moles as a function of time.

$FIAP_C$ values for Rb, Sr, Mo, Tc, Cs and U are plotted in Figure 6. In general, a higher release during the initial time intervals is observed for uranium and the group of elements: Cs, Mo, Tc, Rb and Sr. This fast initial dissolution observed in uranium can be attributed to the dissolution of the oxidized surface layer present at the beginning of the experiment. For the rest of elements typically considered as a part of the IRF, this fast release is assumed to come mainly from the more accessible and open surfaces (i.e. gap and cracks). At this point of the experiment is difficult to identify the different release stages because more experimental dat are needed for further conclusions. For this reason, sampling will be continued and this work will be done in the coming months.

Figure 6: Cumulative FIAP as a function of time.

151

Fractional release Normalized to Uranium (FNU)

FNU values were also calculated in order to compare with uranium in reference to matrix release, see Table 1. All elements from this group showed higher fractional release compared to U (FNU>1), specially cesium with ratios of one order of magnitude higher than the rest.

Table 1: *FNU values calculated and cumulative time in days.*

Time (d)	0.01	0.17	1.17	4.17	8.17	21.17	49.17
Rb	14	7	3	3	2	3	4
Sr	9	5	5	5	5	4	6
Mo	21	11	5	3	3	3	4
Tc	13	7	3	3	3	4	6
Cs	151	95	65	48	38	34	35

Estimation of the IRF(%)

The IRF determinations are based on FIAP results presented in previous section. Only those elements whose release was faster than uranium were considered as contributors of the IRF. The calculation of IRF does not include the matrix contribution and for this reason FIAP of uranium was substracted in each case. At this point, IRF was calculated after ~50 days of experiment. The higher values are obtained for Cs with a fraction of 0.45% and for the rest of the elements IRF values are comprised between ~0.04% for Rb and Mo and ~0.07% for Sr and Tc.

Conclusions and Future work

Instant release fraction experiment with cladded fuelsegment has started and preliminary results for the first 50 days of experiments are reported. The experimental data show no uranium secondary phase precipitation following this methodology. Elements Cs, Mo, Tc, Rb and Sr follow similar trends as observed in other studies with higher fractional release compared to uranium and therefore, are identified as IRF. Specially, caesium clearly presents the higher release compared to the rest. The higher release found at the beginning of the experiment is assumed to come mainly from the gap and also from the two fractured faces of this sample. However, these assumptions are preliminary and more experimental data are needed to make more specific conclusions. These data will be recalculated and compared after the experimental inventory determination planned in the framework of the project.

Acknowledgement

References

Gonzalez-Robles, E. (2011).   Study of Radionuclide Release in Commercials UO_2 Spent Nuclear Fuels. Doctoral thesis, Universitat Politècnica de Catalunya, Barcelona, Spain.

Hanson, B., Stoub, R.B. (2004). Re-examining the dissolution of Spent Fuel: a comparison of different Methods for calculating Rates. Materials. Research. Society. Symposium. Proceedings, 824, 89-94.

Iglesias, E., Quinones, J. (2008). Analogous Materials for Studying Spent Nuclear Fuel: The Influence of Particle Size Distribution on the Specific Surface Area of Irradiated Nuclear Fuel. Applied Surface Science, 254, 6890-6896.

ORIGEN-ARP (2000). Automatic Rapid Process for Spent Fuel Depletion, Decay and Source Term Analysis "NUREG/CR-0200". Revision 6. Volume1, Section D1, ORNL/NUREG/CSD2/V1/R6.

Forsyth, R. (1995). Spent Nuclear Fuel. A Review of Properties of Possible Relevance to Corrosion Processes. SKB TR-95-23.

Van der Lee, J., Dewindt, L. (2000). CHESS Tutorial (version 3.0). Ecole des Mines de Paris, Fontainebleau, France.

DETERMINATION OF DISSOLUTION RATES FOR DAMAGED AND LEAKING VVER FUEL STORED IN WATER

Emese Slonszki[*], Zoltán Hózer

Centre for Energy Research Hungarian Academy of Sciences (HU)

* Corresponding author: emese.slonszki@energia.mta.hu

Abstract

Within the FIRST-Nuclides project dissolution rates of several isotopes from VVER fuel were determined for two pH in the coolant based on activity measurements at the Paks NPP. The present report summarizes data, calculation methods and compares the calculated and fitted dissolution rates of isotopes during and after the incident of Unit 2 of Paks NPP and during the wet storage of the leaking fuel assembly (No. 70873) of Unit 4 of Paks NPP. The dissolution rates were different in the two evaluated conditions which is attributed to the pH.

Introduction

The objective of MTA EK contribution to WP3 in the framework of FIRST-Nuclides project is the determination of dissolution rates for several isotopes from damaged and leaking VVER fuel assemblies stored in water for several years. The characterization of VVER fuel was already carried out in the first year of this project (Hózer and Slonski, 2012).

The dissolution rates were calculated for two datasets:

1. Fuel assemblies were damaged during an incident in a cleaning tank at the Paks NPP in 2003. The thirty damaged fuel assemblies were then stored in a special service area of the spent fuel storage pool for almost four years. The measured activity concentrations over time allowed us to calculate release rates for several isotopes.
2. A leaking fuel assembly was identified in 2009 at the Paks NPP. A special measurement programme was carried out in the spent fuel storage pool to investigate the activity release from the leaking fuel rod at wet storage conditions. The data from this programme was used for the calculation of dissolution rates.

1. Calculation of release rates

Several isotopes were measured during and after the incident of Unit 2 of Paks Nuclear Power Plant and during the wet storage of No. 70873 leaking fuel assembly of Unit 4 of Paks Nuclear Power Plant. Concentrations of those isotopes were measured regularly and their decay corrected integrated releases were estimated in this work. It involves 11 isotopes and uranium in the first case and 13 isotopes and uranium in the second case. We used two methods for determination of the release rates:

1. First of all we calculated the corrected integrated releases of every isotope from the measured activity data. After that these data were divided by the total time which belongs to measurement (the elapsed time from the first measurement to the last measurement). The calculated release rate values are given by this method.

2.   In the other case linear fitting was applied to the corrected integrated releases data which was resulted the fitted release rates. These procedures are described in the following Chapter 1.1.

1.1. Release rates for damaged VVER fuel

1.1.1. Calculation methods

Activity concentrations in the coolant between 11th April 2003 and 8th January 2007 have been used (Hozer et al., 2009; Hózer et al., 2010; Slonsky et al., 2009). One example of datasets (^{137}Cs) is shown in Figure 1. The data were provided by the Paks Nuclear Power Plant. Measurements were available from the pit with the cleaning tank, from the spent fuel storage pool and from the reactor system. Several measurements were taken before and after the filters of the purification system.

Figure 1: *History of ^{137}Cs activity concentration in the pit with the cleaning tank of Unit 2.*

It was supposed in the evaluation process, that the measured activity concentration was typical for the total volume of water connected to the cleaning tank with damaged fuel.

Aims of this work to evaluate the activity release of radionuclides first of all for the first two weeks which period describes the incident and the other hand the about 4 year's period which corresponds to the wet storage. The elapsed time since the incident was divided into short periods, which were characterized by stabilized technological conditions (considering the flowrate of water purification system and volume of coolant) allowing us to consider constant release rate during a given period. It was supposed that the release rate was constant during these short periods. The number of periods was different for the different isotopes, since the cation and anion filters were used at different times and either they worked together or separate only the anion filters during the water purification. So if only the anion filter operated, flowrate of water purification system was zero at cations in the calculation. For example in the case of ^{137}Cs isotope 53 periods were identified.

The operation of water purification system was considered using the flowrate and efficiency values. The positions of gates between the reactor pool and between the spent fuel storage pool were taken into account. When the gate was closed, only the volume of the spent fuel storage pool was used and if this gate was opened the volume of pools were added.

The release rate was calculated for each period and the total release was determined as the result of integration over the total calculated time. The release rate was calculated in three different ways.

1. Linear fitting was applied to those periods, where the activity continuously increased. That was typical for periods without the operation of water purification system.

2. Monotone decreasing or constant activities were typical for periods with operation of water purification system. In this case the following expression was applied for each isotope:

$$\alpha = g_f \frac{C - C_0 * e^{-g_f * \Delta t / M}}{1 - e^{-g_f * \Delta t / M}} \tag{1}$$

where:

α	–	dissolution rate of the given isotope (Bq/h);
g_f	–	flowrate of water purification system (kg/h);
C	–	activity concentration at the beginning of the period (Bq/kg);
C_o	–	activity concentration at the end of the period (Bq/kg);
Δt	–	period (h);
M	–	mass of water (kg).

3. In the third case the average activity value was multiplied by the flowrate of the water purification system. This approach was applied when the scatter of the measured points did not allow us to use the above methods (there were too few measured points). These periods could not be characterized by a constant dissolution rate that is why an average value was considered.

The real flowrate of the water purification system was corrected by the efficiency of filters. For this reason the efficiency ε was calculated from activity concentrations before and after the filters.

$$\varepsilon = \frac{C_{before} - C_{after}}{C_{before}} \tag{2}$$

where:

ε	–	efficiency
C_{before}	–	activity concentration before the filter (Bq/kg);
C_{after}	–	activity concentration after the filter (Bq/kg).

The efficiency ε was multiplied by the flowrate g_f. This efficient flowrate was used in the calculation of dissolution rates. The purification efficiency was calculated for each isotope and for each period.

The inventory of radioactive fission products continuously decreased after shutdown and during the storage of spent fuel in the cleaning tank. To compare with the initial inventory and the results of analytical work, corrections were applied for decay. These corrected values were higher than the measured values. The physical meaning of the corrected values relates to the time of the incident, simulating what the total release would have been at that time. The correction was made using this exponential formula:

$$e^{\lambda t} \tag{3}$$

where:

λ	–	decay constant (1/s),
t	–	elapsed time from the incident to the end of the given period (s).

Activity release of each period was corrected using formula (3) and the total release for the isotopes considered for 4 years was calculated as the sum of the individual periods. First of all this value was divided by the total time - from the incident until removing of damaged fuel assemblies – giving the "calculated release rate" of the isotope (Table 1). Alternatively, a linear fitting was applied to the corrected integrated release data and yielded release rate for every examined isotope.

The activity concentration of uranium was given in µg/L and converted stoechiometrically to a concentration of UO_2 using the ratio of molar mass of UO_2 and ^{238}U (270/238).

Finally, the release rates refer to the isotope inventory of incident (Table 1 and Table 3).

1.1.2. Results

Based on the calculated integrated releases the total measuring period can be divided into two parts. The activity of the first two week describes the incident while the other parts of period correspond to the wet storage. After the incident the change in the release rate was influenced first of all by the decay of short lived isotopes. However the water chemistry conditions played important role, too, which is illustrated in Figure 2 that shows the trend of ^{238}Pu and ^{242}Cm activity and the pH. The pH decreased from 7 to 4–4.5 due to the increase of the boric acid concentration from 15 g/kg to 21 g/kg and the lead to increase of ^{242}Cm and ^{238}Pu activity by two and three orders of magnitude (Figure 2 and Table 2). Similar effect was observed for other isotopes as well at the same time.

The uranium concentration (µg/L) measurements started in five month after the incident, so there are no uranium data for the time period close to the incident. Using the available data the amount of dissolved UO_2 was calculated and compared to the original mass of the fuel. Using this approach a relative release or dissolution rate was calculated, that is similar to the release rates of the radioactive isotopes. The data shows that 1.8 % (71.5 kg) of the total mass (3,969 kg) of the UO_2 was dissolved during the four years of wet storage after the incident. This means that 19 days were necessary for the dissolution of 1 kg UO_2 into the coolant and the average release rate of $UO_2 = 6.08 \cdot 10^1$ g/d.
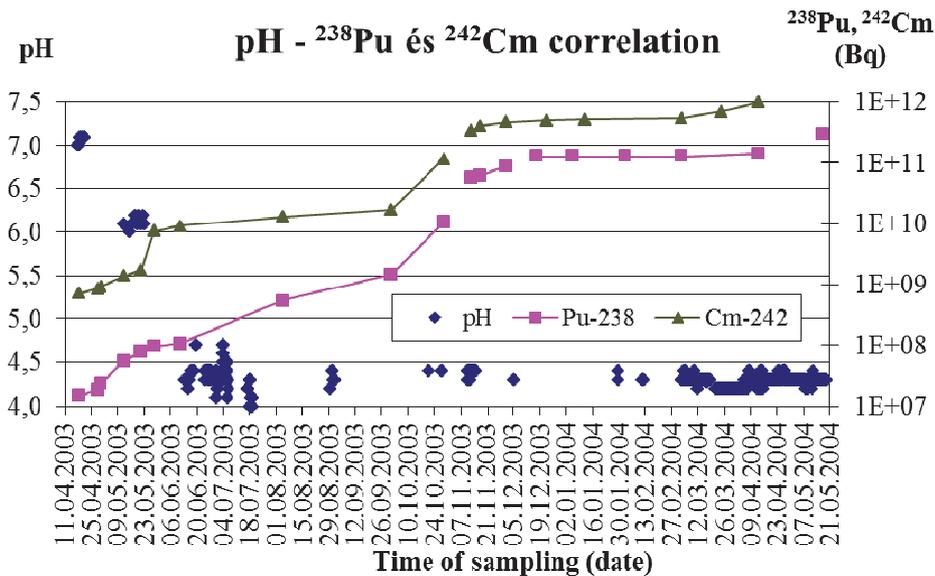
Figure 2: Change of pH and ^{238}Pu and ^{242}Cm activity concentration.

Table 1: *Calculated and fitted release rates of the gamma radiant isotopes.*

Isotope	Isotope inventory (Bq)	Calculated release rate (1/d)	Fitted release rate (1/d)	
			Incident pH≈7	Wet storage pH≈4-4.5
^{144}Ce	1.20E+17	1.27E-05	2.00E-05	**1.20E-05**
^{140}Ba	1.16E+17	2.71E-05	4.15E-05	**1.45E-05**
^{131}I	4.15E+16	1.38E-04	5.78E-04	**2.31E-06**
^{137}Cs	7.22E+15	2.10E-05	1.33E-04	**1.66E-05**
^{134}Cs	5.69E+15	2.76E-05	1.69E-04	**2.11E-05**
^{125}Sb	5.75E+14	6.75E-06	-	**7.85E-06**
^{154}Eu	2.32E+14	2.94E-05	-	**2.30E-05**
^{155}Eu	1.22E+14	3.78E-05	-	**2.70E-05**

Table 2: *Calculated and fitted release rates of the alpha radiant isotopes and UO_2.*

Isotope	Isotope inventory (Bq)	Calculated release rate (1/d)	Fitted release rate (1/d)	
			pH≈7 (incident+2 months)	pH≈4-4.5
^{242}Cm	9.25E+14	4.42E-05	1.80E-07	**5.16E-05**
^{238}Pu	7.36E+13	3.62E-05	8.94E-08	**4.10E-05**
^{244}Cm	2.31E+13	2.05E-05	2.70E-08	**1.93E-05**
UO_2	3969 kg	1.53E-05	-	**1.70E-05**

Two fits were made for the measured isotopes (column 4 and 5 in Table 1 and Table 2), one for the interval of the incident and one for the interval of the wet storage. In case of the long lived isotopes the fitted and calculated release rates during the wet storage agree well. For most isotopes the fitted value is below the release rate which was calculated from the integrated releases (Table 1 and Table 2). The fitted release rates of ^{144}Ce and ^{238}Pu isotopes approximate best the calculated release rates, the differences are about 5%. In case of caesium and europium isotopes these values were between 20% and 30%. At the same time the calculated release rates of ^{125}Sb and curium isotopes exceed the fitted release rates by about 15%. The fitted release rate of UO_2 overestimates the calculated release rate by 11%. The two applied methods independently confirm that the results are reasonable.

1.2. Release rates for leaking VVER fuel

1.2.1. Calculation methods

The processed activity concentration data of isotopes were from the measurements between 27th April 2009 (reactor shutdown) and 3rd May 2010. The release rate of isotopes was estimated on the direct measurements from the spent fuel storage pool of Unit 4.
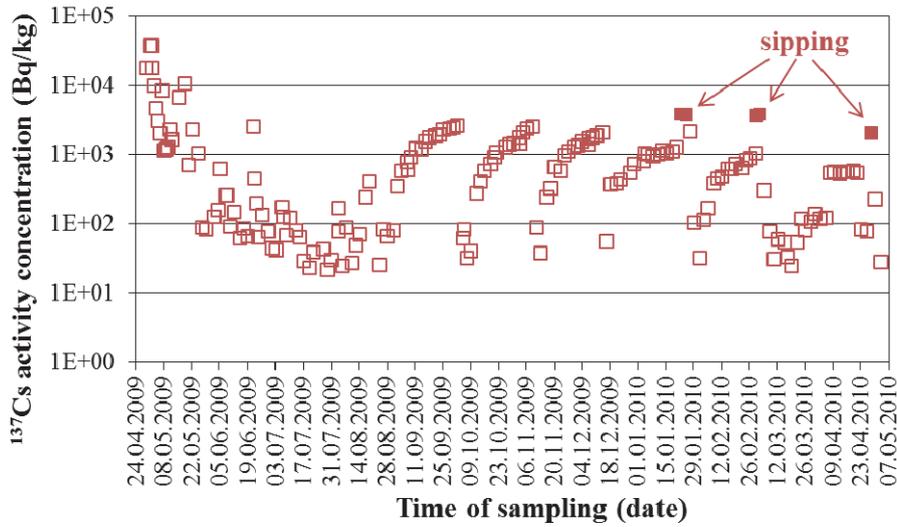
Figure 3: *History of ^{137}Cs activity concentration in the spent fuel storage pool of Unit 4.*

The calculation method is the same as the calculation method of damaged VVER fuels (Chapter 1.1.1). So the elapsed time since the reactor shutdown was divided into short periods even as before too. Also the number of periods was different for the different isotopes. For example in the case of ^{137}Cs isotope 31 periods were identified.

The method of evaluation of release rates corresponds with the above described calculation. It should be noted that only those releases were used in this evaluation which were characterized by steady-state release rates; the transients (e.g. sipping which technique was used for the identification of leaking fuel assemblies) were not taken account of (Figure 3). The isotope inventory of the reactor shutdown was used to correct the integrated releases.

1.2.2. Results

In case of the No. 70873 leaking fuel assembly, the fitted release rates of isotopes approximate well the calculated release rates.

Table 2: *Calculated and fitted release rates of isotopes.*

Isotope	Isotope inventory (Bq)	Calculated release rate (1/d)	Fitted release rate (1/d)
^{95}Zr	7.40E+13	3.92E-08	**3.79E-08**
^{106}Ru	7.61E+12	2.43E-07	**2.37E-07**
^{137}Cs	1.59E+12	6.24E-06	**5.83E-06**
^{134}Cs	1.08E+12	6.55E-06	**6.09E-06**
^{125}Sb	1.12E+11	6.66E-06	**6.79E-06**
^{154}Eu	3.74E+10	4.53E-06	**3.82E-06**
^{155}Eu	2.35E+10	1.18E-05	**7.89E-06**
UO_2	0.955 kg	8.98E-08	**7.54E-08**

The release rates of the ^{125}Sb gave the best agreement. The fitted release rates of the other examined isotopes underestimate their calculated release rates (Table 4). The difference is below 7% for the ^{95}Zr, ^{106}Ru, ^{137}Cs and ^{134}Cs isotopes, while this value for the ^{154}Eu isotope is below 20%. The most significant difference is in case of ^{155}Eu by 33%. The fitted release rate of UO$_2$ underestimates the calculated release rate by 16%.

Summary

The dissolution rates for VVER fuel stored in water for long periods were determined on the basis of data from the Paks NPP. The two datasets provided information on slightly different conditions: in both cases the water temperature was similar, but in cases of damaged fuel the pH of coolant was significantly lower compared to the leaking fuel. This effect can explain the observed differences in dissolution rates (Figure 4).
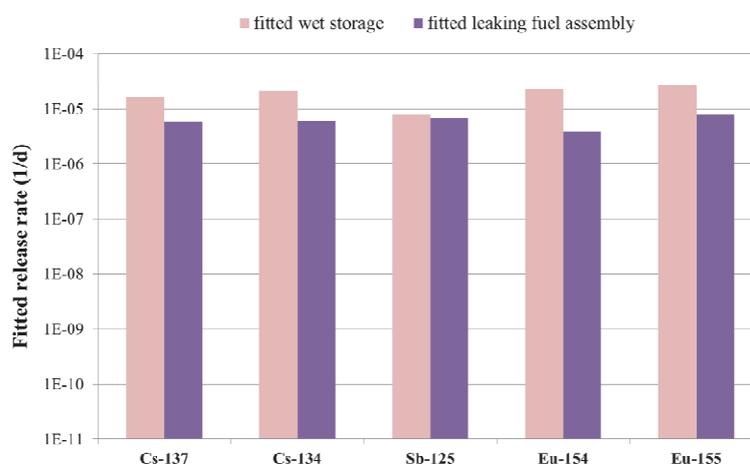
Figure 4: *Comparison of the fitted release rate of long lived isotopes.*

During the wet storage of the damaged VVER fuel the fitted release rate range of long lived isotopes was $1·10^{-5}$-$3·10^{-5}$ L/d (only the release rate of ^{125}Sb isotope fell slightly short of this range with about $8·10^{-6}$ L/d) (Table 2). These values are three to six times higher than the release rate of leaking VVER fuel (Figure 4).

The release rates of ^{125}Sb isotope show the best agreement of all isotopes when comparing the damaged and leaking fuel under wet storage.

Following a review of the reliability of measured data, the dissolution rates were determined for eleven isotopes in case of damaged fuel and for seven isotopes in case of leaking fuel. Additionally uranium dissolution rates were calculated in both cases. In most of the cases the release rates of individual isotopes were comparable to that of uranium.

Our calculated release rates may be regarded as a conservative upper limit compared to the expected releases in the groundwater of deep geological repository since the release from the fuels took place in the spent fuel storage pool with high boric acid concentration.

Future work

The data produced for VVER fuel should be compared to other dissolution rates that will be determined in the framework of the FIRST-Nuclides project. Furthermore, the present VVER specific data can be used for the estimation of migration of fission product from deep geological repository with VVER fuel.

References

Hózer, Z., Slonszki, E. (2012). Characterisation of Spent VVER-440 Fuel to Be Used in the FIRST-Nuclides project. In: 1st Annual Workshop Proceedings of the Collaborative Project "Fast / Instant Release of Safety Relevant Radionuclides from Spent Nuclear Fuel". Bernhard Kienzler, Volker Metz, Lara Duro, Alba Valls (eds.), 1st Annual Workshop Proceedings – 7th EC FP – FIRST-Nuclides. 9th – 11th October 2012, Budapest, Hungary, 87-101., http://dx.doi.org/10.5445/KSP/1000032486.

Hózer, Z., Szabó, E., Pintér, T., Baracska Varjú, I., Bujtás, T., Farkas, G., Vajda, N. (2009). Activity Release from Damaged Fuel during the Paks-2 Cleaning Tank Incident in the Spent Fuel Storage Pool. Journal of Nuclear Materials, 392, 90–94.

Hózer, Z., Aszódi, A., Barnak, M., Boros, I., Fogel, M., Guillard, V., Győri, Cs., Hegyi, G., Horváth, G.L., Nagy, I., Junninen, P., Kobzar, V., Légrádi, G., Molnár, A., Pietarinen, K., Perneczky, L., Makihara, Y., Matejovic, P., Perez-Feró, E., Slonszki, E., Tóth, I., Trambauer, K., Tricot, N., Trosztel, I., Verpoorten, J., Vitanza, C., Voltchek, A., Wagner, K.C., Zvonarev, Y. (2010). Numerical Analyses of an Ex-Core Fuel Incident: Results of the OECD-IAEA Paks Fuel Project. Nuclear Engineering and Design, 240, 538–549.

Slonszki, E., Hózer, Z., Pintér, T., Baracska Varjú, I. (2009). Activity Release from the Damaged Spent VVER-Fuel during Long-Term Wet Storage. Radiochimica Acta, 98, 231-236.

SPENT FUEL LEACHING EXPERIMENTS AND LASER ABLATION STUDIES PERFORMED IN STUDSVIK - STATUS AND PRELIMINARY RESULTS

Olivia Roth[*], Anders Puranen, Jeanett Low, Michael Granfors, Daqing Cui, Charlotta Askeljung

Studsvik Nuclear AB (SE)

* Corresponding author: olivia.roth@studsvik.se

Abstract

This paper presents the status of the experiments performed at Studsvik Nuclear AB within the EURATOM FP7 Collaborative Project "Fast / Instant Release of Safety Relevant Radionuclides from Spent Nuclear Fuel (CP FIRST-Nuclides)".

The main focus of the investigations is to explore the effects of additives and dopants on the fast/instant release of fission products such as Cs and I. These effects are studied in spent fuel leaching experiments. Experiments will also be performed to investigate the feasibility of measuring fast/instant release of Se and ^{14}C during spent fuel leaching.

Furthermore, laser ablation investigations have been performed to study the radial distribution of I, Xe and Cs and to explore any correlation to the fission gas release (FGR) and instant release leach rates of the corresponding fuel samples.

Introduction

This paper describes ongoing efforts at Studsvik Nuclear AB within the EURATOM FP7 Collaborative Project "Fast / Instant Release of Safety Relevant Radionuclides from Spent Nuclear Fuel (CP FIRST-Nuclides)".

The aim of the project is to study the fraction of fission and activation products that are fast/instantly released from spent nuclear fuel upon contact with aqueous media. The fraction consists of readily soluble phases in the gap between fuel and cladding, cracks and grain boundaries. Some of these fission and activation products have a long half-life and are for this reason important for the safety assessment of deep repositories for spent nuclear fuel.

At the Studsvik Hot Cell laboratory, spent fuel leaching studies have been conducted since around 1980. During 1990-1996 a comprehensive research program was initiated aiming at mapping the most important parameters influencing the stability of spent nuclear fuel in water (Forsyth, 1997). Since then the program has been extended with leaching experiments of high burn-up fuel and instant release experiments (Johnson et al., 2012; Zwicky et al., 2011).

In these previous experiments, standard UO_2 fuel has been used. Today new fuel types with additives and dopants are taken into use in commercial reactors. The additives and dopants affects properties such as grain size and fission gas release which in turn may affect the instant release behavior of the fuel. The main objective of this study is to investigate how these changes in the fuel matrix affect the instant release process.

Sample selection and preparation

The sample selection and preparation has been described in (Roth and Puranen, 2012).

The six high burn-up fuels chosen for the studies are listed in Table 1. The FGR values in Table 1 are based on rod puncturing and gas analysis and the calculated BU values are based on core calculations. The methods are described in (Roth and Puranen, 2012).

Table 1: Fuels selected for investigation at Studsvik.

Sample name	Reactor type	Fuel type	FGR[1] [%]	Calculated BU (rod average) [MWd/kg U]
D07	BWR	Std UO$_2$	~1.6	50.2
L04	BWR	Std UO$_2$	~3.1	54.8
5A2	BWR	Std UO$_2$	~2.4	57.1
C1	BWR	Al/Cr doped UO$_2$	~1.4	59.1
VG81	PWR	Gd doped UO$_2$	~2.2	54.4
AM2K12	PWR	Std UO$_2$	~4.9	70.2

[1] *Based on rod puncturing and gas analysis as described in* (Roth and Puranen, 2012).

Spent fuel leaching studies

Sample preparation

Spent fuel leaching studies will be performed using samples from 6 different fuel rods. Before the start of the leaching experiment each fuel segment is gamma scanned to identify pellet-pellet interfaces, thereafter samples are cut from the segment. The samples are cut at mid-pellet positions as shown in Figure 1. Each sample consists of approximately 2 fuel pellets including cladding.
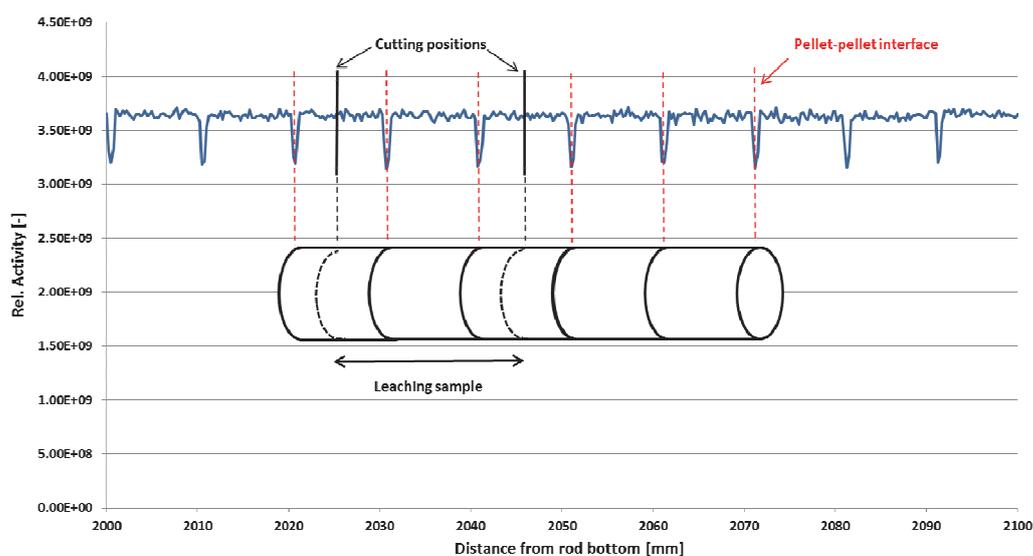
Figure 1: Schematic picture of leaching sample position relative to gamma spectrum.

The samples are leached as cladded fuel segments, fuel fragments + separated cladding or fuel powder. The fuel segments are weighed before the start of the leaching experiments. Two different methods to obtain the samples consisting of fuel fragments + separated cladding have been employed; (1) *cutting* - the cladding is cut axially and bent open which causes the fuel fragments to detach from the cladding, (2) *crushing* – the fuel is gently crushed by hitting and pressing the cladding with a hammer. The fuel fragments are collected and leached together with the cladding (and any remaining fuel still sticking to the inside of the cladding).

In a next step the leaching of powdered specimens will be performed using a simultaneous grinding and leaching technique described by (Stroes-Gascoyne et al., 1995). The objective of this method is to expose the grain boundaries by grinding the fuel down to the same size range as the individual fuel grains. This would ideally make the entire grain boundary inventory available for leaching. By combining the grinding and leaching into one wet grinding step surface oxidation and temperature effects (from the friction of grinding) can be minimized.

Experimental Setup

The leaching experiments are performed in a Hot Cell at the Studsvik Hot Cell laboratory. Leaching of cladded fuel segments and fuel fragments + separated cladding is performed in glass flasks. Each flask contains 200 mL leaching solution (10 mM NaCl + 2 mM NaHCO$_3$). Cladded fuel segments are placed in a 'basket' made of platinum wire. Fuel fragments + separated cladding are placed in glass baskets with filter bottom. The baskets are attached to stop cocks and immersed in the leaching solution. The experiments are performed under aerated, stagnant conditions (no stirring).

The leaching is performed in a cumulative way in which the leaching solution is completely exchanged at every sampling interval. After 1 d, 7 d, 21 d, 63 d, 92 d and 182 d (resulting in a cumulative leaching time of 365 d), the stopcock and fuel basket is transferred to a new leaching flask containing a fresh leaching solution. Samples of the old leaching solutions are withdrawn from the used leaching flasks and analysed by ICP-MS and gamma analysis (^{137}Cs). In order to calculate the leached fraction of the fuel inventory up to a given leaching time the analysed concentrations are thus added to the results of the prior samplings.

Figure 2 shows the general set-up for the leaching experiments.
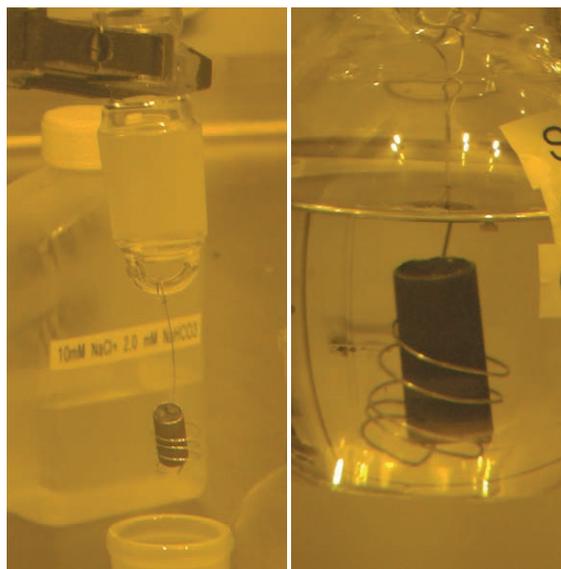
Figure 2: *General pictures of leaching experiments a) cladded fuel in Pt-basket, b) Pt-basket with cladded fuel immersed in leaching solution.*

All aqueous samples from the leaching studies are removed from the hot cell and transported to the chemistry laboratory where the samples are centrifuged (and filtered if necessary in the case of powdered samples) and analysed for Cs and I with ICP-MS.

Status of leaching experiments

In August 2012, the leaching of two cladded fuel segments (D07 and L04) was started and in September 2012, the leaching of two fuel fragments + separated cladding (C1 and 5A2) was started. For these series 6 contact periods have elapsed with a total contact time of ~1 year for each sample.

In March 2013, the leaching of one fuel fragment + separated cladding (VG81) was started, for this sample 5 contact periods have elapsed.

The analysed data from the leaching experiments is under evaluation, a selection of preliminary data is shown below.

The leaching of the powdered sample is planned to start in November 2013.

The status of the leaching experiments is summarized in Table 2.

Table 2: *Status of leaching experiments.*

Sample name	Sample type	Start of leaching
D07	cladded fuel segment	Aug 2012
L04	cladded fuel segment	Aug 2012
5A2	fragments + separated cladding (cut)	Sept 2012
C1	fragments + separated cladding (cut)	Sept 2012
VG81	fragments + separated cladding (crushed)	March 2013
AM2K12	powder	Planned Nov 2013

Preliminary results

Preliminary results from parts of the leaching studies have been published in Roth et al. (2012) and Roth et al. (2013). In Figure 3-4 results from the leaching of sample C1 and 5A2 are shown. In Figure 3 the ^{137}Cs and ^{129}I cumulative release fractions are presented. As can be seen the figure, for the Al/Cr doped fuel the release fraction of iodine is higher than that of cesium as expected from previous results (Johnson et al., 2012) whereas the relationship is reversed for the standard fuel. A parallel study using a different sample preparation method has shown that the deviation in the iodine data for the standard fuel can probably be explained by loss of iodine during the decladding of the fuel (Roth et al., 2013). Lower release from the doped sample can probably (partly) be attributed to the larger grain size of the fuel which decreases the probability of fission products migrating to the grain boundaries, a behaviour that is also reflected by the lower fission gas release of the C1 rod.
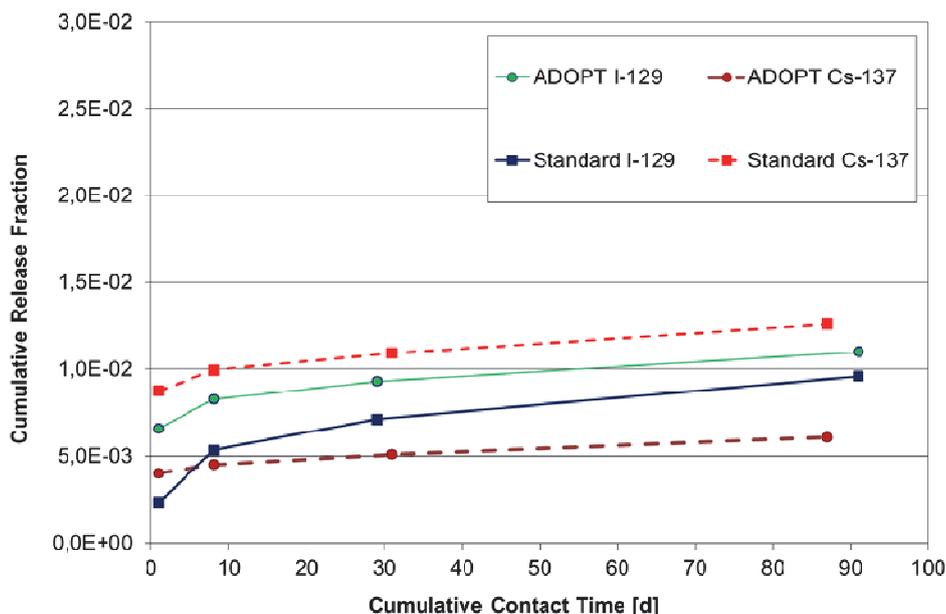
Figure 3: ^{137}Cs *and* ^{129}I *cumulative release fractions from standard and Al/Cr doped fuel.*
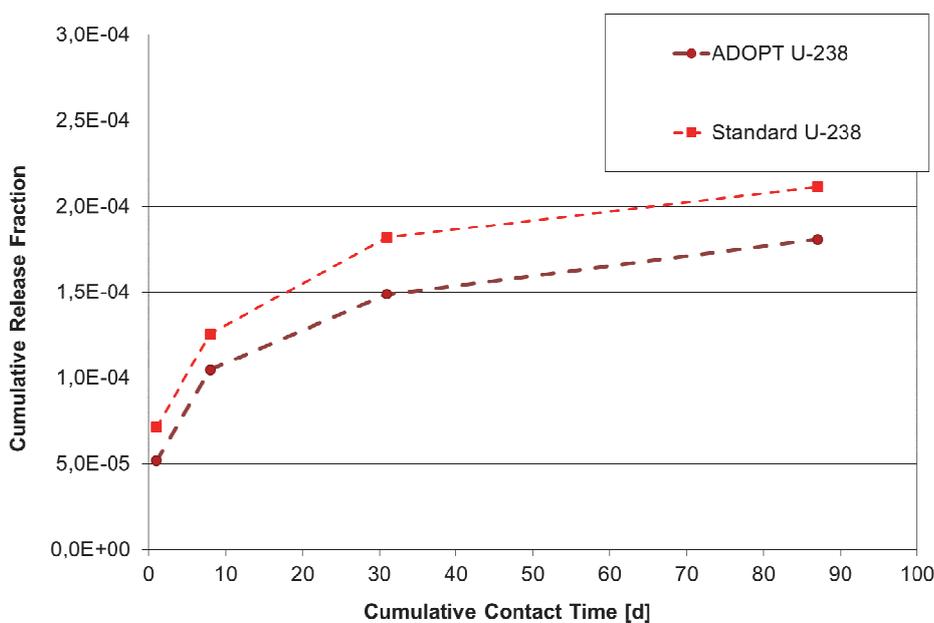
Figure 4: ^{238}U *cumulative release fractions from standard and Al/Cr doped fuel.*

Figure 4 shows the cumulative release fractions of ^{238}U. As can be seen in the figure the release is somewhat lower from the Al/Cr doped fuel. The same behaviour is observed for e.g. ^{144}Nd and ^{153}Eu.

Further analysis of this data is underway and the results are should be considered as preliminary.

Selenium and ^{14}C analysis

A method for analysis of Se and ^{14}C will be tested. Selenium analysis will be performed using hydride generation ICP-MS. If convincing selenium isotopic ratios consistent with a fissiogenic origin are obtained,

167

efforts to determine the selenium speciation in the leaching solution will also be made (by control of the selenium redox state and hydride generation or by chromatography). Preliminary results on the first leaching samples analysed by ICP-MS indicate fissiogenic ^{82}Se levels close to the detection limit (without modifications for specific analysis of selenium). Analysis of ^{14}C will be performed using a method with liquid scintillation.

Analysis by LA-ICP-MS

Laser Ablation Inductively Coupled Plasma Mass Spectroscopy (LA-ICP-MS) analysis was applied on fuel cross-sections from the standard UO$_2$ fuel 5A2 and from the Al/Cr additive fuel C1. For both fuels the samples were cut out from neighbour pellets to the samples used for the leaching studies.

The LA technique consists of a pulsed laser that ablates the material to be studied (20 Hz, spot size typically ~10 or ~60 μm diameter). A carrier gas (He or <1% H$_2$ in He) transports the created aerosol for analysis to an Inductively Coupled Plasma Mass Spectrometer (ICP-MS). The complete system is adapted for Hot Cell use (Granfors et. al., 2012). Calibration is performed by ablation on reference materials, such as the NIST 610, 612 glasses (Jochum et. al., 2011). For UO$_2$ based materials results are typically reported as the mass fraction relative to ^{238}U. Figure 5 shows an overview image of the fuel cross section from the standard sample 5A2 after laser ablation.
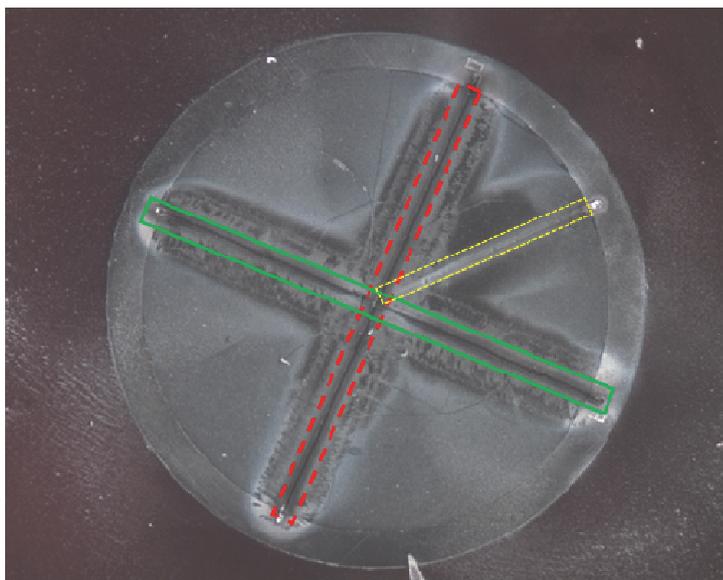
Figure 5: *Overview of sample 5A2 after laser ablation.*

The red dashed line in Figure 5 corresponds to the radial laser ablation profiles in Figure 6, the green solid line corresponds to the profiles in Figure 7. The dotted yellow line corresponds to the profiles in Figure 8.
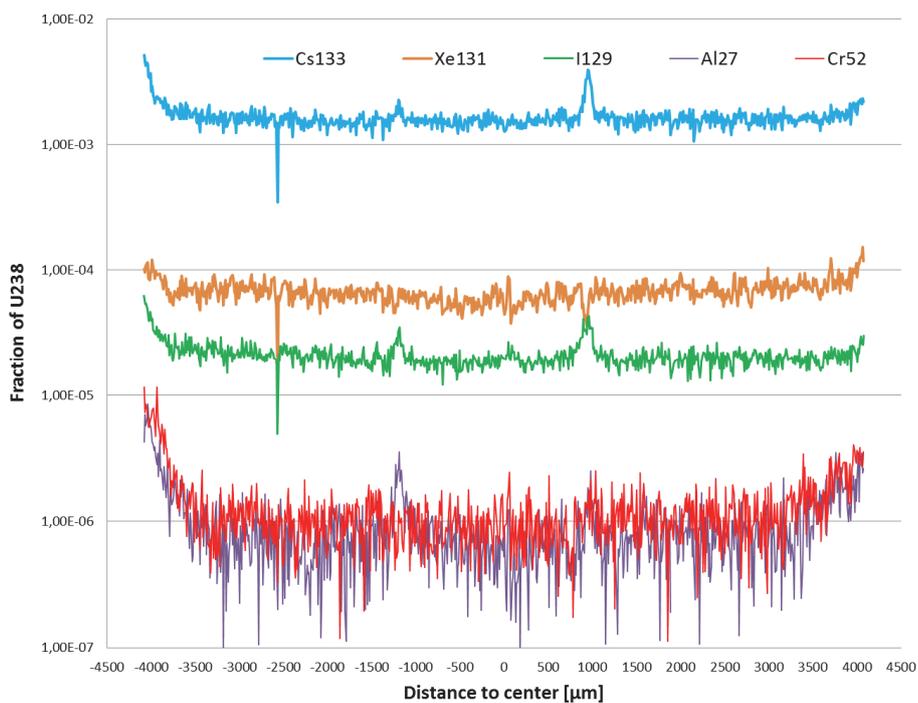
Figure 6: *Ablation profiles on 5A2 along the red dashed track in figure 5 (60 µm beam).*
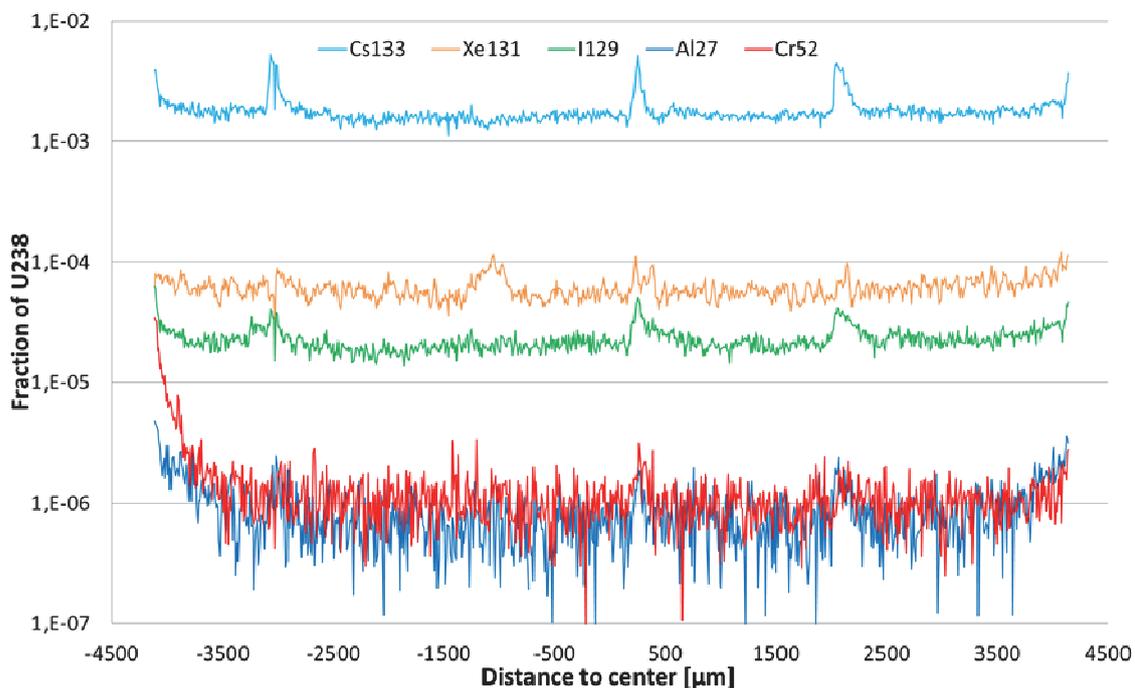
Figure 7: *Ablation profiles on 5A2 along the green track in figure 5 (60 µm beam).*

As can be seen in Figures 6 and 7 it appears that the cesium and iodine profiles follow each other. The cesium and iodine peaks, such as the one at ~1,000 µm in Figure 6 are typically associated with visible cracks in the fuel. Overall the cesium, iodine and xenon profiles are rather flat in the interior of the pellet (no excessive linear heat rates during operation).
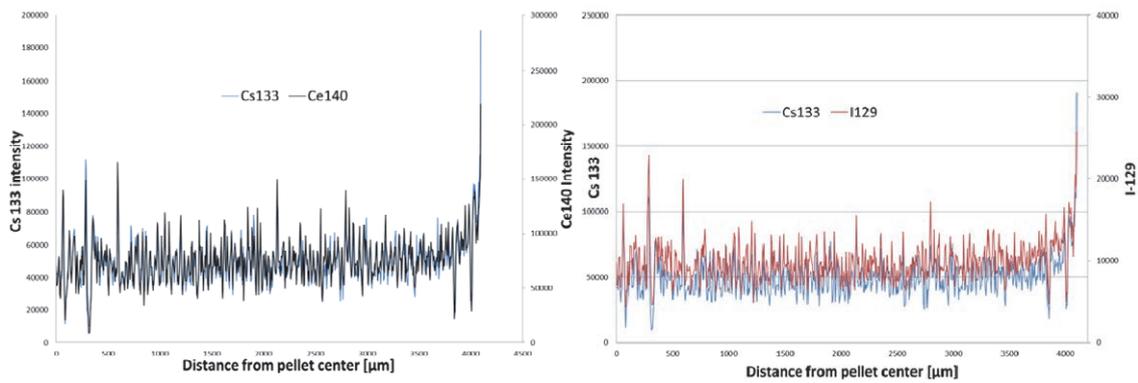
Figure 8: *Ablation profiles on 5A2 along the yellow dotted track in figure 5. Left, overlaid Cs-133 & Ce-140 profiles. Right, overlaid Cs-133 & I-129 profiles (10 µm beam).*

Figure 8, left, shows overlaid profiles of ^{133}Cs and the rather immobile lanthanide ^{140}Ce, which approximately follows the radial burnup profile of the fuel. Since the radial ^{133}Cs and ^{140}Ce profiles are nearly identical (10 µm beamsize) it suggests very limited cesium redistribution during the power operation. Figure 8 right, shows the nearly overlapping ^{133}Cs and ^{129}I profiles from the same ablation track.

Figure 9 shows an overview image of the fuel cross section from the additive sample C1 after laser ablation.
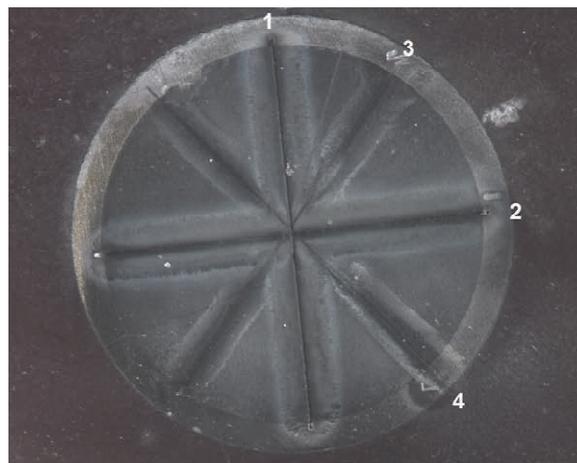
Figure 9: *Overview of additive sample C1 after laser ablation.*
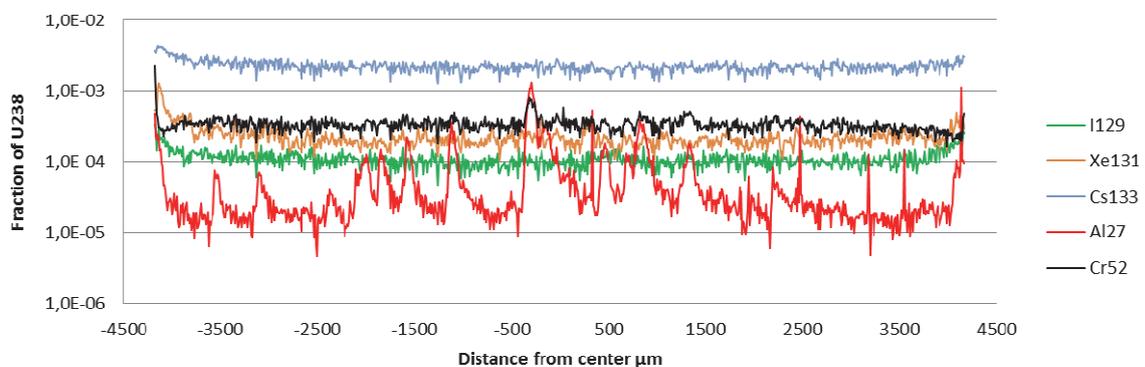
Figure 10: *Ablation profiles on sample C1 along the track marked 1 in Figure 9 (60 µm beam).*
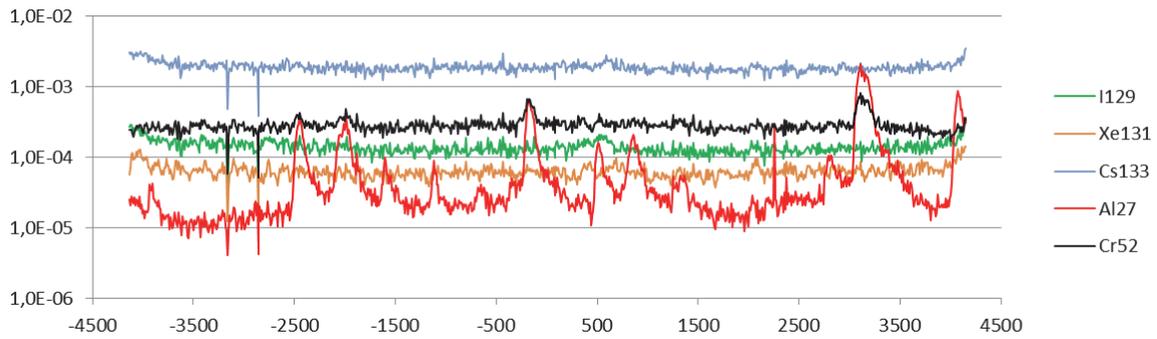
Figure 11: Ablation profiles on sample C1 at the 4th passage in the track marked 1 in Figure 9 (60 μm beam).
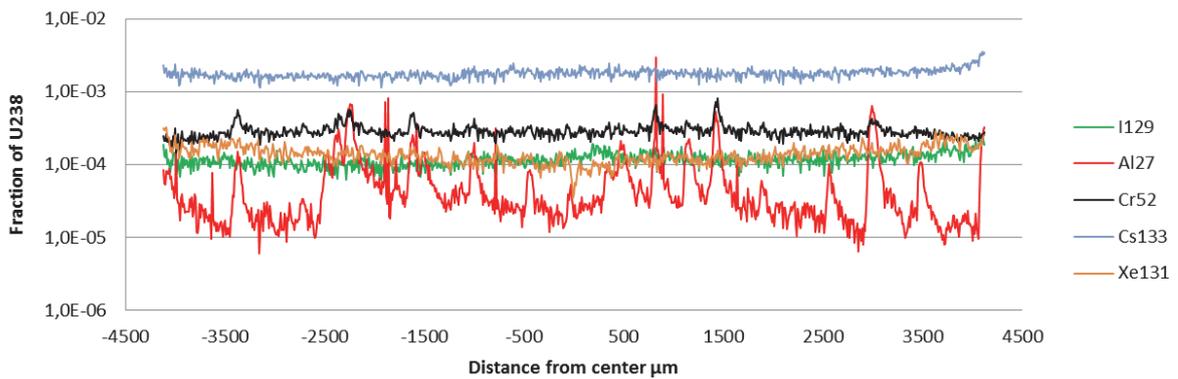
Figure 12: Ablation profiles on sample C1 along the track marked 2 in Figure 9 (60 μm beam).

As can be seen in Figures 10-12, the cesium, iodine and xenon profiles are rather flat. The aluminium additive on the other hand shows a very heterogeneous distribution, which is expected given the low solubility of Al_2O_3 in the UO_2 matrix. The chromium additive appears to be rather homogenously distributed in the fuel, although there appears to be some correlation with the aluminium rich areas. It should be noted that a significant fraction of the Cr_2O_3 could be expected to be dissolved in the UO_2 matrix. Figure 11 shows the result of repeated reanalysis (4th passage) of the same laser ablation track as in Figure 10. The passages have ablated away a few μm of material. The iodine and cesium profiles appear to be rather consistent during the multiple passages. The xenon intensities does however decrease, this is probably due to beam induced xenon depletion of the material (fission gas release due to the vibration from the impacting beam). The peaks in the chromium and aluminium profiles also change with multiple passages, supporting that the peaks for these elements are highly localized, such as in grain boundaries.
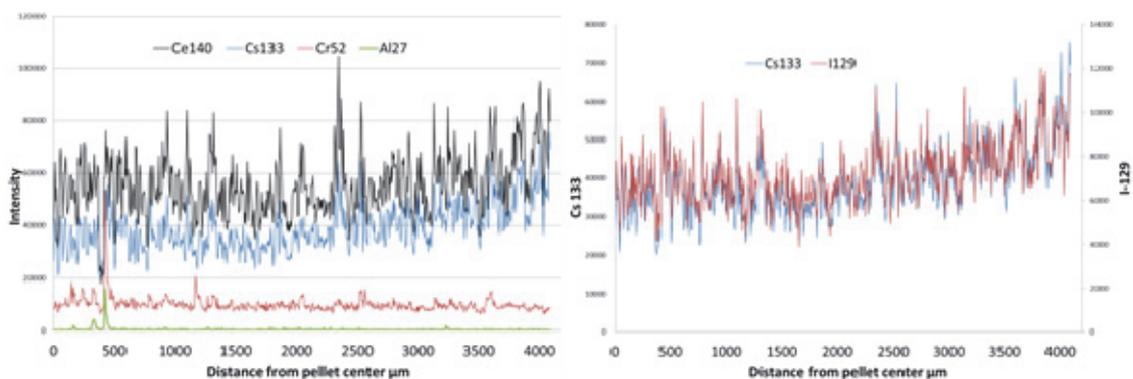
Figure 13: Ablation profiles on C1 in the fine track between 1 & 3 in Figure 9 (10 μm beam).

171

Figures 13 (left) shows that the intensity profiles of cesium and cerium are very similar also for the additive fuel. Figure 13 (right) shows the very similar Cs and I profiles for the additive fuel.
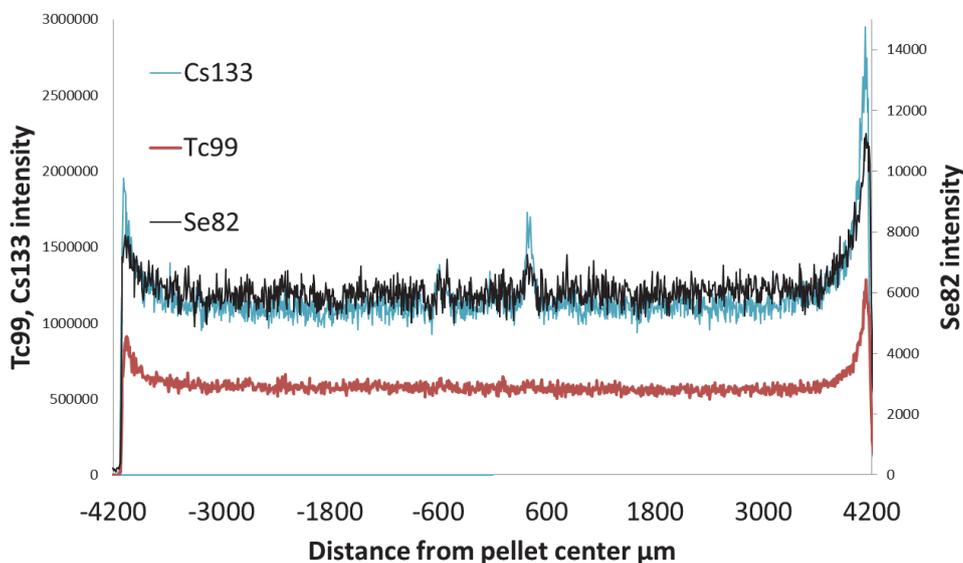
Figure 14: *Ablation profiles on sample C1 (60 μm beam).*

Figure 14 shows another radial profile from sample C1 that crosses a pellet crack at ~600 µm. Selenium (^{82}Se) was tentatively identified, as can be seen from the overlaid ^{82}Se and ^{133}Cs profiles they have very similar radial distribution. The insert shows the overlaid ^{133}Cs and ^{129}I profiles at the location of the crack.
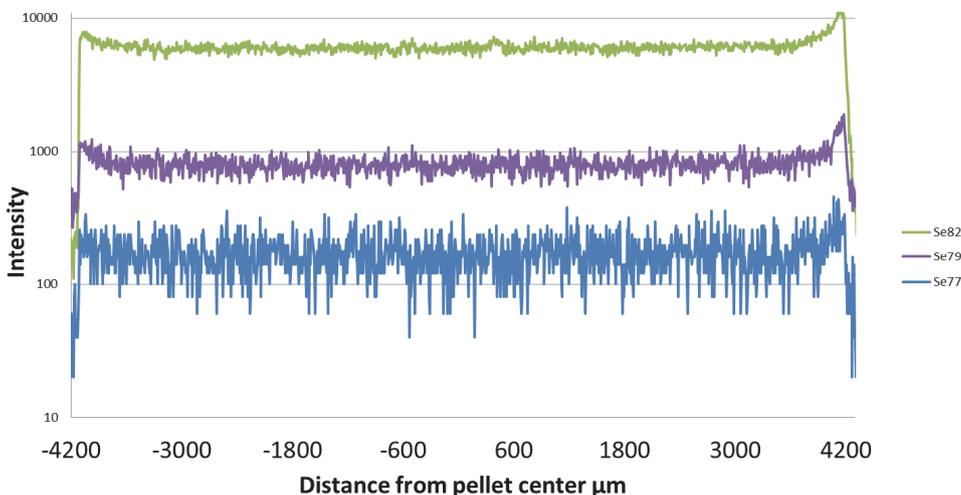
Figure 15: *Ablation profiles on sample C1 (60 μm beam).*

Figure 15 shows the radial profiles of mass 77, 79 and 82, which should all be dominated by isotopes of selenium, which shows a very good agreement between calculated and measured ratios as shown below.
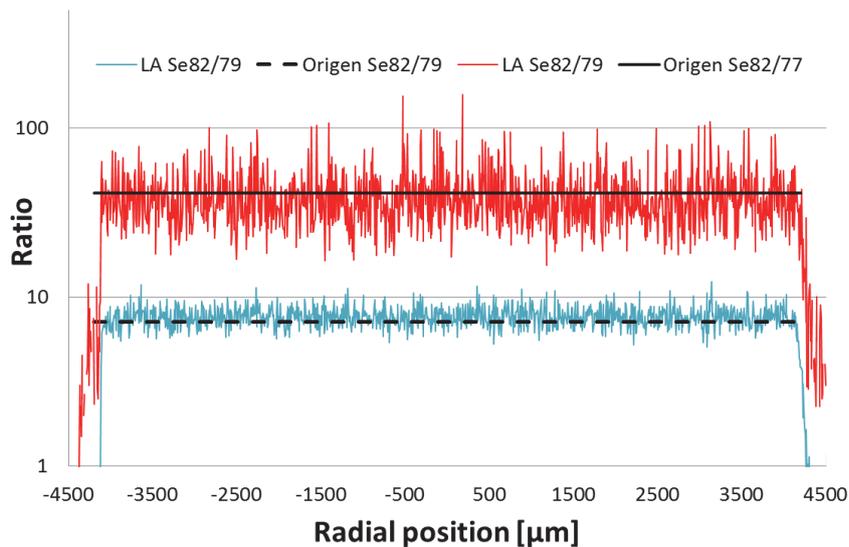
Figure 16: *Comparison of Se isotope ratios from LA and average values calculated by the Origen code, sample C1 (60 μm beam).*

Figure 16 shows the radial isotopic ratios of mass 82/79 and by 82/77 obtained by LA and the good agreement with the calculated average $^{82}Se/^{79}Se$ and $^{82}Se/^{77}Se$ ratios obtained by the Origen code. Similar results were also obtained from sample 5A2 (not shown).

In summary the findings of the LA study on both pellets indicate cesium and iodine profiles that are very similar and appear to follow the radial burnup profile (as indicated by ^{140}Ce). Cesium, iodine and to some extent selenium also appear to collect in some fuel cracks. Selenium was tentatively identified by the good agreement of the isotopic ratios of mass 77, 79 and 82 with the calculated inventory. For the additive pellet chromium and especially aluminum are heterogeneously distributed in the pellet.

Further analysis of the LA data is underway and the results should be considered as preliminary.

Acknowledgement

References

Forsyth, R. (1997). The SKB Spent Fuel Corrosion Program – An Evaluation of Results from the Experimental Program Performed in the Studsvik Hot Cell Laboratory, SKB TR 97-25.

Granfors, M. et al. (2012). Radial profiling and isotopic inventory analysis of irradiated nuclear fuel using laser ablation ICP-MS". Proceedings of Top Fuel 2012, 2nd – 6th September 2012, Manchester, UK.

Jochum, K.P., Weis, U., Stoll, B., Kuzmin, D., Yang, Q., Raczek, I., Jacob, D.E., Stracke, A., Birbaum, K., Frick, D.A., Günther, D., Enzweiler, J. (2011) Determination of Reference Values for NIST SRM 610–617 Glasses Following ISO Guidelines. Geostandards & Geoanalytical Reserch, 35, 397-429.

Johnson, L., Günther-Leopold, I., Kobler Waldis, J., Linder, H.P., Low, J., Cui, D., Ekeroth, E., Spahiu, K., Evins, L.Z. (2012). Rapid Aqueous Release of Fission Products from High Burn-Up LWR Fuel: Experimental Results and Correlations with Fission Gas Release. Journal of Nuclear Materials, 420, 54-62.

Pearce, N., Perkins, W., Westgate, J., Gorton, M., Jackson, S., Neal, C., Chenery, S. (1997). A Compilation of New and Published Major and Trace Element Data for NIST SRM 610 and NIST SRM 612 Glass Reference Materials. The Journal of Geostandards and Geoanalyses, 21 06/97, 115-144.

Roth, O., Puranen, A. (2012). Selection of Materials, Preparations and Experimental Set-Up. 1st Annual Workshop Proceedings of the Collaborative Project "Fast/Instant Release of Safety Relevant Radionuclides from Spent Nuclear Fuel". 1st Annual Workshop Proceedings – 7th EC FP – FIRST-Nuclides. 9th – 11th October 2012, Budapest, Hungary, KIT Scientific Reports 7639, 137-144.

Roth, O., Low, J., Granfors, M., Spahiu, K. (2013). Effects of Matrix Composition on Instant Release Fractions From High Burn-Up Nuclear Fuel. Mater. Res. Soc. Symp. Proc., 1518, 145-150.

Roth, O., Low, J., Spahiu K. (2013). Effects of Matrix Composition and Sample Preparation on Instant Release Fractions from High Burnup Nuclear Fuel. Submitted to Mater. Res. Soc. Symp. Proc.

Stroes-Gascoyne, S., Moir, D.L., Kolar, M., Porth, R.J., McConnell, J.L., Kerr, A.H. (1995). Measurement of Gap and Grain-Boundary Inventories of ^{129}I in Used CANDU Fuels. Mat. Res. Soc. Symp. Proc., 353, 625-631.

Zwicky, H-U., Low, J., Ekeroth, E. (2011). Corrosion Studies with High Burnup Light Water Reactor Fuel; Release of Nuclides into Simulated Groundwater during Accumulated Contact Time of up to Two Years. SKB TR-11-03.

POSTERS

FIRST Nuclides

7th Framework Programme Collaborative Project:

Fast / Instant Release of Safety Relevant Radionuclides from Spent Nuclear Fuel (FIRST-Nuclides)

EURATOM 7

Objectives

Understanding the fast / instant release of radionuclides from high burn-up spent UO_2 fuels in geological repositories.

- Experimental investigations of irradiated fuel.
- Provide for improved data for the fast/instant release fraction for high burn-up spent UO_2 fuel.
- Study correlations between the Fission Gas Release and non-gaseous fission products, in particular ^{129}I, ^{79}Se and ^{135}Cs.
- Reduce uncertainties with respect ^{129}I, and ^{14}C releases.
- Determine the chemical form of the relevant elements.
- Discuss the impact of the results on the peak-dose.

Consortium

The project is implemented by a consortium with 10 **Beneficiaries** from 7 EURATOM Signatory States, and the EC Institute for Transuranium Elements:

KIT   AMPHOS²¹   itu   JÜLICH   PSI

SCK·CEN   CNRS   ctm   EM   Studsvik

Associated Groups: Groups participating in the project at their own costs with specific RTD contributions or particular information exchange functions. **End-User Group:** Waste Management / Regulating Organizations.

Structure of the project

WP 1: Samples and tools: Selection, characterization and preparation of materials and set-up of tools.

WP 2: Gas release + rim and grain boundary diffusion: Experimental determination of fission gases release. Rim and grain boundary diffusion experiments.

WP 3: Dissolution based release: Dissolution based fast/instant radionuclide release.

WP 4: Modelling: Modelling of migration/retention processes of fission products in the spent fuel structure.

WP 5: Knowledge, reporting and training: Knowledge Management, State-of-the-Art report, general reporting, documentation up-date, dissemination and training.

WP 6: Project management.
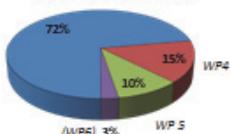
Figure 1. Use of staff resources committed for different types of activities within the project.

Experimental (WP 1 - WP 3) 72%   15% WP4   10%   (WP6) 3%   WP 5

Details of the experimental programme (WP 1-WP 3):

- Chemical form, specifically for fission gases, ^{135}Cs, ^{129}I, ^{14}C compounds, ^{79}Se, ^{99}Tc and ^{126}Sn.
- Determination of gap and grain boundary inventories.
- Dependency of fast/instant release on
  - UO_2 fuel and the respective manufacturing process,
  - evolution of higher burn-up and burn-up history,
  - linear power and fuel temperature history, ramping processes, and storage time.
- Accessibility / transport properties on grain boundaries.
- Exchange processes along the grain boundaries.
- Transition between instant/fast release and radiolytically driven matrix corrosion.

*Table 1. Fuel data under investigation from PWR and BWR*

	PWR	BWR
Discharge (manufacturer)	1989 -2008 (AREVA)	2005 – 2008 (AREVA/ Westinghouse)
Cladding Material/diameter/ thickness (mm)	Zry-4-M5 / 9.50 - 10.75 / 0.62 - 0.73	Zyr 2 / 9.84 - 10.2
Pellet Enrich.(%) /grain size (μm) / den. (g·cm⁻³)	2.8 - 4.3 / 5 - 40 / 10.41	3.5 - 4.25 % / 6 - 25 / 10.52
Irradiation BU (GWd/t) / cycles	45 - 70.2 / 2 - 14	50.2 - 59.1 / 5 - 7
Lin. Power (W/cm)	186 -306	160 - 200
FGR (%)	4.9 – 26.7	1.4 – 3.1

Enrich = enrichment, den = density, BU = burn up, Lin = linear

Modelling (WP 4)

- Fission product migration on grain boundaries.
- Effects of fractures in the pellets.
- Effects of holes/fractures in the cladding.
- Chemical state of relevant elements.

Figure 2. Microstructure of the pellet. (Different grain size)

Original grain   Rim

Dissemination, Mgt* and Training (WP 5-WP6):

Duration of the CP: 01 Jan. 2012 to 31 Dec. 2014

Funding: Total Costs: 4 741 261 €
     EC Contribution: 2 494 513 €

Events: 2nd Annual Workshops: *(October 2013)*

Mgt = Management
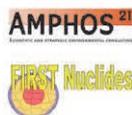
Numerical modelling of Spent Nuclear Fuel saturation with water under laboratory and repository conditions

*Marek Pękala, Andrés Idiart, Olga Riba and Lara Duro

Amphos 21 Consulting S.L, Barcelona (Spain) *marek.pekala@amphos21.com

INTRODUCTION AND OBJECTIVES

A factor that can significantly impact Performance Assessment results (PA) is the Instant/Fast Release Fraction (IRF) – a fraction of the radionuclide inventory that can be mobilised "instantly" upon exposure of the Spent Nuclear Fuel (SNF) to the intruding groundwater. Wetting of the fuel surfaces, if sufficiently slow, may be an important factor limiting the release rate for some radionuclides. The objective of this work is to quantify the time of SNF saturation with water and its potential impact on the IRF.

METHODOLOGY

Main assumptions:

Serna et al. (2006)

- ❖ Primary water flow is through "large" diameter crack network (mean of 20μm)

- ❖ Porosity assumed unconnected
- ❖ Grain boundaries assumed not to participate in water flow

Romano et al. (2007) – left
Thomas et al. (1989) – right

- ❖ Secondary water flow through "small" diameter crack network (arbitrary mean of 0.1 μm)

IAEA-TECDOC-CD-1635

Reference Pellet Definition:

Willford (1984)

Oguma (1983)
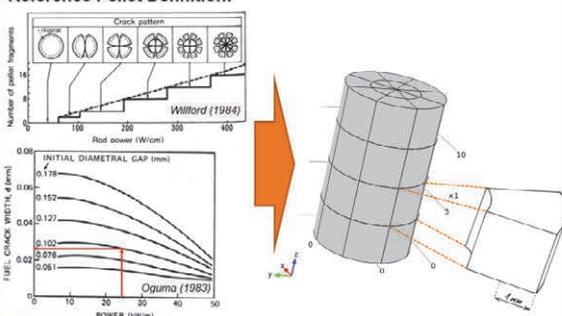
Parameterisation:

- ❖ Retention curve approximated from cracks statistics (Zhang and Fredlund, 2003)
  - ○ Mean aperture (20 μm and 0.1 μm)
  - ○ Standard deviation of apertures: 50 % and 100 %
  - ○ Apertures follow log-normal distribution
- ❖ Van Genuchten parameters fitted to retention curve
- ❖ Saturated permeability evaluated from the "cubic law" (de Marsily 1986)
- ❖ Interconnected voidage: Reference Pellet = 0.02 (estimated from crack geometry), sub-μm scale = 0.1 (assumed)
- ❖ Fracture compressibility & Residual water content = 0

Numerical implementation:
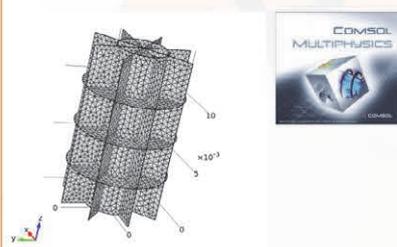
- ❖ Model implemented into Comsol Multiphysics (finite element code)
  - ○ Modified "Fracture Flow Interface" for the Reference Pellet
  - ○ "Richards Interface" for the sub- μm scale model
- ❖ Pellet finite element mesh consists of 10,500 triangle elements (or 50,000)
- ❖ Sub-μm scale 1D model discretised over 1 mm using 1,000 equidistant elements

Initial and Boundary Conditions:

Relative Standard Deviation (RSD) of cracks apertures [%]	Initial Saturation [‰]	Boundary water pressure [cm]
50	1	5
100	0.1	5

RESULTS

Time to saturation – Reference Pellet:

RSD [%]	Initial Saturation = 1 ‰	Initial Saturation = 0.1 ‰
50	1 sec	1 min
100	1 min	2 hour
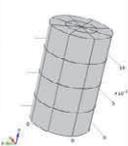
Time to saturation (Sub-μm aperture case solved over 1 mm length):

RSD [%]	Initial Saturation = 1 ‰	Initial Saturation = 0.1 ‰
50	5 sec	1 min
100	2 hour	1 year
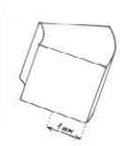
DISCUSSION AND CONCLUSIONS

- ❖ First saturation results obtained for low boundary water pressures characteristic of laboratory conditions (leaching experiments)
- ❖ Saturation strongly depends on (unknown in detail) water retention properties of the crack system
- ❖ Small-aperture (sub-μm) cracks are expected to saturated over times much longer (months to years) than those for large (here 20 μm) cracks (hours)
- ❖ Saturation with water could represent an additional process (besides rapid dissolution) to contribute to IRF

[1] IAEA, International Atomic Energy Agency Report, IAEA-TECDOC-CD-1635 [2] de Marsily G. (1986). Quantitative Hydrogeology.Academic Press, Inc. [3] Oguma M. (1983). Cracking and relocation behaviour of nuclear fuel pellets during rise to power. Nuclear Engineering and Design, 76, 35. [4] Romano A., Horvath M. I. and Restani R. (2007). Evolution of porosity in the high-burnup fuel structure. Journal of Nuclear Materials 361, 62-68. [5] Serna J., Tolonen P., Abeta, S. Watanabe S., Kosake Y., Sendo T and Gonzales P. (2006). Experimental observations on fuel pellet performance at high burnup. Journal of Nuclear Science and Technology 43, 1-9. [6] Thomas L. E., Knoll R. W., Charlot L. A. Coleman J. E. and Gilbert E. R. (1989). Storage of LWR spent fuel in air, Volume 2 – Microstructural characterization of low-temperature oxidized LWR spent fuel. Pacific Northwest Laboratory Report, PNL-6640. [7] Willford R. E. (1984). A cracked-fuel constitutive equation. Nuclear Technology, 67, 208 . [8] Zhang L. and Fredlund D. G. (2003). Characteristics of water retention curves for unsaturated fractured rocks. Second Asian Conference on Unsaturated Soils, UNSAT-ASIA 2003. Osaka, Japan.

PRESENTATIONS BY ASSOCIATED GROUPS

INTEGRATING USED FUEL DEGRADATION MODELS INTO GENERIC PERFORMANCE ASSESSMENT

David C. Sassani*, Carlos F. Jové-Colón, Philippe F. Weck

Sandia National Laboratories (USA)

*Corresponding author: dsassan@sandia.gov

Within the Used Fuel Disposition Campaign (UFDC) of the United States Department of Energy Office of Nuclear Energy (DOE-NE), we have investigated used fuel (UF) degradation and radionuclide mobilization (UFD&RM) and implemented/produced a set of models encompassing radiolytic processes, UF matrix degradation, instant release fractions (IRF) of key radionuclides, and first-principles atomistic models for UO_2 and its potential corrosion products. The goals of this collaborative effort (among three different national laboratories: Argonne National Laboratory [ANL]; Pacific Northwest National Laboratory [PNNL]; and Sandia National Laboratories [SNL]) are to enhance the understanding of UF degradation processes and the technical bases for safety analyses in a range of generic disposal environments. In addition to these modeling efforts, integrated experimental studies are being conducted at both ANL and PNNL to evaluate and validate (and ultimately expand) process models for radiolytic phenomena and UF matrix degradation in various geologic disposal conditions. Integration and coupling of these process models into a generic performance assessment model (GPAM) is one focus of SNL efforts within the generic analyses of the Engineered Barrier System (EBS) for various repository environments. As discussed below, the present work has produced a set of models for implementation into the GPAM as an initial step towards an enhanced coupled model of source-term processes.

USE OF IRF DATA IN THE SAFETY CASE FOR THE FINNISH DISPOSAL PROJECT

Barbara Pastina

Saanio & Riekkola Oy, Helsinki (FI)

At the end of 2012, Posiva Oy presented the license application to construct a spent fuel repository in Finland. The license application comprises several components, including a safety case addressing the long-term safety of the repository after its closure (Posiva, 2012). One of the outcomes of the safety case is the assessment of the consequences of radionuclide release scenarios. The assessment is carried out by modelling the releases from the spent fuel and their transport in the geosphere and up to the biosphere. The source term for the radionuclide release model consists of four components: 1-the UO_2 matrix, 2-the gaps and grain boundaries, 3-the cladding and other Zr-based alloys, 4-metallic structures of the fuel assembly (Posiva, 2013). There are currently important uncertainties in the releases from the gap and grain boundaries that are managed by increasing the level of conservatism of the source term. For example, the fraction of radionuclides susceptible to be located in the gaps and/or grain boundaries is set to be released instantaneously at the time of the initial canister release (hence the term Instant Release Fraction, IRF).The objectives of the FIRST-Nuclides project fulfil the need to reduce the uncertainties and provide realistic data on the relevant radionuclide release for the safety case leading to an increased confidence in capability of predictions.

The three key IRF radionuclides that contribute to the doses to the biosphere are ^{14}C, ^{36}Cl and ^{129}I. Other radionuclides are included in the IRF are: ^{135}Cs, ^{137}Cs, ^{10}Be, ^{107}Pd, ^{90}Sr, ^{99}Tc, ^{79}Se and ^{126}Sn. Of particular interest to the safety case are the uncertainties in the following

- Speciation and partitioning of activation products and ^{14}C
- Quantification of the IRF and correlation with fission gas release (FGR) measurements
- Correlation between the irradiation history (e.g., burnup, linear power rating) and the IRF

Concerning the last bullet, the importance of correlating spent fuel data (e.g. irradiation history) with measurements of FGR or IRF has been recognized in the previous studies leading to FIRST-Nuclides.

Within the FIRST-Nuclides project, spent fuel from one of the Finnish nuclear power plants is undergoing leaching measurements at Studsvik (see S+T "Spent Fuel Leaching Experiments and Laser Ablation Studies Performed in Studsvik – Status and Preliminary Results" pag. 161, from Roth et al.). The results from these tests will be used in the next safety case in support of the operational license application, due in 2020. Gathering additional data (e.g. short-term leaching, FGR) on well characterised fuel is recommended to reduce, if possible, the conservativeness of IRF assumptions in the safety case.

Acknowledgment

References

Posiva, 2012. Safety case for the disposal of spent nuclear fuel at Olkiluoto - Synthesis 2012. POSIVA 2012-12. Posiva Oy, Eurajoki, Finland.

Posiva, 2013. Safety case for the disposal of spent nuclear fuel at Olkiluoto - Models and Data for the Repository System 2012. POSIVA 2013-01. Posiva Oy, Eurajoki, Finland

THE CHARACTERISTICS AND LEACHING BEHAVIOUR OF AGR SPENT FUEL – AN OVERVIEW OF CURRENT UK RESEARCH

Cristiano Padovani[1], Charlotta Askeljung[2], Mark Cowper[3], David Hambley[4], Zoltan Hiezl[5], Bill Lee[5]

[1]Nuclear Decommissioning Authority, Radioactive Waste Management Directorate (UK)
[2]Studsvik Nuclear AB, Studsvik Nuclear AB (SE)
[3]AMEC Clean Energy Europe (UK)
[4] Spent Fuel Management and Disposal, UK National Nuclear Laboratory (NNL) (UK)
[5] Imperial College London, Centre for Nuclear Engineering (UK)

The UK has a large and diverse inventory of radioactive wastes (NDA, 2011a). Wastes unsuitable for surface disposal are currently destined for disposal in a geological disposal facility (GDF). Whilst spent fuel from Advanced Gas Reactors (AGR) has been and is still being reprocessed, it is likely that, at the time in which reprocessing facilities will close, a significant fraction of such fuel will not have been reprocessed and may require disposal in a GDF (NDA, 2011b).

This talk will describe current R&D planned or being carried out in the UK to understand the characteristics and leaching behaviour of spent AGR fuel, in support of the development of a safety case for its disposability in a GDF. Current activities include experimental work on active samples as well as experimental and modelling work on inactive surrogates (SIMFUEL). This work is still in early stages so only preliminary results will be presented.

Work on active samples is being carried out on three AGR samples extracted from a currently operating power station. Key characteristics of the fuel rods from which samples were extracted are an average burn-up of 37 MWd/KgU with a fission gas release (FGR) of 8.4% (considered representative of high-burn up/FGR) and two fuel rods with average burn-up of 30 MWd/kgU and 27 MWd/kgU respectively and with a FGR of about 1.1% and 0.2% respectively (considered representative of average burn-up/FGR). The samples were extracted in regions of the rods intended to allow, as far as practicable, a meaningful comparison (the specific position in the rod determining important factors such as temperature history and local burn-up). Fuel fragments and cladding are being exposed to a 0.01 M NaCl, 0.002 M $NaHCO_3$ solution at room temperature and in naturally aerated conditions. Instant release fraction (IRF) and long-term dissolution rates are being measured on key radionuclides with ICP-MS. The sample preparation, leaching methodology and leaching conditions were selected to allow a comparison with data previously obtained in other disposal programmes on Light Water Reactor (LWR) fuels in similar conditions (e.g. Johnson et al., 2012), from which formula to calculate the IRF as a function of fuel burn-up were derived (e.g. Thetford and Karney, 2011; Trivedi et al., 2012).

Work on inactive samples is mainly focused on the use of SIMFUEL, a surrogate of spent fuel manufactured with depleted uranium and non-radioactive isotopes of key fission products (Strausberg and Murbach, 1963). SIMFUEL samples intended to replicate the expected chemical composition of AGR fuels after a decay period of 100 years (the composition is not expected to change dramatically over longer periods) and initial average burn-ups of 25 MWd/kgU ('low-doped') and 43 MWd/kgU ('high-doped') have being manufactured at Springfields through a cold pressing and sintering process in hydrogen atmosphere. Samples have then been characterised with optical/SEM microscopy and EDX to evaluated their morphology (porosity and composition of precipitates phases). This work (Figure 1) indicated the formation of the 'grey phases' ((Ba, Sr)(Zr, RE)O_3 oxide precipitates) and ε-phases (Mo-Ru-Rh-Pd metallic precipitates), typically observed in spent fuel (Thomas

et al., 1992; Hiezl et al., 2013). Preliminary electrochemical measurements (cyclic voltammetry) carried out on 'pure' UO_2 and SIMFUEL samples indicated much more prominent oxidation/reduction peaks in SIMFUELS samples, which have been associated with the lattice damage and hyper-stoichiometric conditions expected in spent fuels (Rauff-Nisthar et al., 2013). Leaching tests and modelling studies (Cooper et al., 2013) are currently underway. Work is also under way to understand the whether the presence of steel cladding in close proximity to the fuel affects dissolution and to examine the incorporation of actinides in secondary phases formed during UO_2 dissolution.
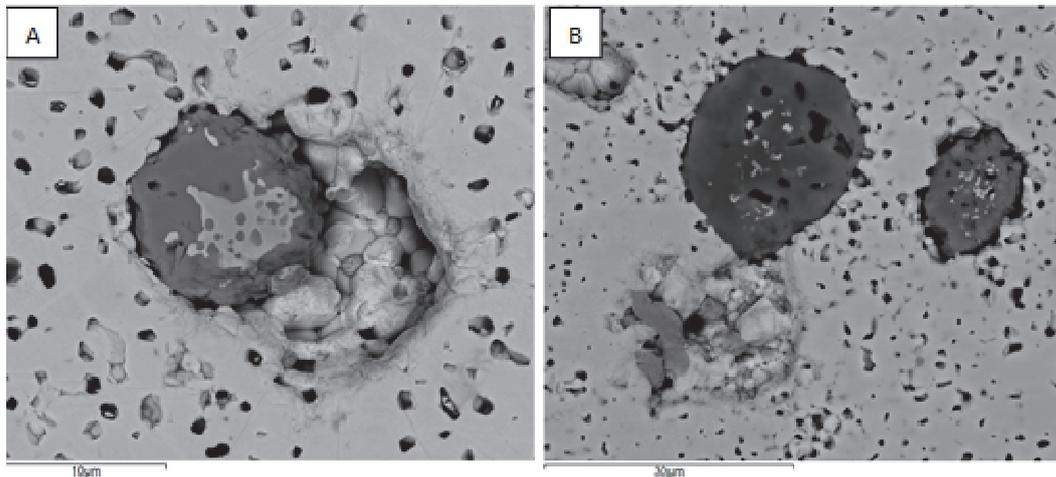
Figure 1: A: SEM-BS image of a typical oxide precipitate present in the low-doped sample; B: Different type of secondary phases in the highly doped SIMFuel sample.

Acknowledgements

References

Nuclear Decommissioning Authority and Department of Energy and Climate Change (2011). The 2010 UK Radioactive Waste inventory – Main report. URN 10D/985 NDA/ST/STY(11)0004.

Nuclear Decommissioning Authority (2011). Strategy (effective from April 2011). ISBN978-1-905985-26-5.

Johnson, L., Günther-Leopold, I., Kobler Waldis, J., Linder, H.P., Low, J., Cui, D., Ekeroth, E., Spahiu, K., Evins, L.Z. (2012). Rapid aqueous release of fission products from high burn-up LWR fuel: Experimental results and correlations with fission gas release. Journal of Nuclear materials, 420, 1-3.

Thetford, R., Karney, G. (2011). Overview of the UK Spent Fuel Inventory - Evaluation of the Instant Release Fraction. Serco reportTAS/ENV/E.004027.02.

Trivedi, D., Wareing, A., Mignanelli, M. (2012). Assessment of Potential release from Spent AGR Fuel in a Geological Disposal Facility. NNL (10) 11377.

Strausberg, S., Murbach, E.W. (1963). Multicycle Reprocessing and Refabrication Experiments on Sintered UO$_2$-fissia Pellets. I&EC Process Design and Development, 2, 228-231.

Thomas, L.E., Beyer, C.E., Charlot, L.A. (1992). Microstructural Analysis of LWR Fuels at High Burnup. Journal of Nuclear Materials, 188.

Hiezl, Z., Hambley, D., Lee, W. E. (2013). Preparation and characterisation of UO$_2$-based AGR SIMFUEL. Proceedings of Scientific Basis for Waste Management 2013, MRS Proceedings (submitted).

Rauff-Nisthar, N., Boxall, C., Farnan, I., Hiezl, W.L.Z., Perkins, C., Wilbraham R. (2013). Corrosion Behavior of AGR Simulated Fuels – Evolution of the Fuel Surface. Corrosion in Nuclear Energy Systems: From Cradle to Grave "ECS Transactions", 53.

Cooper, M.W.D., Middleburgh, S.C., Grimes R.W. (2013). Partition of Soluble Fission Products Between the Grey Phase, ZrO$_2$ and Uranium Dioxide. Journal of Nuclear Materials, 438, 238-245.

CORROSION BEHAVIOUR OF AGR SIMULATED FUELS – EVOLUTION OF THE FUEL SURFACE

N. Rauff-Nisthar[1], C. Boxall[1], I. Farnan[3], Z. Hiezl[2], W. Lee[2], C. Perkins[4] and R. Wilbraham[1]

[1]Engineering Department, Lancaster University (UK)
[2]Department of Earth Sciences, University of Cambridge (UK)
[3]Department of Materials, Imperial College London (UK)
[4]National Nuclear Laboratory (UK)

In the UK, the vast proportion of spent nuclear fuel (SNF) is from indigenous Advanced Gas-cooled Reactors (AGRs). AGRs, whilst using UO_2-based fuel, employ CO_2 as coolant and are graphite moderated. Further, the fuel assembly cladding is comprised of $^{20/25}$Nb stainless steel (20% Cr, 25% Ni) rather than zircalloy as is the case in Pressurised Water Reactors (PWRs). Consequently, AGR fuel has unique characteristics that need to be evaluated in order to satisfy safety case requirements before it can be disposed of in a geological repository.

Hydrogen peroxide concentrations in the near-field are expected to lie in the vicinity of 100 μmol/dm^3 (Corbel et al., 2006). This locally oxidising environment may convert U(IV) to U(VI), so allowing U to pass into solution, with the possibility of re-precipitation of oxidised U(VI) back onto the fuel pellet surface, generating secondary mineral phases such as schoepite. The peroxide minerals studtite $(UO_2)O_2(H_2O)_4$ and metastudtite $(UO_2)O_2(H_2O)$ are stable in H_2O_2-bearing environments even at low $[H_2O_2]$. As such, studitite layers may form a barrier for retarding SNF corrosion and could retain radionuclides either within their structure or by surface adsorption. Whether more or less corrosion obtains in the presence of the studtites is a generic research question for all UO_2-based SNF, not just AGR SNF.

Pure UO_2 pellets and SIMFUEL pellets simulating 25 GWd/t$_U$ and 43 GWd/t$_U$ burn-up were fabricated at the UK NNL. Using Raman spectroscopy, we have studied the effect of the SIMFUEL dopants on the UO_2 crystal structure. We have also studied the effect of exposure to hydrogen peroxide solutions on the SIMFUEL surface.
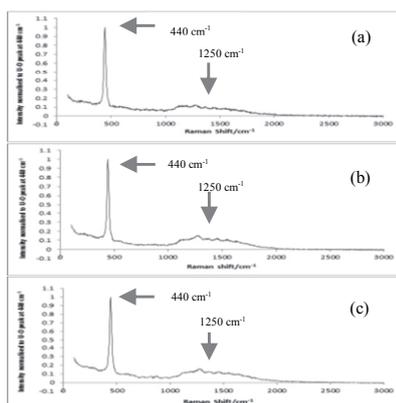

Figure 1: *Micro-Raman spectra of an undoped UO_2 sample: (a) as received; and after 1 h exposure to (b) oxygenated water and (c) 100 μmol/dm^3 H_2O_2*
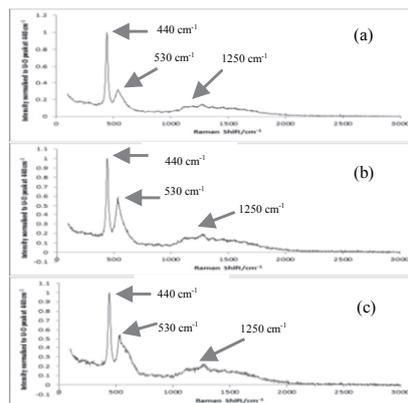
Figure 2: *Micro-Raman spectra of a 25 GWd/tU SIMFUEL sample: (a) as received; and after 1 h exposure to (b) oxygenated water and (c) 100 μmol/dm^3 H_2O_2*
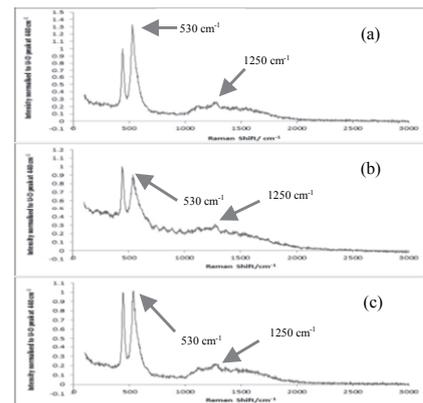
Figure 3: *Micro-Raman spectra of a 43 GWd/tU SIMFUEL sample: (a) as received; and after 1 h exposure to (b) oxygenated water and (c) 100 μmol/dm^3 H_2O_2*

Samples prepared in the absence of dopants exhibit the cubic fluorite structure expected of UO_2 and show no change in their Raman spectra upon treatment with oxygenated water or solutions of aqueous hydrogen peroxide (Figure 1). A peak associated with lattice damage (470 – 600 cm^{-1}) is observed from both 25 and 43 GWd/t$_U$ burn-up SIMFUEL, reflecting the introduction of dopant-associated lattice defects into the UO_2 matrix (Figures 2 and 3). As might be expected, the peak intensity is greater for the 43 GWd/t$_U$ sample. An increase in the lattice damage peak is observed when the 25 GWd/t$_U$ burn-up SIMFUEL is exposed to water and subsequently H_2O_2 for 1 h, suggesting that the structure at the surface is becoming more distressed. This is consistent with additional point defects being established as the concentration of interstitial oxygen is increased in the lattice via H_2O_2 induced surface oxidation of the SIMFUEL.
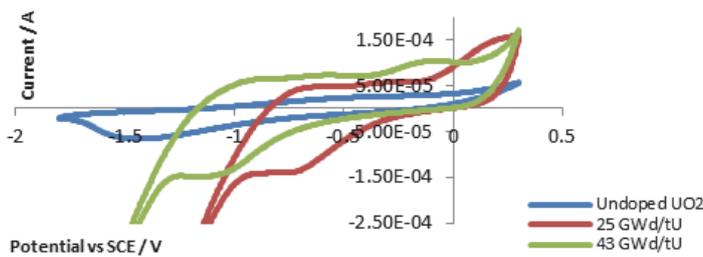

Figure 4: *Cyclic Voltammogram of Undoped UO$_2$, 25 GWd/t$_U$ and 43 GWd/tU SIMFUEls in modified simplified Groundwater, sparged with Argon.*

Exposure of the 43 GWd/t$_U$ SIMFUEL to the same concentration of hydrogen peroxide results in a decrease in damage peak intensity, suggesting peroxide driven dissolution of defected structures is occurring. Preliminary cyclic voltammetric studies on the same samples (Figure 4) also indicate greater electrochemical / redox activity upon increased simulated burn-up, most especially increased susceptibility of UO_{2+x} at grain boundaries (feature at ~-0.6V) and UO_2 in grain bodies (peak at ~-0.1V) to oxidation.

References

Corbel, C., Sattonnay, G., Guilbert, S., Garrido, F., Barthe, M.F., Jegou, C. (2006). Addition versus Radiolytic Production Effects of Hydrogen Peroxide on Aqueous Corrosion of UO2. Journal of Nuclear Materials, 348, 1-17.

Burakov, B.E., Strykanova, E.E., Anderson, E.B. (1996). Secondary Uranium Minerals on the Surface of Chernobyl "Lava". MRS Proceedings, 465, 1309.

He, H., Broczkowski, M., O'Neil, K., Ofori, D., Semenikhin, O., Shoesmith, D. (2012). Corrosion of Nuclear Fuel (UO2) Inside a Failed Nuclear Waste Container: A Review of Research Conducted Under the Industrial Research Chair Agreement Between NSERC, NWMO and Western University (January 2006 to December 2010). NWMO, TR-2012-09.

He, H., Shoesmith, D. (2010). Raman Spectroscopic of Defect Structures and Phase Transition in Hyper-Stoichiometric UO2. Phys. Chem. Chem. Phys., 12, 8109 – 8118.

ISSUES SURROUNDING ATOMISTIC MODELLING OF UK SPECIFIC AGR FUEL

Michael Cooper

Centre for Nuclear Engeneering (UK)

There are a number of unusual features in AGR fuel that could cause different behaviour to that of PWR fuel. For example, due to higher AGR operating temperatures and the annular nature of the AGR fuel pellet there is a significantly different temperature profile across the pellet. Additionally, AGR fuel uses a stainless steel cladding which has a lower oxygen pick up than Zircalloy, potentially resulting in a more hyper-stoichiometric fuel.

In this work atomistic simulation is used to investigate the effect of off-stoichiometry on fission product segregation to secondary oxide phases, such as ZrO_2 and $CrUO_4$ at the fuel-clad interface or $(Ba,Sr)ZrO_3$ precipitates. Significant segregation of trivalent fission products to ZrO_2 and $BaZrO_3$ was seen from stoichiometric UO2 but not from hyper-stoichiometric UO_{2+x}.

For the investigation of temperature dependent effects work has been done to create a UO_2 potential description that performs well over a large temperature range (300 – 3000 K). The validation of this new many-body potential against experimental data is also presented here.